



Synthesis and mechanical properties of elastomers made by sequential-IPNs

Thitima Limpanichpakdee

► To cite this version:

Thitima Limpanichpakdee. Synthesis and mechanical properties of elastomers made by sequential-IPNs. Chemical Physics [physics.chem-ph]. Université Pierre et Marie Curie - Paris VI, 2017. English. NNT : 2017PA066315 . tel-01718214

HAL Id: tel-01718214

<https://theses.hal.science/tel-01718214>

Submitted on 27 Feb 2018

HAL is a multi-disciplinary open access archive for the deposit and dissemination of scientific research documents, whether they are published or not. The documents may come from teaching and research institutions in France or abroad, or from public or private research centers.

L'archive ouverte pluridisciplinaire **HAL**, est destinée au dépôt et à la diffusion de documents scientifiques de niveau recherche, publiés ou non, émanant des établissements d'enseignement et de recherche français ou étrangers, des laboratoires publics ou privés.

Université Pierre et Marie Curie

ED 397 : Physique et Chimie des Matériaux

Laboratoire Sciences et Ingénierie de la Matière Molle / Equipe Soft Polymer Networks

Synthesis and mechanical properties of elastomers made by sequential-IPNs

Par Thitima LIMPANICHPAKDEE

Thèse de doctorat de Chimie et Physico-chimie des Polymères

Dirigée par Costantino Creton et Jutta Reiger

Soutenance prévue le 14 Novembre 2017

Devant un jury composé de :

François GANACHAUD	DR CNRS - l'INSA Lyon - Lyon	Rapporteur
Guillaume MIQUELARD	MCF à CNAM - Paris	Rapporteur
Laurent CHAZEAU	Professeur à l'INSA Lyon - Lyon	Examineur
Laurent BOUTEILLER	DR CNRS - Université P. et M. Curie - Paris 6	Examineur
Jutta RIEGER	CR à l'Université P. et M. Curie - Paris 6	Co-encadrante
Costantino CRETON	DR CNRS – ESPCI Paris	Directeur de thèse

« Dans la vie, rien n'est à craindre, tout est à comprendre. »

Marie Curie

Acknowledgement

My PhD thesis would not be finished, if I did not get kindly support from many people behind me. I would like to express my gratitude to them who are a part of my achievement.

Foremost, I am really appreciated and I would like to express my sincere gratitude to my advisor, Costantino Creton. Thanks for all of your support and to broaden my knowledge in mechanical field, thanks for your generosity with your time, encouragement, motivation, enthusiasm, and immense knowledge, I am really overwhelm and appreciated. Also, I would like to express my gratitude to Jutta Rieger, my kindly co-supervisor who give me an advice and tech me in a polymer chemistry and a latex synthesis. Special thanks to Jutta who let me synthesized latexes at her lab.

Furthermore, I like to thank Jean-Luc Cornillon, Materials research and development director in Asia and Jean-Philippe Weber, Semi-finished designer manager at Michelin ROH, who always support and motivate me during my work and my study.

Moreover, I would like to thank Christian Frégnny, the director of the lab SIMM at ESPCI, for accepting me as a PhD student and for all the things offered to me to carry out my thesis. Most importantly, I would like to thank all the members in my jury: François Ganachaud, Guillaume Miquelard-Ganier, Laurent Chazeau and Laurent Bouteiller. I am appreciated for your time and suggestions. I will follow your recommend and thank for the evaluations on my thesis.

Many thank also give to the people at SIMM lab, ESPCI and LCP Lab, UPMC who provide me technical knowledge, discussion, technical support and suggestion, including Pierre Millereau, Guylaine Ducouret, Guillaume Chatte, Natacha Goutay, André Pontes da Costa, Etienne Ducrot, Hui Gao, Stéphanie Roi, Mengxing Li, Ludovic Olanier, Freddy martin, Armand Hakopian, Gilles Garnaud. In addition, my years in SIMM lab was passed so quickly because of there are many friendship and fun. I wish to thank all of SIMM member, LCP member and Thai students in Paris for the great memory, especially I like to thank Ekkachai Martwong, Jingwen zhao, Laure Bluteau, Yinjun Chen, Davide Colombo, Paul Elziere, Robert Gurney, Louis Keal, Romain Dubourget, Corentin Trégouë, Eak Eakkarin, Nam Thanyanan, Ploy Avasaya, Elle Suwanna and etc.

Finally, I am truly in debt to my patents, for their endless support. Although my father did not wait to see my PhD graduation, I am certainly that he must be happy and be pound of me. Many thank give to my sisters and my little brother who always give me a power and suggestions during I faced some obstacles. A special thanks goes to Baramée Patamaprom, my husband, thanks for your advice, your love and your support, thanks to be with me during difficult and joyful circumstances.

This thesis was done, at SIMM laboratory under the financial support from Franco-Thai scholarship and Michelin ROH Co., Ltd

Abbreviations

NMR	Nuclear Magnetic Resonance
SEC	Size Exclusion Chromatography
DLS	Dynamic Light Scattering
TEM	Transmission electronic microscopy
IPNs	Interpenetrating polymer networks
Semi-IPN	Semi-interpenetrated network
SIN	simultaneous interpenetrating network
IEN	Interpenetrating elastomeric networks
SN	Simple network
DN	Double network
TN	triple networks
QN	quadruple networks
HyS _{maj}	major loop hysteresis (hysteresis at the 1 st cycle)
HyS _{mi}	minor loop hysteresis (hysteresis at the 2 nd repeating loop)
HyS _{maj} /W	The normalized hysteresis
Def _{res}	residual deformation or permanent set
E _{maj}	initial modulus of major loop hysteresis
T _g	glass transition temperature
PSA	Pressure sensitive adhesive
RTV	Room temperature vulcanization
HTV	High temperature radical cure
CTNs	carbon nanotubes
GO	graphene oxide
POSS	polyhedral oligomeric silsesquioxane
CBA	cellulose acetate butyrate
PDMS	Poly(dimethylsiloxane)
PDMS-V ₇₇₀	Poly(dimethylsiloxane), vinyl dimethylsiloxy terminated, M _w 770 g.mol ⁻¹
PDMS-V _{6k}	Poly(dimethylsiloxane), vinyl dimethylsiloxy terminated, M _w 6000 g.mol ⁻¹
PDMS-V _{17k}	Poly(dimethylsiloxane), vinyl dimethylsiloxy terminated, M _w 17000 g.mol ⁻¹

PDMS-H ₄₀₀	poly(dimethylsiloxane) hydride terminated, M _w 400 g.mol ⁻¹
D ₄ H	2,4,6,8-Tetramethylcyclotetrasiloxane
Pt	Platinum-divinyltetramethyldisiloxane complex in xylene
H _{D4}	Hydride of 2,4,6,8-Tetramethylcyclotetrasiloxane
V _{6k}	Vinyl of Poly(dimethylsiloxane), vinyl dimethylsiloxy terminated, M _w 6000 g.mol ⁻¹
V _{17k}	Vinyl of Poly(dimethylsiloxane), vinyl dimethylsiloxy terminated, M _w 17000 g.mol ⁻¹
% V/V	Percentage volume per volume
% V/W	Percentage volume per weight
FTIR	Fourier transform infrared spectroscopy
TA	Thermal annealing process
VOC	volatile organic compounds
RAFT	reversible addition fragmentation chain transfer
PEO	poly(ethylene oxide)
P(BA-co-BDA)	poly[(n-butyl acrylate)-co-(1,4-butanediol diacrylate)]
PAA-b-PBA	poly(acrylic acid)-block-poly(n-butyl acrylate)
PBA	poly(n-butyl acrylate)
PAA	poly(acrylic acid)
ACPA	4,4'-Azobis(4-cyanovaleric acid)
BDA	1, 4-Butanediol diacrylate
DVB	Divinylbenzene
Fe ³⁺	Iron (III) acetylacetonate
HMP	2-hydroxyethyl-2-methylpropiophenone
KPS	Potassium persulfate
NaOH	Sodium hydroxide
NH ₄ OH	Ammonium hydroxide solution
PDAME	Poly(<i>N</i> , <i>N</i> -dimethylamino ethyl acrylate) trithiocarbonate
SDS	Sodium dodecyl sulfate
TMS	(Trimethylsilyl)diazomethane solution
TTCA	2-(Dodecylthiocarbonylthio)-2-methyl propionic acid

PISA	polymerization induced self-assembly
TMS	(trimethylsilyl) diazomethane
THF	Tetrahydrofuran
TEM	Transmission electronic microscopy
P(BA-co-BDA)	poly[(n-butyl acrylate)-co-(1,4-butanediol diacrylate)]
TA	Thermal annealing process

Symbols

E	Young's modulus
E_e	Young's modulus from entanglements
E_c	Young's modulus from crosslinks
F	Force
G	Shear modulus
G'	Shear storage modulus
G''	Shear loss modulus
M_n	Number average molar mass
M_w	Weight average molar mass
$M_n(\text{th})$	Theoretical number average molar mass
$M_n(\text{exp})$	Experimental number average molar mass
M_c	average molecular weight between crosslinks
M_e	average molecular weight between entanglements
Q	Swelling ratio
R	Ideal gas constant
t	Time
T	Temperature
V	Volume
ε	Strain
ε_c	Strain at break
σ	Stress
σ_t	True stress
σ_{mooney}	Mooney stress
λ	Deformation ratio
λ_c	Deformation ratio at break
T_c	Critical transition temperature
W	Strain energy density
N_c	Number of monomer units between cross-links
r	end-to-end distance
r_0^2	mean square end to end distance for unstressed chain
A	inversed mean square end to end distance for unstressed chain
k	Boltzmann's constant
T	temperature.

L^{-1}	inverse Langevin function
ρ	density of the polymer
N_A	Avogadro's number
W	strain energy density
F_{el}	elastic free energy
$A^*(T)$	a constant depend on the temperature
ξ	cycle rank
Γ	energy release rate of fracture
c	initial length of the crack
C	strain-dependent empirical correction
ϕ	weight fraction
r_e	effective stoichiometric ratios
τ	shear stress
η	steady shear viscosity
τ'	elastic stress
τ''	viscous stress
N_c	number of chemical crosslinks
N_e	number of entanglements
$W_{sol} \%$	Sol fraction
Q	swelling ratio
$P_n \cdot$	polymeric radical
$\overline{M}_n(th)$	number-average molar mass
M_M	molar mass of the monomer
$[RAFT]$	Concentration of the RAFT agent
M_{RAFT}	molar mass of the RAFT agent
$\% \text{ Conv.}$	conversion percentage
$\% \text{ coag}$	weight percentage of latex coagulation
D_z	average diameter of the latex particles
PDI	Polydispersity index obtained from DLS
M_w/M_n	Polydispersity index obtained from SEC

Table of content

General introduction.....	1
Chapter 1: Introduction to polymer physics and interpenetrating polymer network.....	5
Introduction.....	7
1. Basic concepts of rubber elastic.....	8
1.1 Elasticity of a single molecule.....	8
1.2 Elasticity of a three-dimensional polymer network.....	10
2. Continuum theories of rubber elasticity.....	12
2.1 Affine network model.....	12
2.2 Phantom network theory.....	13
2.3 Slip-tube model.....	14
2.4 Mooney-Rivlin model.....	15
3. Mechanical behavior of polymers.....	17
3.1 Stress-Strain behavior of polymers.....	17
3.2 Fracture mechanics in polymers.....	18
3.3 Energy dissipation.....	19
3.3.1 The Mullins effect.....	20
3.3.2 Permanent set.....	22
3.3.3 Hysteresis.....	23
3.3.4 Anisotropy.....	24
4. Interpenetrating Polymer Networks (IPNs).....	25
4.1 Sequential IPNs.....	25
4.2 Simultaneous Interpenetrating Network (SIN).....	25
4.3 Latex IPNs.....	26
4.4 Gradient IPNs.....	27
4.5 Thermoplastic IPNs.....	27
4.6 Semi-IPNs.....	28
5. Conclusions and objectives of the manuscript.....	29
References.....	30
Chapter 2: Synthesis of silicone multiple networks.....	35
Introduction.....	37
1. Silicones	38

1.1	General features of silicones.....	38
1.2	Crosslinking of Silicones.....	39
1.1.1	Room Temperature Vulcanization (RTV).....	40
1.1.2	Heat-activated radical cure or High Temperature Vulcanization (HTV).....	40
1.1.3	Transition metal catalyzed hydrosilylation or addition cure.....	43
1.3	State of the art in silicone elastomer.....	43
2.	Method and synthesis.....	45
2.1	Chemicals and reagents.....	45
2.2	Synthesis and reaction conditions.....	46
2.2.1	Synthesis of the silicone highly crosslinked network.....	46
2.2.2	Silicone loosely crosslinked network.....	48
2.2.3	Extraction of the uncrosslinked fraction.....	49
2.2.4	Drying process.....	50
2.3	Stoichiometry study of silicone highly crosslinked network (1 st network).....	50
2.4	Stoichiometry study of silicone prepolymer (2 nd network without crosslink).....	52
2.4.1	Curing time of the silicone prepolymer.....	52
2.5	Stoichiometry study of silicone loosely crosslinked network (2 nd network with crosslink).....	55
2.6	Silicone multiple networks.....	56
2.6.1	Swelling process.....	56
2.6.2	Synthesis and reaction conditions of the multiple networks.....	58
	Conclusion.....	62
	References.....	63

Chapter 3: Mechanical properties and characterization of silicone multiple networks....	69
Introduction.....	71
1. Materials and methods.....	72
1.1 Rheology experiments	72
1.1.1 Steady shear testing.....	72
1.1.2 Dynamic mechanical testing.....	73
1.2 Mechanical testing experiments.....	74
1.2.1 Tensile test.....	75
1.2.2 Step-cycle extension.....	76
1.2.3 Fracture in a single edge notch test.....	77
2. Effect of Stoichiometry on the mechanical properties of simple silicone networks.....	79
2.1 Silicone highly crosslinked networks (1 st network).....	79

2.1.1	Stoichiometry of silicone small mesh size networks, using PDMS-V _{6k}	79
2.1.2	Stoichiometry of silicone large mesh size networks, using PDMS-V _{17k}	82
2.1.3	Selection of the 1 st networks: summary.....	85
2.2	Silicone loosely crosslinked networks (2 nd network).....	85
2.2.1	Optimization of the stoichiometry of silicone prepolymer without any crosslinker	86
2.2.2	Dynamic rheology of silicone prepolymer without crosslinker.....	87
2.3	Loosely crosslinked networks of silicone.....	90
3.	Silicone multiple networks.....	92
3.1	Silicone multiple networks based on PDMS-V _{6k} made in solvent.....	92
3.2	Silicone multiple networks based on PDMS-V _{17k} synthesized in the bulk.....	95
3.3	Silicone multiple networks based on PDMS-V _{17k} made in solvent.....	98
4.	Energy dissipation characteristic of silicone multiple networks.....	102
5.	Fracture mechanic of silicone multiple networks.....	103
	Conclusion.....	105
	References.....	106
 Chapter 4: Synthesis of latex double network films.....		107
	Introduction.....	110
1.	Latex.....	111
1.1	General feature and application of latex.....	111
1.2	Emulsion polymerization.....	112
1.3	RAFT polymerization.....	114
1.4	Block copolymers through RAFT-mediated polymerization.....	117
1.5	Surfactant free core-shell latex mediated by RAFT polymerization.....	118
1.6	Latex film formation process.....	119
1.7	State of the art and aims of this study.....	123
2.	Method and synthesis.....	125
2.1	Chemicals and reagents.....	125
2.2	Latex characterization methods.....	127
2.2.1	Gravimetric analysis.....	127
2.2.2	Nuclear Magnetic Resonance (NMR).....	128
2.2.3	Size Exclusion Chromatography (SEC).....	128
2.2.4	Dynamic Light Scattering (DLS).....	130
2.2.5	pH-meter.....	130
2.2.6	Transmission Electronic Microscopy (TEM).....	130
2.3	P(BA-co-BDA) crosslinked latex synthesized by radical emulsion polymerization.....	130

2.4	PAA-b-PBA core-shell latex synthesized by RAFT emulsion polymerization.....	132
2.4.1	PAA-TCC macro-RAFT agent.....	133
2.4.2	PAA-b-PBA latex.....	135
2.4.3	PAA-b-PBA latex with crosslinked PBA-core.....	143
2.4.4	PAA-b-PBA latex with Na ⁺ counter ion.....	146
3.	Latex film formation.....	148
3.1	Drying process and conditions.....	148
3.2	PAA-b-PBA film with added PADAME.....	151
3.3	P(BA-co-BDA) and PAA-b-PBA films with added PAA homopolymer.....	153
3.4	Thermally annealed latex film.....	155
4.	Latex double network films.....	157
4.1	Swelling study of latex film.....	158
4.2	PBA elastomer, serving as an interpenetrating network to DN.....	159
4.3	Latex double network synthesis and conditions.....	160
4.4	HMP consumption effect.....	163
	Conclusion.....	166
	References.....	167

Chapter 5: Structure and Mechanical properties of latex films and DN made from latex films

	Introduction.....	174
	Part I: Mechanical properties of latex films.....	179
1.	Mechanical properties of the PBA, serving as an interpenetrating network for DN films.....	180
2	The differences between P(BA-co-BDA) latex films and PAA-b-PBA core-shell latex films..	182
2.1	P(BA-co-BDA) crosslinked latex films (0.5 mol% BDA).....	182
2.2	PBA-b-PAA core-shell latex films.....	183
2.3	Differences between crosslinked latex, P(BA-co-BDA), and core-shell latex, PAA-b-PBA.....	185
3	Mechanical results of PAA-b-PBA core-shell latex films with modified compositions.....	191
3.1	PAA-b-PBA latex film with a crosslinked PAA-Shell.....	191
3.1.1	Crosslinked PAA-shells by added PADAME.....	191
3.1.1-1	SN films of PAA-b-PBA with added PADAME.....	191
3.1.1-2	DN films based on PAA-b-PBA with added PADAME.....	192
3.1.2	Ionic interactions through PAA deprotonation with NaOH instead of NH ₄ OH....	196
3.1.2-1	SN films of PAA-b-PBA with Na ⁺ counter ions.....	197
3.1.2-2	DN films based on PAA-b-PBA with Na ⁺ counter ions.....	197

3.2	PAA-b-PBA latex film with a crosslinked PBA-core.....	201
3.2.1	Crosslinked PBA-core by BDA.....	201
3.2.1-1	SN films of PAA-b-PBA crosslinked by BDA.....	201
3.2.1-2	DN films based on PAA-b-PBA crosslinked by BDA.....	202
3.2.2	Crosslinked PBA-core by DVB.....	206
3.3	The effect of the M_n on the PAA (shell thickness).....	207
3.3.1	SN films of PAA-b-PBA with different M_n of the PAA.....	208
3.3.2	DN films based on PAA-b-PBA with different M_n of the PAA.....	208
3.4	The effect of the PBA-core size on the PAA-b-PBA latex film	212
3.4.1	SN films of PAA-b-PBA with different M_n of the PBA	212
3.4.2	DN films based on PAA-b-PBA with different M_n of the PBA.....	213
3.5	PAA-b-PBA films with added PAA _{5k}	217
3.5.1	Standard latex (PAA 2.5k, PBA 100k) with added PAA _{5k}	217
3.5.1-1	SN films of PAA-b-PBA with added PAA _{5k}	217
3.5.1-2	DN films based on PAA-b-PBA with added PAA _{5k}	218
3.5.2	High M_n PBA latex, (PAA2.5k, PBA200k) with added PAA _{5k}	221
3.5.2-1	SN films of (PAA2.5k, PBA200k) with added PAA _{5k}	222
3.5.2-2	DN films based on (PAA2.5k, PBA200k) with added PAA _{5k}	222
	Part II: Summary and discussion of the mechanical properties of the different SN and DN films..	227
1.	Method of data analysis.....	228
2.	Swelling equilibrium of modified latex films.....	231
3.	Toughness of DN films.....	232
4.	Dissipation energy in DN films.....	235
5	Fracture toughness of DN films.....	237
	Conclusion.....	238
	References.....	240
	Chapter 6: General conclusion and outlook.....	243
	References.....	247
	Annexes.....	249
	Annex: A.....	251
	Annex: B.....	253

- General Introduction -

Elastomers are materials composed of long flexible chain-like molecule. Through a crosslinking or a curing process, uncrosslinked polymers which can easily change their shape and flow under the stress, transform into a permanent shape and display a large reversible deformability up to strains of several hundred percent. Elastomers have been developed and applied in many applications used in industry and in our daily life. In order to broaden their usage, many recent publications in this decade seek to reinforce the mechanical properties of elastomeric materials.

Reinforcing elastomer with reinforcing nanofillers is one of the major approaches to bring the performance to elastomer. Reinforcing fillers such as carbon black, precipitated silica and nanoclay have been well known to give high mechanical reinforcement to many kinds of elastomers such as polybutadiene rubber, styrene-butadiene rubber, polyisoprene rubber, silicone rubber etc. However, using of filler may also have some limitations in some case, especially at high temperature where the fracture toughness of filled elastomers always decreases. In addition, in high tech or in advanced materials, fillers have been found the insufficient of biocompatibility; some fillers are toxic, and straining color. To fulfill those specifications, loosely entangled polymers have been developed but they exhibit very weak mechanical properties. Thus, in order to overcome these obstacles many strategies have been pioneered and most of them using a network design strategy.

Interpenetrating polymer networks or IPNs is one possible network design strategy to toughen networks but generally has been applied to hydrogels. IPNs have been also developed in elastomeric materials, however, if the two networks are synthesized simultaneously phase separation may occur due to the incompatibility of the two or more elastomers. Recently, novel IPNs have been developed successfully to reinforce acrylate elastomers by using two networks with different mechanical characteristics: a soft and extensible network, and a rigid and highly crosslinked network. These multiple networks based on acrylates exhibits an extremely large increase in toughness and fracture resistance. The reinforcement mechanism was attributed to the presence of sacrificial bonds or overstressed bond in the rigid network which was designed to break in a distributed way in the entire material before macroscopic failure occurs.

Inspired from the success of the acrylate IPNs using sacrificial bonds, our objective is to broaden this effective reinforcement strategy to different materials, i.e. silicone elastomers and acrylate latex films. Silicone is an elastomer, which has been widely applied in medical devices due to its biocompatibility, water and chemicals resistant properties. In general, silicone elastomers are reinforced mechanically by filling them with precipitated silica. Developing novel silicone networks based on IPNs we hope to obtain silicone elastomers mechanically reinforced without using any particulate fillers, resulting in high performance silicones, better biocompatible silicones and more transparent materials. In our study we focus on network design and selected stoichiometric ratio of the composition in order to achieve as high a mechanical performance as possible.

In addition, it is the first time to our knowledge that acrylate elastomers are reinforced by using a latex film. In our study, we synthesize poly(acrylic acid)-block-poly(n-butyl acrylate) or PAA-b-

PBA highly asymmetric amphiphilic diblock copolymers, inspired by recent work designing PAA-b-PBA block copolymers by using the RAFT emulsion polymerization induced self-assembly (PISA) technique. In our work, the PAA-b-PBA latex has been modified by different methods: for example by introducing ionic polymers or ionic counter ions to create PAA-shells with physical crosslinks, by introducing chemical crosslinks to the PBA-core and by increasing the M_n of PAA or PBA etc. Modified latexes and a standard latex have first been prepared before creating double network films by swelling the film with BA monomer and subsequently polymerizing it by UV. In this study, a PBA lightly crosslinked network is interpenetrating through the PBA-core of the precursor film due to its similar hydrophobicity, resulting in a homogenous distribution of PAA shells through the entire material.

This manuscript is divided into six chapters:

Chapter one is devoted to important background information. The basic concept of elastomeric material, the continuum theories of rubber elasticity used throughout this manuscript and the mechanical testing and properties of the elastomer are explained.

The second chapter is dedicated to the silicone elastomers. We first provide background information on the special characteristics of silicone, applications, synthesis method and literature review. Then, the specific synthesis of simple silicone networks and multiple networks that we used in this study are described in detail.

Chapter 3 is then dedicated to the characterization of the physical and mechanical properties of simple silicone networks and multiple networks and the results are discussed.

In Chapter 4, we introduce first the latex synthesis techniques and film formation process. Then the details of the latex synthesis, either standard latex or modified latexes, are presented and discussed. Finally, the preparation method to prepare dry films from the latex and the swelling by butyl acrylate monomer and subsequent polymerization are addressed.

Chapter 5 presents and discusses the mechanical properties of the dry films obtained either from the drying of latex directly or from polymerization of butyl acrylate swollen films. The differences in the mechanical properties between the films are then discussed as a function of the changes made to the latex structure.

Finally, an overall conclusion of all studies is made in chapter 6 along with outlooks.

-CHAPTER 1-

Introduction to polymer physics and interpenetrating polymer networks

Chapter 1: Introduction to polymer physics and interpenetrating polymer networks.....	5
Introduction.....	7
1. Basic concepts of rubber elasticity.....	8
1.1 Elasticity of a single molecule.....	8
1.2 Elasticity of a three-dimensional polymer network.....	10
2. Continuum theories of rubber elasticity.....	11
2.1 Affine network model.....	11
2.2 Phantom network theory.....	13
2.3 Slip-tube model.....	14
2.4 Mooney-Rivlin model.....	15
3. Mechanical behavior of polymers.....	16
3.1 Stress-Strain behavior of polymers.....	16
3.2 Fracture mechanics in polymers.....	17
3.3 Energy dissipation.....	18
3.3.1 Mullins effect.....	19
3.3.2 Permanent set.....	21
3.3.3 Hysteresis.....	22
3.3.4 Anisotropy.....	23
4. Interpenetrating Polymer Networks (IPNs).....	23
4.1 Sequential IPNs.....	23
4.2 Simultaneous Interpenetrating Network (SIN).....	24
4.3 Latex IPNs.....	25
4.4 Gradient IPNs.....	25
4.5 Thermoplastic IPNs.....	26
4.6 Semi-IPNs.....	26
5. Conclusion and objective of the manuscript.....	27
References.....	29

Introduction

Elastomers are extensible polymers with generally some viscoelastic nature. During World War II synthetic elastomers were developed due to the limited supply of natural rubber in Asia. From ancient times to the present, elastomers have been constantly developed and applied in many products used in our daily life. In order to broaden their usage, there is a large body of literature in the last few decades, where one of the major objectives is to mechanically reinforce elastomers without using particulate fillers. Interpenetrating polymer networks (IPNs) is a possible method to reinforce elastomers while avoiding filler usage. An IPNs is composed of two or more polymer networks which are at least partially interlaced on a molecular scale but not covalently bonded to each other and cannot be separated unless chemical bonds are broken.¹

In this introductory chapter, the basic concepts of elastic soft materials, either at the single chain level or the 3D polymer network level, are first reviewed. Then the continuum theories of rubber elasticity used in this manuscript are explained. The second part of the chapter focuses on the mechanical behavior of elastomers: stress-strain curve, hysteresis behavior and fracture mechanics, which will be needed to characterize the material properties in our study. The methods of synthesizing IPNs, which is the technique used to reinforce elastomers in our study, will be described. Finally, the objectives of the thesis and the general approach which has been followed will be exposed.

1. Basic concepts of rubber elasticity

1.1 Elasticity of a single molecule²

Elastomeric materials are composed of long flexible chain-like molecules. Before crosslinking, conventional rubbers are composed of high molecular weight chains, and can change shape and flow under stress if the polymer is above its glass transition temperature (T_g). Focusing on an isolated chain, generally the chain moves randomly by Brownian motion during chain transformation in a stress-free state as illustrated in Figure 1-1(a). The elastomeric chain can also adopt an oriented conformation under an applied force, resulting in a stretched chain under the tensile force as presented in Figure 1-1(b). When the chain is relaxed, the average end-to-end distance is r_0 , which increases to r when the sample is stretched.

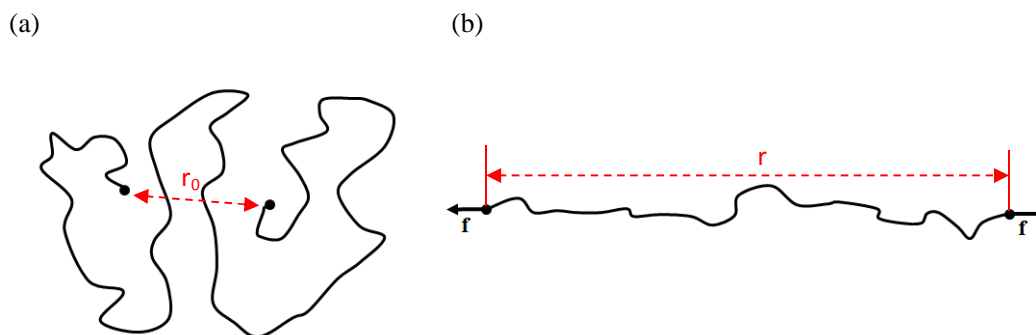


Figure 1- 1: Polymer chain, (a) Random chain, and (b) oriented chain^{2,3}

The isolated chain can form a wide variety of conformations, governed by three factors³

- i) The statistics of random processes
- ii) A preference for certain sequences of bond arrangements
- iii) The exclusion of some hypothetical conformations that would require parts of the chain to occupy the same volume in space

The occupied-volume exclusion for an isolated chain has been explained by Flory in 1969.⁴ It was argued that in the bulk state, the excluded volume interaction is balanced by the neighboring chains. The excluded volume interaction thus can be ignored in the melt state. The end-to-end distance (r) in the melt state is governed by Gaussian statistics for sufficiently long chains, starting from the tension-displacement relation as showed in Eq 1.1

$$f = Ar \quad (\text{Eq. 1 - 1})$$

Where f is a tensile force, and r is the average distance between the ends of the chain, shown in Figure 1-1 (b) and A is the inversed mean square end-to-end distance (r_0^2) for the unstressed chain, derived from the general equation of the Helmholtz free energy as presented in Eq. 1-2 where k is the Boltzmann's constant and T is the absolute temperature.

$$A = \frac{3kT}{r_0^2} \quad (\text{Eq. 1 - 2})$$

In the case where the elastomeric molecule is replaced by a hypothetical chain consisting of a large number (n) of rigid segments, the freely jointed chain model can be applied with the assumption that each rigid segment is of length l , (Figure 1-2), then:

$$r_0^2 = nl^2 \quad (\text{Eq. 1 - 3})$$

In this case r_0^2 is independent of temperature, because a fully random link arrangement is assumed. The tension f in Eq. 1-1 arises individually from an entropic mechanism; that is, from the tendency of the chain to adopt conformations of maximum randomness, and not from any energetic preference for one conformation over another. The tension f is then directly proportional to the absolute temperature T .

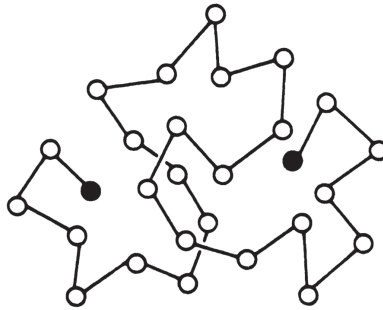


Figure 1- 2: Freely jointed chain model²

For real chains, a polymer consists of a large number n of primary valence bonds along the chain backbone, and r_0^2 can be determined as shown in Eq.1-4

$$r_0^2 = C_\infty nl^2 \quad (\text{Eq. 1 - 4})$$

Where the coefficient C_∞ is the degree to which this real molecule departs from the freely jointed model (Eq.1-3). C_∞ is found to vary from 4 to 10, depending on the chemical structure of the molecule and on temperature. Thus, $C_\infty^{1/2}l$ may be regarded as the effective bond length of the real chain, a measure of the stiffness of the molecule.

Cotton et al.⁵ claimed that the tension-displacement relation as presented in Eq 1-1 is reasonably accurate only for relative short distances r , less than about 1/3 of the fully stretched chain length. Unfortunately, there is no model describing tension in real chains at larger end separations. Therefore, the freely jointed chain model is applied to determine tension as in Eq.1-5

$$f = (kT/l)L^{-1}(r/nl) \quad (\text{Eq. 1 - 5})$$

Where L^{-1} denotes the inverse Langevin function. An expansion of this relation in terms of r/nl is given by:²

$$f = (3kTr/nl^2) \left[1 + \left(\frac{3}{5} \right) \left(\frac{r}{nl} \right)^2 + \left(\frac{99}{175} \right) \left(\frac{r}{nl} \right)^4 + \left(\frac{513}{875} \right) \left(\frac{r}{nl} \right)^6 + \dots \right] \quad (\text{Eq. 1 - 6})$$

The relation between tension and end-to-end distance described in Eq 1-5 is clearly different from the Gaussian relation, shown in Eq. 1-1. Therefore, in the theory of rubber elasticity, the tension-displacement relation of a single chain can be explained by Eq. 1-1 for the polymer at small deformation and by Eq. 1-5 in large deformation.

1.2 Elasticity of a three-dimensional polymer network

Generally, an elastomer starts as a liquid-like material, called polymer melt, which can flow at temperatures above its T_g . In order to prevent this behavior and keep the permanent structure, a small number of intermolecular chemical bonds or crosslinks are introduced into the polymer melt to form a crosslinked elastomer which behaves as a three-dimensional molecular network structure, as shown in Figure 1-3.

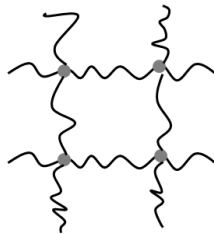


Figure 1- 3: Idealized structure of a crosslinked polymer network

However, without the crosslinker, a high molecular weight polymer has a temporary network structure. The liquid-flow like properties of uncrosslinked elastomers are inhibited due to the presence of entanglements, a sort of molecular intertwining with a spacing (in the melt state) characteristic of a particular molecular structure. The average molecular weight between entanglements (M_e) of some polymers, determined by flow viscosity measurements is presented in Table 1-1.

Polymer	M_e (g.mol ⁻¹)
Polyethylene	1150
Cis-1,4-Polybutadiene	2000
Cis-1,4-Polyisoprene	6800
Poly (dimethylsiloxane)	12000
Polystyrene	18100

Table 1- 1: The average molecular weight between entanglements (M_e) for polymeric melts, obtained from flow viscosity measurements ⁶

The entanglements in elastomers show a behavior similar to the crosslinking points, thus if we consider the entanglements as temporary crosslinks, the effective number N of network chains per unit volume should become the sum of the effective number of chains between chemical crosslinks (N_c) and between entanglements (N_e), as shown in Eq.1-7 and Eq.1-8

$$N_e = \rho N_A / M_e \quad (\text{Eq. 1 - 7})$$

$$N_c = \rho N_A / M_c \quad (\text{Eq. 1 - 8})$$

where ρ is the density of the polymer, N_A is Avogadro's number, and M_c and M_e are the average molecular weight between entanglements and between crosslinks, respectively. The elasticity of three-dimensional polymer can be calculated by many of theories, which are described in following section.

2. Continuum theories of rubber elasticity

To interpret the physical behavior of the conformation of the single chain and the behavior of the strands in the network, there are many constitutive models based on different assumptions. The related models applied in our study are now explained in more detail in this section.

2.1 Affine network model

The affine network model is based on the simple main idea of the macroscopic deformation of a polymer network. The assumption of the affine network model is that the deformation of polymer chains at the macroscopic scale is directly proportional to that of individual chains and the end of each individual chain is permanently attached to the elastic nonfluctuating background.⁷ The elastic background in this model is assumed to deform affinely and the distance between chain ends (X_1 and X_2) changes with the same deformation gradient as the macroscopic deformation. The schematic diagram of this hypothesis is presented in Figure 1-4.

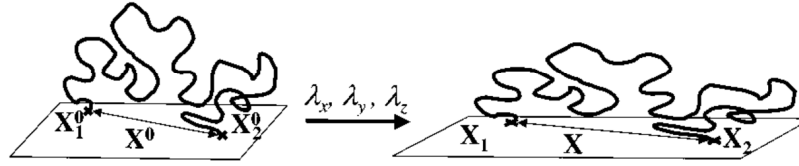


Figure 1- 4 : Schematic diagram of the affine network model.⁷

The elastic free energy (F_{el}) of the single chain is related to the distribution function of end-to-end vectors for the Gaussian distribution as shown in Eq.1-9.

$$F_{el} = A^*(T) + \frac{3}{2} kT \frac{\langle r^2 \rangle}{\langle r^2 \rangle_0} \quad \text{Eq. 1 - 9}$$

Where $A^*(T)$ is a temperature- dependent constant, $\langle r^2 \rangle_0$ is the average of the mean-square end –to–end vector in the undeformed state as explained in section 1.1, and r is the average distance between the ends of the chain

The elastic free energy of the network relative to the undeformed state, based on affine network model ($\Delta F_{el,Affine}$), is calculated by the sum of the free energy of individual chains (Eq. 1-1) and the result is presented in Eq. 1-10

$$\Delta F_{el,Affine} = \frac{3kT}{2\langle r^2 \rangle_0} \sum_v (r^2 - \langle r^2 \rangle_0) = \frac{3}{2} v kT \left(\frac{\langle r^2 \rangle}{\langle r^2 \rangle_0} - 1 \right) \quad \text{Eq. 1 - 10}$$

Where ν is the number of chains per unit volume in the network and $\langle r^2 \rangle$ is the end-to-end vector in the deformed state averaged over the ensemble of the chains which is

$$\langle r^2 \rangle = \langle x^2 \rangle + \langle y^2 \rangle + \langle z^2 \rangle \quad Eq. 1 - 11$$

In the affine model all the junction points of the network are assumed to be embedded and each Cartesian component of the chain end-to-end vector transforms linearly with macroscopic deformation.

$$x = \lambda_x x_0, \quad y = \lambda_y y_0, \quad z = \lambda_z z_0 \quad Eq. 1 - 12$$

Therefore,

$$\langle x^2 \rangle = \lambda_x^2 \langle r_0^2 \rangle, \quad \langle y^2 \rangle = \lambda_y^2 \langle r_0^2 \rangle, \quad \langle z^2 \rangle = \lambda_z^2 \langle r_0^2 \rangle \quad Eq. 1 - 13$$

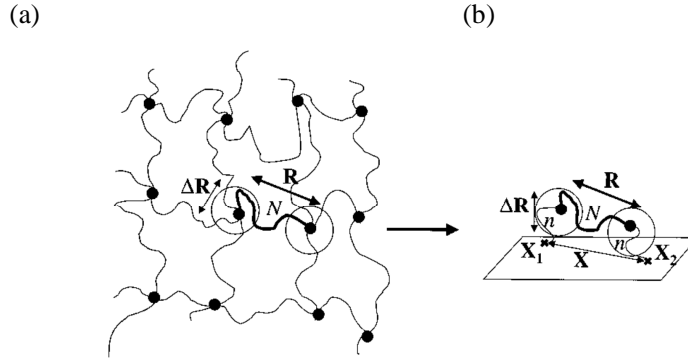
From the assumption provided in Eq.1-13, and substitution in Eq. 1-10,

$$\Delta F_{el,Affine} = \frac{1}{2} \nu k T (\lambda_x^2 + \lambda_y^2 + \lambda_z^2 - 3) \quad Eq. 1 - 14$$

where k is the Boltzmann constant, T is the absolute temperature and $\lambda_x, \lambda_y, \lambda_z$ are the components of the stretch ratio ($\lambda = \varepsilon + 1$).

2.2 Phantom network model

Different from the affine network model, the phantom network model is defined as a network where the chains are connected to each other by fluctuating crosslinks or junctions.⁸ In general, the model of rubber elasticity is based on the hypothesis of Gaussian chains and non-fluctuating crosslinking points. However, there are some arguments indicating that the affine model of rubber network should be refined to accurately represent the deformation of the rubber.⁹ The Phantom network model considers that the crosslinks in the bulk fluctuate around their average position as described in Figure 1-5.⁷ The magnitude of fluctuations determines the macroscopic deformation of the network which refer to the deformation of individual chains.

Figure 1- 5 : Schematic diagram of Phantom network model.⁷

As opposed to the individual chain, the single-chains are connected to the elastic background through the effective chains (see figure 1-5 (b), where n is an effective chain). The position of the effective chains are randomly distributed due to the randomness of the cross-linking process. A network chain with its two effective chains is defined as a combined chain (Figure 2b).⁷ Thus, The phantom network model is equivalent to the affine network model of combined chains. The elastic free energy of the phantom network model is presented in Eq. 1-15.⁷

$$\Delta F_{el,phantom} = \frac{1}{2} \nu kT \left(1 - \frac{2}{\phi} \right) \sum_{\alpha} \lambda_{\alpha}^2 \quad Eq. 1 - 15$$

Where ϕ is a functionality of the network cross-links, and λ_{α} is a coefficient of network deformation along the major axis of deformation ($\alpha = x, y, z$).

In summary, both models, Affine network model and Phantom network model, are based on an unrestricted network. The difference between these two models is only the front factor. Some studies show that the Phantom network model is closer to real elastomers.^{10, 11, 12} Thus the phantom network model has become the basis of further development in the theory of rubber elasticity.⁷

2.3 Slip-tube model⁷

The slip-tube model is a molecular model which was developed to predict the elastic large strain behavior of networks that are both entangled and crosslinked (i.e. low levels of crosslinking). The assumptions of the slip-tube model are based on the combination between the slip-link model and the tube model. In the tube model, which has been developed for entangled melts, the confining potential, acting on a given network strand is assumed to be formed collectively by many neighboring strands. In the slip-link model, the assumption is that each entanglement is formed by a pair of chains. The

entanglements may be trapped by the crosslinking process, and the slip-links allow the chains to slide along.

In the slip-tube model, the basic concept is that the permanent entanglements, created by the chemical crosslinks, act as slip-links connecting neighboring chains. The slip-links are allowed to pass through each other but each of them can slide along up to a limited distance. If this certain fixed distance is small compared to the average distance between neighboring chains, the model can be reduced to the affine model. In contrast, if the fixed distance is long due to a large sliding, the slip-links pass through each other and the topological constraints are locally released. Last, if the fixed distance is equal to the chain length between crosslinks the slip-link model transforms into the phantom network model.¹³ The topological constraints imposed by the neighboring network chains are represented by virtual chains attached to the elastic nonfluctuating background at one end and ending with slip-links at the other as presented in Figure 1-6.

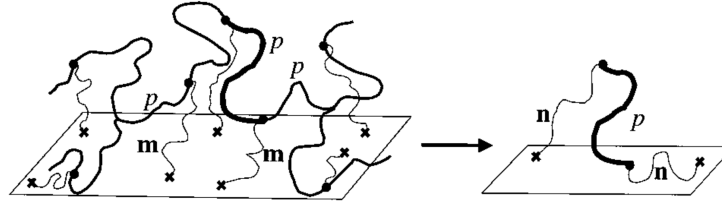


Figure 1- 6: Schematic diagram of slip-tube model.⁷

The elastic free energy of the chains calculated by the slip-tube model ($\Delta F_{el,slip-tube}$) can be defined as shown in Eq.1-16.

$$\Delta F_{el,Slip-tube} = \Delta F_{el,Phantom} + \frac{1}{2} \nu k T L \sum_{\alpha} \left(\frac{\lambda_{\alpha}}{g_{\alpha}^{1/2}} + \frac{g_{\alpha}^{1/2}}{\lambda_{\alpha}} \right) - \nu T S(g_{\alpha}) \quad Eq. 1 - 16$$

Here, L is the number of slip-links per network chains and g_{α} is the redistribution parameter which depends on the number of monomers along the axis α (component x, y and z direction) in the deformed network. The function $S(g_{\alpha})$ is the entropy of the degree of freedom corresponding to different positions of slip-links along the chain.

The elastic free energy of the slip-link model can be calculated and in uniaxial extension the reduced stress (mooney ratio) $f^*(\lambda^{-1})$ is given by Eq. 1-17.

$$f^*(\lambda^{-1}) = G_c + \frac{G_e}{0.74\lambda + 0.61\lambda^{-\frac{1}{2}} - 0.35} \quad Eq. 1 - 17$$

where G_c is the phantom modulus which is equal to the modulus of crosslinked network, G_e is the entanglement modulus and λ is the extension ratio.

2.4 Mooney-Rivlin model

The Mooney-Rivlin model is a phenomenological hyperelastic material model which was proposed by Melvin Mooney in 1940. In uniaxial extension or compression, the Mooney-Rivlin model can be written as Eq. 1-18.^{14, 15,16}

$$\sigma = \left(2C_1 + \frac{2C_2}{\lambda} \right) \left(\lambda - \frac{1}{\lambda^2} \right) \quad \text{Eq. 1 - 18}$$

Where C_1 and C_2 are constant values determined by fitting data.

The Mooney- Rivlin equation, in general, does not explain the physical mechanisms behind the nonlinear elastic behavior. They are merely curve-fits of various polynomials to test data which the coefficients used in mechanical analyses.

3. Mechanical behavior of polymers

3.1 Stress-Strain behavior of polymers

The behavior of polymeric materials can be divided into three main types; brittle plastic, tough plastic, and elastomer. Brittle plastics have elastic moduli of a few GPa and a linear stress-strain curve up to the fracture point with a small deformation, normally 2% to 5 % elongation (Figure 1-7 (a)). Polymers showing this kind of behavior are mostly in the glassy state at room temperature or have a high glass transition temperature (T_g) such as poly(methyl methacrylate); T_g 110°C^{17} , polystyrene; T_g 100°C^{17} , and poly(acrylic acid); T_g 106°C^{18} .

However, some glassy polymers such as polycarbonate exhibit a tough plastic behavior, this type of behavior is generally observed for semi-crystalline polymers, with an amorphous fraction above the T_g such as polyethylene, polyethylene terephthalate, polytetrafluoroethylene, polyamide-11, polyamide-12 and isotactic polypropylene (Figure 1-7 (b)). The initial modulus or Young's modulus of these polymers is typically a bit lower than for the brittle plastics but remains in the GPa range. The stress-strain curve shows a yield point and is followed by extensive elongation and sometimes necking.

For an elastomer behavior, the initial modulus is in the MPa range, the stress-strain curve is highly non-linear and the deformation is mostly reversible up to elongations at break that can be several hundred % (Figure 1-7 (c)) and the T_g of the polymer is below room temperature. This kind of behavior can be found in many elastomers such as natural rubber, silicone rubber, styrene-butadiene rubber, nitrile rubber etc.

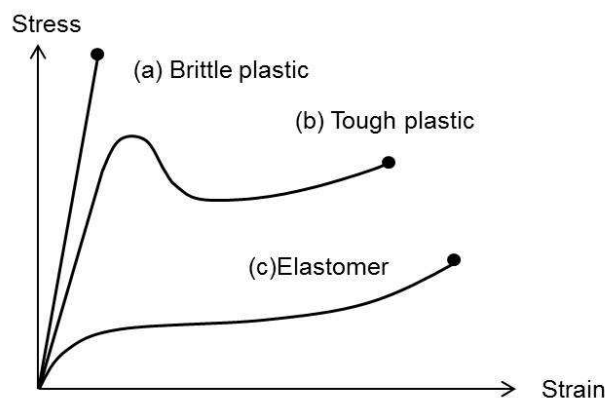


Figure 1- 7 : Stress- strain curve of three types of polymeric material ¹⁹

3.2 Fracture mechanics in polymers

The fracture mechanics approach is based on the quantification of the energy per unit area required to propagate a crack. This approach has been developed for small deformations and linear elastic materials. The fracture toughness can be described as the value of the energy release rate (\mathcal{G}) where the crack starts to propagate. The energy release rate is a quantity that can be calculated from the elastic properties of the material, test geometry, crack length and applied stress far from the crack. It corresponds to the elastic energy available from the sample to propagate the crack and is proportional to the square of the applied load. At the point where the crack starts to propagate, $\mathcal{G} = \Gamma$ where Γ is called the fracture energy. This fracture energy typically depends on the loading rate and at vanishing loading rate or high temperature is called threshold value Γ_0 .

For rubbers, several approaches have been developed to quantify the fracture toughness, or the fracture energy, as a material property. Rivlin and Thomas²⁰ and then Greensmith²¹ proposed a simple method to determine the strain energy release rate \mathcal{G} in the case of single edge notched specimens with the following equation:

$$\mathcal{G} = 2 \times K \times W(\lambda) \times c \quad \text{Eq. 1 – 19}$$

where $W(\lambda)$ is the strain energy density, c is the length of the crack and K is a strain-dependent empirical correction associated with the lateral contraction of the sample in extension. When the notched sample is stretched, λ increases and when it reaches λ_c , stretching at the crack propagates and $\mathcal{G} = \Gamma$.

The strain energy density $W(\lambda_c)$ is obtained by integration of the stress strain curve of the un-notched sample up to λ_c as presented in Figure 1-8.

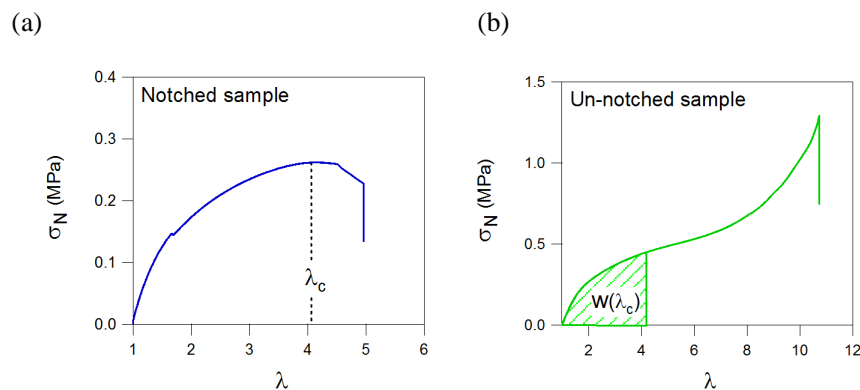


Figure 1- 8: The strain energy density ($W(\lambda_c)$) calculated by the area under the curve of stress-strain relation in a single edge notched test

The strain dependence correction factor K determined experimentally by Greensmith can be approximated by

$$K = \frac{3}{\sqrt{\lambda}} \quad \text{Eq. 1 - 20}$$

Thus, by introducing Eq. 1-20 into Eq.1-19, and applying the propagation condition we obtain the relation of the fracture energy given by Eq.1-21. It should be noted that this equation is used in this study in order to determine the fracture energy of materials.

$$\Gamma = \frac{6cW(\lambda_c)}{\sqrt{\lambda_c}} \quad \text{Eq. 1 - 21}$$

3.3 Energy dissipation

Energy dissipation is one of the most important properties of elastomers. A fine understanding of the dissipation mechanisms is the key to optimize the reinforcement of the mechanical properties. Energy dissipation in large strain which is very relevant for fracture, is normally determined by loading-unloading cyclic extension. The stress-strain curve of such a test can be analyzed after the test and many properties such as the called Mullins effect, the permanent set, hysteresis, and anisotropy, can be determined as summarized in Figure 1-9.

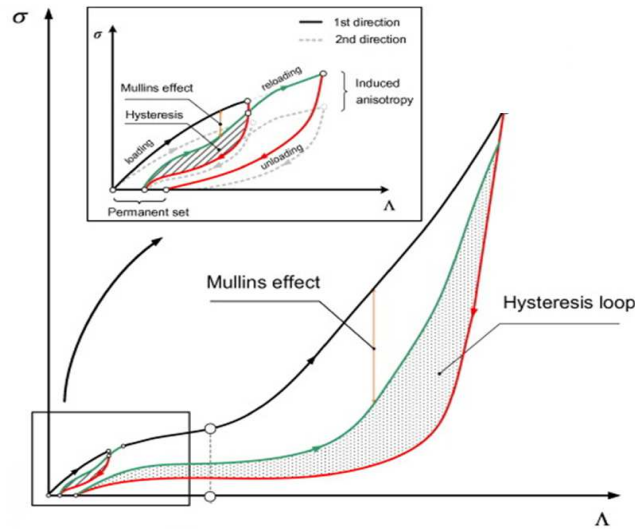


Figure 1- 9: Energy dissipation analysis from the stress-strain curves obtained with the loading-unloading cyclic extension test.²²

3.3.1 The Mullins effect

The strain softening mechanism, the amplitude of which depends on the maximum loading reached in a previous extension, is generally found in filled elastomers²³, crystalline elastomer²⁴, soft-hard block copolymers²⁵, and also in double network gels²⁶ and elastomers^{27, 28}. This behavior, which corresponds to a change in the structure of the material with increasing strain, was first investigated by Mullins and Tobin²⁹ in filled and unfilled natural rubber, and has been known since then as the Mullins effect. The Mullins effect is generally characterized in elastomeric materials in a uniaxial extension test by a cyclic load-unload step extension as shown in Figure 1-10.

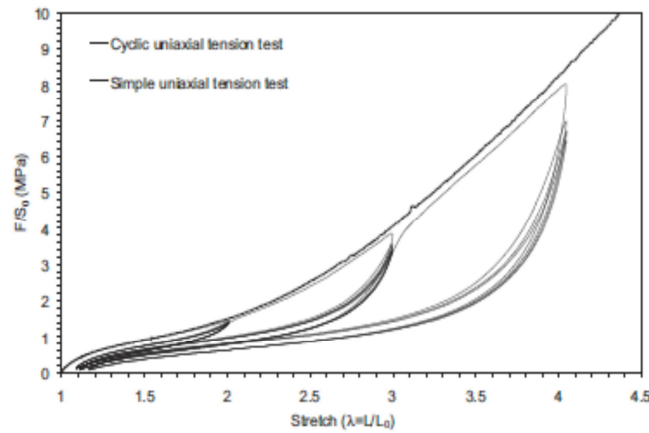


Figure 1- 10: Stress-strain curve of a 50 phr (~20 vol%) carbon-black filled styrene butadiene rubber in simple uniaxial extension with a loading-unloading step extension increasing the maximum stretch every 5 cycles²³

The softening behavior of materials which exhibit the Mullins effect can be summarized as²³

- i) a lower stress can be found at the same applied strain after the first cyclic extension
- ii) after a small number of cycles at the same extension level, the material response is nearly stationary
- iii) the softening increases progressively when increasing the maximum stretch

The Mullins effect is controlled by the structure of the material. In the case of a filled rubber, the spatial distribution of filler particles and the interactions between filler and matrix are the important parameters. The physical mechanisms behind the Mullins effect were summarized by Diani et al.²³, and are presented in Table 1-2.

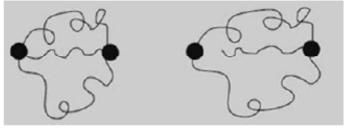
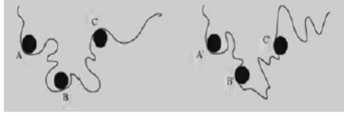
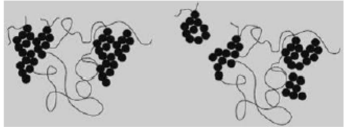
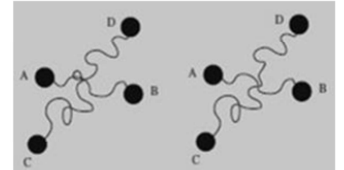
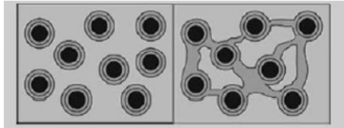
Sketch	Physical Source
	Bond rupture
	Molecules slipping
	Filler rupture
	Disentanglement
	Double-layer model

Table 1- 2: The different possible physical mechanisms behind the Mullins effect
as summarized by Diani et al²³

In the literature, the Mullins effect was interpreted in many different ways, the most common of which is by the permanent rupture of chemical bonds. The idea of this physical mechanism is based on the bond scission of chemical crosslinks and main chain bonds of elastomer which can occur both in filled elastomers^{30, 31, 32} and in tough hydrogels (DN hydrogels and multifunctional hydrogels)^{26, 33, 34}. This breaking of covalent bonds contributes then significantly to the irreversible stress-softening observed upon the initial extension. An alternative interpretation of the Mullins softening found in the literature for filled elastomer^{35, 36, 37} and tough hydrogel^{34, 38} is the disentanglement which can accommodate the induced anisotropy. The removal of entanglements causes a chain slippage, resulting in the stress-softening in material.

In filled elastomers, molecules adsorption and desorption was first explained by Houwink³⁹, who claimed that elastomer molecules can slip over the surface of the fillers and re-attach elsewhere. The newly created bonds exhibit the same physical properties as the original bonds, but they are located at different places. This adsorption/desorption process triggered by deformation causes the change of material entropy, resulting in the stress softening in filled elastomer. In addition, in the case of highly filled systems, the filler can form a physically connected network and the rupture of the

contacts between fillers (affecting electrical conductivity for example) is another possible mechanism causing a Mullins effect in filled elastomers.⁴⁰

Additionally, another model, was developed to explain the physical mechanisms of reinforcement and softening in filled elastomer claimed by Montes et al.^{41, 42} It is based on the idea that the filler is surrounded by a glassy layer which progressively softens as the temperature changes. This model has initially been used to predict the abnormal dependence of the temperature dependence of the small strain modulus and the softening occurring at very small strains also called the Payne effect. However, the same physical mechanism could be active in large strain and be responsible for the Softening in large strain called Mullins effect.

Extensions of the model have also been proposed by Fukahori.^{43, 44, 23} where filled elastomer are represented by spherical particles surrounded by a double layer structure of rubber embedded in a crosslinked rubbery matrix. The inner layer represents the polymer in a glassy state, while the outer layer is made of the constrained polymer. During the extension, the outer layer gets oriented and extends, and finally connects with the other outer neighbor layers to create a super-network. During unloading, the super-network is not able to hold the stress and it can return to the previously extended state and changes to support the stress when the stretch exceeds the extension previously applied. The entropic forces of super-network are responsible for the Mullins effect recovery.

3.3.2 Permanent set

The permanent set or residual stretch (λ_{res}) is the remaining extension of the material after undergoing a cyclic extension test. When elastomers are subjected to a load-unload cycle, a remaining residual extension is usually observed, which is due to a permanent or temporary change in structure.

Permanent set has been reported after the first cycle and generally the subsequent cycles slightly increase its level until the response becomes approximately constant after a few cycles (Figure 1-11).^{45, 46, 47} In most cases, a permanent set is present after unloading elastomers. This was not taken into account in the initial description of the Mullins effect.

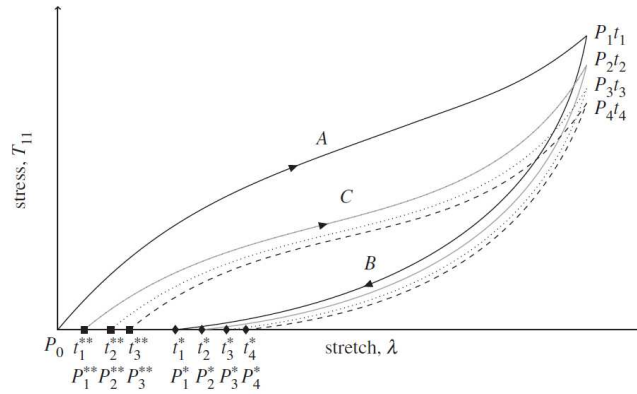


Figure 1- 11: loading-unloading mechanical test with the presence of residual strain in a filled elastomer where P_0 is the starting point, P_x is a point at maximum loading, P_x^{**} is a point at complete unloading (stress = 0), t_x is a time at loading, and t_x^{**} is a time at unloading ⁴⁵

In filled elastomers, permanent set has been reported to have a relation with Mullins softening⁴⁷, loading strain⁴⁷, filler amount⁴⁸, and the nature of the filler.⁴⁹ The effects of filler on permanent set have been reported as follows ⁴⁹

- i) The permanent set is higher when the filler particles are smaller and the filler has a higher specific surface area.
- ii) Stronger interactions between polymer and filler reduce the compression set.
- iii) Fillers with polar surfaces may give a poor permanent set because of preferential adsorption of the crosslinker (sulfur) and creation of a more crosslinked layer around the particles.

3.3.3 Hysteresis

Hysteresis in the stabilized cycle is different in nature from the Mullins hysteresis. It can be found in many elastomers, especially filled elastomers, which have an ability to dissipate a significant fraction of energy upon deformation. Unlike the Mullins hysteresis which is due to a permanent change in structure with increasing strain, the stabilized cycle hysteresis is caused by internal friction, which resists the extension or contraction.⁵⁰ Hysteresis of the material can be calculated as the energy in the area between loading and unloading cyclic loops in the stabilized stress-strain curve as shown in Figure 1-12. As shown in Figure 1-10 two types of hysteresis can be characterized: the first or major cycle hysteresis (Mullins hysteresis) and the stabilized or minor cycle (which can be in principle any of the subsequent cycles but which is normally the second cycle).

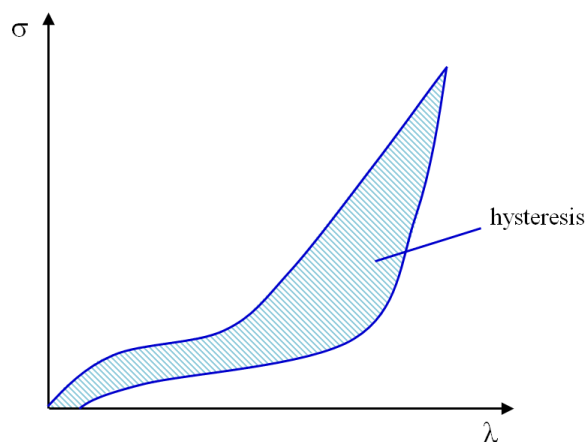


Figure 1- 12: The calculation of hysteresis energy.

The physical explanations of the hysteresis and Mullins effect have been widely reported in the literature. Papkov et al.⁵¹ claimed that, the softening can be associated with a relatively slow motion of chains. After the first deformation, a chain rearrangement due to slippage of the chains at the surface of the filler is the main reason for the permanent softening. In subsequent load-unload cycles, the hysteresis will remain the same, as long as the strain does not exceed the maximum value reached in previous cycles. However, mechanisms of hysteresis are crucially dependent on the detailed structure and are only observed in heterogeneous materials that either undergo a change in structure when deformed or have an internal friction dissipative mechanism. The reader is referred to the excellent review of Diani et al.²³ on the subject.

3.3.4 Anisotropy

It should be noted also that the elastomer softening which is usually observed under uniaxial loading and is known as Mullins effect is a directional softening, i.e. during the deformation of the elastomer, polymer chains can go through re-alignment or re-orientation which then induce an anisotropic material behavior in the subsequent cycles. This has been in particular studied in detail by Vacherand and Diani for a model filled elastomer^{23, 52, 53}.

4. Interpenetrating Polymer Networks (IPNs)

Interpenetrating polymer networks or IPNs are a combination of two or more polymers in the network form. In an IPNs, at least one of the networks is polymerized or crosslinked in the immediate presence of the other(s).^{54, 55, 56} IPNs are in essence a specific type of polymer blend. The first pioneering work was reported in 1914 by Jonas Anylswoth^{54, 57} who reinforced phenol-formaldehyde resin with crosslinked rubber. However the term of IPNs came about much later in 1960, introduced by Millar who developed PS/PS IPNs to be used as ion exchange resin.⁵⁷ IPNs have been then extensively studied in the literature. Nowadays, IPNs are classified into 6 mains types.

4.1 Sequential IPNs

In sequential IPNs, polymer network I is synthesized first to create the base network. Then the polymer network I is immersed into the monomer bath containing monomer II, crosslinker II, and activator. The swollen polymer I is finally polymerized in situ to create IPNs^{54, 55}. The procedure of this process is explained in Figure 1-13.

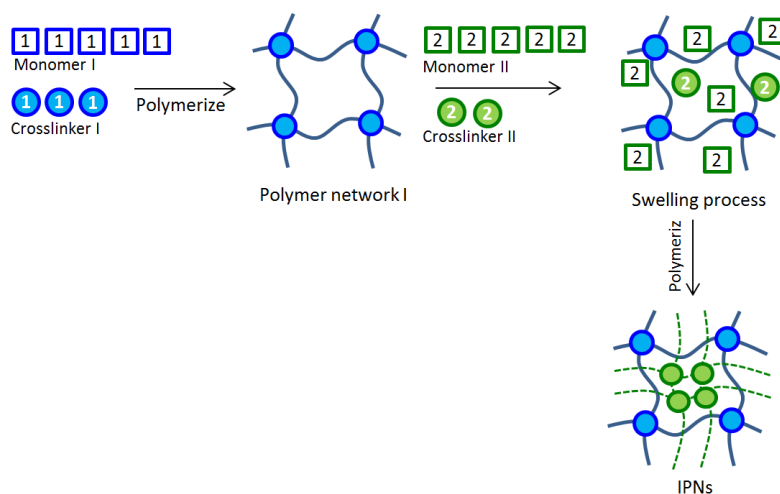


Figure 1- 13: Sequential IPNs process to prepare interpenetrating polymer networks.⁵⁴

4.2 Simultaneous Interpenetrating Network (SIN)

The simultaneous interpenetrating network method or SIN is a synthesis method where IPNs are made by mixing monomers or linear polymers, crosslinkers, initiator, etc., of both polymers to form a homogeneous fluid. The two polymer components are then simultaneously polymerized by independent, noninterfering reactions as the procedure presented in Figure 1-14.

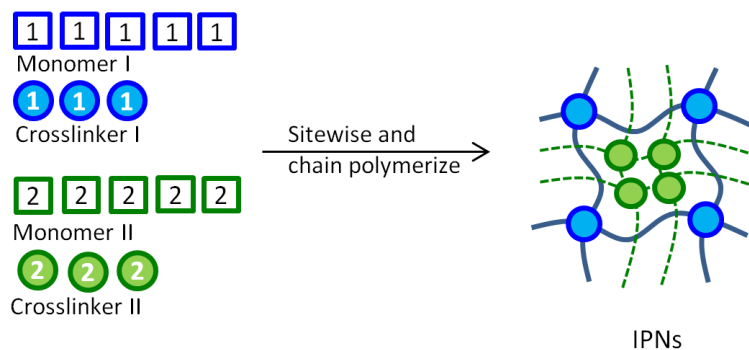


Figure 1- 14: SIN process for preparing interpenetrating polymer networks.⁵⁴

SIN create IPNs by controlling the rates of polymerization kinetics of the two polymer systems which can generally proceed in three ways⁵⁵: (i) the simultaneous gelation of both polymers, (ii) a sequential polymerization of the pre-polymer mixture, and (iii) the introduction of a larger or smaller number of graft sites between the two polymers.

A major advantage of SINs over sequential IPNs is the ease of the process. For example, the mixture can be prepolymerized until just short of the gel point, followed by pumping into a mold or die, with continued polymerization. The main disadvantage of the method is however that the structure is much less well controlled and some level of macroscopic phase separation often occurs.

4.3 Latex IPNs

The IPNs created from latexes are referred to as micro-IPNs due to the fact that IPNs of both latexes appear on a single latex particle within the micro-scale. To prepare latex IPNs, a crosslinked polymer I in latex form is prepared as the seed latex, followed by the addition of polymer II, crosslinker and activator. Upon polymerization, polymer II creates the IPNs inside the latex particles of polymer I, formed as a latex IPN or core-shell latex IPNs, presented in Figure 1-15.^{55, 58, 59} Latex IPNs contain two kinds of polymer and crosslinks in one latex particle.

Another way to create latex IPNs is by Interpenetrating Elastomeric Networks (IEN). In this method, two different latexes are mixed together, along with crosslinking agents and initiator or catalyst. Usually a poly(urethane-urea) latex was mixed with one of the polymer latexes.⁵⁵ Then the dried film is created at high temperature in order to generate the crosslinking of each polymer. The final product of IEN is a crosslinked latex with polymers blending.

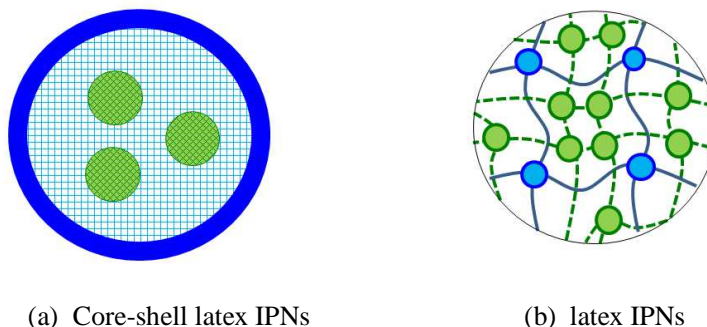


Figure 1- 15: latex-IPNs from the two different preparation process, (a) core-shell latex IPNs prepared by IEN, and (b) latex-IPNs prepared by seed emulsion polymerization

4.4 Gradient IPNs

Gradient IPNs are another method to create IPNs. A distinct specificity of gradient IPN is that heterogeneous IPNs materials are created. An extreme example of gradient IPNs is a material consisting of a layered or laminated material, where the gradient in composition is a discontinuous step change.⁵⁵ The crucial advantage of gradual gradient IPNs over other IPNs is the improvement of structural integrity in which the delamination may be avoided.

The preparation step of gradient IPNs involves partial swelling of polymer network I with a monomer II mixture (including crosslinker II and initiator), followed by rapid polymerizing before the swelling becomes uniform through diffusion. Thus, the overall material can be made with polymer network I predominantly on one surface, and polymer network on the other surface, with a gradient composition filling between two plates of polymer networks.

4.5 Thermoplastic IPNs

Thermoplastic IPNs are a kind of polymer blend, formed with physical crosslinking. There are several distinct types of physical crosslinks such as block copolymers, ionomer formation, and partially crystalline polymers, used in thermoplastic IPNs.⁵⁵ The employment of a crosslinking system in these IPNs may be either the same or a different physical crosslinking method. Thermoplastic IPNs can be synthesized by two general methods; i) mechanical blending of the two polymers in the melt stage, ii) chemical blending, by the swollen of monomer II into polymer I or dissolving polymer I in monomer II, following the polymerization of polymer II in situ.

4.6 Semi-IPNs

Semi-IPNs can be synthesized by a sequential or a simultaneous process. However, in this method, the crosslinker II (used to create polymer network II) is absent. The overall product of semi-IPNs is a polymer network I with linear polymers embedded as shown in Figure 1-16. To indicate the process used for IPNs product, product IPNs made by a sequential process are called semi-IPNs and the ones made by a simultaneous process are pseudo-IPNs.

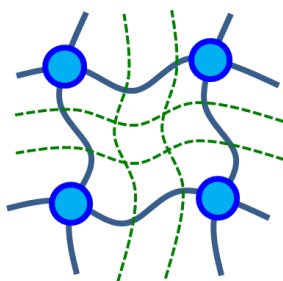


Figure 1- 16: Chemical network structure of semi-IPNs where blue colour represents polymer I and green colour shows polymer II.

5. Conclusions and objectives of the manuscript

In order to reinforce and develop toughened elastomeric materials without addition of particulate fillers and with minimal introduction of viscoelasticity, network design is required. In 2014, the first network design of acrylate elastomers based on sequential IPNs was pioneered by Ducrot et al.^{27, 28} By using the sacrificial bonds of the toughening network (polymer network I) the IPNs showed significant improvements in mechanical properties with a simultaneous increase in stiffness and toughness.

Our objective is to develop sequential IPNs containing sacrificial bonds with two extremely different materials; i) Silicone elastomers, and ii) poly(acrylic acid)-block-poly(n-butyl acrylate) or PAA-b-PBA core-shell latexes. Silicone elastomers are generally biocompatible non-reactive elastomers that are stable, and resistant to extreme environments and temperatures. Silicone elastomers are usually reinforced by using nanoparticles of filler such as silica. The filler content changes the dominant characteristics of the elastomer, introduces a Mullins effect³¹ and can sometimes cause the toxicity. By using a controlled network design, we hope to develop new modified IPNs silicone network fully reinforced mechanically in an analogous way as double network acrylates.

Furthermore, we will develop a new type of IPNs based on PAA-b-PBA core-shell latexes. Inspiration for this work comes from the work of Chenal et al.^{60, 61, 62} The latexes they synthesized were prepared by the polymerization induced self-assembly method (PISA). A polyacrylic acid (PAA) RAFT macro-initiator was synthesized first and used to initiate the RAFT polymerization of a hydrophobic n-butyl acrylate monomer. At the end of the controlled polymerization, particles with a core-shell structure were obtained where the shell thickness was controlled by the PAA block length (typically only a few kg.mol⁻¹ and the core was composed of the PBA block (typically 100 kg.mol⁻¹ or more). To prepare IPNs, the core-shell latex is first dried to form a latex film under controlled conditions. Then a sequential polymerization is carried out by first swelling the dry latex with n-butyl acrylate monomer and then carrying out a UV polymerization of the swollen film. To swell the film, the BA monomer and the hydrophobic crosslinker must diffuse through the PBA cores and PAA shells, producing the final latex film as a homogeneous IPNs. PAA is a glassy polymer, since its T_g is around 106 °C.^{63, 64} Thus at ambient temperature, the PAA shells included in the latex IPNs films act as a continuous percolating rigid filler throughout the material providing a significant stiffening to the elastomer with a very low volume fraction of filler.

The manuscript is divided in 6 chapters. Chapters 2 and 3 are dedicated to the silicone IPN system and describes first the synthesis and characterization method and then the mechanical properties. Chapters 4 and 5 focus on the latex IPNs with a similar split between synthesis and mechanical properties and finally chapter 6 provides a general conclusion.

References

1. Wilkinson, A.D.M.a.A., *IUPAC. Compendium of Chemical Terminology*. 2nd ed. (the "Gold Book") ed. 1997, Oxford: Blackwell Scientific Publications.
2. Gent, A.N., *Chapter 1 - Rubber Elasticity: Basic Concepts and Behavior*, 2013. (The Science and Technology of Rubber (Fourth Edition)), Academic Press: Boston. p. 1-26.
3. Gent, A.N. and A.G. Thomas, *Forms for the stored (strain) energy function for vulcanized rubber*. Journal of Polymer Science, 1958. **28**(118): p. 625-628.
4. Flory, P.J. and M. Volkenstein, *Statistical mechanics of chain molecules*. Biopolymers, 1969. **8**(5): p. 699-700.
5. Cotton, J.P., B. Farnoux, and G. Jannink, *Neutron Diffraction in Dilute and Semidilute Polymer Solutions*. The Journal of Chemical Physics, 1972. **57**(1): p. 290-294.
6. Fetters, L.J., et al., *Packing Length Influence in Linear Polymer Melts on the Entanglement, Critical, and Reptation Molecular Weights*. Macromolecules, 1999. **32**(20): p. 6847-6851.
7. Rubinstein, M. and S. Panyukov, *Elasticity of Polymer Networks*. Macromolecules, 2002. **35**(17): p. 6670-6686.
8. Heinrich, G., E. Straube, and G. Helmis, *Rubber elasticity of polymer networks: Theories*, 1988. (Polymer Physics), Springer Berlin Heidelberg: Berlin, Heidelberg. p. 33-87.
9. Staverman, A.J., *Properties of phantom networks and real networks*, 1982. (Polymer Networks), K. Dušek, Editor, Springer Berlin Heidelberg: Berlin, Heidelberg. p. 73-101.
10. Valentín, J.L., et al., *Uncertainties in the Determination of Cross-Link Density by Equilibrium Swelling Experiments in Natural Rubber*. Macromolecules, 2008. **41**(13): p. 4717-4729.
11. Flory, P.J. and B. Erman, *Theory of elasticity of polymer networks*. 3. Macromolecules, 1982. **15**(3): p. 800-806.
12. Arruebarrena, V.A.F., *Manifestations of the Mullins effect in filled elastomers*, 2016. (Thesis submitted to Doctoral degree of Philosophy): University of Nottingham. p. 260.
13. F. Horkay, G.B.M., *Polymer network and gel*, 2007. (Physical Properties of Polymers Handbook), J.E. Mark, Editor, Springer-Verlag New York.
14. Mooney, M., *A Theory of Large Elastic Deformation*. Journal of Applied Physics, 1940. **11**(9): p. 582-592.
15. Mooney, M., *The Thermodynamics of a Strained Elastomer. I. General Analysis*. Journal of Applied Physics, 1948. **19**(5): p. 434-444.
16. Sperling, L.H., *Crosslinked Polymers and Rubber Elasticity*, 2005. (Introduction to Physical Polymer Science), John Wiley & Sons, Inc. p. 427-505.
17. Peterlin, A., *The Physics of Glassy Polymers*, R. N. Haward, Ed., Halsted Press, New York, 1973. 620 pp. \$45.00. Journal of Polymer Science: Polymer Letters Edition, 1973. **11**(10): p. 655-655.

18. Chern, C.-S., *Applications of Emulsion Polymers*, 2008. (Principles and Applications of Emulsion Polymerization), John Wiley & Sons, Inc. p. 223-247.
19. Sperling, L.H., *Mechanical Behavior of Polymers*, 2005. (Introduction to Physical Polymer Science), John Wiley & Sons, Inc. p. 557-612.
20. Rivlin, R.S. and A.G. Thomas, *Rupture of rubber. I. Characteristic energy for tearing*. Journal of Polymer Science, 1953. **10**(3): p. 291-318.
21. Greensmith, H.W. and A.G. Thomas, *Rupture of rubber. III. Determination of tear properties*. Journal of Polymer Science, 1955. **18**(88): p. 189-200.
22. Dargazany, R., V.N. Khiêm, and M. Itskov, *A generalized network decomposition model for the quasi-static inelastic behavior of filled elastomers*. International Journal of Plasticity, 2014. **63**: p. 94-109.
23. Diani, J., B. Fayolle, and P. Gilormini, *A review on the Mullins effect*. European Polymer Journal, 2009. **45**(3): p. 601-612.
24. Mullins, L., *Effect of Stretching on the Properties of Rubber*. Rubber Chemistry and Technology, 1948. **21**(2): p. 281-300.
25. Buckley, C.P., D.S.A.D. Focatiis, and C. Prisacariu, *Unravelling the mysteries of cyclic deformation in thermoplastic elastomers*, 2011. (Constitutive Models for Rubber VII). p. 3-10.
26. Webber, R.E., et al., *Large Strain Hysteresis and Mullins Effect of Tough Double-Network Hydrogels*. Macromolecules, 2007. **40**(8): p. 2919-2927.
27. Ducrot, E., et al., *Toughening Elastomers with Sacrificial Bonds and Watching them Break*. Science, 2014. **344**(6180): p. 186-189.
28. Ducrot, E., *Innovative tough elastomers: Designed sacrificial bonds in multiple networks*, 2013. (Unpublished doctoral dissertation): University Pierre and Marie Curie, Paris, France.
29. Mullins, L. and N.R. Tobin, *Theoretical Model for the Elastic Behavior of Filler-Reinforced Vulcanized Rubbers*. Rubber Chemistry and Technology, 1957. **30**(2): p. 555-571.
30. Bueche, F., *Molecular basis for the mullins effect*. Journal of Applied Polymer Science, 1960. **4**(10): p. 107-114.
31. Clough, J.M., et al., *Covalent Bond Scission in the Mullins Effect of a Filled Elastomer: Real-Time Visualization with Mechanoluminescence*. Advanced Functional Materials, 2016. **26**(48): p. 9063-9074.
32. Blanchard, A.F. and D. Parkinson, *Breakage of Carbon-Rubber Networks by Applied Stress*. Industrial & Engineering Chemistry, 1952. **44**(4): p. 799-812.
33. Gong, J.P., *Why are double network hydrogels so tough?* Soft Matter, 2010. **6**(12): p. 2583-2590.
34. Li, J., et al., *A facile method to fabricate hybrid hydrogels with mechanical toughness using a novel multifunctional cross-linker*. RSC Advances, 2017. **7**(56): p. 35311-35319.

35. Ma, C., et al., *Molecular insight into the Mullins effect: irreversible disentanglement of polymer chains revealed by molecular dynamics simulations*. Physical Chemistry Chemical Physics, 2017. **19**(29): p. 19468-19477.
36. Hanson, D.E., et al., *Stress softening experiments in silica-filled polydimethylsiloxane provide insight into a mechanism for the Mullins effect*. Polymer, 2005. **46**(24): p. 10989-10995.
37. Hamed, G.R. and S. Hatfield, *On the Role of Bound Rubber in Carbon-Black Reinforcement*. Rubber Chemistry and Technology, 1989. **62**(1): p. 143-156.
38. Shams Es-haghi, S., A.I. Leonov, and R.A. Weiss, *Deconstructing the Double-Network Hydrogels: The Importance of Grafted Chains for Achieving Toughness*. Macromolecules, 2014. **47**(14): p. 4769-4777.
39. Houwink, R., *Slipping of Molecules during the Deformation of Reinforced Rubber*. Rubber Chemistry and Technology, 1956. **29**(3): p. 888-893.
40. Dannenberg, E.M. and J.J. Brennan, *Strain Energy as a Criterion for Stress Softening in Carbon-Black-Filled Vulcanizates*. Rubber Chemistry and Technology, 1966. **39**(3): p. 597-608.
41. Montes, H., F. Lequeux, and J. Berriot, *Influence of the Glass Transition Temperature Gradient on the Nonlinear Viscoelastic Behavior in Reinforced Elastomers*. Macromolecules, 2003. **36**(21): p. 8107-8118.
42. Berriot, J., et al., *Evidence for the Shift of the Glass Transition near the Particles in Silica-Filled Elastomers*. Macromolecules, 2002. **35**(26): p. 9756-9762.
43. Fukahori, Y., *New progress in the theory and model of carbon black reinforcement of elastomers*. Journal of Applied Polymer Science, 2005. **95**(1): p. 60-67.
44. Fukahori, Y., *Generalized Concept of the Reinforcement of Elastomers. Part 1: Carbon Black Reinforcement of Rubbers*. Rubber Chemistry and Technology, 2007. **80**(4): p. 701-725.
45. Rickaby, S.R. and N.H. Scott, *Transversely isotropic cyclic stress-softening model for the Mullins effect*. Proceedings of the Royal Society A: Mathematical, Physical and Engineering Science, 2012. **468**(2148): p. 4041-4057.
46. Buckley, C.P., D.S.A. De Focatiis, and C. Prisacariu, *Unravelling the mysteries of cyclic deformation in thermoplastic elastomers*, 2011. (Constitutive Models for Rubber VII), CRC Press. p. 3-10.
47. Mullins, L., *Permanent Set in Vulcanized Rubber*. Rubber Chemistry and Technology, 1949. **22**(4): p. 1036-1044.
48. Dorfmann, A. and R.W. Ogden, *A constitutive model for the Mullins effect with permanent set in particle-reinforced rubber*. International Journal of Solids and Structures, 2004. **41**(7): p. 1855-1878.
49. *Particulate-Filled Polymer Composites, Second Edition* ed. R.N. Rethon. 2003: Smithers Rapra Press. 556.

50. Bauman, J.T., *Rubber Stress-Strain Behavior*, 2008. (Fatigue, Stress, and Strain of Rubber Components), Carl Hanser Verlag GmbH & Co. KG. p. 9-18.
51. Papkov, V.S., et al., *Energy investigation of the softening of siloxane rubbers during deformation*. Polymer Mechanics, 1975. **11**(3): p. 329-333.
52. Diani, J., M. Brieu, and P. Gilormini, *Observation and modeling of the anisotropic visco-hyperelastic behavior of a rubberlike material*. International Journal of Solids and Structures, 2006. **43**(10): p. 3044-3056.
53. Diani, J., M. Brieu, and J.M. Vacherand, *A damage directional constitutive model for Mullins effect with permanent set and induced anisotropy*. European Journal of Mechanics - A/Solids, 2006. **25**(3): p. 483-496.
54. Sperling, L.H. and V. Mishra, *The current status of interpenetrating polymer networks*. Polymers for Advanced Technologies, 1996. **7**(4): p. 197-208.
55. Zhi-zhong, Y. and E.M. Pearce, *Interpenetrating polymer networks and related materials*, L. H. Sperling, Plenum, New York, 1981, 265 pp. Price: \$35.00. Journal of Polymer Science: Polymer Letters Edition, 1982. **20**(4): p. 244-245.
56. Comstock, M.J., *Interpenetrating Polymer Networks, Copyright, 1993 Advisory Board, FOREWORD, ABOUT THE EDITORS*, 1994. (Interpenetrating Polymer Networks), M.J. Comstock, Editor, American Chemical Society. p. i-ix.
57. Mathew, A.P., *Interpenetrating Polymer Networks: Processing, Properties and Applications*, 2013. (Advances in Elastomers I: Blends and Interpenetrating Networks), P.M. Visakh, et al., Editors, Springer Berlin Heidelberg: Berlin, Heidelberg. p. 283-301.
58. Sheu, H.R., M.S. El-Aasser, and J.W. Vanderhoff, *Phase separation in polystyrene latex interpenetrating polymer networks*. Journal of Polymer Science Part A: Polymer Chemistry, 1990. **28**(3): p. 629-651.
59. El-Aasser, M.S., et al., *Morphology, design and characterization of IPN-containing structured latex particles for damping applications*. Colloids and Surfaces A: Physicochemical and Engineering Aspects, 1999. **153**(1): p. 241-253.
60. Chenal, M., *Particules cœur-écorce par polymérisation raft en émulsion pour des matériaux nanostructurés sans solvants*, 2013. (Thèse de doctorat Physique et Chimie des matériaux): University Pierre and Marir Curie, Paris, France. p. 265
61. Chenal, M., L. Bouteiller, and J. Rieger, *Ab initio RAFT emulsion polymerization of butyl acrylate mediated by poly(acrylic acid) trithiocarbonate*. Polymer Chemistry, 2013. **4**(3): p. 752-762.
62. Chenal, M., et al., *Soft nanostructured films with an ultra-low volume fraction of percolating hard phase*. Macromol Rapid Commun, 2013. **34**(19): p. 1524-9.
63. Haynes, W.M., *CRC Handbook of Chemistry and Physics, 93rd Edition*. 2016: CRC Press.

64. Park, J.-K., et al., *Effect of drying conditions on the glass transition of poly(acrylic acid)*. Polymer Engineering & Science, 1991. **31**(12): p. 867-872.

-CHAPTER 2-

Synthesis of silicone multiple networks

Chapter 2: Synthesis of silicone multiple networks.....	35
Introduction.....	37
1. Silicones	38
1.1 General features of silicones.....	38
1.2 Crosslinking of Silicones.....	39
1.1.1 Room Temperature Vulcanization (RTV).....	40
1.1.2 Heat-activated radical cure or High Temperature Vulcanization (HTV).....	40
1.1.3 Transition metal catalyzed hydrosilylation or addition cure.....	43
1.3 State of the art in silicone elastomer.....	43
2. Method and synthesis.....	45
2.1 Chemicals and reagents.....	45
2.2 Synthesis and reaction conditions.....	46
2.2.1 Synthesis of the silicone highly crosslinked network.....	46
2.2.2 Silicone loosely crosslinked network.....	48
2.2.3 Extraction of the uncrosslinked fraction.....	49
2.2.4 Drying process.....	50
2.3 Stoichiometry study of silicone highly crosslinked network (1 st network).....	50
2.4 Stoichiometry study of silicone prepolymer (2 nd network without crosslink).....	52
2.4.1 Curing time of the silicone prepolymer.....	52
2.5 Stoichiometry study of silicone loosely crosslinked network (2 nd network with crosslink).....	55
2.6 Silicone multiple networks.....	56
2.6.1 Swelling process.....	56
2.6.2 Synthesis and reaction conditions of the multiple networks.....	58
Conclusion.....	62
References.....	63

Introduction

Silicone chemistry is the basis of high performance elastomers which have many unique properties such as a very low glass transition temperature, outstanding thermal stability, high hydrophobicity and biocompatibility.^{1, 2, 3} However, silicones have weak intermolecular interactions between polymer chains which generally results in poor mechanical properties. In order to improve the mechanical properties, the most common strategy has been to introduce nanofillers into the system. Although, fillers have a proven efficiency to reinforce elastomers, using fillers also impacts the bulk density, may change a bit the glass transition temperature, causes energy dissipation, and also may affect the bio-compatibility properties.

The mechanical properties of silicone elastomers can also be modified without introducing fillers by simply blending different polymers^{4, 5}, using interpenetrating networks (IPNs)^{6, 7} and synthesizing copolymers^{2, 8}. These methods use a combination between two or more different polymers to obtain a synergy of their unique properties. Our study will focus on IPNs networks. It has been recently reported by Ducrot^{9, 10, 11} that by using a prestretched network interpenetrated into extensible networks, the prestretched network could randomly break bonds and dissipate energy in the bulk before the material fails, resulting in an improvement in both stiffness at low strain and toughness at high strains. This mechanical reinforcement technique utilizes sacrificial bonds and has been first developed in elastomeric systems with acrylate elastomers¹⁰.

In our study, we will attempt to expand this “sacrificial bonds” technique to silicone elastomers. The core, or breakable network, will be designed as a well crosslinked network and the penetrating network, as an extensible network. The reinforced silicone network will be synthesized by using the hydrosilylation reaction with a sequential interpenetrating network technique. The effective stoichiometric ratio between silicone hydride end groups (Si-H) and unsaturated vinyl groups grafted on polydimethyl siloxane (PDMS-V) will be designed and optimized independently for the prestretched core network and for the penetrating network. Then the selected stoichiometric ratios will be later used to create silicone multiple networks. The synthesis method and the controlled conditions to study the effect of the stoichiometric ratio and to create silicone multiple networks will be exposed now.

2. Silicones

1.2 General features of silicones

Silicones are a family of polymeric materials which are composed of an inorganic-organic backbone (Si-O). There are two monovalent organic radicals that attach to each silicon atom (R_2Si-O)¹², as shown in Figure 2-1. Due to its excellent properties: thermal stability, chemical stability, electrical resistance and low surface energy, silicone polymers have found a variety of applications such as membranes^{13, 14}, electronic and optical devices^{15, 16}, sealants¹⁷ and biomedical applications^{18, 19, 20}. In this decade alone, approximately 3000 commercial silicone products were put on the market¹. Some examples of large commercial applications of silicones, divided by category, are listed in Table 2-1.

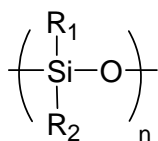


Figure 2- 1: General structure of the silicone polymer backbone

From the first commercialization of silicones in the early 1940's up to the present time, the most widely recognized silicone is Poly(dimethylsiloxane) or PDMS, a linear chain of siloxane backbone with $R_1 = R_2 = \text{Methyl } (-CH_3)$ as shown in Figure 2-2. PDMS can be prepared by two general methods, a ring opening reaction of cyclic silicone oligomers and a condensation of linear silicone oligomers.²¹ PDMS at low molar mass is a viscous fluid at room temperature while PDMS at high molar mass is in a gummy state which shows a markedly viscoelastic behavior. However, this material is able to dissolve in organic solvents such as toluene, cyclohexane etc.

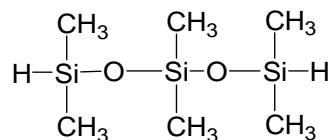


Figure 2- 2: Poly(dimethylsiloxane) structure

Silicone type	Application
Fluid - PDMS - Organo functional siloxane	Greasing hypodermic needles, Breast implants, Anti-foaming, Release agent, Additive of paint and ink, Lubricants, Softening, Processing aids
Compound (Grease like silicone) - Silica + PDMS	Sealing and lubricant agent, , Anti-foaming, Insulator compound
Gel (unreinforced elastomer) - Crosslink PDMS	Cushioning material, Wound interface, Soft matrix for drug release, Silicone gel for scar treatment
Elastomers - Crosslinked PDMS - Reinforced with silica - Finished cured system	Soft and resilient material for medical device, Tube, Catheters, Finger joints, Fabric coating, Sealant and adhesive, Release liner, Cooking mold, Insulator
Pressure sensitive adhesive (PSA) - Silicate resin in PDMS	Film-former, Silicone PSA tape, Protective film

Table 2- 1 : Commercial silicone products and applications.^{1, 22}

In order to reinforce the mechanical properties and improve the chemical and solvent resistance of PDMS, a crosslinking process is required to create a network between each polymer chains and form a silicone elastomer. In this state, a silicone elastomer does not dissolve when immersed into organic solvents, but it is still able to swell in some organic solvents such as toluene or cyclohexane etc. However the crosslinked network of a silicone elastomer is still relatively mechanically brittle.²¹ Therefore, many publications up to now have focused on the mechanically reinforcement of silicone elastomers especially by using nanoparticle fillers such as silica²³, nanoparticle²⁴, clay²⁵ and mica flakes.²⁶

1.3 Crosslinking of Silicones

As discussed above PDMS is a fluid at room temperature and requires a crosslinker to create a network between each silicone chain through a vulcanizing, crosslinking or curing process. There are several possible manners to vulcanize a silicone. However the most common techniques are ²⁷

1. The incorporation of tri- or tetrafunctional silanes that can react under ionic conditions.
2. The use of a functional group R in the PDMS polymer (R= methyl, vinyl or hydrogen) to form a network.

Using these 2 techniques, there are 3 main different methods to cure a silicone elastomer.

1.3.1 Room Temperature Vulcanization (RTV)

Room temperature vulcanization is a method that takes advantage of the displacement of ligands of PDMS chain ends. An organosilicon crosslinking agent is used to interact with siloxanol end groups in the presence of a catalyst under anhydrous conditions.²¹ The reaction occurs at room temperature, therefore the term of RTV is related to the process of curing. The rate of the substitution reaction depends on the leaving group during the crosslinking process. In general the selected leaving groups are oximes, carboxylates and alkoxides.²⁷

RTV curing can be with a single or duo package system.²¹ The single package system is more convenient, since all the components are premixed together. The system usually needs the use of an excess of the multifunctional crosslinking agent to interact with the siloxanol end groups of the silicone chains in the presence of a catalyst. This one component system has the drawback of a relatively long curing time because of the requirement of diffusion of moisture to react with the residual multifunctional crosslinker. Also the curing silicone rubber from this system possess multifunctional end groups which could be hydrolyzed and condensed when exposed to the atmospheric moisture.²¹ The duo package system requires the mixing of two separate components. One component contains a multifunctional organosilicone crosslinker and a catalyst while another part contains hydride-terminated PDMS and filler. The system is prepared with equivalent chemistry, thus after the two components are mixed, the curing proceeds relatively fast at room temperature.

1.2.2 Heat-activated radical cure or High Temperature Vulcanization (HTV)

High temperature radical cure of silicones arise from peroxides. Generally, peroxides decompose at a temperature around 150°C to create the radical.²¹ There are two different types of radical cure commonly used; radical H[•] and vinyl group. In the first, peroxides are used to initiate radicals H[•] which are abstracted from a methyl group in PDMS and form silylmethyl radicals (SiCH₂[•]). The silylmethyl radicals crosslink by coupling or by addition to a small amount of pendent vinyl groups. This process provides a high efficiency, although the efficiency drops at high conversion due to the viscosity of the product.²⁷ In addition this process produces byproducts such as phenols that needs to be removed from the elastomer. In the second method, vinyl groups which are more reactive toward radicals than alkanes (to H[•] subtraction), can form a crosslinked network at low temperature in the presence of less reactive “vinyl-specific” peroxides.²⁷ This system also creates byproducts that need to be removed either by heat stripping or by titration.

1.2.3 Transition metal catalyzed hydrosilylation or addition cure

Addition cure by hydrosilylation is widely used in the silicone industries.²⁸ The reaction is useful for functionalizing siloxane monomers and polymers and also is good to crosslink polysiloxane. The hydrosilylation reaction only occurs with the help of catalysts; platinum catalyst, palladium, peroxides, UV light and azidonitriles to conjugate the end group of the silicon hydride (Si-H) bond to unsaturated groups of PDMS ($\text{Si}-\text{CH}=\text{CH}_2$ or $\text{Si}-\text{C}\equiv\text{CH}$). The reaction performs rapidly from room temperature to high temperature under mild conditions.²⁷ One example of hydrosilylation reaction in which a vinyl-terminated PDMS reacts with a tetrafunctional hydrosilane, tetrakisdimethylsiloxy silane is shown in Figure 2-3.²⁹ By this method, the reaction shows a high efficiency and provides a high conversion, without any byproduct²⁹ and is relatively free from side reactions.²¹

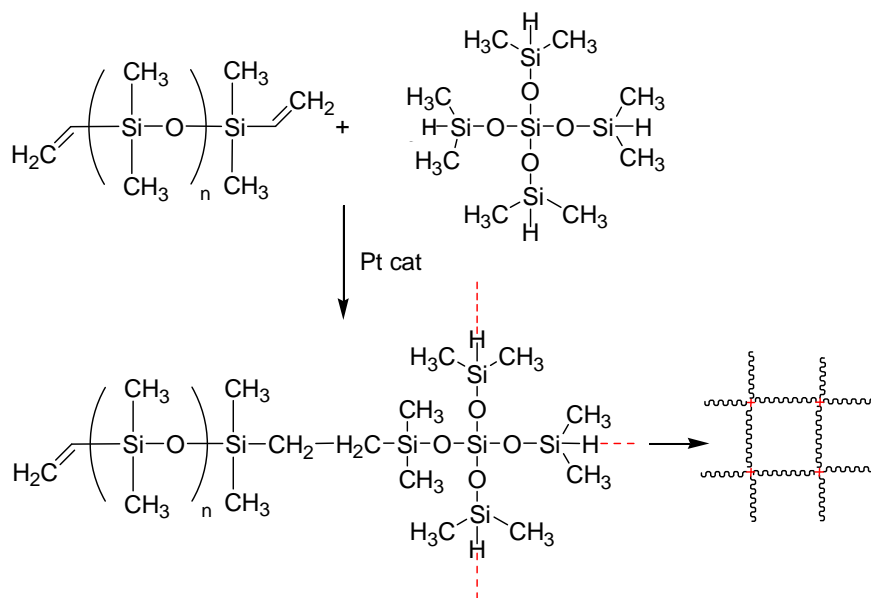


Figure 2- 3 : Hydrosilylation reaction by Pt catalyst

Platinum (Pt) catalysts are mostly used to perform hydrosilylation curing due to their ability to solubilize in the polymer.³⁰ One class of platinum compounds used as platinum catalysts for hydrosilylation reactions are Pt(0) complexes. An example of such a catalyst is Karstedt's catalyst (Figure 2-4) which is formed by the reaction of divinyl-tetramethyldisiloxane with chloroplatinic acid.²⁸

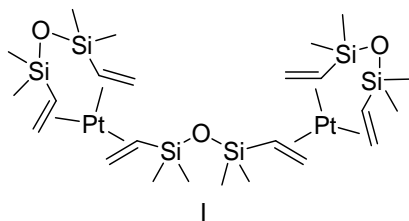


Figure 2- 4: Karstedt's catalyst structure

The mechanism for the platinum-catalyzed hydrosilylation of alkenes ($C=C$) has been proposed by Chalk and Harrod³¹ in 1964, as shown in Figure 2-5. At first, the oxidative addition of the Si-H bond in PDMS hydride terminated occurs with a metal center of the catalyst and forms an intermediate including the H-[Pt]-Si moiety. Then alkenes ($C=C$) of multifunctional organosilicones insert into the resulting H-[Pt] bond and forms H-C-C-[Pt]-Si. Finally, H-C-C-[Pt]-Si subsequently undergoes a reductive elimination of the adduct of Si-C-C-H products and returns to the Pt metal catalyst form.³²

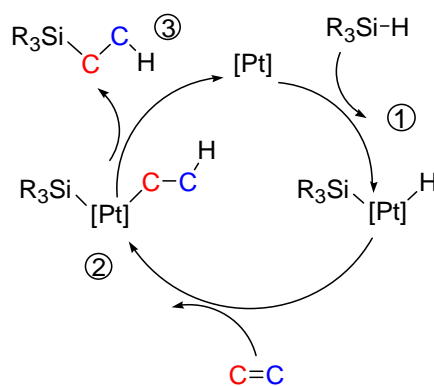


Figure 2- 5: Chalk-Harrod cycle

In our study, the technique of the hydrosilylation reaction will be used to synthesize the polymer chains of silicone PDMS and also to crosslink the polymer to form the silicone elastomer. The Karstedt's catalyst will be used to initiate and perform the reaction. The technique and reaction conditions which are used in our study will now be presented in the following section.

1.4 State of the art in silicone elastomers

As discussed in the introduction of this chapter silicone elastomer have distinct properties such as outstanding thermal stability, chemical resistance, good dielectric properties, and good biocompatibility.^{1,3} Silicone elastomers are however relatively weak elastomers.^{1,33} Fillers are a good option to reinforce them and are generally added into silicone elastomers. In particular silica nanofillers are widely used to improve the mechanical properties of silicone elastomers. These nanofillers with average particle sizes in the range of 1-100 nm showed a high performance in enhancing mechanical properties. For example the use of small amounts of nanofiller (~10 vol%) can improve the properties of the polymer such as heat resistance, strength, stiffness, flame retardancy etc. and the small particle size will only slightly affect the bulk properties of polymers such as density and light transmission.³⁴ (note that other nanofillers have been also developed for silicone elastomers such as clay nanolayers^{35, 36}, graphene^{37, 38}, carbon nanotubes (CNTs)^{39, 40, 41}, nanosilica⁴², polyhedral oligomeric silsesquioxane (POSS)^{43,44} etc.) Silica particles and silicone polymer chains have a strong filler-polymer interaction due to the hydrogen bonds created between silanols on the silica surface and oxygen atoms of the polymer chain.³³ Moreover in order to improve the interaction between silica and polymer there are many publications focusing on the modification of silica surfaces by surface treatment. Two approaches are normally used for surface modification: physical adsorption of some chemical on the filler surface and permanent surface modification by passivating part of silanol groups present on the surface of the particles.³³

However, using the filler to reinforce the polymer also carries some disadvantages. Due to the extremely high surface activity of nanofillers filler-filler interactions between these particles gives them a tendency to agglomerate and aggregate, creating micron size filler clusters causing a loss of transparency.³³ The blending of filler particles into the polymer before crosslinking often leads to inhomogeneities³³ and requires special processes to fabricate filler/ polymer composites. Moreover, incorporating high volume fractions of fillers also could affect the bulk density of the polymer⁴⁵, increase energy dissipation⁴⁶ and affect biocompatibility^{47, 48, 49} which limits their application. In addition, it has been reported that some types of filler could influence the glass transition temperature of the polymer matrix.^{50, 51}

Using polymer blends, co-polymers and interpenetrating polymer networks (IPNs) are alternative techniques to reinforce silicones without using fillers. These techniques combine the unique properties of two or more different polymers to form the networks with a good balance of properties. The IPNs technique in silicone networks has been first developed in the 1960's by Sperling and Frish.⁵² However, silicone based IPNs are less interesting due to the incompatibility between silicones and most organic polymers and having uniquely flexible chains, it is difficult to trap them in the non-equilibrium structures of the IPNs.⁵² However the mechanical properties of silicone based IPNs have

been developed with a thermoplastic polymer. In 1995, Hamurcu et al.⁵³ synthesized full- and semi-IPNs based on PDMS/polystyrene, PDMS/polybutadiene and PDMS/poly(glyceryl propoxy triacrylate) where PDMS was used as a host network. It was found that both IPNs network of PDMS/polystyrene and PDMS/poly(glyceryl propoxy triacrylate) exhibited superior mechanical and elastomeric properties when comparing with pure silicone networks. However, this IPNs networks showed two separated T_g indicating that a phase separation occurred.

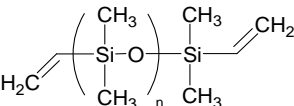
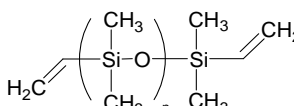
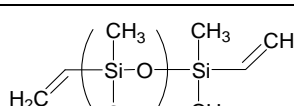
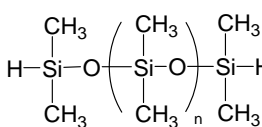
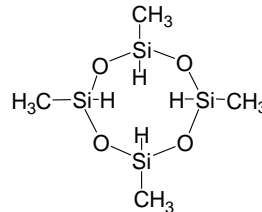
Furthermore, the thermal and mechanical properties of PDMS were improved by creating interpenetrated networks with cellulose acetate butyrate (CBA).⁵⁴ It has been claimed that the INPs of PDMS/CAB were miscible avoiding phase separation and they were called true IPNs. PDMS also could be combined with two different partner polymer networks using the IPNs architecture. In 2002 Huang et al.⁵⁵ studied phase separation of PDMS and polymethacrylate (PMAC). PDMS, blended with polyacrylate (PAC) was used as the host network. The sequential interpenetrating network technique was used to incorporate PMAC into the host network. It has been found that the glass transition temperature (T_g) of the IPNs materials change as a function of the concentration of PMAC and PDMS, the transition peak at low temperature being dominated by PMAC (T_g) and the transition peak at high temperature zone dominated by the PDMS (T_g).

In our study the mechanical properties of the PDMS networks will be reinforced by another PDMS network, by using a sequential interpenetrating networks technique. The introduction of prestretched chains as sacrificial bonds, a technique which has been recently investigated in acrylate-based unfilled elastomers by Ducrot et al.^{9, 10, 11} will be expanded to silicone systems in our study. The usage of prestretched chains which can break and dissipate energy before the material fails is the advantage of the sacrificial bonds technique to reinforce networks in stiffness and toughness.³⁴ In our study, the host PDMS network is designed as a rigid network to provide the stiffness while the interpenetrating network designed as an extensible network to serve as an extensible matrix. The incorporation of the same polymeric system avoids phase separation while the different mechanical characteristics of host and guest network can be tuned for better mechanical properties.

3. Method and synthesis

2.1 Chemicals and reagents

Chemical substrates and solvents for the synthesis of silicone networks are listed in Table 2-2. All chemical reagents and solvents were used as received without any further purification. Poly(dimethylsiloxane), vinyl dimethylsiloxyl terminated or PDMS-V of different molar masses were used as silicone oligomeric precursors, while hydride terminated poly(dimethylsiloxane) (PDMS-H) and 2,4,6,8-Tetramethylcyclotetrasiloxane (D₄H) were used as chain extender and crosslinker respectively. Karstedt's catalyst or Platinum-divinyltetramethyldisiloxane complex was used as a catalyst to cure the silicone elastomers by hydrosilylation reaction.

Notation	Chemical Name	Semi-develop formular	M _w (g.mol ⁻¹)	Purity	Origin
PDMS-V ₇₇₀	Poly(dimethylsiloxane), vinyl dimethylsiloxyl terminated		770	95%	ABCR
PDMS-V _{6k}	Poly(dimethylsiloxane), vinyl dimethylsiloxyl terminated		6000		ABCR
PDMS-V _{17k}	Poly(dimethylsiloxane), vinyl dimethylsiloxyl terminated		17200		ABCR
PDMS-H ₄₀₀	poly(dimethylsiloxane) hydride terminated		400- 500		ABCR
D ₄ H	2,4,6,8Tetramethylcyclotetra siloxane		240.51	99.5%	Aldrich

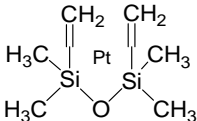
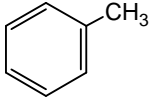
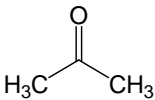
Pt	Platinum-divinyltetramethyldisiloxane complex in xylene			(2.1-2.4%) Pt	ABCR
Toluene	Toluene		92.14	99.5%	Sigma, VWR
Acetone	Acetone		58.08	99.5%	Sigma, VWR

Table 2- 2: Chemicals and reagents

2.2 Synthesis and reaction conditions

In our synthesis, poly(dimethylsiloxane), vinyl dimethylsiloxyl terminated (PDMS-V) was crosslinked with 2,4,6,8-Tetramethylcyclotetrasiloxane (D_4H) by the hydrosilylation reaction and poly(dimethylsiloxane) hydride terminated (PDMS-H) was used to chain extend PDMS-V. The Karstedt's catalyst was served as the initiator to trigger the reaction between vinyl ($=CH_2$) end group of PDMS-V and hydride ($-H$) of PDMS-H or D_4H . The basic principle of sequential interpenetrating networks (IPNs) was described in chapter 1. In our study, silicone elastomers were investigated by using 2 different systems: a highly crosslinked network which is a rigid network and a loosely crosslinked network which controls the extensibility of the material. The stoichiometric ratio between vinyl groups of the PDMS-V chains and the $-H$ of the D_4H crosslinker (in the highly crosslinked system) or the PDMS-H (in the loosely crosslinked system) were optimized separately in order to obtain the highest modulus (for the highly crosslinked system) and the highest extensibility simultaneous increase in stiffness and extensibility. Then the silicone loosely crosslinked network was interpenetrated into the more crosslinked network by using a sequential polymerization technique. The products after this process were called silicone multiple networks.

2.2.1 Synthesis of the silicone highly crosslinked network

Two types of rigid networks of well crosslinked silicone (or 1st networks) were used in our study: a small mesh size and a larger mesh size (Figure 2-6). These two different 1st networks were prepared by using PDMS-V with $M_w = 6 \text{ kg.mol}^{-1}$ and PDMS-V with $M_w = 17.2 \text{ kg.mol}^{-1}$ respectively. The networks were synthesized by crosslinking PDMS-V with D_4H crosslinker via a hydrosilylation

reaction at room temperature. Toluene was added into the system in order to decrease the viscosity of the PDMS-V and also to decrease the entanglement density of silicone chains in the final product as reported by Urayama et al.^{11, 56, 57}

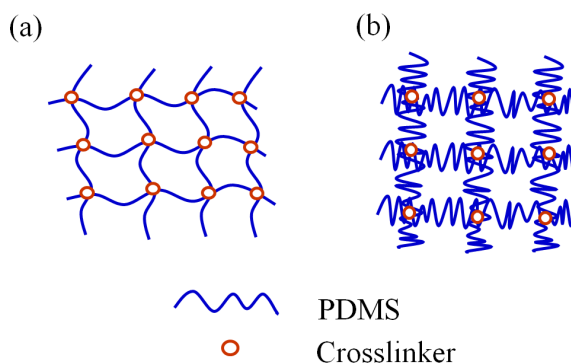


Figure 2- 6: Ideal rigid network of (a) PDMS small mesh size (b) PDMS large mesh size

In our synthesis, we apply the duo-package technique, which is used in the room temperature vulcanizing method of silicones. In general, this technique prepares 2 packages of different ingredients before mixing them to produce a cured network at room temperature. The first component of the reactive mixture consists of multifunctional organosilicones with the catalyst while the other contains silanol-terminated PDMS and filler.²¹ However in our system, in order to increase the homogeneity of the network; the first reagent, composed of PDMS-V, D₄H crosslinker and one half of the toluene were smoothly stirred about 10 minutes. The second reagent, consisted of 20 ppm (part per million) of Pt Karstedt's catalyst and the other half of the toluene were mixed well before being introduced into the first reagents. The two reagents were mixed by continued stirring for a few minutes and then the solution was injected with a syringe into the prepared glass mold as shown in Figure 2-7.

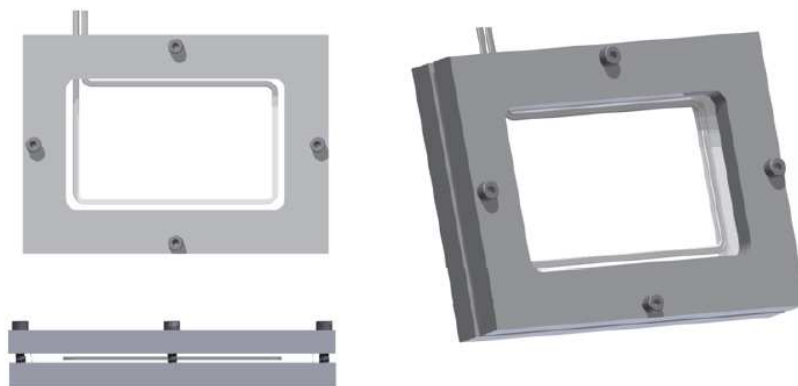


Figure 2- 7: Glass mold for preparing silicone networks.¹¹

The glass mold in our study consisted of two glass plates, steel spacers and a teflon tubing to seal the mold. In order to avoid the problem of the final sample sticking to the glass mold, the glass surfaces were covered with a PET thin film before placing them into the metal frame. The whole setup was tightened to ensure a good contact of the glass plates with the spacers and the tubing. Metallic spacers were used to control the thickness of the final silicone network sample, which was about 1 mm. The Teflon tubing with an external diameter around 1.8 mm was compressed and acted as an O-ring seal. The curing procedure was carried out at room temperature for 12 hr. before removing the sample from the mold, washing, and drying it.

Moreover, we also investigated the same silicone 1st networks synthesized in solvent-free conditions. In this synthesis, we used only 0.005% V/W of total composition to dilute the Pt catalyst concentration since the high concentration of Pt catalyst showed a premature curing after the first drop of Pt catalyst. The sample preparation procedure of the solvent-free system was the same as in the presence of solvent; however, the toluene did not introduce in the both component, the mixed component was kept at -20 °C before adding the catalyst and the reaction was made at -20 °C for 12 hr. The curing took place at -20 °C in order to avoid hydrogen bubbles inside the curing samples, which were produced from the hydrosilylation reaction. The solvent free system had a high viscosity during the curing process that might trap hydrogen gas and cause the presence of bubbles inside the curing samples. Thus, in this system a slow reaction was required to give the hydrogen gas enough time to diffuse out of the sample.

2.2.2 Silicone loosely crosslinked network

A loosely crosslinked silicone network was used to swell the silicone rigid network. Based on the multiple network design optimized for a acrylates, the important desired property of this 2nd network is its extensibility. The network should be soft and extensible as much as possible but should be only loosely connected to the first network.¹¹ PDMS-V MW 770 g.mol⁻¹ was mixed with PDMS-H MW 400-500 g.mol⁻¹ and in some cases a small amount of D₄H crosslinker was also introduced. The composition was mixed for about 15 minutes and kept at -20 °C for an hour in order to prevent an occasional immediate reaction, which happens after introducing the Pt Karstedt's catalyst to the system. In this formula, PDMS-H was used to extend the chain length of PDMS-V₇₀₀ while D₄H was used to crosslink and maintain the stability of network (Figure 2-8). Low molecular weights starting precursors are needed to be able to swell the highly crosslinked network (1st network) before polymerization of this second network occurs.

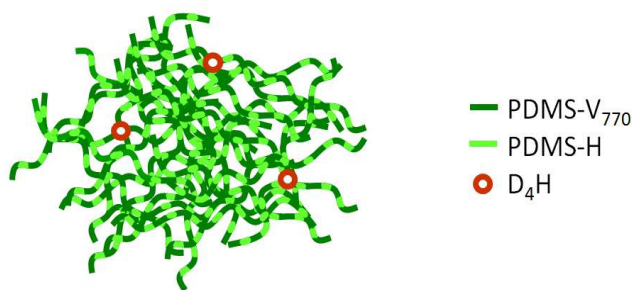


Figure 2- 8: Ideal chain of silicone loosely crosslink network

The 30 ppm of Pt Karstedt's catalyst was diluted in toluene to 0.001% V/W of total composition in order to avoid the flash reaction after adding the catalyst. The two components were mixed and stirred for 5 minutes before pouring in to the mold. For this network, we used cylindrical molds of polypropylene to cure the sample. We found that the loose network always stuck to the glass mold. Even when using a PET thin film to cover the glass, the cured network could not be removed intact from the glass mold. To overcome this problem, many surfaces have been tried to demold the silicone loosely crosslinked network such as polyethylene, silicone and PTFE. Finally we found that the silicone loosely crosslinked network showed the least bonding to polypropylene. The dimensions of the polypropylene mold are exhibited in Figure 2-9. For curing, the sample was placed in the oven in which an oven's tray was controlled by a tubular spirit level, to keep a constant thickness. The curing took place at 70 °C for 40 hr. The reaction conditions for the loosely crosslinked network were determined by a couette viscometer study.

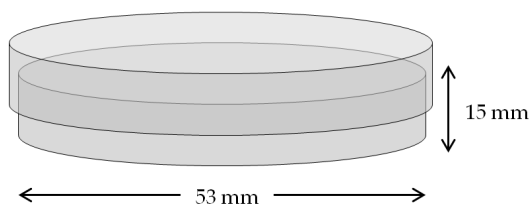


Figure 2- 9: Polypropylene cylindrical mold for silicone loosely crosslink network

2.2.3 Extraction of the uncrosslinked fraction

The extraction process was performed only for the silicone highly crosslinked network and for silicone multiple networks. The objective of washing the samples after completing the curing reaction is to remove free chains, unreacted components and also catalysts trapped inside the network.

In silicone multiple networks, the sample was first removed from the mold and immediately immersed into a toluene bath in which the solvent was changed every day. After a day of immersion,

the sample absorbed a large amount of solvent and became much larger and fragile, thus the solvent's changing needed to be carefully done otherwise the samples might crack and break. We found that by drying the samples at a room temperature through a slow evaporation of solvent, the dried samples usually break into pieces. This phenomenon has been explained elsewhere and indicates that the evaporation process of solvent creates residual stresses inside the polymer sample.⁵⁸ In order to deswell the samples we used a mixture of a good and poor solvent in which the good solvent was toluene and the poor solvent was acetone. After four days of washing, the solvent bath was changed from a toluene bath to a mixed solvent of toluene/acetone, 75/25 % V/V and for the fifth to seventh day we used the a toluene/acetone, 50/50 %, 25/75% and 0/100% V/V respectively.

However for the silicone highly crosslinked network in which the network is not thick, the deswelling process could start with a solvent mixture toluene/acetone, 50/50 % V/V in day four, then continue to toluene/acetone, 0/100 % V/V the day after.

2.2.4 Drying process

After the extraction process, silicone simple networks and multiple networks were fully dried, first under a laboratory fume hood for 2 hr and then under vacuum at 80 °C for one night. Finally, the samples were stored at room temperature until later use.

2.3 Stoichiometry study of silicone highly crosslinked network (1st network)

In order to create sacrificial bonds and improve the mechanical properties of silicone multiple networks, the 1st network is designed to be as rigid as possible. In principle, a fully crosslinked silicone 1st network is expected, if every vinyl terminated group of PDMS-V can react with a hydride of D₄H crosslinker. In other words, a stoichiometric ratio of vinyl (V) and hydride of crosslink (H_{D4}) of 1 to 1 or [1:1]. However, because of the lack of information on the precise amount of vinyl of PDMS-V and hydride of D₄H crosslinker, stoichiometric ratios need to be studied and experimentally optimized.

In our system, two parameters to create the network were adjusted, i) toluene composition , and ii) network mesh size controlled by the M_w of PDMS-V. The prepared samples and their compositions are listed on Table 2-3 for PDMS-V $M_w = 6 \text{ kg.mol}^{-1}$ and Table 2-4 for PDMS-V $M_w = 17.2 \text{ kg.mol}^{-1}$.

Toluene/polymer (% V/W)	Stoichiometric ratio		PDMS-V _{6k} (g)	D ₄ H (g)	Pt Karstedt (ppm)
	V _{6k}	H _{D4}			
66.66/33.33	1	1.3	2.395	0.062	20
66.66/33.33	1	1.35	2.395	0.065	20
66.66/33.33	1	1.4	2.395	0.067	20
66.66/33.33	1	1.5	2.395	0.072	20
66.66/33.33	1	1.6	2.395	0.077	20
0/100	1	1.3	2.096	0.055	1 ^(a)
0/100	1	1.35	2.096	0.057	1 ^(a)
0/100	1	1.4	2.096	0.059	1 ^(a)
0/100	1	1.5	2.096	0.063	1 ^(a)

Table 2- 3: Formulation and stoichiometric ratio of 1st network at PDMS-V M_w 6 kg.mol⁻¹, ^(a) with a toluene solvent at 0.005% V/W of total composition

Toluene/polymer (% V/W)	Stoichiometric ratio		PDMS-V _{17k} (g)	D ₄ H (g)	Pt Karstedt (ppm)
	V _{17k}	H _{D4}			
66.66/33.33	1	1.4	2.432	0.024	20
66.66/33.33	1	1.5	2.432	0.026	20
66.66/33.33	1	1.6	2.432	0.027	20
66.66/33.33	1	1.7	2.432	0.029	20
0/100	1	1.4	6.007	0.059	1 ^(a)
0/100	1	1.5	6.007	0.063	1 ^(a)
0/100	1	1.6	6.007	0.067	1 ^(a)
0/100	1	1.7	6.007	0.071	1 ^(a)

Table 2- 4: Formulation and stoichiometric ratio of 1st network at PDMS-V M_w 17200 Kg.mol⁻¹, ^(a) with a toluene solvent at 0.005% V/W of total composition

2.4 Stoichiometry study of silicone prepolymer (2nd network without crosslink)

A silicone loosely crosslinked network or 2nd network is introduced as interpenetrating network in silicone multiple networks. The important feature of this network is its extensibility and loose coupling with the stiff network. In order to optimize this network we proceeded in two steps. In a first step, we prepared a highly viscous fluid by using only PDMS-V and a chain extender PDMS-H. Then by modifying this composition with very small amounts of D₄H crosslinker, we could test the effect of a light but controlled crosslinking. PDMS-V at $M_w = 770 \text{ g.mol}^{-1}$ (PDMS-V₇₇₀) is selected as a precursor because of its low viscosity and small molecular size which is an important property to be able to swell the 1st network before forming silicone multiple networks. The chain length of PDMS-V₇₇₀ is then first extended by using a hydrosilylation reaction with a hydride group of PDMS-H at M_w 400-500 g.mol^{-1} (PDMS-H₄₀₀). To optimize the properties of this composition, the stoichiometric ratio of vinyl group of PDMS-V₇₇₀ (V₇₇₀) and hydride of PDMS-H₄₀₀ (H₄₀₀) are systematically studied.

The composition and stoichiometric ratio between V₇₇₀ and H₄₀₀ in 2nd network study are presented in Table 2-5.

Stoichiometric ratio		PDMS-V ₇₇₀	PDMS-H ₄₀₀	Pt Karstedt
V ₇₇₀	H ₄₀₀	(g)	(g)	(ppm)
1	0.5	1	0.292	30
1	1	1	0.584	30
1	1.2	1	0.701	30
1	1.35	1	0.789	30
1	1.38	1	0.807	30
1	1.4	1	0.818	30
1	1.42	1	0.830	30
1	1.45	1	0.847	30
1	1.5	1	0.877	30

Table 2- 5: Formulation and stoichiometric ratio of 2nd network without crosslink

2.4.1 Curing time of the silicone prepolymer

The curing time of this silicone network is also important. In our study, we were confronted with some problems in setting the curing time of the 2nd network. At first, the silicone loosely crosslinked

network was cured at room temperature for 24 hr following the reaction condition of Pt Karstedt's catalyst. However after the characterization of the mechanical properties by rheometry, we found that the viscosity of the loosely crosslinked networks had significantly changed during storage. This phenomenon came from the higher viscosity of the 2nd network and made the curing process more difficult to complete. In order to avoid this issue, the curing time of the loosely crosslinked network was studied.

Seven different stoichiometric ratios between vinyl groups of PDMS-V₇₇₀ (V₇₇₀) and hydride of PDMD-H (H₄₀₀) were chosen to study the effect of the curing time on the final properties. The sample's composition and stoichiometric ratio as used in this study are shown in Table 2-6. First, PDMS-V₇₇₀ and PDMS-H₄₀₀ were mixed for 15 min and stored at -20°C for an hour. Then another part composition, 30 ppm of Pt Karstedt's catalyst was diluted to 0.005 % V/W of toluene and stored at 4 °C until used.

The two-part mixture was then mixed and stirred for a few minutes before pouring in into the cup of a couette viscometer. The method of this rheology test can be found in Chapter 3. The curing of the sample was tested at a temperature of 60 °C which was controlled by water circulation passing through the couette geometry. The test was performed in a dynamic time sweep test at a control frequency 6.28 rad/s and constant strain rate of 0.1%.

Stoichiometric ratio		PDMS-V ₇₇₀	PDMS-H ₄₀₀	Pt Karstedt
V ₇₇₀	H ₄₀₀	(g)	(g)	(ppm)
1	1.350	2.241	1.768	30
1	1.360	2.241	1.781	30
1	1.365	2.241	1.788	30
1	1.370	2.241	1.794	30
1	1.375	2.241	1.801	30
1	1.380	2.241	1.807	30
1	1.400	2.241	1.834	30

Table 2- 6: Formulation and stoichiometric ratio of the 2nd network without crosslinker for the curing time study

The rheology test showed that depending on the stoichiometry, the 2nd network had different final characteristics and also needed different curing times (Figure 2-10 (a)). At a stoichiometric ratio [1: 1.36]; [V₇₇₀: H₄₀₀] G' and G'' data at long curing time showed that the 2nd network behaved as a viscous fluid. After increasing the ratio of H₄₀₀ to [1: 1.37] the polymer remained a viscous fluid yet

with higher values of G' and G'' . Finally at the ratio [1: 1.38] the polymer became a soft solid as indicated by $G' > G''$. The extensive result and selected stoichiometric ratio will be clearly discussed in Chapter 4.

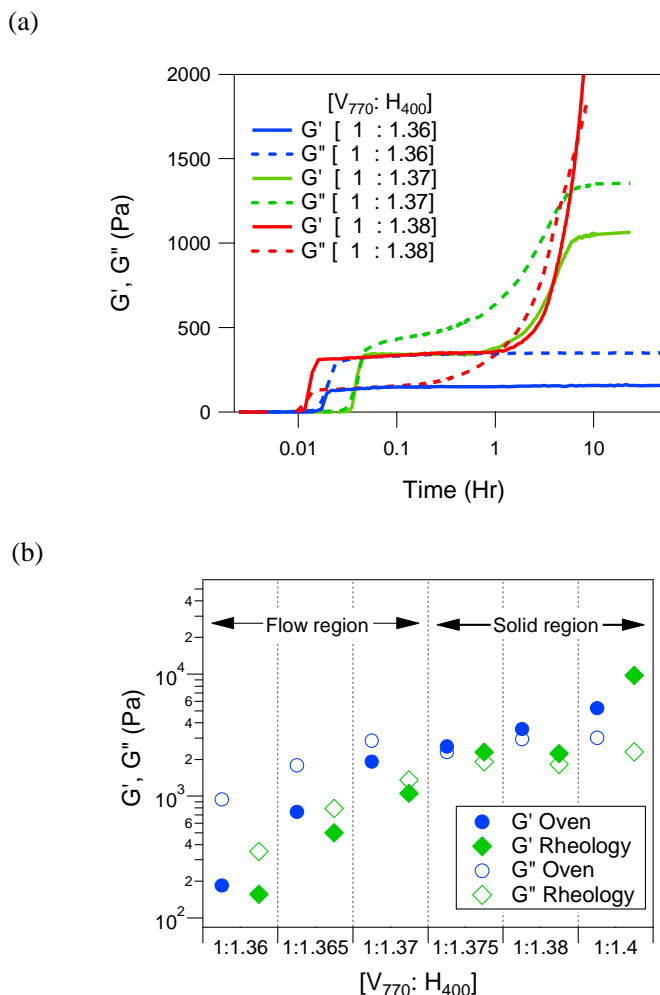


Figure 2- 10: Reaction time of the silicone 2nd network without crosslinker (a) by the couette viscometer, and (b) the comparison with the dynamic mechanical behavior of the 2nd network cured in the oven at 60 °C for 40 hr. and in the couette viscometer at 60°C, frequency 6.28 rad/s for 30 hr

Passing the gelling point was an unwanted property and in order to avoid this we kept the stoichiometric ratio of V_{770} to H_{400} below [1:1.38]. Moreover, if we considered the reaction time, it was found that at the lower H_{400} amount, the reaction reached its equilibrium point faster. However as we focused on the stoichiometric ratio giving materials below the gel point, the ratio [1:1.37], which imposed a reaction time around 30 hr was selected.

Because the curing in the couette viscometer occurs with an applied frequency of 6.28 rad/s, we speculated that this could accelerate the reaction and result in a faster time to equilibrium. Therefore,

in order to make sure that the loosely crosslinked networks were fully cured. We extended the reaction time to 40 hr when curing at 60°C in the oven in quiescent conditions. The comparison between the dynamic mechanical properties of the 2nd network which cured in the oven at 60 °C for 40 hr and cured inside the couette viscometer at 60°C, at a frequency of 6.28 rad/s for 30 hr. is shown in Figure 2-10 (b). The samples cured in the oven were prepared with the same preparation procedure as in section 2.4 and their linear viscoelastic properties were characterized (in the full cured conditions) in a parallel plates TA ARES rheometer a constant frequency of 6.28 rad/s at room temperature. The curing by the two methods did not result in very different values of G' and a little different ones for G''. Both curing methods confirm the gelling point of the 2nd network at a stoichiometric ratio [1:1.375].

2.5 Stoichiometry study of silicone loosely crosslink network (2nd network with crosslink)

In the previous section, the studied silicone polymer without crosslinker provides a highly viscous polymer at the optimized stoichiometric ratio. However, if purely entangled networks are used as the interpenetrating network, they may flow out of the 1st network over time and without connections with the first network they may not reinforce mechanically the network.⁵⁹ For this reason, in this study a small amount of crosslinker is added to the loosely crosslinked network. As we showed in the curing time study above, the gelling point of the 2nd network is at a stoichiometric ratio of V₇₇₀ to H₄₀₀ [1:1.375]. Thus, stoichiometric ratios near this gelling point [1:1.37] were selected in this study. The compositions and stoichiometric ratios used in this study were chosen to maintain the Vinyl/SiH ratio constant and are shown in Table 2-7.

stoichiometric ratio			PDMS-V ₇₇₀	PDMS-H ₄₀₀	D ₄ H	Pt Karstedt
V ₇₇₀	H ₄₀₀	H _{D4}	(g)	(g)	(g)	(ppm)
1	1.36	0.01	2.433	1.934	0.004	30
1	1.34	0.03	2.433	1.906	0.011	30
1	1.32	0.05	2.433	1.877	0.019	30
1	1.27	0.10	2.433	1.806	0.038	30

Table 2- 7: Formulation, stoichiometric ratio and % D₄H (W/W) of 2nd network

2.6 Silicone multiple networks

Silicone multiple networks were synthesized by the multiple sequential interpenetrating network process. The 1st network or highly crosslinked silicone, is swollen with the small precursor molecules of the loosely crosslinked network. One or two sequences of swelling/polymerization can then provide the multiple networks of silicone. The procedure to prepare silicone multiple networks is presented in this part.

2.6.1 Swelling process

The equilibrium swelling ratio of the 1st network is a key factor determining the relative fraction of each network. A first network that is less swellable is undesired due to the need of carrying out several sequential swelling and polymerization steps to sufficiently dilute the 1st network in the silicone multiple network to obtain a mechanical reinforcement. In order to understand the swelling behavior, various silicone 1st networks were swollen to equilibrium with the precursors of the 2nd network.

The 2nd network precursor baths of PDMH-V₇₇₀, PHMS-H₄₀₀ and D₄H were prepared at room temperature. In this swelling study, the Pt Karstedt's catalyst was not introduced for better swelling control. The silicone 1st network was cut in a rectangular shape of 2×2 cm. and the initial weight was measured (W_i) before immersing the sample into the mixing precursor bath. The bath was kept at room temperature without light exposure. At regular intervals the samples were taken out, cleaned with tissue paper before recording their weight (W_t). The swelling was continued up to 48 hr and the % swelling could be calculated by using Eq.2-1. The composition of 1st network and 2nd network used in this study are shown in Table 2-8.

$$\%swelling = \left(\frac{W_t - W_i}{W_i} \right) \times 100 \quad Eq. 2 - 1$$

(a) 1st network

Sample	Toluene/polymer (% V/W)	Stoichiometric ratio		PDMS-V (g)	D ₄ H (g)	Pt Karstedt (ppm)
		V	H _{D4}			
SN _{6k,66%} T	66.66/33.33	1	1.35	2.096	0.057	20
SN _{6k,0%} T	0/100	1	1.5	6.237	0.188	1 ^(a)
SN _{17k,66%} T	66.66/33.33	1	1.5	2.289	0.240	20
SN _{17k,0%} T	0/100	1	1.6	6.150	0.069	5 ^(a)

(b) 2nd network

stoichiometric ratio			PDMS-V ₇₇₀ (g)	PDMS-H ₄₀₀ (g)	D ₄ H (g)	Pt Karstedt (ppm)
V ₇₇₀	H ₄₀₀	H _{D4}				
1	1.35	0.02	4.482	3.536	0.014	0

Table 2- 8: Formulation and stoichiometric ratio of (a) 1st network and (b) 2nd network used in the swelling study, ^(a) with a toluene solvent at 0.001% V/W of total composition

The equilibrium swelling ratios for each 1st network are shown in Figure 2-11. We found that for the silicone small mesh size network in which the 1st network was created by PDMS-V_{6k} the equilibrium swelling was approached after 9 hr. On the other hand, the silicone with a larger mesh size network, synthesized with the PDMS-V_{17k} started to reach an equilibrium swelling at 15 hr. This behavior may be due to a lower collective diffusion coefficient of PDMS precursors into the looser mesh due to entanglements. Moreover, the silicone 1st network made in the presence of toluene showed a slightly decreased % swelling after their maximum point.

Thus, we set the swelling time of the 1st network for fabricating silicone multiple networks at 15 hr. in order to reach an equilibrium swelling and absorb the largest amount of small molecules. However, since the 1st network of PDMS-V_{6k} synthesized in the absence of solvent shows a lower %swelling (~100%) which was not efficient for silicone multiple network creation. It was decided not to use this 1st network to synthesize multiple networks.

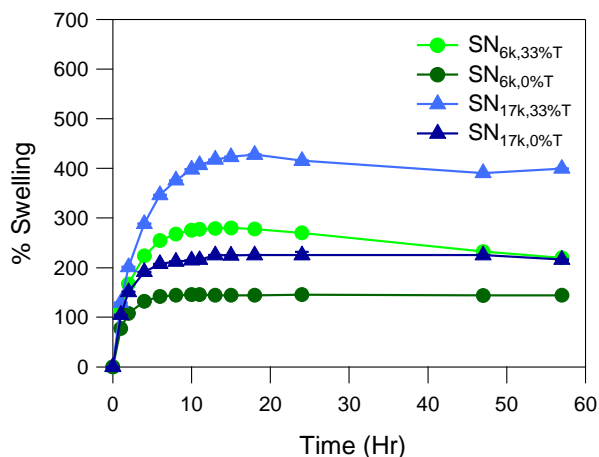


Figure 2- 11: Rate of swelling of silicone 1st network

2.6.2 Synthesis and reaction conditions of the multiple networks

Silicone multiple networks were prepared by first swelling the dry first network (as described above) in the solution of the precursors of the silicone 2nd network and then carry out the polymerization step in sequence. First, the bath of the precursor solution needs to be prepared. PDMS-V₇₇₀, PDMS-H₄₀₀ and D₄H crosslinker were prepared in a 20 ml tube and stirred about 10 minutes before storing at -20°C for an hour. Then the Pt Karstedt's catalyst was diluted with a small amount of toluene 0.001 % V/W of total composition and added to the cold 2nd network solution. The tube was stirred for a few minutes before pouring it into a container and kept at -20°C until needed. A piece of 1st network, core network was prepared and weighted before immersing it into 2nd network liquid bath rapidly. The solution was maintained at -20°C for one night to avoid reaction before swelling (about 15 hr following the equilibrium swelling ratio of 1st network). Then the swelled 1st network was removed from the bath and gently cleaned with a tissue paper to eliminate the excess of small molecules. The sample was then placed on a release liner before curing in an oven at 60 °C for 40 hr, and post cured at 100°C for 2 hr. After curing the sample was removed and washed and dried as discussed in the previous section. The final samples were stored at room temperature until later use. These samples were named silicone double network (DN).

To prepare other multiple networks, which were triple networks (TN) or quadruple (QN) networks, the same procedure was repeated using the silicone (n) networks as the starting material and carrying out the swelling, washing and drying step as described previously. The final product is then a silicone (n+1) networks which could be TN or QN depending on the starting network. The method to prepare silicone multiple networks is described schematically in Figure 2-12.

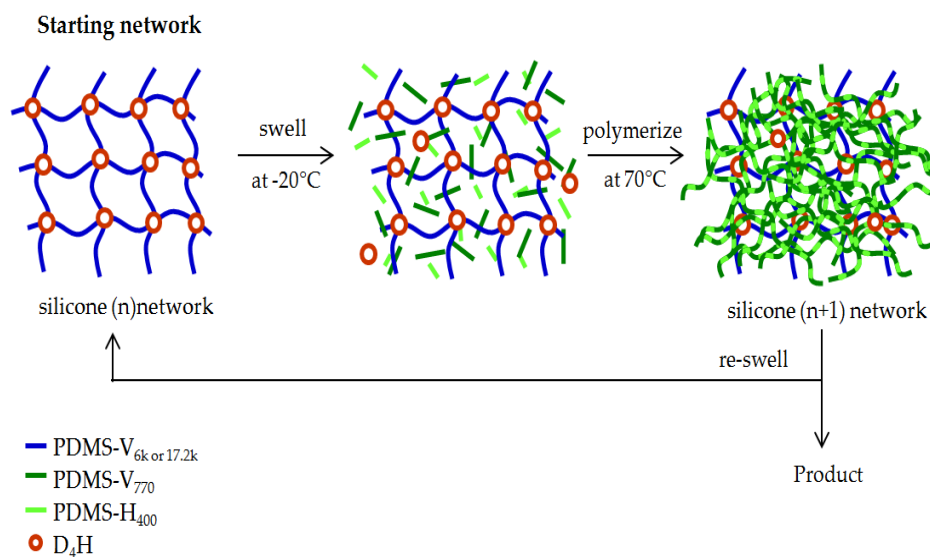


Figure 2- 12: silicone multiple networks procedure.

The effect of introducing a small amount of crosslinker in the interpenetrating network was also studied. The stoichiometric ratios and formulation of silicone 1st networks and interpenetrating network or 2nd networks which have been used in silicone multiple network are summarized in Table 2-9.

(a) 1st network

Sample	Toluene/polymer (% V/W)	Stoichiometric ratio		PDMS-V (g)	D ₄ H (g)	Pt Karstedt (ppm)
		V	H _{D4}			
SN _{6k,66%T}	66.66/33.33	1	1.35	2.096	0.058	20
SN _{17k,66%T}	66.66/33.33	1	1.5	2.289	0.240	20
SN _{17k,0%T}	0/100	1	1.6	6.150	0.069	5 ^(a)

(b) 2nd network

stoichiometric ratio			PDMS-V ₇₇₀ (g)	PDMS-H ₄₀₀ (g)	D ₄ H (g)	Pt Karstedt (ppm)
V ₇₇₀	H ₄₀₀	H _{D4}				
1	1.36	0.01	6.403	5.089	0.010	30
1	1.36	0.02	6.403	5.052	0.020	30
1	1.36	0.03	6.403	5.014	0.030	30

Table 2- 9 : Formulation and stoichiometric ratio of (a) 1st network and (b) 2nd network used to create silicone multiple networks, ^(a) with a toluene solvent at 0.001% V/W of total composition

To determine the composition of the final silicone multiple networks sample, we calculated the weight fraction of silicone (n+1) network ($\phi_{wt}^{(n)}$) from the initial weight of the starting network or silicone (n) network ($W_{i(n)}$) and the weight of the final sample after swelling ($W_{f(n+1)}$) by following the Eq.2-2

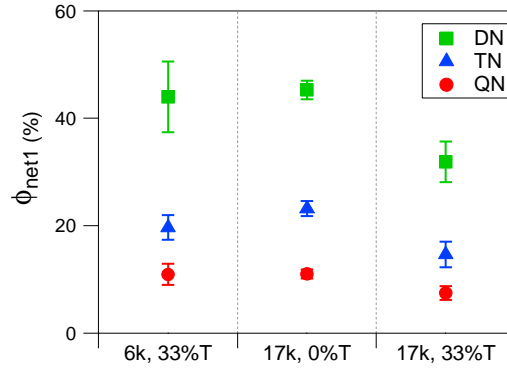
$$\phi_{wt}^{(n)} = \frac{W_{i(n)}}{W_{f(n+1)}} \quad \text{Eq. 2 - 2}$$

The prestretching of the chains of the first network (λ_0) can be calculated from Eq.2-3.

$$\lambda_0 = \frac{1}{(\phi_{wt}^{SN})^{1/3}} \quad \text{Eq. 2 - 3}$$

In our study, we prepared multiple networks from three different 1st networks; SN_{6k,66%T}, SN_{17k,0%T}, and SN_{17k,66%T}. The compositions of the silicone multiple networks made from each starting network are shown in Table 2-10. For each system we used three different crosslinker amounts in the interpenetrating network were and although the crosslinker quantity should not in principle affect to the swelling behavior of the 1st network, we found that for the silicone 1st network with short mesh size (SN_{6k,66%T}) there was some variation of the equilibrium swelling (Figure 2-13(a)). Moreover, it was clearly shown that introducing toluene when synthesizing the 1st network can increase its equilibrium swelling ratio as shown by the lower value of ϕ_{net1} in the multiple networks prepared from the SN_{17k,66%T} comparing with the SN_{17k,0%T}. Unsurprisingly, because of the higher swelling ratio in the system SN_{17k,66%T}, the prestretching of the chains of the 1st network in this system was also higher compared with that of the others (Figure 2-13(b))

(a)



(b)

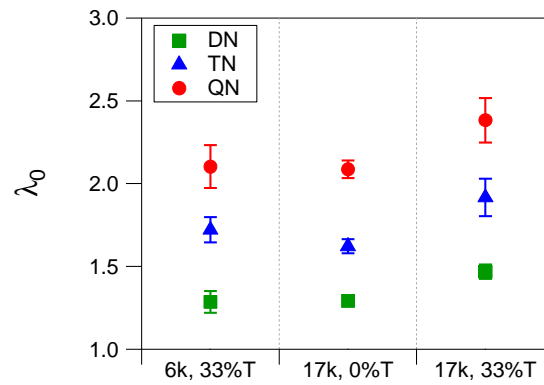


Figure 2- 13: Characteristics of silicone multiple networks, (a) weight fraction of the 1st network in different synthesis systems, and (b) prestretching λ_0 of the chains of the 1st network in different synthesis systems.

Silicone multiple networks of PDMS-V 6 kg.mol⁻¹ with 66% wt toluene

sample	[0.01 H _{D4}]					[0.02 H _{D4}]					[0.03 H _{D4}]				
	$\Phi_{\text{SN},0}$	$\Phi_{\text{net2},1}$	$\Phi_{\text{net2},2}$	$\Phi_{\text{net2},3}$	λ_0	$\Phi_{\text{SN},0}$	$\Phi_{\text{net2},1}$	$\Phi_{\text{net2},2}$	$\Phi_{\text{net2},3}$	λ_0	$\Phi_{\text{SN},0}$	$\Phi_{\text{net2},1}$	$\Phi_{\text{net2},2}$	$\Phi_{\text{net2},3}$	λ_0
SN	100				1	100				1	100				1
DN	44	56			1.31	42	58			1.33	56	44			1.21
TN	21	46	34		1.69	17	47	36		1.81	22	38	40		1.67
QN	13	31	33	23	1.98	11	30	32	27	2.09	9	34	31	25	2.24

Silicone multiple networks of PDMS-V 17.2 kg.mol⁻¹ with solvent-free system

sample	[0.01 H _{D4}]					[0.02 H _{D4}]					[0.03 H _{D4}]				
	$\Phi_{\text{SN},0}$	$\Phi_{\text{net2},1}$	$\Phi_{\text{net2},2}$	$\Phi_{\text{net2},3}$	λ_0	$\Phi_{\text{SN},0}$	$\Phi_{\text{net2},1}$	$\Phi_{\text{net2},2}$	$\Phi_{\text{net2},3}$	λ_0	$\Phi_{\text{SN},0}$	$\Phi_{\text{net2},1}$	$\Phi_{\text{net2},2}$	$\Phi_{\text{net2},3}$	λ_0
SN	100				1	100				1	100				1
DN	48	52			1.28	46	54			1.29	45	55			1.30
TN	25	42	33		1.59	22	41	37		1.67	24	42	34		1.62
QN	11	32	27	29	2.06	10	32	28	30	2.15	12	30	29	30	2.05

Silicone multiple networks of PDMS-V 17.2 kg.mol⁻¹ with 66% wt toluene

sample	[0.01 H _{D4}]					[0.02 H _{D4}]					[0.03 H _{D4}]				
	$\Phi_{\text{SN},0}$	$\Phi_{\text{net2},1}$	$\Phi_{\text{net2},2}$	$\Phi_{\text{net2},3}$	λ_0	$\Phi_{\text{SN},0}$	$\Phi_{\text{net2},1}$	$\Phi_{\text{net2},2}$	$\Phi_{\text{net2},3}$	λ_0	$\Phi_{\text{SN},0}$	$\Phi_{\text{net2},1}$	$\Phi_{\text{net2},2}$	$\Phi_{\text{net2},3}$	λ_0
SN	100				1	100				1	100				1
DN	34	66			1.43	29	71			1.52	32	68			1.46
TN	17	49	33		1.79	13	49	39		2.00	13	49	38		1.97
QN	7	37	28	27	2.39	9	33	31	27	2.24	6	37	31	26	2.51

Table 2- 10: Compositions of silicone multiple networks, prepared from silicone 1st networks of Table 2-9 (a), Φ is showed in percentage (%) and Φ_{net2} is volume fraction of silicone 2nd network in multiple network

Conclusion

In this chapter, we have described the synthesis of multiple interpenetrated networks based on polydimethyl siloxane. Silicone multiple networks were created by sequential swelling and polymerization steps in order to progressively stretch the first network strands and create sacrificial bonds inside the material to dissipate energy and delay the macroscopic fracture of the material. The core network of the PDMS multiple network was designed to be a well crosslinked stiff network while the PDMS interpenetrating network was designed to be extensible to expand the dissipative volume. Both types of PDMS networks were synthesized via a hydrosilylation reaction. The optimal stoichiometric ratio or effective stoichiometric ratio (r_e) was determined for each network separately by maximizing the elastic modulus and targeting the gel point respectively. Silicone multiple networks were made from 3 different 1st networks: a small mesh size network made from PDMS- V_{6k} precursors in the presence of 66%wt toluene ($SN_{6k, 66\%T}$), and two large mesh size network made either from PDMS- V_{17k} in the absence of solvent ($SN_{17k, 0\%T}$) or from PDMS- V_{17k} in the presence of 66%wt toluene ($SN_{17k, 66\%T}$). Three different amounts of crosslinker have been used as the interpenetrating network in each silicone 1st network. Now, in the next chapter we will focus on the mechanical properties of the samples described in this chapter.

References

1. Clarson, S.J., *Silicones and Silicone-Modified Materials: A Concise Overview*, 2003. (Synthesis and Properties of Silicones and Silicone-Modified Materials), American Chemical Society. p. 1-10.
2. Rasappa, S., et al., *Rapid, Brushless Self-assembly of a PS-b-PDMS Block Copolymer for Nanolithography*. Colloids and Interface Science Communications, 2014. **2**(Supplement C): p. 1-5.
3. Stricher, A.M., et al., *How I met your elastomers: from network topology to mechanical behaviours of conventional silicone materials*. RSC Advances, 2015. **5**(66): p. 53713-53725.
4. Rajan, K.P., et al., *Blends of Thermoplastic Polyurethane and Polydimethylsiloxane Rubber: Assessment of Biocompatibility and Suture Holding Strength of Membranes*. International Journal of Biomaterials, 2013. **2013**: p. 240631.
5. Li, J.P., et al., *Efficient hydrosilylation reaction in polymer blending: An original approach to structure PA12/PDMS blends at multiscales*. Polymer, 2017. **112**(Supplement C): p. 10-25.
6. Hillerström, A., et al., *Transparency and wettability of PVP/PDMS-IPN synthesized in different organic solvents*. Journal of Applied Polymer Science, 2009. **114**(3): p. 1828-1839.
7. Turner, J.S. and Y.L. Cheng, *Preparation of PDMS–PMAA Interpenetrating Polymer Network Membranes Using the Monomer Immersion Method*. Macromolecules, 2000. **33**(10): p. 3714-3718.
8. Klasner, S.A., et al., *Synthesis and Characterization of a Poly(dimethylsiloxane)–Poly(ethylene oxide) Block Copolymer for Fabrication of Amphiphilic Surfaces on Microfluidic Devices*. Langmuir, 2009. **25**(17): p. 10390-10396.
9. Ducrot, E., et al., *Toughening Elastomers with Sacrificial Bonds and Watching them Break*. Science, 2014. **344**(6180): p. 186-189.
10. Ducrot, E. and C. Creton, *Characterizing Large Strain Elasticity of Brittle Elastomeric Networks by Embedding Them in a Soft Extensible Matrix*. Advanced Functional Materials, 2016. **26**(15): p. 2482-2492.
11. Ducrot, E., *Innovative tough elastomers: Designed sacrificial bonds in multiple networks*, 2013. (Unpublished doctoral dissertation): University Pierre and Marie Curie, Paris, France.
12. Yilgör, E. and I. Yilgör, *Silicone containing copolymers: Synthesis, properties and applications*. Progress in Polymer Science, 2014. **39**(6): p. 1165-1195.
13. Zhou, H., et al., *PDMS/PVDF composite pervaporation membrane for the separation of dimethyl carbonate from a methanol solution*. Journal of Membrane Science, 2014. **471**: p. 47-55.

14. Firpo, G., et al., *Permeability thickness dependence of polydimethylsiloxane (PDMS) membranes*. Journal of Membrane Science, 2015. **481**(Supplement C): p. 1-8.
15. Larmagnac, A., et al., *Stretchable electronics based on Ag-PDMS composites*. Sci Rep, 2014. **4**: p. 7254.
16. Morent, R., et al., *Adhesion enhancement by a dielectric barrier discharge of PDMS used for flexible and stretchable electronics*. Journal of Physics D: Applied Physics, 2007. **40**(23): p. 7392-7401.
17. de Buyl, F., *Silicone sealants and structural adhesives*. International Journal of Adhesion and Adhesives, 2001. **21**(5): p. 411-422.
18. Prauzner-Bechcicki, S., et al., *PDMS substrate stiffness affects the morphology and growth profiles of cancerous prostate and melanoma cells*. J Mech Behav Biomed Mater, 2015. **41**: p. 13-22.
19. Genchi, G.G., et al., *Bio/non-bio interfaces: a straightforward method for obtaining long term PDMS/muscle cell biohybrid constructs*. Colloids and Surfaces B: Biointerfaces, 2013. **105**: p. 144-151.
20. Peterson, S.L., et al., *Poly(dimethylsiloxane) thin films as biocompatible coatings for microfluidic devices: Cell culture and flow studies with glial cells*. Journal of Biomedical Materials Research Part A, 2005. **72A**(1): p. 10-18.
21. Warrick, E.L., et al., *Silicone Elastomer Developments 1967–1977*. Rubber Chemistry and Technology, 1979. **52**(3): p. 437-525.
22. Andriot, M., et al., *Silicones in Industrial Applications*, 2009. (Inorganic Polymers), R.D. Jaeger and M. Gleria, Editors, Nova Science Publishers Inc: United States.
23. Camenzind, A., et al., *Structure & strength of silica-PDMS nanocomposites*. Polymer, 2010. **51**(8): p. 1796-1804.
24. Kulik, V., et al., *Viscoelastic properties of silicone rubber with admixture of SiO₂ nanoparticles*. Materials Science and Engineering: A, 2011. **528**(18): p. 5729-5732.
25. Kaneko, M.L.Q.A., et al., *High molar mass silicone rubber reinforced with montmorillonite clay masterbatches: Morphology and mechanical properties*. European Polymer Journal, 2010. **46**(5): p. 881-890.
26. Osman, M.A., et al., *Reinforcement of poly(dimethylsiloxane) networks by mica flakes*. Polymer, 2001. **42**(15): p. 6545-6556.
27. Brook, M.A., *Silicon in organic, organometallic, and polymer chemistry*. 2000: J. Wiley.
28. Lewis, L.N., et al., *Platinum Catalysts Used in the Silicones Industry, Their Synthesis and Activity in Hydrosilylation*. Platinum Metals Review, 1997. **41**(2): p. 66.
29. Viers, B.D. and J.E. Mark, *Large-Scale Structures in Some End-Linked Polysiloxane Networks: A Critical Review*, 2007. (Science and Technology of Silicones and Silicone-Modified Materials), American Chemical Society. p. 136-164.

30. Lewis, L.N., et al., *Platinum Catalysts Used in the Silicones Industry*. Platinum Metals Review, 1997. **41**(2): p. 66-75.
31. Chalk, A.J. and J.F. Harrod, *Homogeneous Catalysis. II. The Mechanism of the Hydrosilation of Olefins Catalyzed by Group VIII Metal Complexes I*. Journal of the American Chemical Society, 1965. **87**(1): p. 16-21.
32. Nakatani, N., et al., *Platinum-catalyzed reduction of amides with hydrosilanes bearing dual Si-H groups: a theoretical study of the reaction mechanism*. Dalton Transactions, 2015. **44**(44): p. 19344-19356.
33. Bokobza, L., *Elastomeric composites. I. Silicone composites*. Journal of Applied Polymer Science, 2004. **93**(5): p. 2095-2104.
34. Ponnammma, D., et al., *Rubber Nanocomposites: Latest Trends and Concepts*, 2013. (Advances in Elastomers II: Composites and Nanocomposites), M.P. Visakh, et al., Editors, Springer Berlin Heidelberg: Berlin, Heidelberg. p. 69-107.
35. LeBaron, P.C. and T.J. Pinnavaia, *Clay Nanolayer Reinforcement of a Silicone Elastomer*. Chemistry of Materials, 2001. **13**(10): p. 3760-3765.
36. Pinnavaia, T.J., *Intercalated clay catalysts*. Science, 1983. **220**(4595): p. 365-71.
37. Zhang, J., et al., *Silicone-modified graphene oxide fillers via the Piers-Rubinsztajn reaction*. Journal of Polymer Science Part A: Polymer Chemistry, 2016. **54**(15): p. 2379-2385.
38. Verdejo, R., et al., *Functionalized graphene sheet filled silicone foam nanocomposites*. Journal of Materials Chemistry, 2008. **18**(19): p. 2221-2226.
39. Yadav, S.K., et al., *PDMS/MWCNT nanocomposite actuators using silicone functionalized multiwalled carbon nanotubes via nitrene chemistry*. Journal of Materials Chemistry C, 2013. **1**(35): p. 5463-5470.
40. Ci, L., et al., *Continuous Carbon Nanotube Reinforced Composites*. Nano Letters, 2008. **8**(9): p. 2762-2766.
41. Goldberg, G., et al., *The effect of multiwall carbon nanotubes on the properties of room temperature-vulcanized silicone adhesives*. Journal of Adhesion Science and Technology, 2014. **28**(17): p. 1661-1676.
42. Huang, X., et al., *Reinforcement of polysiloxane with superhydrophobic nanosilica*. Journal of Materials Science, 2009. **44**(17): p. 4522-4530.
43. Baumann, T.F., et al., *Synthesis and characterization of novel PDMS nanocomposites using POSS derivatives as cross-linking filler*. Journal of Polymer Science Part A: Polymer Chemistry, 2009. **47**(10): p. 2589-2596.
44. Pan, G., J.E. Mark, and D.W. Schaefer, *Synthesis and characterization of fillers of controlled structure based on polyhedral oligomeric silsesquioxane cages and their use in reinforcing siloxane elastomers*. Journal of Polymer Science Part B: Polymer Physics, 2003. **41**(24): p. 3314-3323.

45. Deng, S., et al., *Microcrystalline cellulose as reinforcing agent in silicone elastomers*. Carbohydrate Polymers, 2016. **151**: p. 899-906.
46. Heinrich, G. and M. Klüppel, *Recent Advances in the Theory of Filler Networking in Elastomers*, 2002. (Filled Elastomers Drug Delivery Systems), Springer Berlin Heidelberg: Berlin, Heidelberg. p. 1-44.
47. Shajii, L. and J. Paul Santerre, *Effect of filler content on the profile of released biodegradation products in micro-filled bis-GMA/TEGDMA dental composite resins*. Biomaterials, 1999. **20**(20): p. 1897-1908.
48. Chawla, A.S., *Toxicity evaluation of a novel filler free silicone rubber biomaterial by cell culture techniques*. Journal of Biomedical Materials Research, 1982. **16**(4): p. 501-508.
49. Caughman, W.F., et al., *Correlation of cytotoxicity, filler loading and curing time of dental composites*. Biomaterials, 1991. **12**(8): p. 737-740.
50. Bleach, N.C., et al., *Effect of filler content on mechanical and dynamic mechanical properties of particulate biphasic calcium phosphate—polylactide composites*. Biomaterials, 2002. **23**(7): p. 1579-1585.
51. Greenberg, A.R., *Influence of filler chemistry on the glass transition behaviour of a polymer matrix composite material*. Journal of Materials Science Letters, 1987. **6**(1): p. 78-80.
52. Mazurek, M., *Silicone Copolymer Networks and Interpenetrating Polymer Networks*, 2000. (Silicon-Containing Polymers ,The Science and Technology of Their Synthesis and Applications), W.A. Richard G. Jones, Julian Chojnowski, Editor, Springer Netherlands. p. 113-137.
53. Hamurcu, E.E. and B.M. Baysal, *Interpenetrating polymer networks of poly(dimethylsiloxane) with polystyrene, polybutadiene and poly(glycerylpropoxytriacylate)*. Macromolecular Chemistry and Physics, 1995. **196**(4): p. 1261-1276.
54. Vidal, F., et al., *Polysiloxane–Cellulose acetate butyrate cellulose interpenetrating polymers networks close to true IPNs on a large composition range. Part II*. Polymer, 2006. **47**(11): p. 3747-3753.
55. Huang, G.-S., Q. Li, and L.-X. Jiang, *Structure and damping properties of polydimethylsiloxane and polymethacrylate sequential interpenetrating polymer networks*. Journal of Applied Polymer Science, 2002. **85**(3): p. 545-551.
56. Urayama, K. and S. Kohjiya, *Extensive stretch of polysiloxane network chains with random- and super-coiled conformations*. The European Physical Journal B - Condensed Matter and Complex Systems, 1998. **2**(1): p. 75-78.
57. Kohjiya, S., K. Urayama, and Y. Ikeda, *Poly(siloxane) network of ultra-high elongation*. Kautschuk und Gummi Kunststoffe, 1997. **50**(12): p. 868-872.
58. Lee, J.N., C. Park, and G.M. Whitesides, *Solvent Compatibility of Poly(dimethylsiloxane)-Based Microfluidic Devices*. Analytical Chemistry, 2003. **75**(23): p. 6544-6554.

59. Nakajima, T., et al., *True chemical structure of double network hydrogels*. *Macromolecules*, 2009. **42**(6): p. 2184-2189.

-CHAPTER 3-

Mechanical properties and characterization of Silicone multiple networks

Chapter 3: Mechanical properties and characterization of silicone multiple networks.....	69
Introduction.....	71
1. Materials and methods.....	72
1.1 Rheology experiments	72
1.1.1 Steady shear testing.....	72
1.1.2 Dynamic mechanical testing.....	73
1.2 Mechanical testing experiments.....	74
1.2.1 Tensile test.....	75
1.2.2 Step-cycle extension.....	76
1.2.3 Fracture in a single edge notch test.....	77
2. Effect of Stoichiometry on the mechanical properties of simple silicone networks.....	79
2.1 Silicone highly crosslinked networks (1 st network).....	79
2.1.1 Stoichiometry of silicone small mesh size networks, using PDMS-V _{6k}	79
2.1.2 Stoichiometry of silicone large mesh size networks, using PDMS-V _{17k}	82
2.1.3 Selection of the 1 st networks: summary.....	85
2.2 Silicone loosely crosslinked networks (2 nd network).....	85
2.2.1 Optimization of the stoichiometry of silicone prepolymer without any crosslinker	86
2.2.2 Dynamic rheology of silicone prepolymer without crosslinker.....	87
2.3 Loosely crosslinked networks of silicone.....	90
3. Silicone multiple networks.....	92
3.1 Silicone multiple networks based on PDMS-V _{6k} made in solvent.....	92
3.2 Silicone multiple networks based on PDMS-V _{17k} synthesized in the bulk.....	95
3.3 Silicone multiple networks based on PDMS-V _{17k} made in solvent.....	98
4. Energy dissipation characteristic of silicone multiple networks.....	102
5. Fracture mechanic of silicone multiple networks.....	103
Conclusion.....	105
References.....	106

Introduction

In our study, we tried to broaden to silicone systems the scope of the reinforcement technique using interpenetrating networks (IPNs) containing sacrificial bonds. This method has been invented and first used to reinforce hydrogels,^{1,2} creating tough IPNs of highly swollen hydrogels and later was successfully applied to toughen acrylate elastomers.^{3,4} In our study, we synthesized silicone networks via a hydrosilylation reaction, which is different from the polymerization reaction used in the acrylate system (addition polymerization). The details of the synthesis method was presented in Chapter 2. In this chapter, the mechanical properties of silicone simple networks (1st networks or 2nd networks) and silicone interpenetrated multiple networks will be described and discussed.

The silicone 1st network which is a highly crosslinked network was prepared with two different M_w of PDMS-Vinyl terminated (PDMS-V), $M_w = 6 \text{ kg.mol}^{-1}$ (PDMS-V_{6k}) and $M_w = 17 \text{ kg.mol}^{-1}$ (PDMS-V_{17k}), creating different mesh sizes of the network. The silicone 2nd network which is a loosely crosslink network that needs to be extensible and loosely coupled to 1st network was synthesized with a combination of low M_w PDMS-V (for its ability to swell the 1st network), multifunctional SiH chain extenders and crosslinkers. We first determined empirically the best stoichiometric ratios or called effective stoichiometric ratio (r_e) for each silicone systems in order to achieve the best mechanical performance of the networks. For the 1st network we chose the stoichiometric ratio giving the highest modulus, while for the 2nd network we first determined the gel point with linear chain extenders, then positioned ourselves just below the gel point and added small amounts of D₄H crosslinker to vary the extensibility of the network. We determined the optimum ratio r_e of the 4 different systems of silicone 1st network which were PDMS-V $M_w 6 \text{ kg.mol}^{-1}$ (PDMS-V_{6k}) in the presence of solvent and in bulk conditions and PDMS-V $M_w 17 \text{ kg.mol}^{-1}$ (PDMS-V_{17k}) in solvent and in bulk conditions. Once the stoichiometric conditions were fixed, multiple networks were synthesized in several steps as described in chapter 2. The mechanical properties of the resulting silicone multiple networks were characterized first in uniaxial extension to failure and then with step cycle extension tests and fracture toughness tests on single edge notch samples.

In this chapter we will first describe the testing methods and then report the mechanical properties of the silicone multiple networks made from different starting 1st network and with different degrees of crosslink of the 2nd network.

1. Materials and methods

1.1 Rheology experiments

The viscoelastic properties of the silicone loosely crosslinked networks (2nd network) were investigated with an ARES (Advanced Rheometric Expansion System) rheometer from TA instruments. The testing temperature was adjusted with a circulating water bath (Julabo model FS18) and the experiments were controlled and recorded by the TA Orchestrator software from TA instrument.

1.1.1 Steady shear testing

Steady shear testing is used to study the behavior of fluids by using a continuous rotation to apply strain. When a steady shear rate is reached, the shear stress (τ) is measured as a function of the shear rate ($d\gamma/dt$). The steady shear viscosity (η) can be calculated from Eq.3-1.

$$\tau = \eta \frac{d\gamma}{dt} \quad \text{Eq. 3 - 1}$$

We used the steady shear testing to characterize the viscosity and behavior of the silicone 2nd network as a function of stoichiometry. The ARES rheometer was set to the steady shear rate sweep mode with an initial shear rate set at 0.01 s^{-1} and a final shear rate set at 10 s^{-1} . The tests were performed at 25°C controlled by the circulating water bath with the cone and plate geometry, the cone angle was 0.04 radians, the diameter 25 mm (Figure 3-1(a)) and the gap between geometry and the sample load was set to 0.045 mm. However, in some cases, the viscosity of the sample was too high and the gap could not be set. The geometry was then changed to the parallel plates geometry, with a 25 mm diameter and a 1.5-2 mm gap (Figure 3-1(b)).

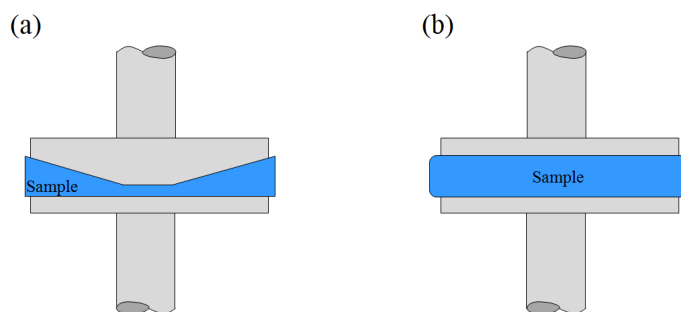


Figure 3- 1: Geometry of ARES rheometer, (a) cone and plate with sample loaded, and (b) parallel plates with sample loaded

1.1.2 Dynamic mechanical testing⁵

Dynamic mechanical testing involves the application of an oscillatory strain to the sample. The resulting sinusoidal stress is measured and correlated with the input strain, so that the viscous and elastic properties of the sample are simultaneously measured. When it is performed in the linear regime, the test method provides a complex modulus (typically an amplitude and a phase shift between stress and strain). The stress signal generated by a viscoelastic material can be separated into two components; an elastic stress (τ'), in phase with the strain, and a viscous stress (τ''), in phase with the strain rate ($d\gamma / dt$) or 90° out of phase with the strain. By separating the stress into these components, both strain amplitude and strain rate dependence of a material can be simultaneously measured.

The viscous and elastic stresses can be related to material properties through the ratio of stress to strain, or modulus. The ratio of the elastic stress to strain is referred to as the elastic (or storage) modulus (G'), and the ratio of viscous stress to strain is referred to as the viscous (or loss) modulus (G''). The complex modulus (G^*) is a measure of the overall resistance of a material to deformation.

Three different operation modes of dynamic mechanical testing were applied to study the mechanical properties of the silicone 2nd network.

- **Dynamic strain sweep**

Dynamic strain sweep was performed in order to determine the limits of linear viscoelasticity and torque levels. The 2nd network samples were tested with the parallel plates geometry, diameter 25 mm with an initial strain 0.01% and final strain 100%. The testing temperature was controlled at 25°C and the frequency of the machine was set at 6.28 rad.s⁻¹ or 1 Hz.

- **Dynamic frequency sweep**

The silicone 2nd networks were characterized in the linear regime with a dynamic frequency sweep in order to analyze the frequency dependent behavior of the samples. The ARES rheometer was set with the parallel plates geometry, diameter 25 mm and the frequency was varied from 0.1 rad.s⁻¹ to 100 rad.s⁻¹. The testing temperature was controlled at 25 °C at the constant strain of 0.5%.

- **Dynamic time sweep**

The dynamic time sweep mode was applied in our study in order to characterize the curing behavior of the silicone 2nd network. The silicone 2nd network compositions; Poly(dimethylsiloxane) vinyl dimethylsiloxy terminated (PDMS-V), Mw 770 g.mol⁻¹, Poly(dimethylsiloxane) hydride terminated (PDMS-H), Mw 400 g.mol⁻¹ and Pt Karstedt's catalyst were introduced into a cup of a Couette geometry (Figure 3-2). The blend of reactants was loaded in the cup until the bob was covered and the test was then carried out at the curing

temperature of 60 °C. The frequency and the strain were set to be constant at 6.28 rad.s⁻¹ or 1 Hz and 0.5 % respectively. The dynamic mechanic properties such as G' , G'' , G^* and tan delta were recorded every 5 minutes along the experiment.

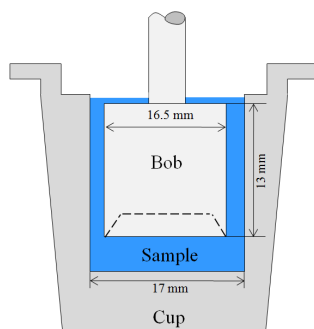


Figure 3- 2: Experimental setup and dimensions of coquette geometry with sample loaded

1.2 Mechanical testing experiments

The tensile tests of the cured silicone materials were carried out on a standard tensile Instron machine, model 5565 fitted with a 10 N or a 100 N load cell. A video extensometer, model SVE was used to follow the relative displacement of markers placed in the homogeneously deformed zone of the sample. The relative uncertainty of the measurement given by the load cell and the video extensometer are respectively 0.1% in the range of 0-100 N and 0.11% at the full scale of 120 mm.

The specimens were cut in to a shape and clamped between pneumatic clamps (Figure 3-3) which allowed a fine control of the pressure in the clamps to avoid slippage or damage of the sample from a too high or too low compressive clamping force. All mechanical tests were performed at room temperature which was controlled at 23-25 °C.

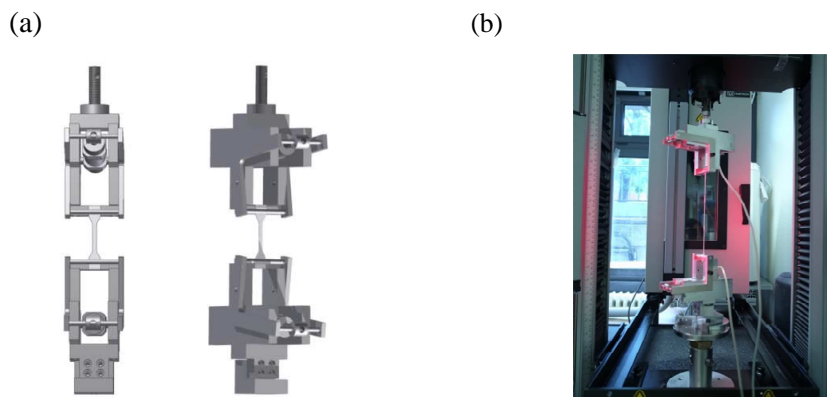


Figure 3- 3: Pneumatic clamps for mechanical testing (a) scheme of the clamp³, (b) picture of the clamps during the tensile test

1.2.1 Tensile tests

Tensile tests in uniaxial tension were performed on the silicone 1st network samples, the silicone 2nd network with crosslink samples and the silicone multiple networks samples. The specimens were cut in a dumbbell shape using a die cutter. The gauge length of the central part used for the strain measurement is around 20 mm. The cross-section is 4 mm in width (w) and a thickness (h) fixed by the samples themselves between 0.5-2.5 mm, depending on the number of sequential swelling/polymerization steps in the silicone multiple networks.

To follow precisely the relative displacement in the deformed zone of the sample, the sample was marked in two spots with a white paint in the center zone to allow the deformation measurement via the video extensometer. The sample dimension with the markers for the tensile test is shown in Figure 3-4.

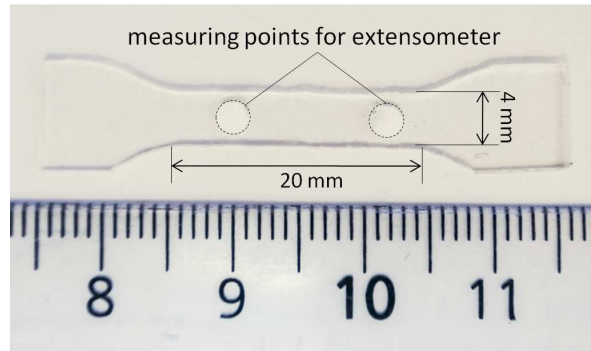


Figure 3- 4: Sample for tensile test

Uniaxial extension tests were carried out at a constant velocity of the crosshead speed of 500 $\mu\text{m.s}^{-1}$ and the typical initial strain rate on the central part of the sample was around 0.02 s^{-1} , with the gauge length around 10 mm.

The force (F) and the strain (ϵ) measured via the video extensometer, were recorded all along the experiment. Nominal stress (σ_N) and stretch ratio (λ) were defined as the tensile force per unit of initial cross sectional area of the sample and the ratio of the length to the initial length as presented in Eq.3-1, Eq.3-2 and Eq.3-3 respectively.

$$\sigma_N = \frac{F}{w \cdot h} \quad \text{Eq. 3 - 2}$$

$$\lambda = \frac{L}{L_0} \quad \text{Eq. 3 - 3}$$

and

$$\lambda = \varepsilon + 1 \quad \text{Eq. 3 - 4}$$

True stress (σ_t) was calculated assuming constant volume deformation as shown in Eq.3-5 and the Mooney stress (σ_{mooney}), represents the mechanical behaviour of the material normalized by that of a neo-Hookean elastomer with an equivalent small strain modulus as shown in Eq.3-6. The Mooney stress or reduced stress has the physical meaning of a strain dependent entropic modulus and is independent of strain for a neo-Hookean elastomer.

$$\sigma_t = \sigma_N \cdot \lambda \quad \text{Eq. 3 - 5}$$

$$\sigma_{\text{mooney}} = \frac{\sigma_N}{(\lambda - 1/\lambda^2)} \quad \text{Eq. 3 - 6}$$

In the small strain regime, the initial modulus or the Young's modulus (E) is the slope of the curve (Eq.3-7), and can be estimated by fitting at small strain ($\varepsilon=0$ to 0.05) and $R^2 \sim 0.99$, Figure 3-5.

$$\sigma_N = E \cdot \varepsilon \quad \text{Eq. 3 - 7}$$

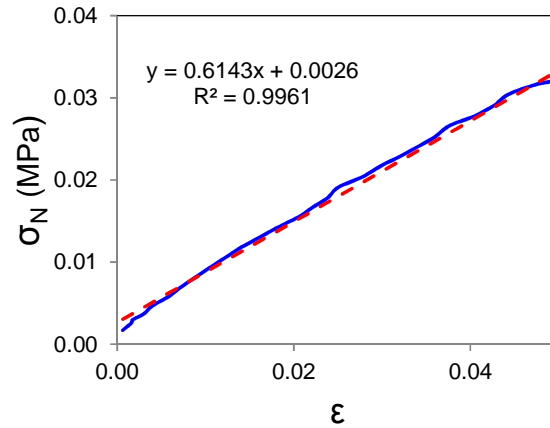


Figure 3- 5: Experimental method to determine the Young's modulus from silicone 1st network, $[V_{6k};H_{D4}]; [1:1.35]$ with toluene 66% v/w

1.2.2 Step-cycle extension

Loading and unloading cycles at incremental values of strain were performed in order to investigate the viscoelastic properties and the potential damage in silicone multiple network elastomers. The samples for step-cycle extension tests were cut in the dumbbell shape, similar to the samples in uniaxial extension test (tensile test).

Step-cycle extension tests were performed at room temperature with a constant velocity of the crosshead of $500 \mu\text{m.s}^{-1}$. For the first cycle, the sample was loaded from $\lambda = 1$ to $\lambda = 2$ and unloaded back to $\lambda \sim 1$ and $F = 0.1 \text{ N}$ (to prevent the compression force). Three identical loading cycles were performed for each λ . Then the strain was increased to $\lambda = 3$ or in λ_{i+1} , where λ_i is a previous extension for 3 cycles. The stretch was increased by 1 for each loop until the sample broke. A typical deformation history for a cyclic deformation test is presented in Figure 3-6. Here again the force (F) and the stretch (λ) measured by the extensometer were recorded all along the experiment.

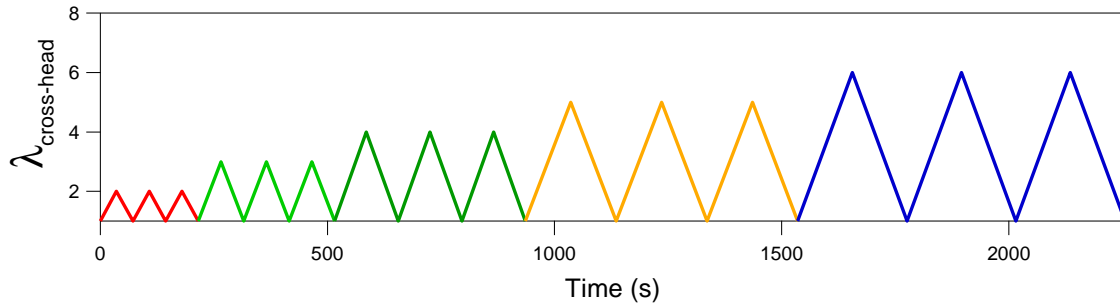


Figure 3- 6: Applied stretch (λ) during a cyclic extension test

1.2.3 Fracture in a single edge notch test

To characterize the fracture toughness of silicone multiple networks, tensile tests on notched samples were performed on the Instron machine. The samples were cut into a rectangular strip, with a total width of 5 mm and a length of about 30 mm. The notch of 1 mm length was made in the middle of a strip, located at the edge of the sample (Figure 3-7). The length of the notch (c) was confirmed from pictures with a gauge using ImageJ.

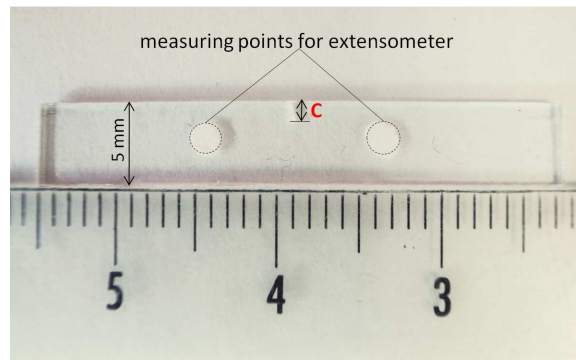


Figure 3- 7: Picture of a typical sample for single edge notch test, $w=5 \text{ mm}$ and $c=1 \text{ mm}$

To determine the fracture toughness, the notched sample was fixed with pneumatic clamps, spaced of 20 mm. This will fix the dimension of the sample: $l = 20$ mm, $w = 5$ mm. The thickness was different for each sample varying from 0.5-2.5 mm. The tests were carried out at room temperature with a crosshead speed of $500 \mu\text{m s}^{-1}$ similar to the test conditions in the tensile test. Force (F) and the stretch (ϵ) measured by the extensometer were recorded all along the experiment.

The fracture energy (Γ) can be determined using the Greensmith approximation⁶ with a single edge notch sample, Γ is given by

$$\Gamma = \frac{6 \times W \times c}{\sqrt{\lambda_c}} \quad \text{Eq. 3 – 8}$$

Where c is the length of the pre-crack, λ_c is the stretch ratio at break in single edge notch experiments and W is the strain energy density. W can be estimated by integration of the nominal stress versus engineering strain of un-notched samples until λ_c (see in chapter 1).

2. Effect of Stoichiometry on the mechanical properties of simple silicone networks

The properties of the silicone 1st and 2nd network which are respectively the principal network and the interpenetrating network in silicone multiple networks, depend crucially on the stoichiometric ratio between their reactants. Although in principle a 1:1 ratio between vinyl and Si-H should give the best results, an excess of Si-H is often used in practice and we discuss here how the composition of the 1st and the 2nd network were optimized.

For the 1st network, we used the uniaxial extension test to measure the modulus of the samples obtained from different stoichiometric ratios. For each composition (short or long PDMS-V) and preparation conditions (in solvent or solvent-free), the stoichiometric ratio resulting in the highest small strain modulus in the fully cured sample was called an effective stoichiometric ratio (r_e). The r_e of each system will be used further to synthesize the 1st networks used for the silicone multiple networks. In addition, to understand better the structure of networks, the uniaxial tensile curve was fitted with the slip tube model proposed by Rubinstein and Panyukov (Chapter 1, section 2) and the respective contribution to the Young's modulus of entanglements (E_e) and permanent crosslinks (E_c) was extracted from the data.

For the silicone 2nd network, first the stoichiometric ratio between PDMS-V₇₇₀ and PDMS-H₄₀₀ was studied and an optimum (just below the gel point) stoichiometric ratio was determined. In other words, the sample presenting the highest viscosity without actually being a solid, was selected as r_e . Then, the D₄H crosslinker was introduced to create silicone 2nd network, while keeping the stoichiometric ratio between vinyl and SiH constant at r_e .

2.1 Silicone highly crosslinked networks (1st network)

2.1.1 Stoichiometry of silicone small mesh size networks, using PDMS-V_{6k}

Silicone 1st networks with different stoichiometric ratios between vinyl end groups of PDMS-V_{6k} [V_{6k}] and silane end groups of D₄H [H_{D4}] have been prepared in both solvent-free conditions (bulk condition) and in the presence of solvent (66 %v/w of toluene to total reactants). After completing the hydrosilylation reaction, initiated by the Pt Karstedt's catalyst, the samples were directly tested in uniaxial tension at 25°C without any step of extraction of the unreacted free chains. The mechanical properties of these networks and the determination of r_e for the PDMS-V_{6k} based networks are presented below.

- Silicone 1st network of PDMS- V_{6k} in bulk conditions

In bulk conditions, the 1st network based on PDMS- V_{6k} shows an increasing modulus with increasing D_4H crosslinker and reaches the highest modulus at $r_e [V_{6k} : H_{D4}]$; [1 : 1.5]. After this point the initial modulus decreases as shown in Figure 3-8. This mechanical behavior was also reported by Chambon et. al⁷ in their stoichiometric study of PMDS-V crosslinked by tetrakis(dimethylsiloxy)silane and they found $r_e = [1 : 1.5]$.

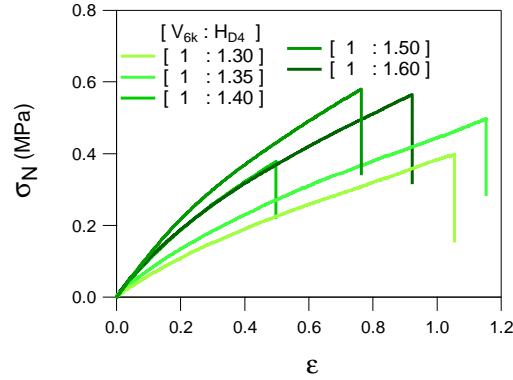


Figure 3- 8: Uniaxial extension of silicone 1st network using PDMS- V_{6k} in solvent- free conditions (without passing extraction process)

A slight increase of the initial modulus and stress at break for $r < r_e$ can also be observed in the Mooney plot (Figure 3-9). The strain softening, characterized by a decrease in Mooney stress with increasing stretch λ , is due to the presence of entanglements between crosslinks and can be found for each stoichiometric ratio, Figure 3-9 (a).

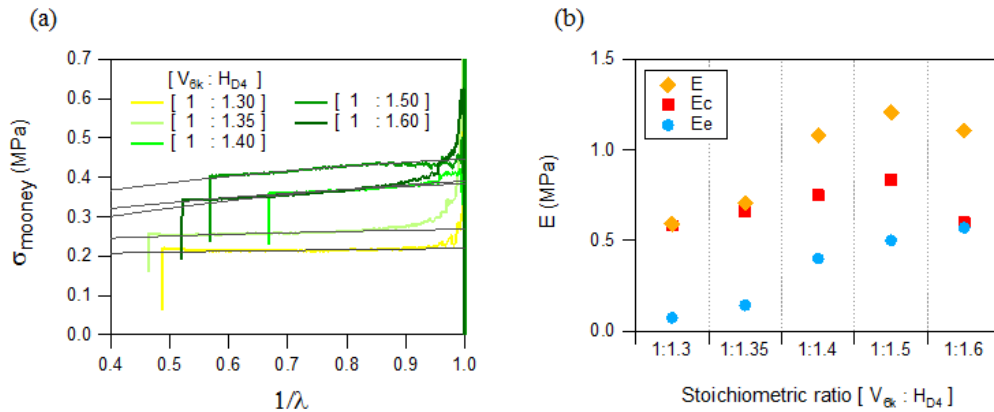


Figure 3- 9: Mooney plot and Young's modulus of silicone 1st network using PDMS- V_{6k} in solvent-free conditions (without passing extraction process), (a) Mooney plot with the best fit (black line) of the Rubinstein-Panyukov equation, and (b) Young's modulus obtained from the initial modulus (E), from the entanglements (E_e) and crosslink contribution (E_c) from the model fit

The best fits of the data with the Rubinstein and Panyukov model are shown as black lines in Figure 3-9 (a). Two parameters are extracted from the fit, the respective contribution of entanglements (E_e) and permanent crosslinks (E_c) to the modulus. The results of these extracted value and initial modulus of networks (E) are summarized in Figure 3-9 (b). We found that, the modulus due to permanent crosslinks goes through a maximum at r_e and suddenly drops at stoichiometric ratio $> r_e$ which is composed of excess crosslinker. This phenomena can be explained by the excess crosslinker creating many pendant chains and blocking the crosslinking process. Interestingly the value of $r = r_e$ giving the highest modulus contains significant entanglements suggesting a very heterogeneous crosslinking structure, while lower values of r_e appear to be much closer to perfect networks but with a lower overall modulus.

Although, r_e was determined for this solvent free system, we decided not to use this system in silicone multiple networks because of its too low equilibrium swelling ratio, about 100% (chapter 2, section 2.6-1). It should be recalled that, a low swelling ratio is not efficient to make silicone multiple networks since a low volume fraction of 1st network requires too many steps.

- The 1st network of PDMS- V_{6k} in the presence of solvent

In this procedure, toluene solvent was introduced during the preparation of the 1st network of PDMS- V_{6k} in the ratio of 2/1 (toluene/reactants) or 66 % v/w of toluene. The samples are test without passing extraction process to determine r_e . Similar to the previous results in bulk condition, the initial modulus increased with the amount of D_4H crosslinker until r_e was reached at $[V_{6k} : H_{D4}]$; [1 : 1.35] as shown in Figure 3-10.

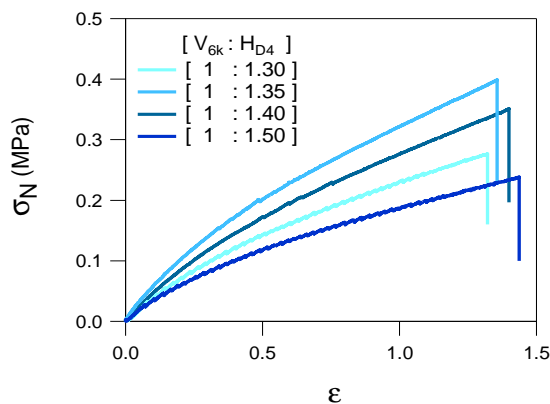


Figure 3- 10: Uniaxial extension of silicone 1st network using PDMS- V_{6k} in solvent system (without passing extraction process)

The entanglements (E_e) and crosslink (E_c), contributions to the modulus are shown in Figure 3-11. As for the solvent free system, E_c is maximal at r_e and continuously decreases for $r > r_e$. The

addition of solvent into the system had the objective to reduce the entanglement density increasing therefore the equilibrium swelling. These phenomena are reflected by the lower value of E_c (Figure 3-11 (b)) compared to the solvent-free system (Figure 3-9 (b)). It is likely that the network is here more homogeneous.

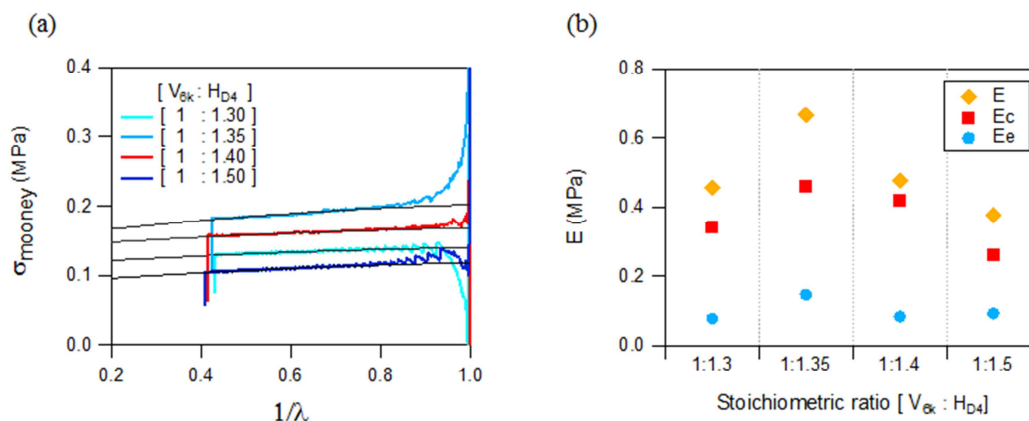


Figure 3- 11: Mooney plot and Young's modulus of silicone 1st network, using PDMS- V_{6k} in the presence of solvent (without passing extraction process), (a) Mooney plot with the best fit (black) of the Rubinstein-Panyukov equation, and (b) Young's modulus from initial modulus (E), from entanglements (E_e) and from crosslinks (E_c)

Although, the same chemical reagents were used to prepare the 1st network in both cases, the addition of solvent during the synthesis step reduces the value of r_e . This might be because the presence of solvent may favor the accessibility of the vinyl reactive sites and therefore reduce the need for excess Si-H. This difference between bulk synthesis and synthesis in the presence of solvent may be even more pronounced for the large mesh size network, made from PDMS- V_{17k} . The PDMS- V_{17k} should in principle create more entanglements and the difference of r_e between solvent-free conditions and solvent should become more obvious.

2.1.2 Stoichiometry of silicone large mesh size networks, using PDMS- V_{17k}

PDMS- V_{17k} was selected to be the large mesh size silicone 1st network. This larger mesh size was designed to increase the equilibrium swelling as shown in chapter 2, section 2.6-1 and therefore to obtain multiple networks with larger levels of prestretching of the 1st network. For this PDMS- V_{17k} based system, the 1st network was also synthesized with two different methods; in bulk conditions, and in solvent. To determine the optimum stoichiometry r_e , the same methods used in PDDMS- V_{6k} network were applied, uniaxial extension at 25°C and estimate of the E_e and E_c by fitting the Mooney stress curve versus λ^{-1} with the Rubinstein-Panyukov model.

- The 1st network of PDMS- V_{17k} synthesized without solvent

Similar mechanical properties as in the small mesh size networks using PDMS- V_{6k} , were observed in this system. The modulus and stress at break increased as a function of the amount of D_4H crosslinker until the r_e was reached at $[V_{17k} : H_{D4}]$; $[1 : 1.6]$ as shown in Figure 3-12.

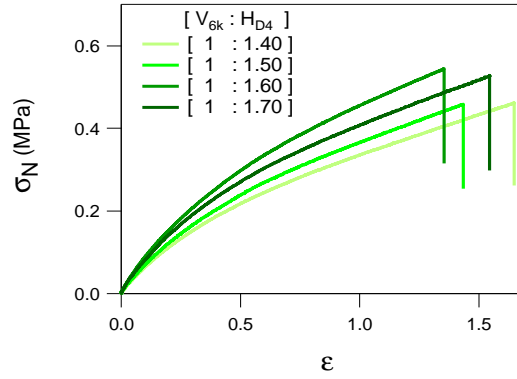


Figure 3- 12: Uniaxial extension of silicone 1st network using PDMS- V_{17k} in the solvent-free system (without passing extraction process)

A clear strain softening can be observed in the Mooney stress plot in Figure 3-13. If the data is fitted with the Rubinstein-Panyukov model E_e , and E_e can be determined. The entanglement contribution to the modulus E_e at the r_e point is a little lower than what was found for the network of PDMS- V_{6k} in bulk (Figure 3-9), but it is within the uncertainty of the model. However the contribution of the crosslinks E_c is much lower for the $SN_{17k, 0\%T}$ than for its 6k counterpart.

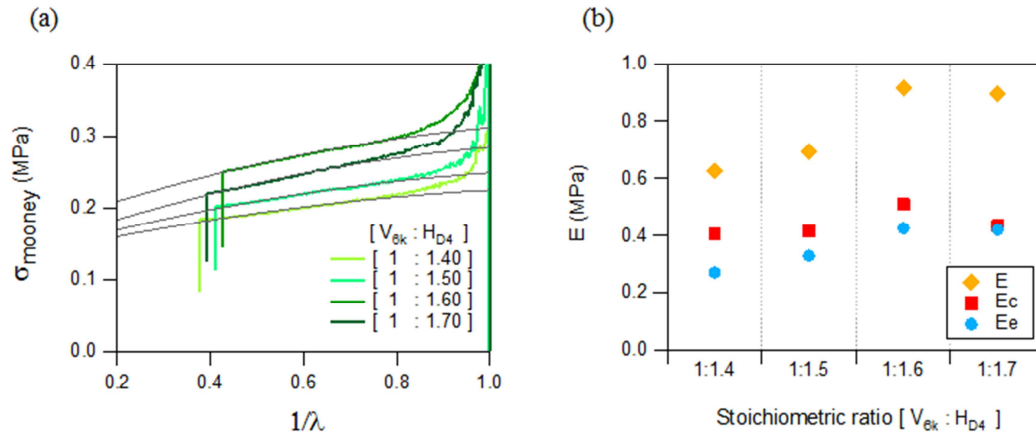


Figure 3- 13: Mooney plot and Young's modulus of silicone 1st network of PDMS- $V_{17.2 \text{ kg.mol}^{-1}}$ in the solvent-free system (without passing extraction process), (a) Mooney plot with the best fit (black) of the Rubinstein-Panyukov equation, and (b) Young's modulus obtained from the initial modulus (E), from the entanglements (E_e) and from the crosslinks (E_c) to the Rubinstein-Panyukov fit

- The 1st network of PDMS-V 17.2 kg.mol⁻¹ in the presence of 66% v/w toluene

The silicone 1st network of PDMS-V_{17k} synthesized in the presence of toluene, is optimized for an $r_e [V_{17k} : H_{D4}]$; [1 : 1.5] as shown by the results of uniaxial extension shown in Figure 3-14.

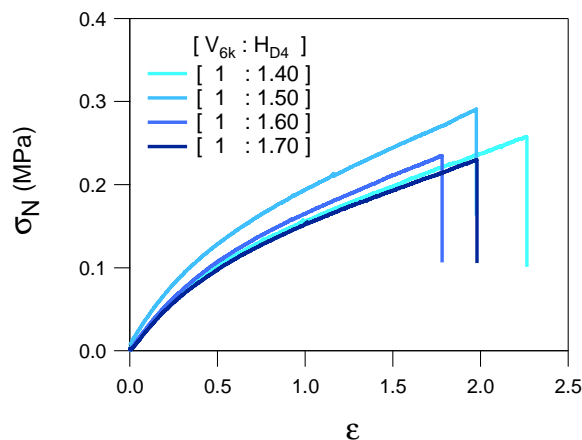


Figure 3- 14: Uniaxial extension of silicone 1st network of PDMS-V 17.2 kg.mol⁻¹ in 66%wt toluene (without passing extraction process)

A similar effect of the presence of solvent, as in the network using of PDMS-V_{6k} is observed here. The E_c obtained for the fit to the Mooney stress is lower than the one obtained in Figure 3.13 with the network prepared in bulk conditions (Figure 3-15). The presence of solvent create a more homogeneous network, resulting in a decrease of E_c .

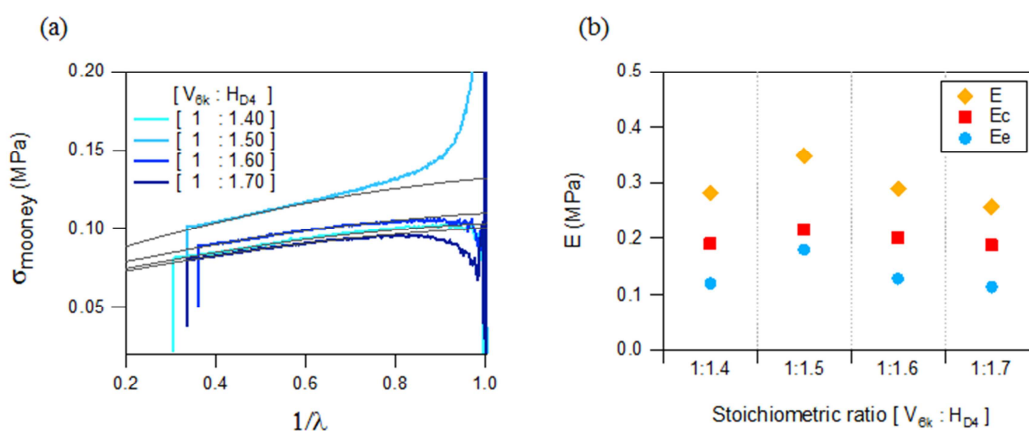


Figure 3- 15: Mooney plot and Young's modulus of silicone 1st network of PDMS-V 17.2 kg.mol⁻¹ in the presence of 66%wt toluene (without passing extraction process), (a) Mooney plot with the best fit (black) of the Rubinstein Panyukov equation, and (b) Young's modulus from initial modulus (E), from the entanglements (E_e) and from the crosslinks (E_c) contributions to the modulus

2.1.3 Selection of the 1st networks: summary

The optimum stoichiometric ratio r_e for the synthesis of the silicone 1st network was determined in 4 different systems by uniaxial extension tests. The respective contribution of crosslinks (E_c) and entanglements (E_e) to the Young's modulus calculated from the best fit to the Rubinstein Panyukov equation are summarized in Table 3-1.

It was found that the presence of solvent during the synthesis decreases the entanglement density of the polymer network resulting in a drop of E_e in the solvent system, comparing to solvent free synthesis conditions, meaning that the 1st network in solvent is more homogenous than the ones made in bulk. Moreover considering the effect of the M_w of the precursors PDMS-V, PDMS-V_{6k} provide a small mesh network and PDMS-V_{17k} creates a larger average mesh and a more extensible network. This effect clearly shows up in the increase of E_c reflecting the higher crosslink density of the network made from the smaller M_w precursor.

Interestingly the bulk condition have an optimized modulus for a larger excess of D₄H crosslinker, and have consequently a larger r_e ratio. We assume that it may be because of the higher viscosity of the precursor solution, that leads to a more difficult access of the D₄H crosslinker to the vinyl reactive sites.

1 st networks	$r_e [V_x : H_{D4}]$	Toughness (kJ.m ⁻³)	E (MPa)	E_c (MPa)	E_e (MPa)
SN _{6k} •0%T	1 : 1.5	257	1.21	0.84	0.50
SN _{6k} •66%T	1 : 1.35	315	0.65	0.46	0.15
SN _{17k} •0%T	1 : 1.6	455	0.83	0.51	0.43
SN _{17k} •66%T	1 : 1.5	357	0.35	0.22	0.18

Table 3- 1: Effective stoichiometry (r_e) and Young's modulus of silicone 1st network in 4 different systems

2.2 Silicone loosely crosslinked network (2nd network)

Silicone 2nd networks were prepared from a mixture of PDMS-precursors; PDMS-V₇₇₀, PDMS-H₄₀₀, and D₄H crosslinker. The main reason to use this composition of precursors was the need to swell the 1st network to synthesize silicone multiple networks. Since silicone 2nd networks alone should be barely crosslinked or not crosslinked at all, the optimal stoichiometric ratio r_e of [V: H] was determined by measuring first the viscosity of the polymer after polymerization. To optimize this system, the crosslinker was initially not introduced. Then a little amount of crosslinker was introduced to determine r_e for a silicone loosely crosslinked network. Uniaxial extension tests were performed in

this second stage to characterize the mechanical properties of the 2nd networks with a light amount of crosslinker.

2.2.1 Optimization of the stoichiometry of silicone prepolymer without any crosslinker

2nd networks with different stoichiometric ratios between vinyl reactive groups of PDMS- V_{770} and Si-H of PDMS- H_{400} , $[V_{770} : H_{400}]$ were prepared and cured at 60°C for 40 hr in an oven. The viscosity of the prepolymer (without crosslinker) was characterized with an ARES rheometer at 25 °C fitted with the cone and plate geometry, the cone angle was 0.04 radians, the diameter 25 mm and the rheometer was used in steady shear mode. The initial shear rate was varied between 0.01 s⁻¹ and 10 s⁻¹. The viscosity of the prepolymer at different stoichiometric ratios is shown in Figure 3-16.

At the lower stoichiometric ratio, the prepolymer after 40 hr of curing has a low viscosity, constant with shear rate. Then the viscosity of the network increases with $[H_{400}]$ and reaches a highly viscous state in the range of stoichiometric ratios $[V_{770} : H_{400}]$ between [1:1.38] and [1 :1.4]. If the ratio further increases the viscosity of the network dramatically decreases and returns to a low viscosity liquid state again at a stoichiometric ratio $[V_{770} : H_{400}] = [1:1.58]$. Because of the huge differences in viscosity, the measurement was performed by using two different plate geometries; cone and plate geometry for the liquid samples and parallel plates geometry for high viscosity samples.

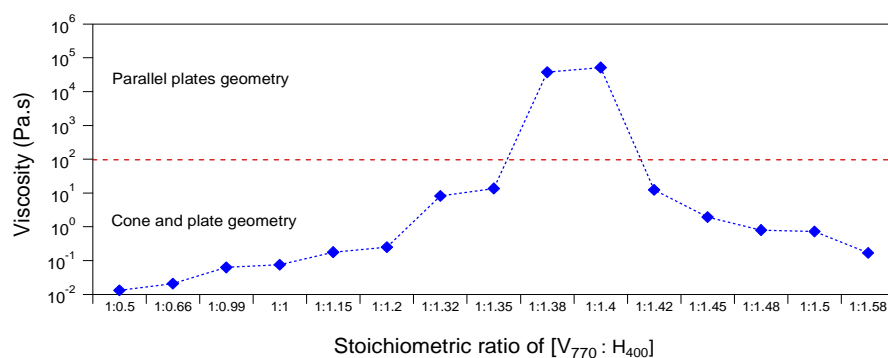


Figure 3- 16: Viscosity of the silicone linear prepolymer without crosslink in different stoichiometric ratio of, $[V_{770} : H_{400}]$.

The viscosity as a function of shear rate of the polymers for each stoichiometric ratio can be found in Figure 3-17. At a stoichiometric ratio [1 : 0.5] to [1 : 1.35] and at stoichiometric ratio [1 : 1.42] to [1 : 1.58] the network shows a newtonian fluid behaviour i.e. the viscosity does not depend on the applied shear rate (Figure 3-17 (a)). In contrast the network at stoichiometric ratios between [1:1.38] to [1:1.4] behaves as a non-newtonian fluid, at these stoichiometric ratios. It is important to

mention that during the test, a significant error is introduced by the slippage of the samples, resulting in the drop in viscosity after a strain rate 0.01 s^{-1} (Figure 3-17 (b)).

Using a rheometer in steady shear mode, we could not determine the r_e of the network due to the slippage occurring during the measurement. Thus, the stoichiometric ratios for the highly viscous compositions [1:1.36] to [1:1.4] were characterized in the dynamic mode with the same rheometer.

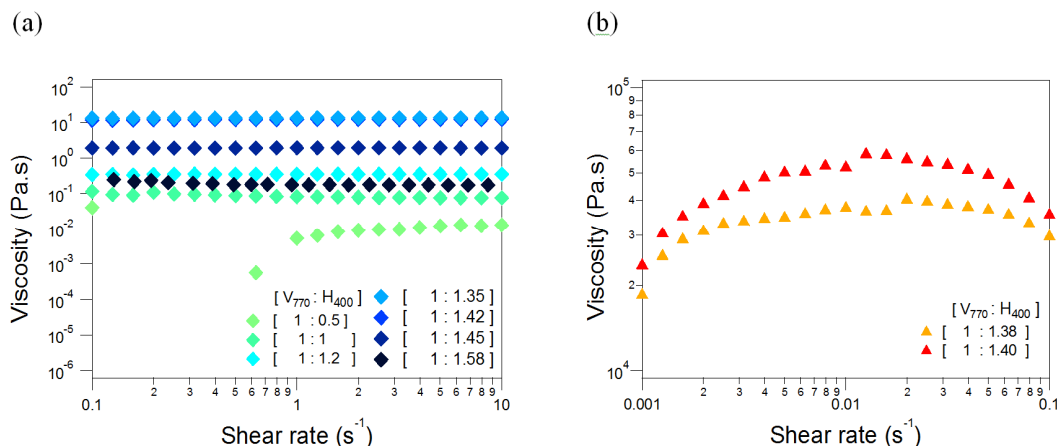


Figure 3- 17: Viscosity measurements of silicone 2nd networks with the ARES rheometer at 25°C in steady shear mode, (a) the measurement with the cone plate geometry in flowing samples and, (b) the measurement with parallel plates geometry in high viscosity samples.

2.2.2 Dynamic rheology of silicone prepolymer without crosslinker

- Dynamic strain sweep (at 1% strain in the linear region)

Dynamic strain sweeps were performed at 25°C with a constant frequency at 1 Hz. The strain was first applied at the start from 0.01% until the storage modulus (G') reduced. The storage modulus (G') and loss modulus (G'') of the samples were observed in the linear viscoelastic region, presented in Figure 3-18. Unsurprisingly, at low stoichiometric ratios, the network behaves like a high viscosity liquid exhibiting a higher loss modulus than storage modulus ($G'' > G'$). However, at higher stoichiometric ratios, starting from [1 : 1.375] to [1 : 1.4] the material shows a viscoelastic solid behavior with a storage modulus higher than the loss modulus ($G' > G''$) and tan delta below 1. This behavior suggests that some crosslinks are present in the networks which may come from some variation in functionality of the PDMS-V₇₇₀, the purity being 95 %. The precursor may contain branched vinyl groups that can crosslink when reacting with PDMS-H₄₀₀.

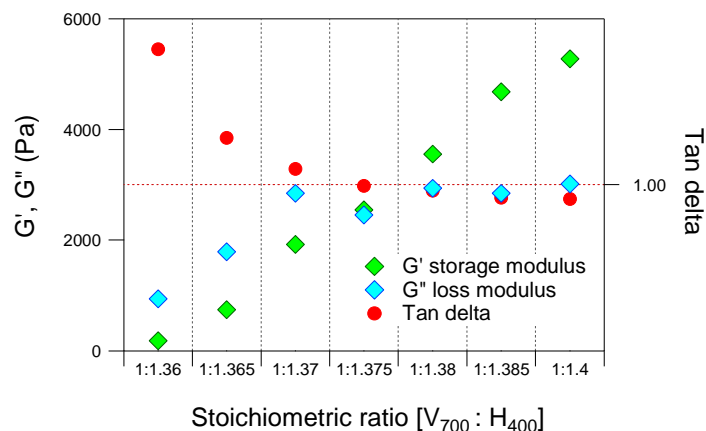


Figure 3- 18: Dynamic modulus of silicone 2nd network without crosslink at 1% strain, 25 °C, and 1 Hz.

To verify the effect of the contamination of the PDMS-V₇₇₀, ATR-FTIR (Bruker tensor 27 FT-IR with OPUS data collection program) was used to analyse the functional groups of PDMS-V₇₇₀ at 25 °C. The IR absorbance of PDMS-V₇₇₀ compared with PDMS-V_{6k} is shown in Figure 3-19. We observed that there were several different FTIR absorbance peaks appearing in PDMS-V₇₀₀ and in particular at 956 cm⁻¹ and 838 cm⁻¹. These two peaks disappear after the reaction with PDMS-H₄₀₀, indicating the absorbance of vinyl groups (Figure 3-20) while the absorbance at 2127 cm⁻¹ and 907 cm⁻¹ indicates the presence of Si-H groups of PDMS-H₄₀₀.^{8, 10, 11} In other literature it was also reported that a peak at wavenumber 956 cm⁻¹ indicated the presence of vinyl end group of PDMS-V¹², however, the origin of the absorbance at 838 cm⁻¹ in PDMS-V₇₇₀ still unclear which may indicate the presence of other reactive groups from impurities.

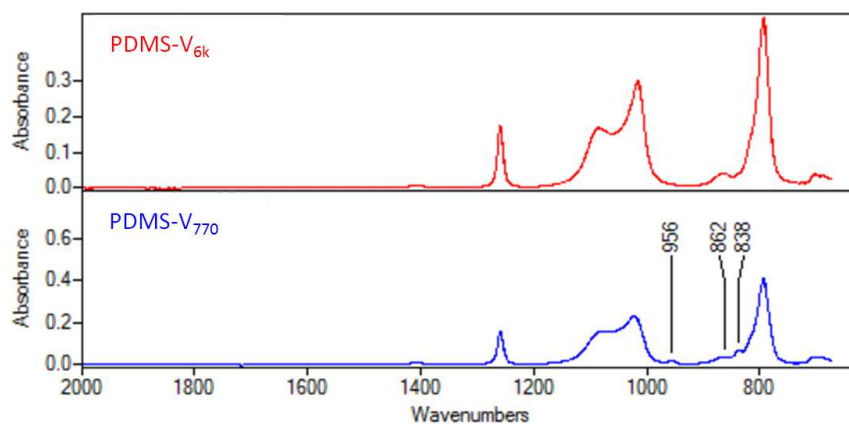


Figure 3- 19: ATR-FTIR spectra of PDMS-V_{6k}, and of PDMS-V₇₇₀.

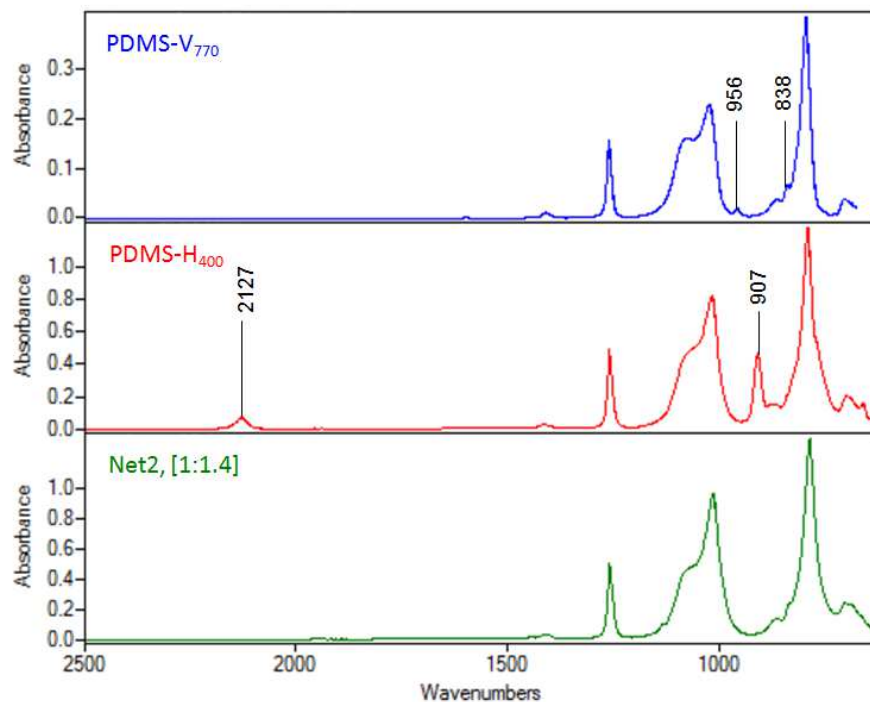


Figure 3- 20: ATR-FTIR spectra of PDMS-V₇₇₀, and of PDMS-H₄₀₀ and silicone 2nd chain at stoichiometric ratio [V₇₇₀ : H₄₀₀] = [1:1.4].

- Dynamic Frequency sweep

In order to characterize the mechanical characteristics of silicone prepolymers near the self-crosslink stoichiometric ratio, the effect of applied frequency was tested in dynamic rheometry in frequency sweep mode at constant 0.5% strain. The test was performed at 25 °C and the frequency was applied from 0.1 rad.s⁻¹ to 100 rad.s⁻¹ or 0.016 Hz to 16 Hz. The dynamic properties of silicone 2nd networks near the self-crosslink point are shown in Figure 3-21.

As expected the applied frequency has an important effect on G' and G'' near the optimal stoichiometric ratio [V₇₇₀ : H₄₀₀], [1:1.36] to [1:1.385]. G' and G'' both increase with applied frequency. The gel point (where both G' and G'' have the same frequency dependence) can be observed at stoichiometric ratio [V₇₇₀ : H₄₀₀], [1:1.375] (Figure 3-21 (d)). Beyond this stoichiometric ratio, [1:1.375] to [1:1.385] the samples turn solid with a low frequency plateau appearing (G' > G'').

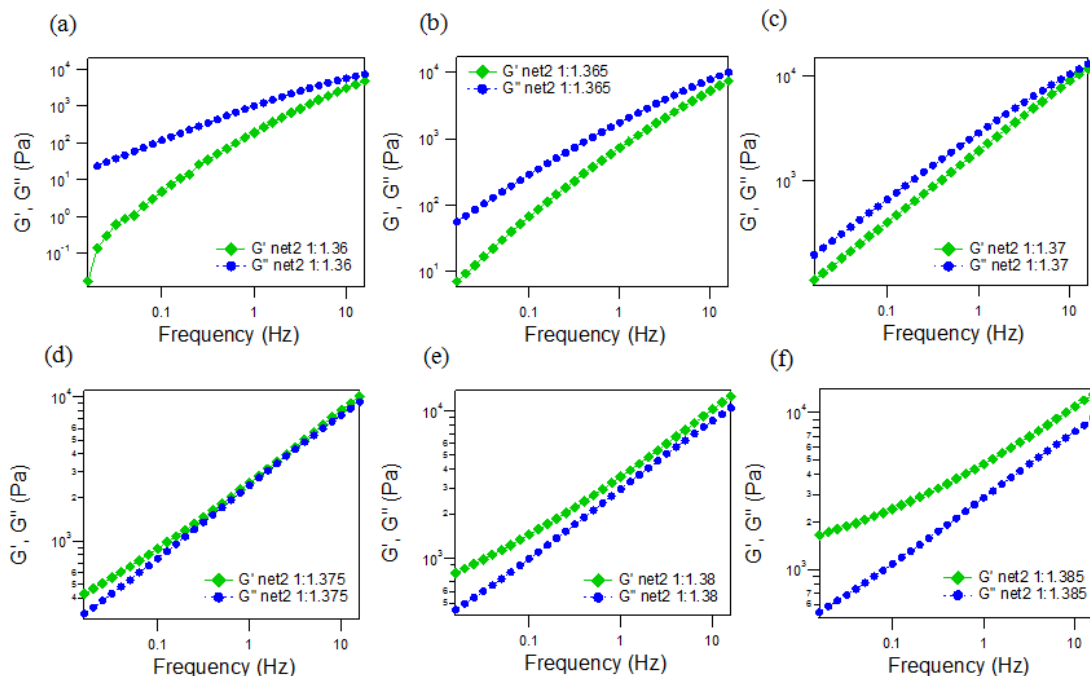


Figure 3- 21: Dynamic modulus at different stoichiometric ratios between vinyl end groups PDMS-V 770 g.mol^{-1} and hydrogen end groups of PDMS-H 400 g.mol^{-1} , $[\text{V}_{770} : \text{H}_{400}]$ of silicone 2nd networks without added crosslinker.

In summary, by using dynamic rheometry we could find the r_c for silicone made from nominally difunctional precursors which was at stoichiometric ratio, $[1:1.4]$. However, at this stoichiometric ratio, the polymer was actually lightly crosslinked by unexpected reactive groups which may come from the impurity of PDAM-V₇₀₀, resulting in the network being too solid. These crosslinks were not easily controllable and would lead to variations between batches. For this reason, we decided to use a lower stoichiometric ratio $[1:1.37]$ to serve as the base 2nd network. However to be able to vary the crosslink density of this second network, we also investigate the properties of a few compositions with a little added D4H crosslinker.

2.3 Loosely crosslinked networks of silicone

A stoichiometric ratio of $[\text{V}_{770} : \text{H}_{400}]$ at $[1:1.37]$ was chosen for the 2nd network in order to be just below the gel point. At this ratio, the polymerization will result in a highly viscous fluid. Yet it was demonstrated that in the absence of coupling between the two networks, a small amount of crosslinker was needed in the second network.¹³ To obtain it, D₄H crosslinker was introduced in the network. The effect of this crosslinker on the mechanical properties of the 2nd network was characterized in uniaxial

extension at 25°C at a crosshead velocity of 500 $\mu\text{m.s}^{-1}$. The stress versus strain plots can be found in Figure 3-22(a).

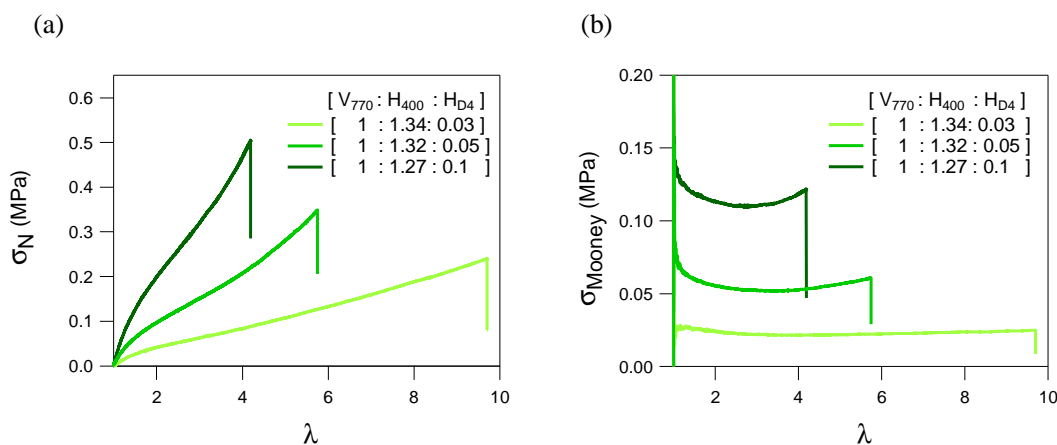


Figure 3- 22: Mechanical properties of standalone silicone 2nd networks, (a) uniaxial extension of silicone 2nd networks, at 25 °C and, (b) Mooney stress versus λ for the 2nd networks.

Unsurprisingly, the initial modulus and stress at break both increase with the amount of crosslinker in the network while the elongation at break decreases. The Mooney stress plot versus λ in Figure 3-22 (b) shows clearly the stiffening which is shifted to lower strains when increasing the amount of crosslinker, indicating the presence of a network. Yet the concomitant strain hardening at low $\lambda = 3$ and the low modulus suggest a very heterogeneous structure.

Given these results, we decided to introduce the crosslinker below [0.03] to the 2nd network since at this stoichiometric ratio the network still has a high elongation and low strain stiffening. Silicone 2nd networks with H_{D4} [0.01] and [0.02] were also synthesized in our study. However, because the samples were too soft and sticky, they could not be cut in a shape for the tensile tests.

3. Silicone multiple networks

Silicone multiple networks were now created by using the sequential interpenetrating network technique. The 1st network prepared with r_e was extracted an unreacted component by extraction process as described in Chapter 2, section 2.2.3. Then, it is first swollen with the precursor molecules of the 2nd network and subsequently polymerized to create a silicone double network (DN). By repeating the swelling step and sequential polymerization, we obtained silicone multiple networks which were triple networks (TN) and quadruple networks (QN). The three different stoichiometric ratios of silicone 2nd network ; [$V_{770} : H_{400} : H_{D4}$]; [1 : 1.36 : 0.01] called as 0.01 H_{D4} , [1 : 1.35 : 0.02] called as 0.02 H_{D4} , and [1 : 1.34 : 0.03] called as 0.03 H_{D4} were used as the interpenetrating network for the three different systems of silicone 1st network that we tested; i) the 1st network of PDMS- V_{6k} prepared in the presence of solvent ($SN_{6k,66\%T}$), ii) the 1st network made from PDMS V_{17k} in the bulk, and iii) the 1st network of PDMS V_{17k} prepared in solvent. It should be noted that the 1st network of PDMS- V_{6k} prepared in the bulk ($SN_{6k,0\%T}$), was not used in multiple networks due to a low swelling ability which was disadvantage in creating the multiple networks.

In this section, the mechanical properties of the silicone multi-networks were characterized with uniaxial extension experiments, step-cycle extensions and fracture in a single edge notch test. The details of the methods and testing conditions can be found in section 1.

3.1 Silicone multiple networks based on PDMS- V_{6k} made in solvent

We discuss first silicone multiple networks synthesized from the 1st network of PDMS- V_{6k} with 66 %w/v toluene. The mechanical properties of SN, DN, TN, and QN with different crosslinker concentrations investigated by uniaxial extension are shown in Figure 3-23 and in Table 3-2.

The 2nd network with [0.01 H_{D4}] does not seem to provide much reinforcement in terms of stiffness. However, beyond [0.01 H_{D4}] the initial tensile modulus (Figure 3-23) and the minimal value of the Mooney stress (Figure 3-24), which is the shear modulus, increase with the amount of D_4H crosslinker added to the 2nd network. Moreover, the Mooney stress plot versus strain in Figure 3-24, shows clearly the increase in the strain stiffening in the multiple networks and the shift of the onset of stiffening towards lower values of λ that one would expect with increasing pre-stretching chains.

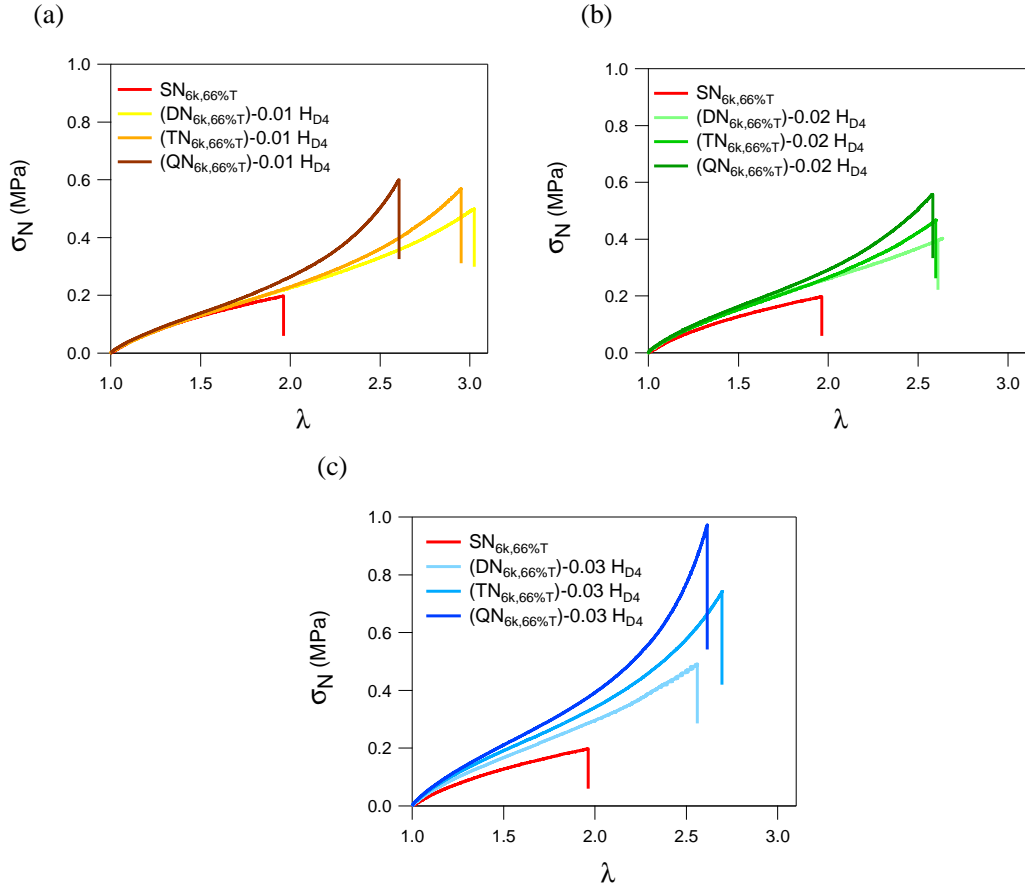


Figure 3- 23: Uniaxial extension properties of silicone multi-networks made from the 1st of PDMS- V_{6k} in solvent system with different D_4H crosslinker amount introduced in the interpenetrating network (2nd network), (a) at $[H_{D4}] = 0.01$ (b) at $[H_{D4}] = 0.02$, and (c) at $[H_{D4}] = 0.03$

[2 nd network]	-	[0.01 H_{D4}]				[0.02 H_{D4}]			[0.03 H_{D4}]		
Silicone network	SN	DN	TN	QN		DN	TN	QN	DN	TN	QN
ϕ_{wt}^{SN} (%)	100	44	21	13		42	17	11	56	22	9
average λ_0	1	1.31	1.69	1.98		1.33	1.81	2.09	1.21	1.67	2.24
E (MPa)	0.35	0.35	0.34	0.35		0.43	0.47	0.49	0.52	0.58	0.67
Toughness (kJ/m ³)	112	480	477	378		359	362	396	379	536	578
$\sigma_{mooney,min}$ (MPa)	0.12	0.13	0.12	0.13		0.15	0.14	0.15	0.13	0.18	0.2

Table 3- 2: Weight fraction of 1st network, prestretch of 1st network chains, initial modulus, toughness and minimum Mooney stress of silicone multi-networks based on PDMS- V_{6k} and 66 % w/v toluene

In the acrylate multiple networks prepared by sequential swelling/polymerization steps, investigated by Ducrot et al.³ they report that the improvement in mechanical properties was due to the

population of stretched chains of the 1st network. The swelling/ polymerization process increase the number of stretched chains of the 1st network, influencing the increase of the initial modulus and the strain stiffening of the acrylate multiple networks at large strains. Moreover, by increasing the crosslinker concentration of the acrylate 1st network, the initial modulus increased and the strain stiffening was visible at lower λ . However in these acrylate networks the loosely crosslinked 2nd network had a minor influence on the stiffness but prevented crack propagation

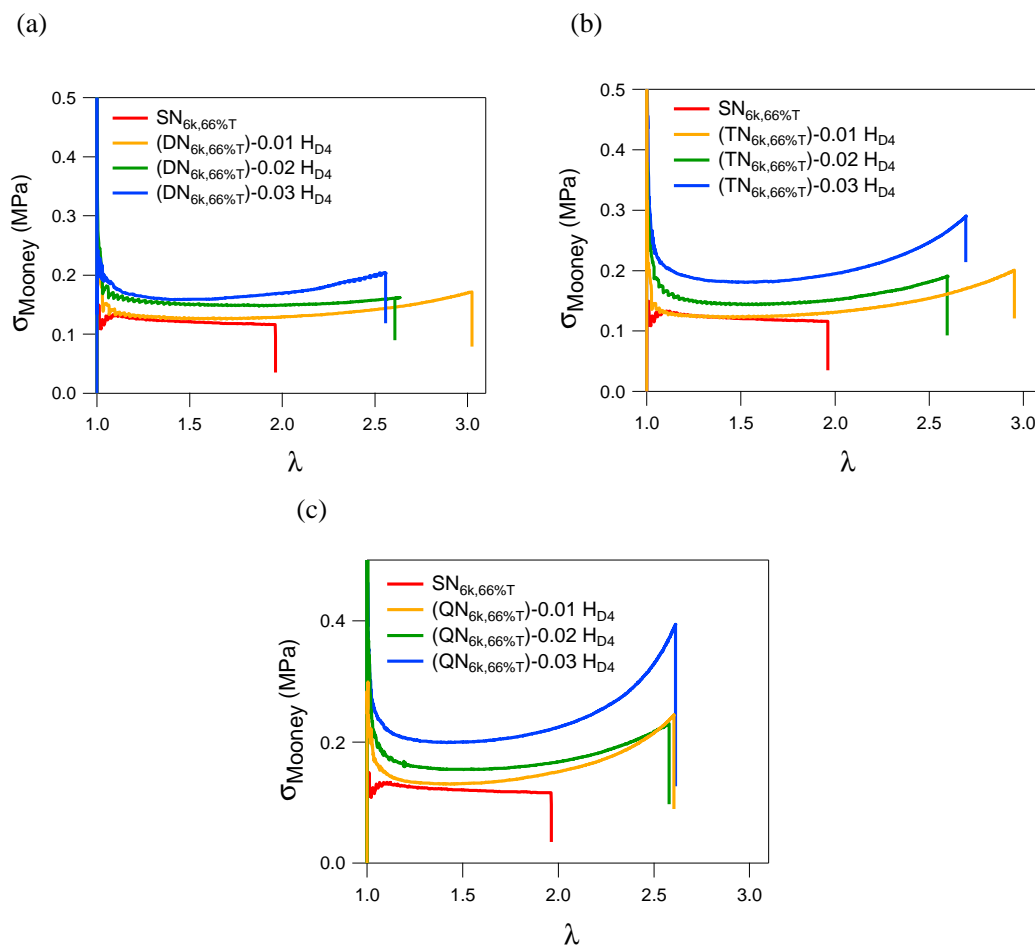


Figure 3- 24: Mooney stress versus λ of silicone multiple network based on PDMS- V_{6k} in solvent system, (a) DN, (b) TN, and (c) QN with different D_4H amount

In contrast, in our silicone systems, we found that the swelling/ polymerization process affects the initial modulus and strain stiffening only on the samples where a relatively high crosslinker amount was introduced in the 2nd network, i.e. a stoichiometric ratio of $[0.02 H_{D4}]$ and $[0.03 H_{D4}]$. For the multiple network with only $[0.01 H_{D4}]$, the initial modulus is similar to the SN (Table 3-2 at $[0.01 H_{D4}]$; $E \sim 0.35$ MPa for DN, TN and QN) and the strain stiffening appears only for the TN. The strain stiffening of silicone multiple networks in $[0.02 H_{D4}]$ and $[0.01 H_{D4}]$ can be observed at $\lambda > 2$ and significantly increases in the samples with $[0.03 H_{D4}]$ at $\lambda > 1.7$ as shown in Figure 3-24.

These results suggest that our silicone 1st network was an imperfect network, composed of loops and dangling chains with many unreacted groups. These free chains may crosslink with the D₄H crosslinker of the 2nd networks during sequential swelling / polymerization process and form linked significant number of connections between the 1st and the 2nd network. The increasing of D₄H concentration in the 2nd network may increase the chance of crosslinking between the 1st and the 2nd network, resulting in the increase in the overall density of elastic chains increasing therefore the initial modulus and shifting the onset of the stiffening to lower values of λ in the overall multiple network. However, the resulting network, while benefitting somewhat from the prestretching of the 1st networks chains, does not have the extensibility needed for a high toughness. From this hypothesis, we can schematically represent the multiple network of PDMS-V_{6k} in the solvent system as shown in Figure 3-25.

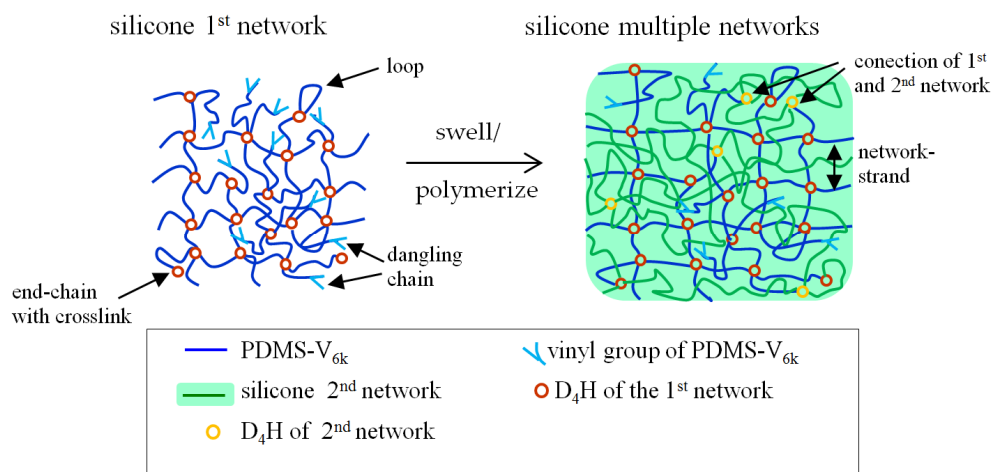


Figure 3- 25: Silicone multiple network of PDMS-V_{6k} with 66 % w/v toluene.

3.2 Silicone multiple networks based on PDMS-V_{17k} synthesized in the bulk

Long chain PDMS-V_{17k} was used to prepare silicone 1st networks with an increased mesh size, resulting in an increased swelling ratio in the silicone multiple networks. The mechanical properties of the silicone 1st network presented in the stoichiometry study, shows that for the PDMS-V_{17k} in the bulk has a higher initial modulus and stress at break than in solvent system (section 2.13). However, the entanglement modulus (E_e) of the network prepared by PDMS-V_{17k} in bulk shows the highest which may indicate to the heterogeneous network. In this section, the silicone 1st network of PDMS-V_{17k} made in the bulk (with extraction unreacted components) was used to make multiple networks by the sequential polymerization technique. The mechanical properties of multiple networks were

characterized by uniaxial extension experiments and the results are shown in Figure 3-26 and Table 3-3.

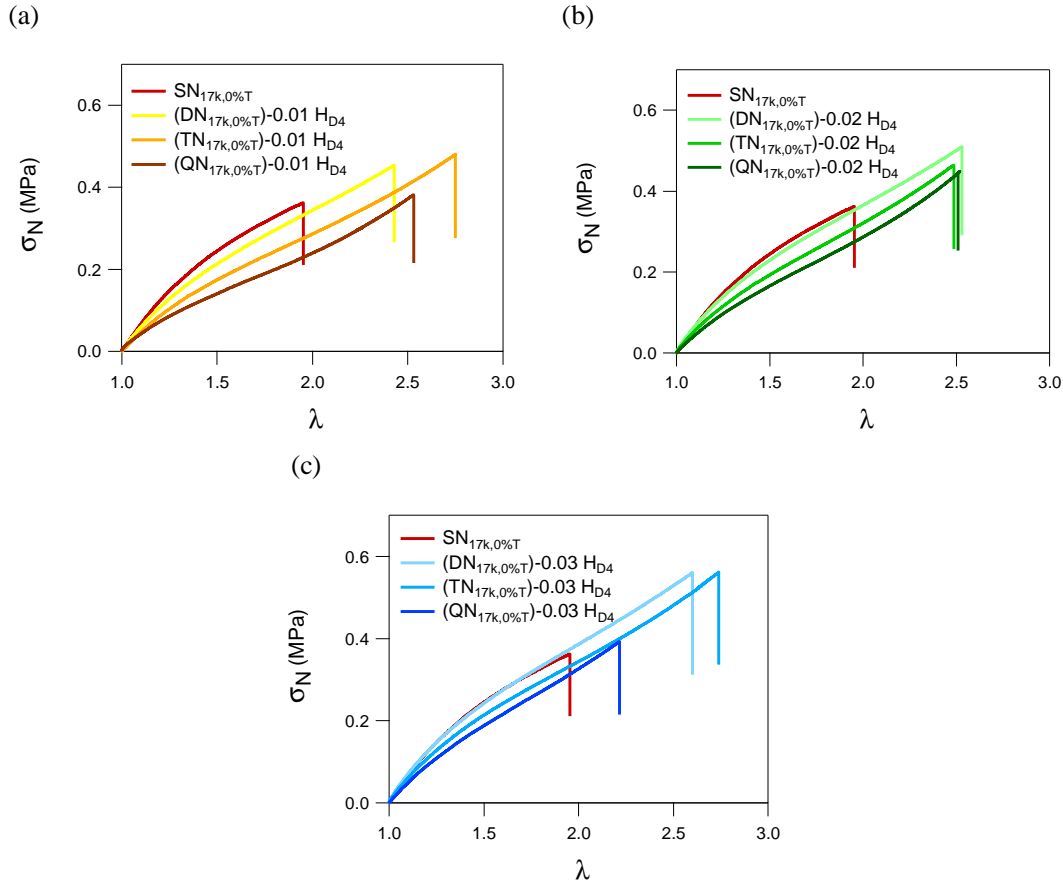


Figure 3- 26: Uniaxial extension properties of silicone multi-network made from the 1st network of PDMS-V_{17k} in bulk with different D_{4H} amount introduced to interpenetrating network (2nd network), (a) at [0.01 H_{D4}], (b) at [0.02 H_{D4}], and (c) at [0.03 H_{D4}]

[2 nd network]	-	[0.01 H _{D4}]			[0.02 H _{D4}]			[0.03 H _{D4}]		
Silicone network	SN	DN	TN	QN	DN	TN	QN	DN	TN	QN
\varnothing_{wt}^{SN} (%)	100	48	25	11	46	22	10	45	24	12
average λ_0	1	1.28	1.59	2.06	1.29	1.67	2.15	1.30	1.62	2.05
E (MPa)	0.68	0.62	0.48	0.42	0.67	0.56	0.44	0.72	0.59	0.5
Toughness (kJ/m ³)	208	372	448	298	447	374	342	511	531	258
$\sigma_{mooney,min}$ (MPa)	0.21	0.2	0.13	0.13	0.21	0.18	0.16	0.22	0.2	0.18

Table 3- 3: Weight fraction of 1st network, prestretch of 1st network chains, initial modulus, toughness and minimum Mooney stress of silicone multi-networks based on PDMS-V_{17k} in bulk

In contrast to our expectations, the modulus of the silicone multiple networks based on the 1st network of PDMS- V_{17k} in the bulk decreased after the swelling/polymerizing process. In general, the introduction of an interpenetrating network increases the stiffness of the network by prestretching the chains of the first network. However, ideal multiple networks were not created successfully in this system. The initial modulus, the stress at break and the toughness decreased with increasing number of swelling/polymerization steps, i.e. $SN > DN > TN > QN$. In summary adding and interpenetrating network to the 1st networks made from PDMS- V_{17k} in the bulk gives the worse mechanical properties. These results suggest that the 1st network may contain many dangling chains, loops and free chains and a very heterogeneous structure. During the swelling process some chain breakage must occur due to the osmotic pressure leading to a reduction of the modulus and to the replacement of these lost crosslinks by entanglements resulting in a decrease of the initial modulus in DN, TN, and QN and a lack of reinforcement.

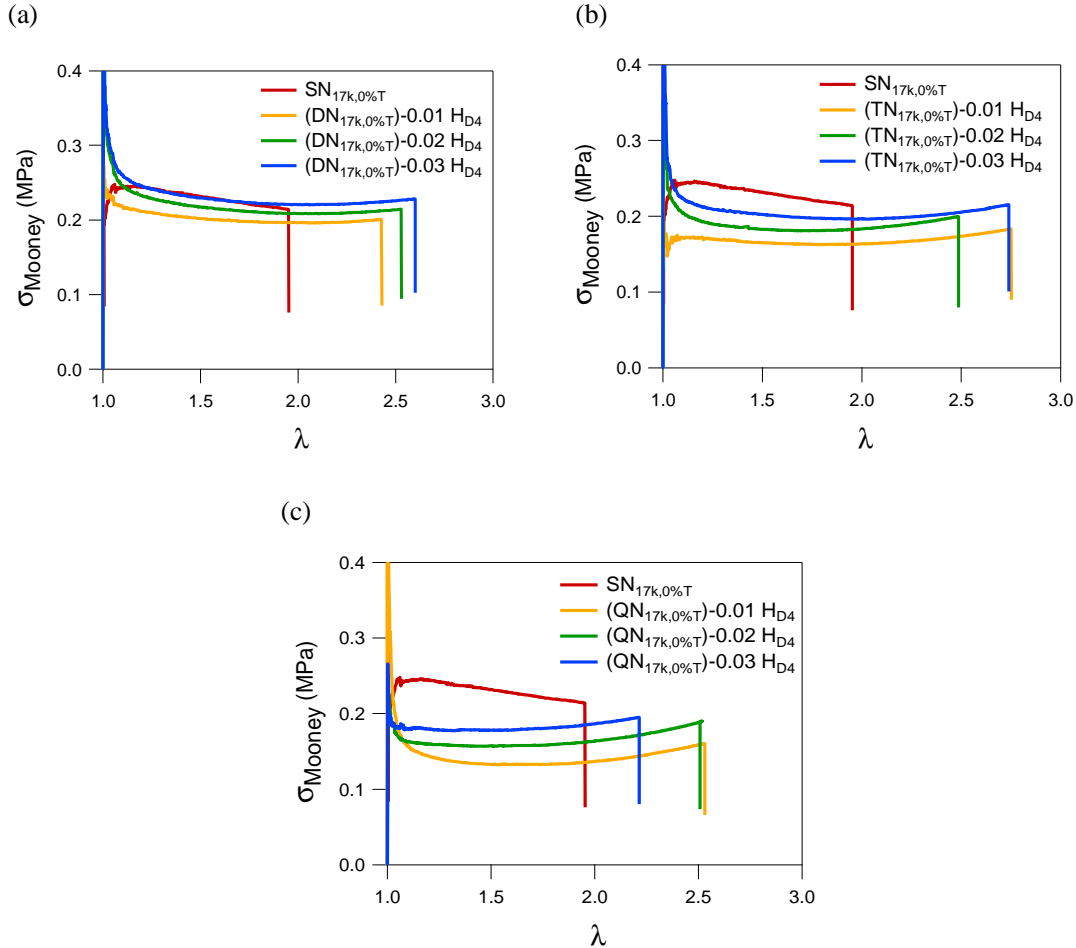


Figure 3- 27: Mooney stress versus λ of silicone multiple network of PDMS- V_{17k} made in the bulk. (a) DN, (b) TN , and (c) QN with different D₄H concentrations

Moreover, the Mooney stress plot versus λ , shown in Figure 3-27, demonstrates that the D_4H amount in the interpenetrating networks has an impact on the mechanical properties of the multiple networks, when $[0.01 H_{D4}] < [0.02 H_{D4}] < [0.03 H_{D4}]$. However, there is a little evidence of reinforcement from stretched chains in the multiple networks and there is little strain stiffening.

In summary the interpenetrating network does not couple much with the PDMS- V_{17k} in the bulk but rather simply swells it. The reduction in modulus is less pronounced with the formulation with more D_4H but remains softer than the starting SN. Also very little strain stiffening is observed suggesting that the chains of the first network are not much prestretched and that some chains may have broken during the swelling step so that the less crosslinked regions may be highly swollen and the more crosslinked regions may be less. This is surprising given the high level of swelling in particular in the QN and suggests a very imperfect network with a lot of dangling chains and loops

By this hypothesis, the 1st network of PDMS- V_{17k} synthesized in the bulk and the multiple networks can be described schematically as presented in Figure 3.28.

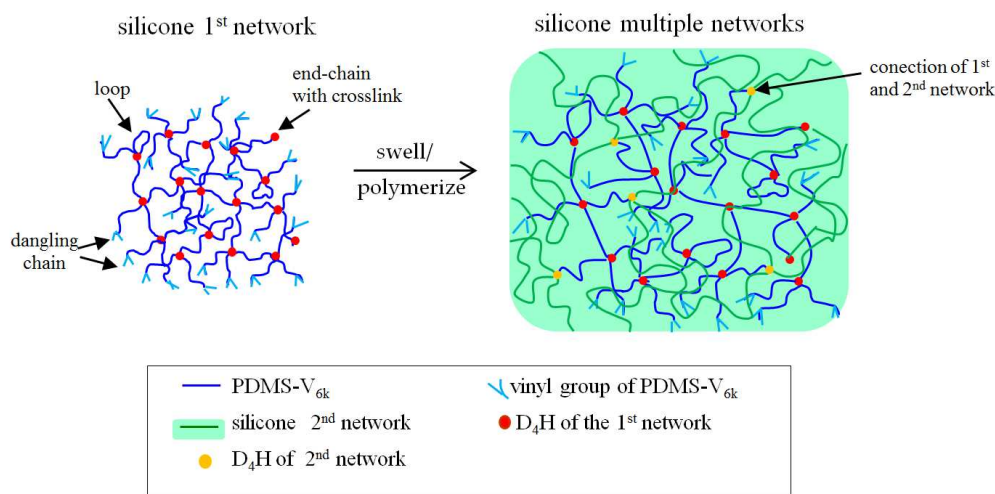


Figure 3- 28: Silicone multi-network of PDMS- V_{17k} in solvent free system.

3.3 Silicone multiple networks based on PDMS- V_{17k} made in solvent

In this system, the silicone multiple networks were designed with a large mesh size, using PDMS- V_{17k} and the toluene was used to decrease the entanglements of the network chains. The mechanical properties of silicone multiple networks compared to the silicone 1st network (SN), in uniaxial extension are shown in Figure 3-29 and in Table 3-4.

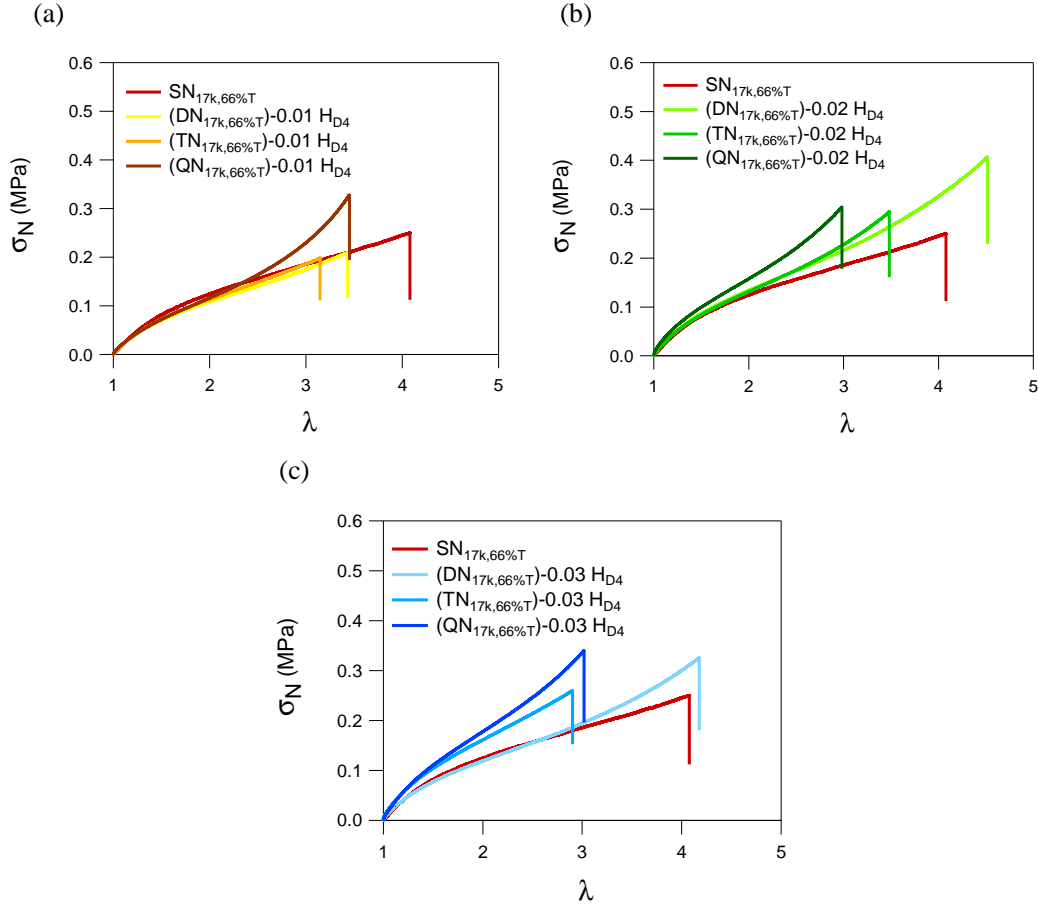


Figure 3- 29: Uniaxial extension properties of silicone multiple networks made from the 1st network of PDMS- V_{17k} in solvent system with different D_{4H} crosslinker amount introduced in the interpenetrating network (2nd network), (a) at [0.01 H_{D4}], (b) at [0.02 H_{D4}], and (c) at [0.03 H_{D4}]

[2 nd network]	-	[0.01 H _{D4}]			[0.02 H _{D4}]			[0.03 H _{D4}]		
Silicone network	SN	DN	TN	QN	DN	TN	QN	DN	TN	QN
ϕ_{wt}^{SN} (%)	100	34	17	7	29	13	9	32	13	6
λ_0	1	1.43	1.79	2.39	1.52	2.00	2.24	1.46	1.97	2.51
E (MPa)	0.22	0.20	0.21	0.23	0.24	0.24	0.36	0.22	0.37	0.33
Toughness (kJ/m ³)	462	290	245	359	710	380	314	526	287	360
$\sigma_{mooney,min}$ (MPa)	0.06	0.06	0.06	0.07	0.07	0.07	0.09	0.07	0.09	0.1

Table 3- 4: Weight fraction of 1st network, average degree of prestretch of the 1st network chains, initial modulus, toughness and minimum Mooney stress of silicone multi-networks based on PDMS-V_{17k} in solvent system

Similarly to multiple networks based on PDMS-V_{6k} (section 3.1), silicone multiple networks made from PDMS-V_{17k} synthesized in the presence of solvent show an increased initial modulus and strain stiffening. The increase of these properties also relate to the amount of D₄H crosslinker in the interpenetrating network. Thus, we can summarize that the silicone 1st network in this system is similar to the one with PDMS-V_{6k} which contains some dangling chains and loops and may crosslink with the D₄H of the 2nd network. The large equilibrium swelling relate to the large mesh size creating by long linear chains.

The strain stiffening of silicone multiple networks is not as dominant as for the silicone multiple networks of PDMS-V_{6k} in the solvent system as shown in section 3.1, Figure 3-23. In this system, the strain stiffening begins at $\lambda = 3$ in the DN and shifts to lower λ in TN and QN for $\lambda = 2.5$ and 2.2 respectively, indicating that the chains of the 1st network continuously stretch due to the swelling/polymerization steps (Figure 3-30). The less pronounced effect of strain stiffening when using PDMS-V_{17k} may be because the longer chains length of the 1st network need a larger swelling ratio to expand and stretch the chains. The stiffening may be more pronounced if we continue performing swelling/polymerization steps and decrease the volume fraction of the 1st network (ϕ_{wt}^{SN}).

In summary for this system, the 1st network chain seem to swell as expected (and this increases the modulus) but we still see a large effect of the added crosslinker in the interpenetrating formulation.

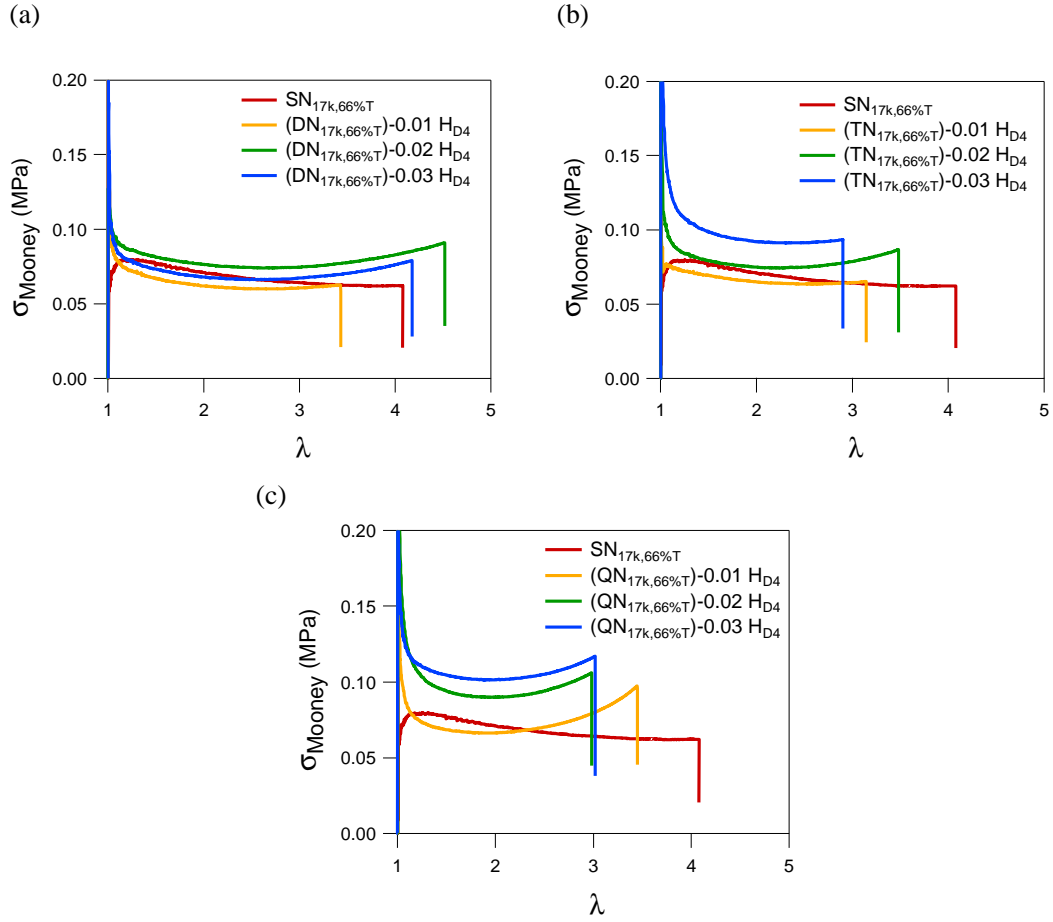


Figure 3- 30: Mooney stress versus λ of silicone multiple network of PDMS- V_{17k} in solvent system. (a) DN, (b) TN, and (c) QN with different $\text{D}_{4\text{H}}$ concentrations

4. Energy dissipation characteristics of the silicone multiple networks

In order to understand the potential dissipation mechanisms involved in loading and unloading the silicone multiple networks, step cycle extension tests were carried out in some selected samples. The samples were chosen among 3 systems, PDMS- V_{6k} in solvent (section 3.1); PDMS- V_{17k} in the bulk (section 3.2); and PDMS- V_{17k} in solvent (section 3.3), namely those showing the best mechanical properties, based on the results of the toughness, and the stress at break. The stress-strain curves of these silicone multiple networks tested with step cycle extension are presented in Figure 3-31.

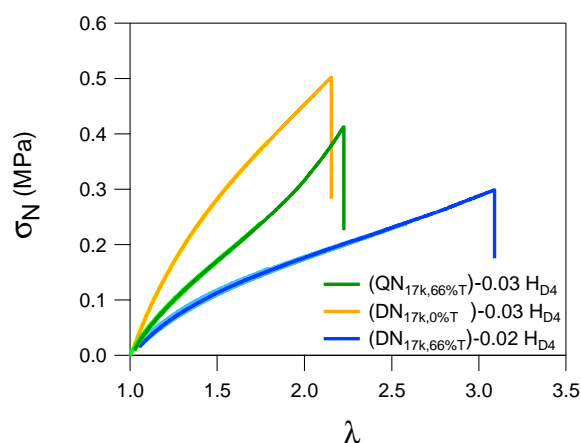


Figure 3- 31: Cyclic extension on silicone multiple networks in different systems

It was found that the mechanical hysteresis of all the silicone multiple networks in the different systems are negligible before macroscopic fracture occurs. There are no viscoelastic dissipations or detectable damage of the sample until the final macroscopic fracture of the samples. Viscoelastic dissipation usually comes from the loose chains or chain connected on one side only. The observed perfect elastic of multiple networks may be because the chains are highly entangled with a reduced mobility and do not have the time to relax during the mechanical testing in this strain rate at $500 \mu\text{m.s}^{-1}$.

Furthermore no evidence of bond scission is detected as one would expect since there is no evidence of softening. This suggests that if any double network effect is present it must be only at the crack tip.

5. Fracture mechanics of the silicone multiple networks

The fracture toughness of the silicone simple networks and of the multiple networks was investigated and analyzed with fracture tests on single edge notch samples. The typical stress-strain curves of notched samples are shown in Figure 3-32 (a) and (b) for silicone 1st network and silicone multiple networks respectively. The fracture toughness of each samples were calculated based on Eq. 3-8, Greensmith model. The results of fracture toughness comparing with initial modulus of the networks are presented in Figure 3.33.

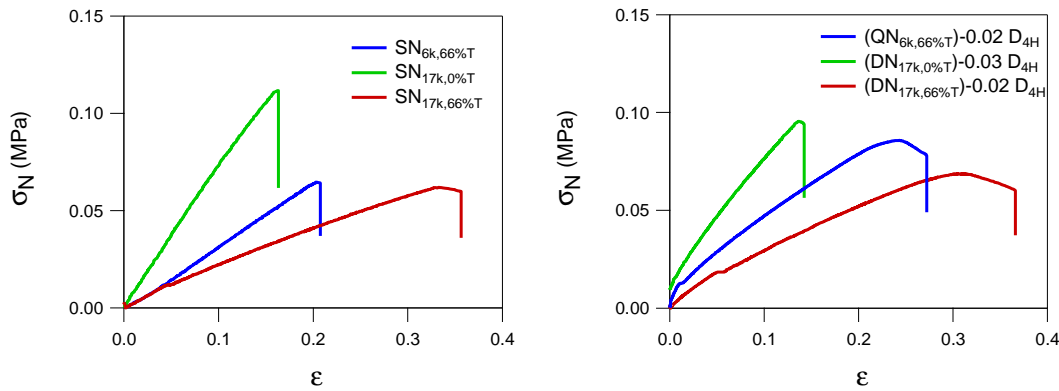


Figure 3- 32: Stress-strain curves on notched samples at 25 °C, (a) simple networks in different 3 systems, and (b) multiple networks in different 3 systems.

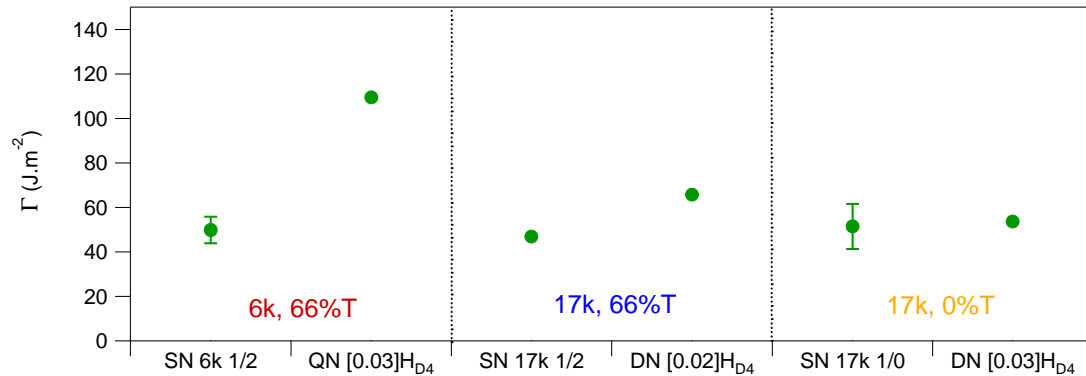


Figure 3- 33: Fracture toughness and initial modulus of silicone simple networks and multiple networks in different 3 systems; PDMS- V_{6k} with 66% toluene (6k, 66% T), PDMS- V_{17k} with solvent free (17k, 0% T), and PDMS- V_{17k} with 66% toluene (17k, 66% T).

The initial modulus in the multiple networks based on PDMS- V_{6k} and PDMS- V_{17k} synthesized in solvent is higher than for their corresponding simple network while no improvement was found in the multiple network based on PDMS- V_{17k} in bulk relative to its corresponding SN. For the fracture

toughness, the multiple network of PDMS- V_{6k} with solvent (6k, 66%T), and PDMS- V_{17k} with solvent (17k, 66%T) show some clear improvement with a Γ value which is about 180-120% greater than the simple network alone. However for the multiple networks of PDMS- V_{17k} synthesized in the bulk (17k, 0%T), the fracture energy was similar to that of the simple network. The result of the fracture toughness confirms that the 1st network in the bulk system probably formed a very heterogeneous network which then swells in a very heterogeneous way and does not create the prestretched chains that would cause strain stiffening and toughening through sacrificial bonds.

Conclusions

Sequential interpenetrating networks have been recently successfully applied in acrylic elastomer to reinforce their mechanical properties. In our study, this technique has been adapted to silicone elastomers via a hydrosilylation reaction to crosslink and create a silicone network, under realistic conditions; presence of oxygen and humidity.

Silicone 1st network, used as the principal network in the multiple networks was synthesized and the best effective stoichiometric ratios (r_e) between vinyl group and hydrogen end group was first determined. Then, the silicone 2nd network, used as the interpenetrating network was also studied and its r_e was optimized before introducing a slight crosslinking level. However, in this study we found that the impurities of PDMS-V₇₀₀ (the precursor of the silicone 2nd networks) showed an uncontrolled crosslinking effect at the r_e and in order to avoid that, we decided to use a stoichiometric ratio between vinyl groups and hydrogen end groups slightly below r_e .

The silicone multiple networks were created using three different silicone 1st network systems; i) PDMS-V_{6k}, ii) PDMS-V_{17k} synthesized in the presence of solvent and iii) PDMS-V_{17k} synthesized in the bulk. Multiple networks were then prepared with sequences of swelling the 1st network with the 2nd network precursors and then polymerize them via the hydrosilylation reaction. Three different D₄H crosslinker amounts were added in the precursors bath during the synthesis. After the swelling/polymerization process, we obtained silicone multiple networks and characterized their mechanical properties. It was found that the multiple networks made from 1st networks prepared in the presence of solvent (66 %w/v of toluene) showed an increase in initial modulus, stress at break and fracture toughness. However, due to the presence of humidity and oxygen during the synthesis and also may be from imprecise stoichiometric ratio, dangling chains and loops are present in the 1st network. Since the same crosslinking reaction (hydrosilylation reaction with pt catalyst) was used in to prepare the multiple networks. Unreacted vinyl end groups can be crosslinked with the 2nd networks chain during swelling/ polymerization process inducing some coupling. Consequently, silicone multiple networks show an improvement in initial modulus and increase in the strain stiffening after introducing higher amount of crosslinker in the interpenetrating network formulation.

In contrast, silicone multiple networks made from 1st network made in the bulk did not show any mechanical reinforcement. The properties of the multiple networks were dominated by the silicone 2nd network. The 1st network was probably a very imperfect network and heterogeneous, containing less and more crosslinked regions, resulting in selective swelling and a lack of reinforcement by stretched chains of the 1st network after sequential polymerization.

Reference

1. Gong, J.P., et al., *Double-Network Hydrogels with Extremely High Mechanical Strength*. Advanced Materials, 2003. **15**(14): p. 1155-1158.
2. Gong, J.P., *Why are double network hydrogels so tough?* Soft Matter, 2010. **6**(12): p. 2583-2590.
3. Ducrot, E., *Innovative tough elastomers: Designed sacrificial bonds in multiple networks*, 2013. (Unpublished doctoral dissertation): University Pierre and Marie Curie, Paris, France.
4. Ducrot, E., et al., *Toughening Elastomers with Sacrificial Bonds and Watching them Break*. Science, 2014. **344**(6180): p. 186-189.
5. *ARES User Manual*. 2003, TA Instruments, Waters LLC, 109 Lukens Drive, New Castle, DE 19720.
6. Greensmith, H.W., *Rupture of rubber. X. The change in stored energy on making a small cut in a test piece held in simple extension*. Journal of Applied Polymer Science, 1963. **7**(3): p. 993-1002.
7. Chambon, F. and H.H. Winter, *Linear Viscoelasticity at the Gel Point of a Crosslinking PDMS with Imbalanced Stoichiometry*. Journal of Rheology, 1987. **31**(8): p. 683-697.
8. Esteves, A.C.C., et al., *Influence of cross-linker concentration on the cross-linking of PDMS and the network structures formed*. Polymer, 2009. **50**(16): p. 3955-3966.
9. Li, Z., *Mesoscopic Adhesion Of Poly(Dimethylsiloxane)- Self-adhesion, Effects of Fillers, Surface Modification and Thin Top Layers*, 2007. (Department of Chemical Engineering and Chemistry): Eindhoven University of Technology, The Netherlands.
10. Lin-Vien, D., et al., *CHAPTER 15 - Organosilicon Compounds*, 1991. (The Handbook of Infrared and Raman Characteristic Frequencies of Organic Molecules), Academic Press: San Diego. p. 251-261.
11. Venkataraman, S.K., et al., *Critical extent of reaction of a polydimethylsiloxane polymer network*. Polymer, 1989. **30**(12): p. 2222-2226.
12. Johnson, L.M., et al., *Elastomeric microparticles for acoustic mediated bioseparations*. Journal of Nanobiotechnology, 2013. **11**(1): p. 1-8.
13. Nakajima, T., et al., *True chemical structure of double network hydrogels*. Macromolecules, 2009. **42**(6): p. 2184-2189.

-CHAPTER 4-

Synthesis of latex double network films

Chapter 4: Synthesis of latex double network films.....	107
Introduction.....	110
1. Latex.....	111
1.1 General feature and application of latex.....	111
1.2 Emulsion polymerization.....	112
1.3 RAFT polymerization.....	114
1.4 Block copolymers through RAFT-mediated polymerization.....	117
1.5 Surfactant free core-shell latex mediated by RAFT polymerization.....	118
1.6 Latex film formation process.....	119
1.7 State of the art and aims of this study.....	123
2. Method and synthesis.....	125
2.1 Chemicals and reagents.....	125
2.2 Latex characterization methods.....	127
2.2.1 Gravimetric analysis.....	127
2.2.2 Nuclear Magnetic Resonance (NMR).....	128
2.2.3 Size Exclusion Chromatography (SEC).....	128
2.2.4 Dynamic Light Scattering (DLS).....	130
2.2.5 pH-meter.....	130
2.2.6 Transmission Electronic Microscopy (TEM).....	130
2.3 P(BA-co-BDA) crosslinked latex synthesized by radical emulsion polymerization.....	130
2.4 PAA-b-PBA core-shell latex synthesized by RAFT emulsion polymerization.....	132
2.4.1 PAA-TCC macro-RAFT agent.....	133
2.4.2 PAA-b-PBA latex.....	135
2.4.3 PAA-b-PBA latex with crosslinked PBA-core.....	143
2.4.4 PAA-b-PBA latex with Na ⁺ counter ion.....	146
3. Latex film formation.....	148
3.1 Drying process and conditions.....	148
3.2 PAA-b-PBA film with added PADAME.....	151
3.3 P(BA-co-BDA) and PAA-b-PBA films with added PAA homopolymer.....	153
3.4 Thermally annealed latex film.....	155
4. Latex double network films.....	157
4.1 Swelling study of latex film.....	158
4.2 PBA elastomer, serving as an interpenetrating network to DN.....	159
4.3 Latex double network synthesis and conditions.....	160
4.4 HMP consumption effect.....	163

Conclusion.....	166
References.....	167

Introduction

A latex is a stable colloidal dispersion of polymer particles in water, meaning that the latex particles will not precipitate or sediment over time. Currently, latexes are used in many applications such as in pigments, surfactants, plasticizing aids and rheological modifiers.^{1, 2} Generally, a latex is synthesized by emulsion polymerization using surfactants as colloidal stabilizers. However, this kind of dried latex usually is sensitive to water uptake (whitening) and requires a low T_g and low modulus component to form a film at room temperature.

In order to improve the latex's stiffness while allowing film formation at room temperature, soft core - hard shell latexes have been developed.^{3, 4, 5} In 2013, Chenal et al.⁶ developed a specific type of soft core - hard shell latex composed of poly(acrylic acid)-block-poly(n-butyl acrylate) or PAA-b-PBA amphiphilic diblock copolymers synthesized by RAFT emulsion polymerization of BA. The latex could be synthesized without presence of surfactant by using the polymerization induced self-assembly (PISA) technique. It was found that only 3 wt% of poly(acrylic acid) or PAA in the resulting nanostructured dried films, resulted in a dramatic improvement in initial modulus without reducing much the strain at break. Inspired by their work, our idea was to use the soft core - hard shell latex as reinforcing polymeric filler in an elastomeric system. To achieve that, a sequential interpenetrating polymer network technique (sequential IPNs) will be used to create a latex double network (latex DN). The mechanical properties of the latex films and latex DN will be characterized further.

In this chapter, we give an overview of latexes, their applications and synthesis methods. In our system, an emulsion polymerization process and the RAFT polymerization technique are involved. The details of the synthesis and characterization methods of conventional latexes and the core-shell latexes are explained here.

1. Latex

1.3 General features and applications of latex

A latex is defined as a stable colloidal dispersion of polymeric particles in water. The polymeric particles of latex are usually a few hundreds of nanometers in diameter. Latex was first discovered in nature from a tree's gum. Natural latex which comes mostly from rubber trees (*Hevea brasiliensis*) is essentially poly(*cis*-1,4-isoprene) emulsified by proteins.¹ In the 20th century, rubber trees planting increased in several Asian countries to support the rubber industries. However, during World War II, the supply of natural latex from Asia was disrupted; the synthetic latex was invented by using an emulsion polymerization. The first commercially synthetic latex was introduced by the Glidden Company in 1984.¹ Since then the use of synthetic latex has rapidly grown and became a part of our daily lives at present. The main reasons for the continuing usage of synthetic latexes are the better control of particle size distribution characterized by polydispersity index (PDI), particle morphology, molar mass distribution or dispersity (M_w / M_n) and the large variety of available chemical compositions. These latex characteristics control the final properties and function of latex materials.⁷ The synthetic latex can be synthesized from a range of monomers, the typical ones are fabricated from acrylates (methyl methacrylate, butyl acrylate, ethylhexyl acrylate), styrene, vinyl acetate and butadiene.¹ In addition, latex can be synthesized with two or more different types of monomers. The different polymer compositions may lead to the formation of a variety of latex particle morphologies ranging from plain spheres to core-shell, hemispheres, salami, and raspberry-type structures as shown in figure 4-1.⁷

Applications of latex expand from basic commodity products and manufacturing aids such as household paints and varnishes, concrete additives, inks, adhesives, tapes, gloves, textile finishes, binders and sealants, all the way to the high value products in a biomedical application for example in drug delivery devices, materials for diagnostic kits and assays.^{1, 2, 7} The range of latex's applications still continuously grows due to the need of reducing volatile organic compounds (VOC).⁸

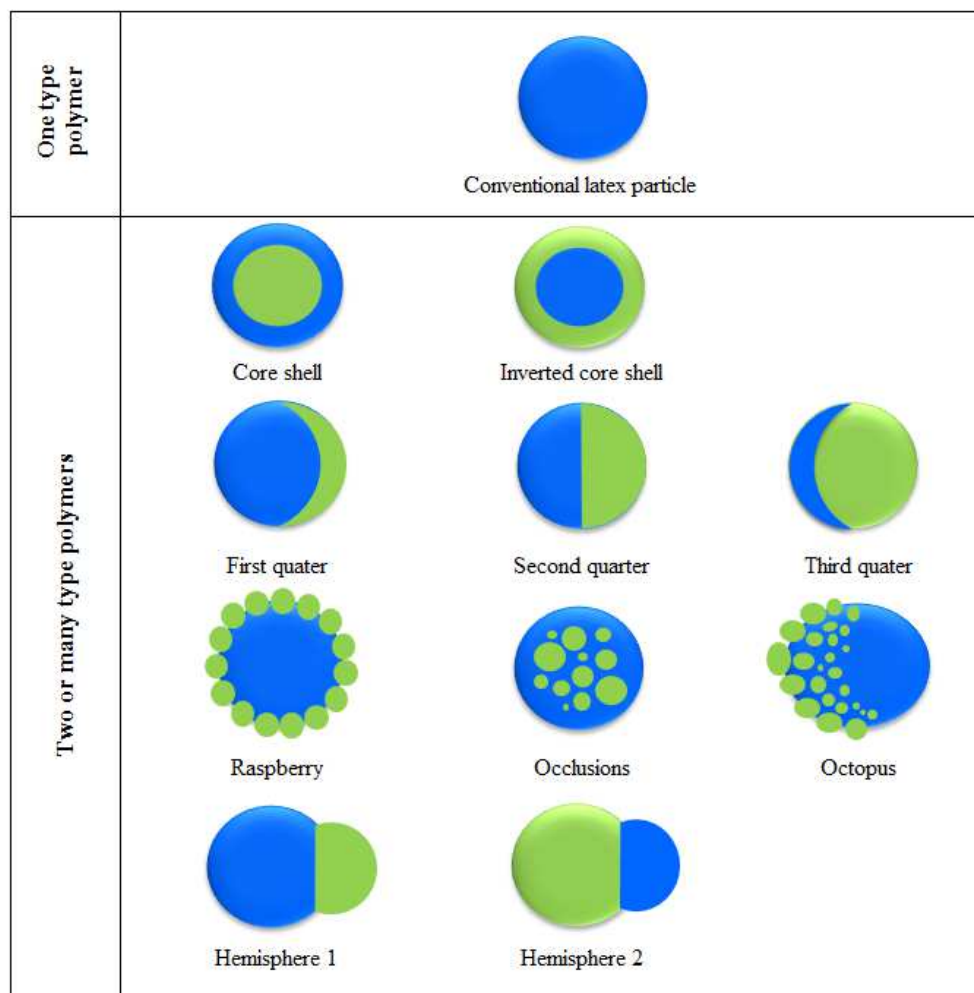


Figure 4-1: Types of polymer latex particles.

1.4 Emulsion polymerization

The most classical way to create latex particles in water is by emulsion polymerization. The main ingredients for this reaction include water, a monomer of low water solubility, water soluble initiator and surfactants. Due to its simplicity, emulsion polymerization is widely used in industry to create a large quantity of latex for some applications such as surface coating (paint, adhesive, etc.) and bulk polymer (poly(styrene-co-butadiene), polychlorobutadiene) etc.⁹

In general, a typical process of emulsion polymerization is an ab-initio emulsion polymerization reaction. According to Harkins, its mechanism is usually separated into three intervals and labeled as Interval I, II and III.^{4, 9, 10, 11}

Interval I:

Interval I is the state of particle formation. An ab-initio polymerization starts from an emulsion of monomer droplets stabilized by surfactants and which are dispersed or emulsified into a few microns in diameter. After, heat is given into the system. The initiator releases free radicals and initiates the polymerization of monomers in micelles, resulting in precursor particles which are small colloidal unstable particles. These particles grow by propagation, coagulation and adsorption of surfactant into colloidal stable particles or mature particles.⁹

Interval II:

The interval II starts when the entire colloid particles turn to mature forms. The particle number density which is the number of particles per unit volume remains constant. At this point, the polymerization continues and new polymer chain are created in the particles while initiation and termination processes maintain a balance over the overall radical concentration.⁴ The particles then continue to grow during this phase by the propagation reaction. The monomer droplets serve as a monomer storage and allow the monomer to diffuse into the particles while maintaining the concentration of monomer constant inside the particle.

Interval III:

The Interval III takes place when all monomer droplets are exhausted.⁴ The remaining monomers in the particles are polymerized and consequently the monomer concentration in the particles decreases. The polymerization continues until all monomers are consumed.

The mechanism of these three intervals could be illustrated in figure 4-2.

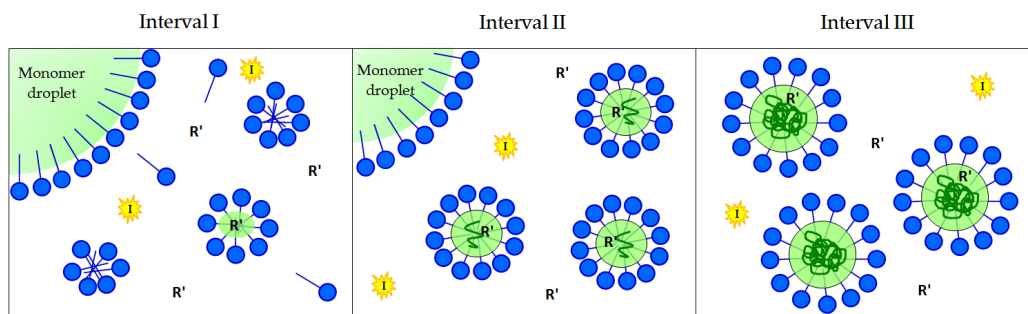


Figure 4- 2: The mechanism of a typical emulsion polymerization with Interval I, II and III; where

—● indicates surfactant molecules, ★ is an initiator, R' is a radical. The micelles are presented as a cluster of surfactant molecules within the interval I and stabilized latex particles exist in the interval III.

1.5 RAFT polymerization

The reversible addition fragmentation chain transfer or RAFT polymerization is one of the reversible deactivation radical polymerization (RDRP, formally called CRP) techniques which allow the control over the polymerization by limiting irreversible termination reactions.¹² RDRP provides access to target molar mass, low molar mass dispersity and defined molecular polymer architectures, such as block copolymers, gradient copolymers, stars and brushes etc.^{7, 13, 14} The RAFT polymerization was invented in 1998 by the Commonwealth Scientific and Industrial Research Organization (CSIRO), Australia. The advantage of RAFT over other RDRP techniques is its compatibility with a wide range of monomers and functional groups, such as vinyl acetate and acrylic acid, and also with a wide range of solvents, including water.^{13, 15}

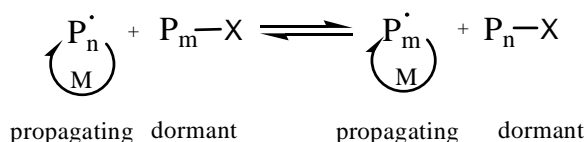


Figure 4- 3: Reversible-deactivation radical polymerization by degenerative chain transfer.¹⁴

The RAFT provides control fundamentally by a degenerative chain transfer process, where the propagating species are in equilibrium with dormant species (Figure 4-3). The RAFT polymerization makes use of a thiocarbonylthio species or RAFT agent (**1** in Figure 4-4) which provides polymerization control by swapping of the thiocarbonylthio functionality (ZC(=S)S-) between growing polymer chains.¹⁴ The effectiveness of the RAFT agent depends on the monomer being polymerized and crucially depends on the properties of the free radical leaving group R and the group Z.¹⁶ The structural features of thiocarbonylthio RAFT agents are explained in Figure 4-4.

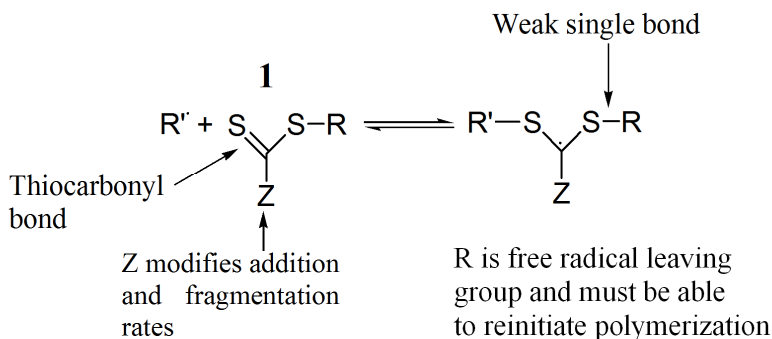
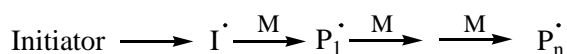


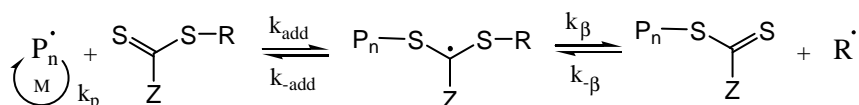
Figure 4- 4: Structural features of thiocarbonylthio RAFT agent (**1**) and the intermediate radical formed on radical addition.^{16, 17}

The RAFT mechanism^{12, 14, 16} (Figure 4-5) begins by the formation of an initiator derived radical (I^\cdot). The radical I^\cdot then propagates with a monomer to create a polymeric radical (P_n^\cdot). In the ideal reaction of the RAFT polymerization, a polymeric radical P_n^\cdot must react efficiently with the thiocarbonyl of the RAFT agent and form an unstable intermediate macromolecular radical, which fragments to release a macromolecular RAFT agent (macro-RAFT agent) and a radical R^\cdot (derived from the RAFT agent) and capable to re-initiate the polymerization. However, in practice, the reverse reaction can occur, resulting in the reformation of P_n^\cdot and RAFT agent. The reversible reaction depends on the effectiveness of the RAFT agent for the type of monomer.

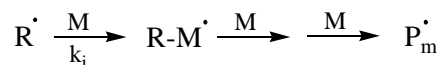
Initiation:



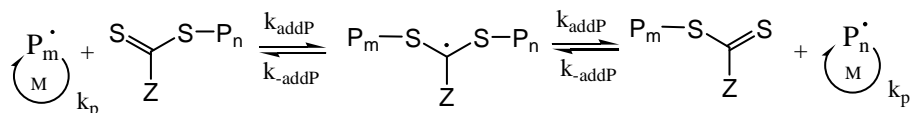
Initialization/ Pre-equilibrium:



Reinitiaion:



Main equilibrium:



Termination:

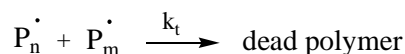


Figure 4- 5: Mechanism of RAFT polymerization.^{14, 16}

The initialization (or pre-equilibrium step)¹⁴ continues until the RAFT agent is fully consumed. Then the reaction shifts to the main equilibrium process, allowing for maximal exchange between growing chains and giving polymers of low molar mass dispersity. After complete polymerization, the majority of the chains will possess a thiocarbonylthio end-group. A large polymer chain end-capped by a RAFT agent is called macro-RAFT agent and it can be activated again for further growth and subsequently give rise to block copolymers.

Side reaction of the initiator or initiator-derived radicals with the RAFT agent have been observed in not well controlled polymerizations.¹⁶ Generally, the creation of the dead chains relates directly to the number of initiator-derived radicals.^{14, 16} Thus in well-designed experiments, a high ratio of RAFT/initiator is selected to diminish the creation of dead chains. The number-average molar mass, $\overline{M}_n(th)$, of polymer formed by the RAFT process can be predicted. In the calculation, the fraction of dead chains should be taken into account.^{14, 15, 16, 18} The theoretical molar mass of macromolecules can be estimated from the concentration of the monomer consumed, the initial RAFT agent concentration and the number of dead chains produced as presented in Eq. 4-1.^{14, 16}

$$\overline{M}_n(th) = \frac{[M]_0 - [M]_t}{[RAFT]_0 + df([I]_0(1 - e^{k_d t}))} \times M_M + M_{RAFT} \quad (Eq. 4 - 1)$$

Where $[M]_0$ and $[M]_t$ are the concentration of the monomer at $t=0$ and $t=t$

M_M is the molar mass of the monomer

$[RAFT]_0$ is the initial concentration of the RAFT agent

$[I]_0$ is the initial concentration of the initiator

M_{RAFT} is the molar mass of the RAFT agent

$df([I]_0(1 - e^{k_d t}))$ is the number of initiator derived chains produced, where d is the average number of chains formed from each radical-radical termination event, f is the initiator efficiency, t is a time in seconds and k_d is the rate coefficient for initiator decomposition. However, in a well-controlled RAFT polymerization, the number of initiator derived chains is low compared to the number of RAFT agent derived chains. Therefore the term $df([I]_0(1 - e^{k_d t}))$ is usually negligible. The simplified equation which is used to predict the number-average molar mass, M_n of the polymer formed by the RAFT process is shown in Eq. 4.2 or in Eq. 4.3 where Conv. is the monomer conversion.

$$\overline{M}_n(th) \approx \frac{[M]_0 - [M]_t}{[RAFT]_0} \times M_M + M_{RAFT} \quad (Eq. 4 - 2)$$

or

$$\overline{M}_n(th) \approx \frac{[M]_0}{[RAFT]_0} \times Conv. \times M_M + M_{RAFT} \quad (Eq. 4 - 3)$$

1.4 Block copolymers through RAFT-mediated polymerization

The simplest and the most common method to synthesize block copolymers using RAFT polymerization is through sequential polymerization.¹⁴ Firstly a polymer chain is generated by RAFT polymerization possessing a thiocarbonylthio end group, which acts then as a macro-RAFT agent. The second step of the RAFT polymerization then continues in the presence of the macro-RAFT agent. The monomer in the second polymerization step will insert to the macro-RAFT. The mechanism of chain extension to create block copolymers is demonstrated in Figure 4-6.

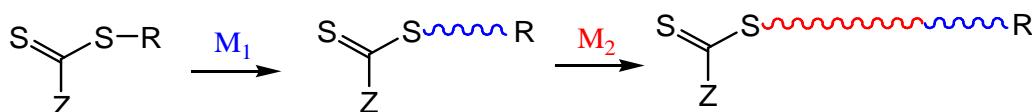


Figure 4- 6: Synthesis of block copolymers via sequential polymerization, M is monomer.

In this process, the R leaving group and the Z-group of the initial RAFT agent must be suitably chosen to control the polymerization of both monomers (M_1 , M_2). If the Z group is not appropriate for one of the two monomers, some control will be lost. For example, if the initial RAFT agent has low activity with M_1 , the macro RAFT agent will have a high molar mass dispersity. On the other hand, if the macro-RAFT agent has low activity with M_2 in the second polymerization step, the polymer block of M_2 will have high dispersity and the final product of block copolymer of M_1M_2 will be contaminated with the homopolymer of M_2 due to inefficient transfer.¹⁴ The molar mass of block copolymers can be predicted using the ratio between the concentration of the monomer in the second polymerization step or $[M_2]$ and the macro-RAFT agent concentration. The theoretical number-average molar mass of block copolymer, $\overline{M}_n(cal)_{block\ copolymer}$ is presented in Eq.4-4.¹⁹

$$\overline{M}_n(th)_{block\ copolymer} \approx \frac{[M_2]_0}{[macro - RAFT]_0} \times Conv. \times M_{M_2} + M_{macro-RAFT} \quad (Eq. 4 - 4)$$

Where $[M_2]_0$ is the concentration of the monomer in the second polymerization step (M_2) at $t=0$

$[macro - RAFT]_0$ is the concentration of the macro-RAFT agent at $t=0$

Conv. is the conversion of monomer in the second step (M_2)

M_{M_2} is the molar mass of the monomer in the second step

$M_{macro-RAFT}$ is the number-average molar mass of the macro-RAFT agent

1.5 Surfactant-free core-shell latexes by RAFT emulsion polymerization

In addition to using conventional radical polymerization, latex particles can also be synthesized by RAFT polymerization which might favor a better control over the particle size and give access to specific morphologies such as a core-shell structure. RAFT can typically be applied to emulsion polymerization and mini-emulsion polymerization in the presence of a RAFT agent and, sometimes, surfactants. However, the presence of surfactants in a latex has the disadvantage to create a latex film in which the surfactants can migrate and create water sensitive regions upon aging. Moreover, the latex particles stabilized with the surfactant can lose their stability during storage because of the dissociation of the surfactant from the particles. Consequently, the latex particles may coagulate, change their properties and are not suitable for further use.⁷ Self-stabilized surfactant-free latexes have been developed in this decade generally based on the polymerization induced self-assembly (PISA) approach. In our study we used this PISA technique to synthesize surfactant-free core-shell latexes.

Polymerization induced self-assembly (PISA)

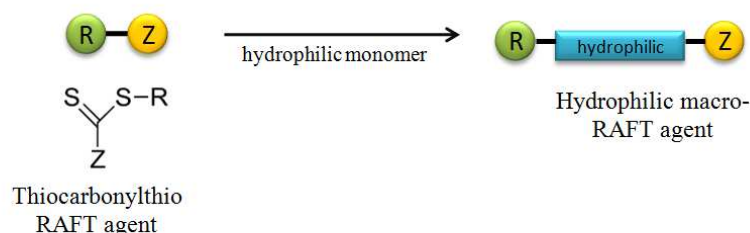
In 2002, Ferguson et al.³ developed the first synthesis of core-shell latex particle by using the self-assembly of amphiphilic block copolymers, created during emulsion polymerization. In their study acrylic acid (AA), a water soluble monomer was first polymerized via RAFT in water in the presence of a RAFT agent (2-((butylsulfanyl)carbothiioyl)sulfanyl)propanoic acid) and an initiator (4,4-azobis(4-cyanopentanoic acid)) to create an oligomeric-RAFT agent. Then the oligomeric -RAFT was used to synthesize a block-like copolymer latex with a hydrophobic segment of poly(butyl acrylate) (PBA) under controlled feed addition of BA to avoid the loss over the polymerization control because of the presence of droplets of BA. After a critical number of BA units added, the diblock copolymer self-assembled to a self-stabilized latex particle with a small shell of PAA and a core constituted of PBA. The number-average molar mass of the formed block copolymer latex measured by GPC and estimated by polystyrene standard calibration was approximately 48 kg.mol⁻¹ while molar mass dispersity was approximately 1.5.

Rieger et al.²⁰ developed self-stabilized core-shell latexes by using poly(ethylene oxide) or (PEO) macro-RAFT agents in the polymerization of styrene (S) and n-butyl acrylate (BA) in an ab initio batch emulsion polymerization (Figure 4-7). In their study the (PEO) macro-RAFT agent was synthesized by esterification of PEO with a RAFT agent. Then the macro-RAFT agent was used in the polymerization of S or BA without avoiding monomer droplets (batch process). They showed that despite the presence of monomer droplets in their system, the diblock copolymer latex presented a high stability, good molar mass control and low molar mass dispersity ($M_w/M_n \approx 1.16-1.2$).

These days, surfactant-free emulsion polymerization under batch ab initio conditions according to the PISA principle has been widely used to synthesize core-shell latexes. Hydrosoluble macro-RAFT agents are used, that serve at the same time as stabilizers and control agents for the polymerization.

Many publications reported that, thanks to well-designed macro-RAFT agents, they could reach controlled ab initio RAFT emulsion polymerization conditions with success without introducing any surfactant. This technique has been applied to many systems for example styrene mediated by poly(acrylic acid)-b-(polystyrene) trithiocarbonate²¹, butyl acrylate mediated by poly(acrylic acid)trithiocarbonate²², n-butyl acrylate and styrene mediated by poly(N,N-dimethylacrylamide)trithiocarbonate²³, styrene mediated by poly(methacrylic acid-co-poly(ethylene oxide) methyl ether methacrylate) trithiocarbonate²⁴ etc.

Step 1: Macro-RAFT preparation in solution



Step 2: Ab initio RAFT emulsion polymerization in batch conditions in water

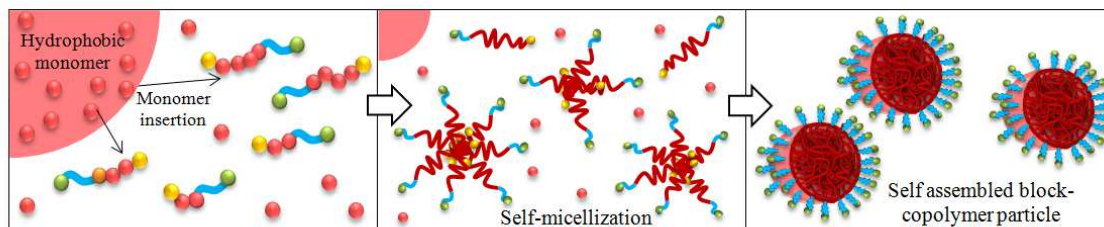


Figure 4- 7: Mechanism of surfactant- free emulsion polymerization under batch ab initio conditions according to the PISA concept.

1.6 Latex film formation process

The film formation process has been reported to have a pronounced influence on the final polymer film properties.¹ Thus, to create a homogenous latex film, the film formation process is crucially important. Conventionally, latex dispersion can form a dried film in three sequential steps; water evaporation, particle deformation and particle coalescence as presented in the Figure 4-8.^{25, 26}

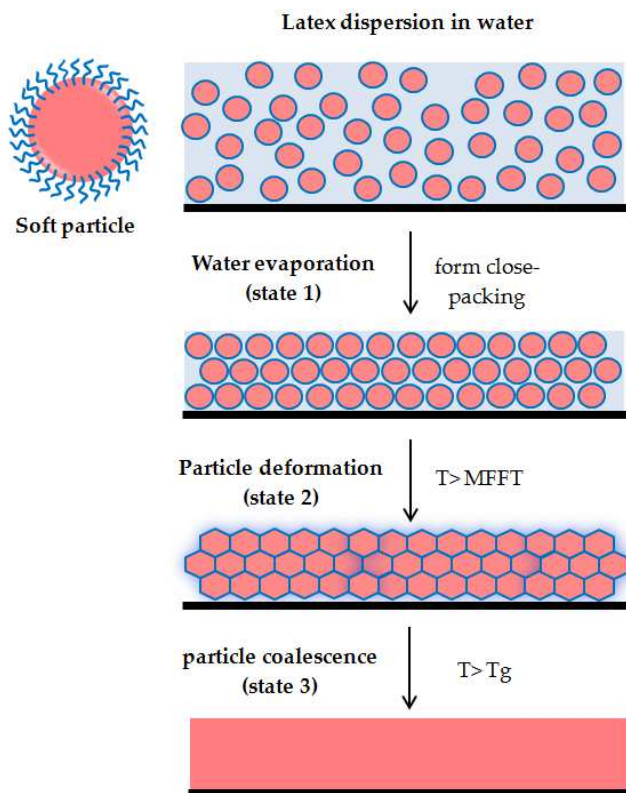


Figure 4- 8: Schematic of the film formation process.

State 1: Water evaporation

The first step of drying (water evaporation) begins when the latex is deposited on a surface and subjected to evaporation. The evaporation rate during this stage is normally constant^{27, 28} and it is quite similar to the evaporation rate of liquid media of latex²⁸. In this stage, two possible arrangements of particles can occur; in the first and preferred case the evaporation rate is constant and layers of close-packed particles form through the thickness of the layer²⁷ (Figure 4-8) and in the second case particles are packed toward the air surface of the latex during evaporation²⁸ (Figure 4-9). If particles accumulate on the top of latex, they may coalesce and form a continuous polymer film during film formation (skin formation), further drying is then limited by the coalesced film and the evaporation rate slows down. Particles packing on the top layer can be generally observed when drying thick layers of latex, for high evaporation rates and in softer polymer latexes¹

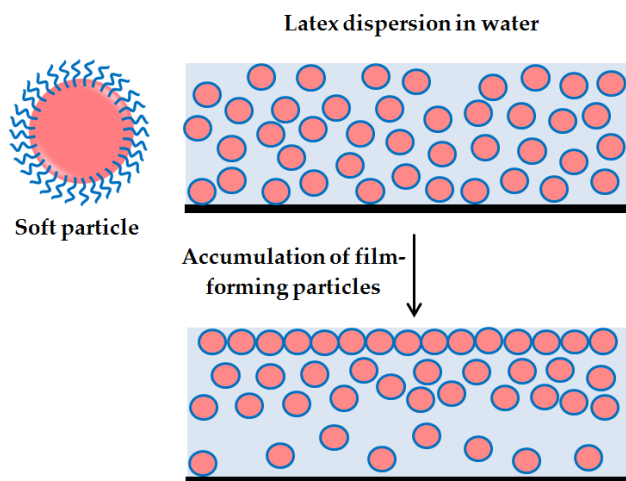
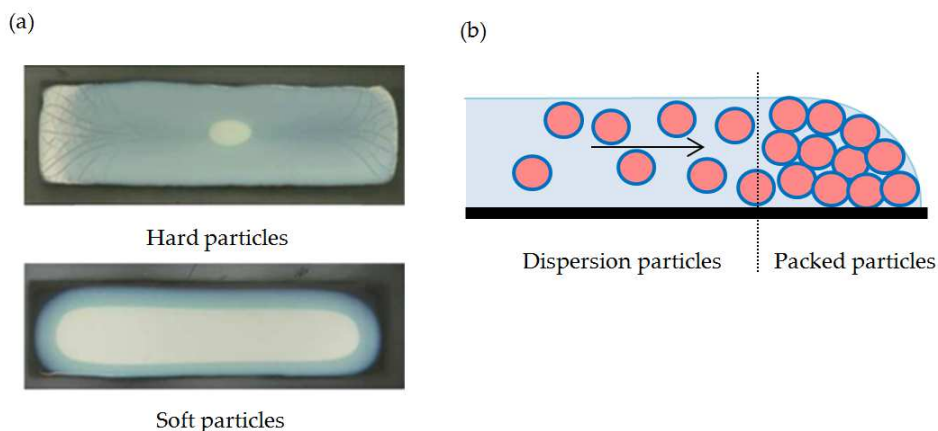


Figure 4- 9: Skin formation during drying process.

In the evaporation process, generally dispersion latexes do not dry in a uniform manner across the film. The edges of the film usually dry first.¹ Divry et al.²⁵ recently studied the drying behavior of hard and soft particle latexes. They found that soft and hard particles had different drying rates. The hard particle latex almost dried with the same rate as free water but the soft latex particle dried more slowly. The slow drying did not come only from skin formation but it also came from non-uniform horizontal drying. The horizontal drying front of hard particle and soft particle are presented in Figure 4-10 (a).

Figure 4- 10: Horizontal drying front of dispersion latex, (a) horizontal drying front of hard and soft particles²⁵, (b) The consolidated particles at the edge of the film

The horizontal drying front occurs through the accumulation of particles at the edge of the film. During the drying process, the height of the latex reduces due to the water evaporation. The particles near the edge begin to consolidate and to form a packed region. The continued evaporation from the

packed region, leads to a flux of water with latex particles from the bulk latex to the edge of the film (Figure 4-10 (b)).^{1, 29}

The observation of skin formation and of the horizontal drying front depends on the latex type, the particle size, dispersion viscosity, initial film thickness, evaporation rate and drying method.^{1, 25, 29}

State 2: Deformation of particles

In this stage after most of the water is evaporated, the particles consolidate into a form of random close-packing. The particles then deform their spherical shape to fill the void space around them. Four major methods of deformation have been proposed including wet sintering, dry sintering, capillary deformation and Sheetz's deformation.^{29, 30}

- Wet sintering^{1, 31}: the deformation of the particles by wet sintering comes from the interfacial tension between the particles and water. When the particles are in the phase of close-packing (particles pressed together), the interfacial area between them is eliminated, and the interfacial free energy is decreased.
- Dry sintering^{32, 1} is analogous to wet sintering. This method assumes that the particles dry completely before losing their shape due to deformation. Therefore the deformation of the particle comes from the particles-air surface tension.
- Capillary deformation^{33, 26} is based on the assumption that the evaporation of water and the deformation of the particles are concurrent phenomena. Capillary forces which are based on the air- water surface tension can generate a large negative pressure and compress the film.
- In contrast to the other methods, Sheetz's deformation³⁴ accounts for the creation of a skin effect during the drying process. As we mentioned above, a skin formation is based on particle accumulation on the surface and coalescence which hinders further evaporation. As the water diffuses through the top surface, it generates a compressive force to the film and causes particle deformation after drying.

The deformation of particles is possible with any of the 4 processes depending on the physical properties of the latex dispersion and also the drying methods.

For monodisperse particles, after water evaporation the particles can be packed into a face-centered cubic pattern where each particle is in direct contact with twelve nearest neighbor particles. This twelve-sided geometry is called rhombic dodecahedron¹, of which the appearance is similar to a natural honeycomb (Figure 4.8).

The deformation process transforms an opaque, cloudy film into a clear and transparent film. The lowest temperature to create the optical transparency film is called the minimum film formation temperature or MFFT which is close to the glass transition temperature of polymers in water.^{1, 35}

State 3: particle coalescence

Coalescence is the term to describe the diffusion of two particles with the elimination of the boundary between them.²⁶ The deformation of particles in stage 2 causes the coalescence of the particles with their nearest neighbors. The polymer chains diffuse across the inter-particle boundaries, resulting in a homogenous and transparent film with increased mechanical strength.^{1, 30, 35}

1.7 State of the art and aims of this study

As mentioned above, Chenal et.al^{6, 2, 22} developed a self-stabilized core-shell latex made of poly(acrylic acid)-block-poly(butyl acrylate), PAA-b-PBA by using surfactant-free RAFT-mediated emulsion polymerization in batch conditions. During the synthesis the formed diblock copolymer, PAA-b-PBA, self-assembles into core-shell latex particles, where poly(acrylic acid) serves as a hard shell and the soft core consists of poly(butyl acrylate). The PAA-b-PBA latex was then used to prepare a film by using a slow evaporation rate in order to obtain homogenous and transparent films.

The mechanical properties of the block copolymer films were then studied (Figure 4-11) by elongational rheology. The mechanical properties revealed that the film was structured in a well-defined percolating network of hard shells, (made of PAA) covalently connected to the soft core, (made of PBA). The existence of such a nanostructure was also confirmed by SAXS. The block copolymer film, which only contained less than 3 wt% of PAA (F2), presented a remarkable increase in both stiffness and toughness compared to a control sample of non-structured film, obtained from a latex of P(AA-co-BA) random copolymer of similar composition (F-R).⁶ In addition, thanks to the absence of a surfactant during synthesis, the PAA-b-PBA films were resistant to water whitening even after 72 hours of immersion in water.

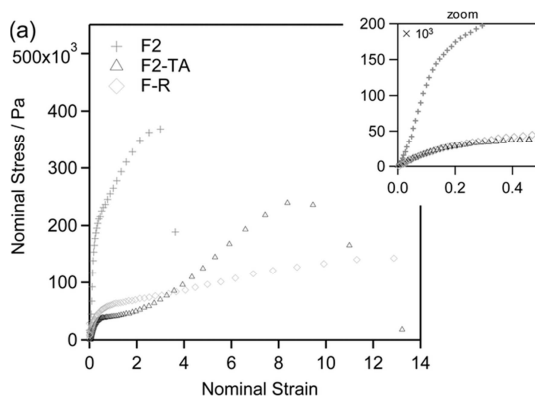


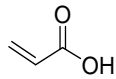
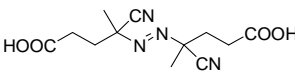
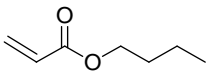
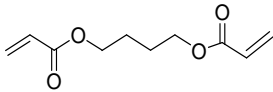

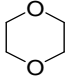
Figure 4- 11: Stress-strain curve of the structured film (F2), of the same film after annealing at 160°C for 3 days (F2-TA) and of the film obtained with a random copolymer (F-R).⁶

Regarding these distinct properties of films prepared from drying latexes, it is now interesting to broaden their application. In our study, a PAA-b-PBA nanostructured film will be created and serve as a polymeric filler with a very low volume fraction of glassy phase (PAA) embedded into a poly (butyl acrylate) elastomer matrix. The sequential interpenetrating network technique (described in chapter 1) will be applied here to facilitate the formation of double network film based on a dried latex as a first physically associated network.

2. Methods and synthesis

2.1 Chemicals and reagents

Chemical substrates and solvents for the synthesis of the acrylate latex films and acrylate double network latex films are listed in table 4-1. Acrylic acid (AA) and n-butyl acrylate (BA) are used as monomers. In general, every purchased acrylate contains a few ppm (parts per million) of radical inhibitor, a hydroquinone or monomethyl ether hydroquinone in order to prevent its self-polymerization. To synthesize polymers, these inhibitors need to be removed from the monomers. In our study, two methods were used, i) passing through an alumina column and ii) distillation under reduced pressure at room temperature. For the latex synthesis, the inhibitors were eliminated from BA by distillation at room temperature. However, for the double network synthesis, the crosslinker, 1,4-butanediol diacrylate (BDA), and BA were passed through an activated alumina to remove the inhibitors. Acrylic acid and others chemical reagents were used as received without any further purification.

Notation	Chemical Name	Semi-develop formula	M _n (g/mol)	Purity	Origin
AA	Acrylic acid		72.06	99%	Aldrich
ACPA	4,4'-Azobis(4-cyanovaleric acid)		280.28	≥98%	Aldrich
BA	n-butyl acrylate		128.17	99%	Aldrich
BDA	1, 4-Butanediol diacrylate		198.22	90%	Aldrich
Di-ether	Diethyl ether		74.12	≥99%	ACROS
Dioxane	1,4 Dioxane		88.11	≥98%	Aldrich

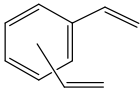
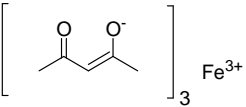
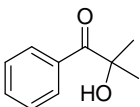
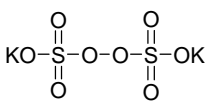
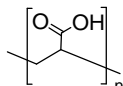
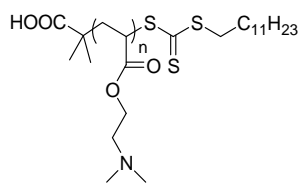
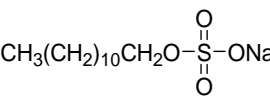
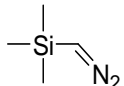
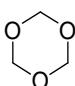
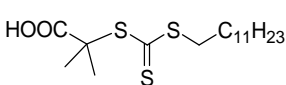
DVB	Divinylbenzene		130.19	80%	Aldrich
Fe ³⁺	Iron (III) acetylacetonate		353.17	97%	Aldrich
HMP	2-hydroxyethyl-2-methylpropiophenone		164.2	97%	Aldrich
KPS	Potassium persulfate		270.32	≥99%	Aldrich
NaOH	Sodium hydroxide	NaOH	40	100%	ACROS
NH ₄ OH	Ammonium hydroxide solution (28-30% NH ₃ basis)	NH ₄ OH	35.05		Aldrich
PAA	Poly(acrylic acid) in water		5000	50% in water	Poly sciences
PADAME (MC300)	Poly(N, N-dimethylamino ethyl acrylate) trithiocarbonate		3350		LCP lab
SDS	Sodium dodecyl sulfate		288.38	≥99%	Fisher
TMS	(Trimethylsilyl)diazomethane solution (2 M in diethyl ether)		114.22		Aldrich
Trioxane	1, 3, 5-Trioxane		90.08	99%	Aldrich
TTCA	2-(Dodecylthiocarbonylthio)-2-methyl propionic acid		364	>99%	LCP lab

Table 4- 1: Chemicals and reagents used in our latex study.

2.2 Latex characterization method

In this study, latex characterizations were performed in two stages; i) in the course of the polymerization, to characterize the conversion of monomers to polymers and to determine the % of residual monomer in the reaction medium, and ii) after polymerization, to characterize their solids content, molar mass of the final latex and also the particle size. The characterization methods are described below.

2.2.1 Gravimetric analysis

Gravimetric analysis is a quantitative determination method based on the mass of solid. In our study this method was used to determine the % solids content of the latex and also to determine the conversion (in %) of volatile monomers transformed to polymers. The method was established considering that after the latex was dried, the volatile contents which are water, NH_4 and volatile monomers should be removed by evaporation and only the solid polymer should remain.

The protocol to define the conversion and the solids content was quite simple. Firstly, about 0.2 ml of latex was dropped into a dry aluminum pan (with an initial weight, W_{pan}). After addition, the mass of latex solution in the pan (m_{wet}) was noted and then the sample was dried first at room temperature overnight and then at 100°C for 20 minutes. After drying, the cooled down sample was reweighed (m_{dry}). The calculation of the % solids content can be found in Eq.4-5. For the calculation of the monomer conversion, non-volatile compounds in the latex, such as RAFT agent (or macro-RAFT agent) and initiator need to be taken into account, since they do not evaporate but still remain with the polymer after drying. The calculation of the degree of conversion (%) of the monomer is presented in Eq.4-6, where m_{NV} is the weight of non-volatile compounds (NV) at the initial state, m_{total} is the weight of all components at the initial state and $m_{Monomer}$ relates to the monomer weight at the initial state.

$$\% \text{ Solid} = \left(\frac{m_{dry} - m_{pan}}{m_{wet} - m_{pan}} \right) \times 100 \quad (\text{Eq. 4 - 5})$$

$$\begin{aligned} \% \text{ Conv.} &= \frac{\left(\frac{m_{dry} - m_{pan}}{m_{wet} - m_{pan}} \right) - \left(\frac{m_{NV}}{m_{total}} \right)}{\left(\frac{m_{monomer}}{m_{total}} \right)} \times 100 \\ &= \frac{\% \text{ solid} - \% \text{ NV}}{\% \text{ monomer}} \end{aligned} \quad (\text{Eq. 4 - 6})$$

The residual latexes with coagulation or precipitation were collected using filtration with a silk membrane. The weight percentage of latex coagulation (% coag.) can be obtained by gravimetric analysis as showed in Eq.4-7 where m_{coag} is the mass of dry coagulate and m_{total} is the mass of total compositions at the initial state.

$$\% \text{ Coag.} = \left(\frac{m_{\text{Coag}}}{\% \text{ Solid} \times m_{\text{total}}} \right) \times 100 \quad (\text{Eq. 4 - 7})$$

2.2.2 Nuclear Magnetic Resonance (NMR)

NMR is used to identify and analyze molecular structures of organic compounds based on a magnetic nuclear spin of ^1H , ^{13}C , ^{15}N , ^{19}F , ^{31}P and so forth.³⁶ In our study, ^1H NMR was used to evaluate the conversion of acrylic acid to PAA-TTC macro-RAFT agent and also to identify its purity.

For NMR analysis, the sample was firstly dissolved in NMR tube series 200 by using deuterated DMSO as the solvent at room temperature. Then, the tube was loaded into the NMR chamber (Bruker Avance 200 MHz) with an observed spectrum at -4 to 16 ppm and residual DMSO (^1H , 2.5 ppm) as an internal reference standard. All the NMR spectra results were treated with TopSpin processing software.

2.2.3 Size Exclusion Chromatography (SEC)

SEC is currently the most commonly used method to analyze the molar mass of synthetic macromolecules and biopolymers.^{37, 38} Through the special chromatography column used, it is assumed that there are no enthalpic interactions between the analyte and the stationary phase, the analyte molecules are only separated according to their hydrodynamic volume.³⁷ However, in reality the analyte compounds containing functional groups such as -SH, -OH, -NH and -COOH need to be discussed in more detail. These functional groups have a tendency to form intermolecular hydrogen bonds and can thus interact with the column packing materials of the SEC.³⁹ In our study, the latex is composed of acrylic acid and therefore contains carboxylic acid groups (-COOH). These groups need to be eliminated in order to prevent adsorption to the SEC column. The methylation technique was used to replace an active hydrogen of the carboxylic acid group by a methyl group (-CH₃) into carboxylic acid group as described below.⁴⁰

Methylation

The latexes composed of acrylic acid were modified by methylation, using (trimethylsilyl) diazomethane (TMS) as described by Couvreur et al. in 2003.⁴¹ In this way, 5 mg of sample was

dissolved in 10 ml of a mixture of THF and water (90: 10, THF: water in volume). The proportion of water was increased when there was a large amount of acrylic acid in the sample. Then, the sample solution was adjusted to pH 2 by using a small amount of hydrochloric acid (HCl 1 M) and stirred for 2 hours. In this state, the solution must be transparent without any coagulation. In case of cloudy appearance, THF and water were added until the solution turned transparent and clear. Then, the yellow solution of TMS was added dropwise in the solution while continuously stirring at room temperature. Upon addition, bubbles of N_2 appeared and the yellow color of TMS slowly turned to colorless. The TMS was continuously added until the solution remained yellow and no bubbles occurred. The reaction mechanism of TMS with the carboxyl group is shown in Fig 4-12.⁴⁰ The solution was constantly stirred at room temperature for 4-6 hours before drying in the aluminum pan at room temperature overnight. After that, the dry methylated sample was dried again at 100 °C for 1 hour in an oven in order to remove all excess water before dissolving in THF for the SEC analyses.

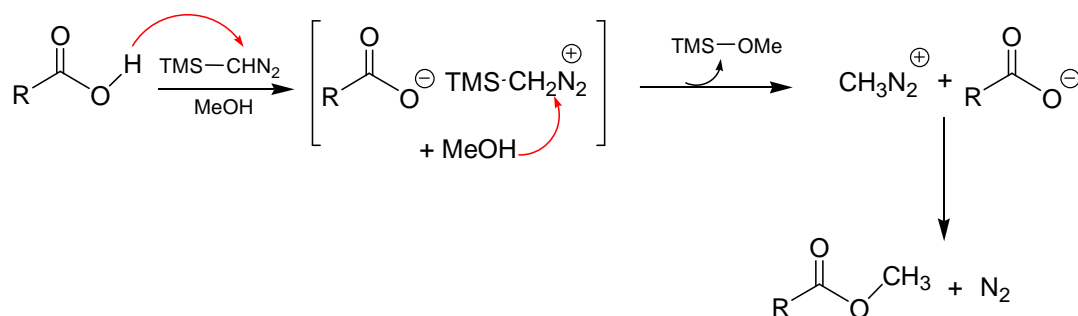


Figure 4- 12: General mechanism for the methylation of carboxylic acids by (trimethylsilyl)diazomethane (in our study MeOH is replaced by water)⁴⁰

Size exclusion chromatography (SEC) in THF

The methylated sample was dissolved into THF solvent containing toluene as a flow-rate marker at the approximate concentration of 5 mg.ml⁻¹. Then, the sample was filtrated with a 0.2 μ m pore-size membrane and placed into the SEC sample chamber for auto-injection to the column. In our study, the SEC was equipped with an integrated solvent and sample delivery module (Viscotek, GPC max). It was operated at a THF flow rate of 1 ml.min⁻¹ with the two columns set at 40°C (PLgel 5 μ m MIXED-C, 7.5 mm \times 300 mm), and a refractive index (RI) detector (Viscotek VE3580) and an Ultra violet (UV-vis) detector (Shimadzu PD-20A/20AV) were used for detection. The data were treated by OmniSEC processing software from Viscotek and the number-average molar mass (M_n) and dispersity (M_w/M_n) were estimated using a polystyrene standard calibration (from polymer laboratories).

2.2.4 Dynamic Light Scattering (DLS)

DLS is a technique that can be used to measure the diameter of latex particles. In our study, a NanoZS90 by Malvern Instrument was used to analyze the diameter of latex particles at 90 degree of scattering by using a laser at 633 nm wavelength. The nanosizer has the capability to measure the particle size from 0.3 nm to 5000 nm diameter.

After the synthesis of the latex, a small amount of latex product was diluted in distilled water. The sample was loaded into the DLS testing tube and placed in the sample cavity of the machine. The test was performed at 25 °C within 3 repetitions. The DLS analyzer was controlled by DTS processing software. The average diameter (Z average, D_z) of the particle size distribution (PDI) of latex particles is defined as the intensity weighed mean hydrodynamic diameter of the total distribution of the particles.

2.2.5 pH-meter

For latex synthesis, the pH of the latex is an important factor and needs to be controlled. A pH meter (Mettler Toledo DL50 Graphix) with a glass microelectrode (Mettler Toledo) was used to adjust and measure the pH of all solutions and latexes used in our study.

2.2.6 Transmission Electronic Microscopy (TEM)

TEM observations were performed by Patricia Beaunier at UPMC with a JEOL 100 CXII TEM instrument operated at an accelerating voltage of 100 kV. Samples for TEM analyses at room temperature were prepared by depositing 3 μ L of the aqueous solution on TEM grids and air drying.

2.3 P(BA-co-BDA) crosslinked latex synthesized by radical emulsion polymerization

For comparison, a latex of poly[(n-butyl acrylate)-co-(1,4-butanediol diacrylate)] or P(BA-co-BDA) was synthesized by conventional radical emulsion polymerization in batch conditions. Therefore, a small amount of 1,4-butanediol diacrylate (BDA) was introduced into the system in order to crosslink the PBA chains in the particles and to prevent the disintegration during the swelling in BA monomer before creating double network films. At first, distilled n-butyl acrylate (BA) monomer, 1,4-butanediol diacrylate (BDA) as a crosslinker, sodium dodecyl sulfate (SDS) as a surfactant and potassium persulfate (KPS) as

an initiator were mixed in distilled water. The detailed composition is presented in Table 4-2. The mixed solution was then stirred in an ice bath under argon atmosphere in order to remove oxygen for 45 minutes. After that, the polymerization took place in an oil bath at 60°C for 3 hours and 30 minutes under a constant stirring at 600 rpm. Before stopping the reaction with an ice bath and oxygen, a small amount of latex sample was taken by a syringe (about 0.2 ml) to check the conversion of the monomer. The conversion (% Conv.) and solids content (% solid) of the resulting P(BA-co-BDA) latex were determined by gravimetric analysis as described in section 4.6.

	<i>TLL01</i>
Name	latex _{no-shell}
Temperature, °C	60
Reaction time, min	210
mol% BDA ^a	0.5
BA conc., mol.L ⁻¹	2.84
KPS conc., mol.L ⁻¹	33.4×10^{-3}
BDA conc., mol.L ⁻¹	14.2×10^{-3}
SDS conc., mol.L ⁻¹	22.1×10^{-3}
% conversion	95
% solids content	26
% coagulation	0
D _z , nm	106
PDI ^b	0.04

Table 4- 2: Reaction conditions and characteristics of P(BA-co-BDA) latex,

^a molar percentage of BDA $\text{mol\% BDA} = n_0(\text{crosslinking agents})/n_0(\text{BA}) \times 100$, ^b polydispersity index obtained from DLS

The P(BA-co-BDA) latex was filtrated by a silk membrane to collect the coagulated latex and define the weight percentage of latex coagulation (% coag). The final P(BA-co-BDA) latex solution was stored at room temperature and any contact with UV light was avoided. To characterize the latex particles, dynamic light scattering (DLS) analyses were used to determine the average diameter of the latex particles (D_z). Unfortunately, we could not measure a molar mass of PBA chains inside the particles since they are crosslinked. The results of % Coag. and D_z of the latex can be found in table 4-

2. The P(BA-co-BDA) latex was named as PBA_{no-shell}. The latex was synthesized with controlled conditions, resulting in a latex without coagulum and low PDI, as measured by DLS.

2.4 PAA-b-PBA core-shell latex synthesized by RAFT emulsion polymerization

The core-shell latex composed of poly(acrylic acid)-block-poly(n-butyl acrylate) diblock copolymers or PAA-b-PBA, has been synthesized by Reversible Addition-Fragmentation Transfer (RAFT) polymerization. As explained above, RAFT polymerization needs a chain transfer agent, called RAFT agent, which contains a thiocarbonylthio compound to control the polymerization and chain's growth.

In our study, the macro-RAFT agent (see section 1.3) was synthesized with acrylic acid (AA) to create a hydrophilic macro-RAFT agent named PAA-TTC. Then, in the second polymerization step, the block copolymer PAA-b-PBA was synthesized by the PAA-TTC. The macro-RAFT agent was chain extended by a PBA block in the formerly described aqueous emulsion polymerization process, using batch conditions. By this method, amphiphilic block copolymers PAA-b-PBA form and beyond a critical length of the PBA block, core-shell latex particles are created. As explained in section 1.5, this approach is called polymerization induced self-assembly or PISA. (The structure of the PAA-b-PBA latex particle is schematically shown in Fig.4-13, in which the PAA is the shell while PBA is the core.

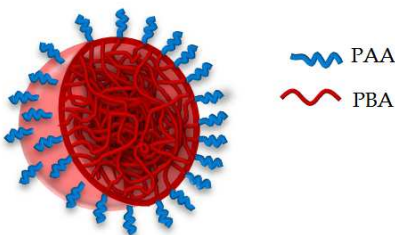


Figure 4- 13: The structure of PAA-b-PBA core-shell latex particles

Different sizes of latex shells and latex cores were investigated in our study. Thin shells containing short PAA segments (2.5 to 6 kg.mol^{-1}), and large core containing long PBA blocks (100 - 200 kg.mol^{-1}). Particles were typically synthesized and the polymerization conditions were optimized. Moreover, we also synthesized latexes with a crosslinked core by using two different crosslinkers; 1,4 butanediol diacrylate (BDA) and divinylbenzene (DVB). These latex particles structures are shown in

Fig 4-14. The used methods and synthesis conditions of these latexes are explained in the following section.

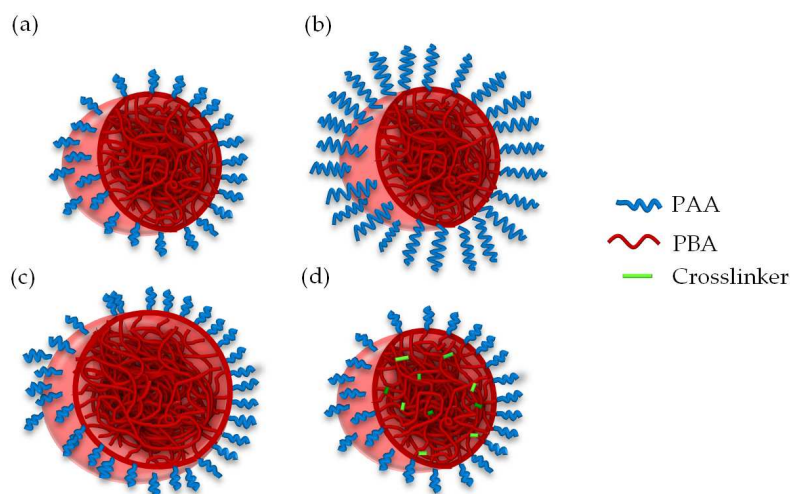


Figure 4- 14: The types of structures of PAA-b-PBA latex particles, which were synthesized. (a) *normal* soft core-hard shell latex, (b) soft core-*thick* hard shell latex (c) *large* soft core-hard shell latex and (d) *crosslinked* soft core-hard shell latex

2.4.1 PAA-TTC macro-RAFT agent

In order to synthesize PAA-b-PBA amphiphilic block copolymers, a poly(acrylic acid) was first synthesized in solution with a RAFT agent (TTCa) to create the PAA-TCC macro-RAFT. The overall procedure is schematically described in figure 4-15.

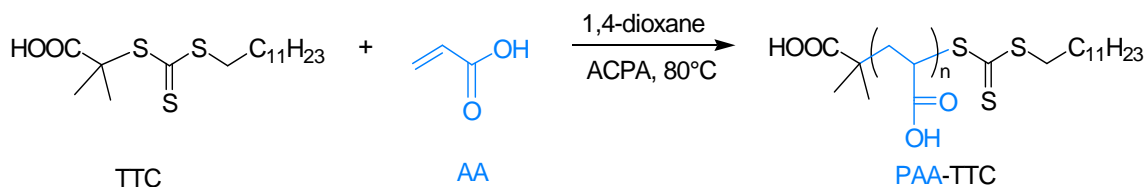


Figure 4- 15: Synthesis of PAA-TTC macro-RAFT agent.

Experimental section

At first, the RAFT agent 2-(dodecylthiocarbonylthio)-2-methyl propionic acid (TTCA, $M = 364 \text{ g.mol}^{-1}$), 1,3,5-trioxane and 4,4'-azobis(4-cyanovaleric acid) or ACPA ($t_{1/2} = 150 \text{ min}$ at 80°C) were dissolved in 1,4-dioxane. After mixing well and dissolving all compounds, acrylic acid (AA) was added to the solution and stirred for a while until the solution was homogeneous. Then, the solution was deoxygenated with bubbling of argon for 30 minutes under cold conditions using an ice bath. The polymerization was carried out at 80°C with continuous stirring at 275 rpm. To verify the conversion of AA monomer, samples were taken during the reaction and dissolved in deuterated DMSO for measuring by ^1H NMR. The signal of 1,3,5-trioxane as an internal reference peak (5.1 ppm) and vinylic proton signals of AA (5.5 ppm) were checked at the initial time (t_0) and also determined at different times (t_x) during the reaction. The monomer conversion was defined by the molar ratio of 1,3,5-trioxane and AA at t_x correlated to their ratio at t_0 with the assumption that 1,3,5-trioxane was not decomposed or polymerized with other ingredients.

After the desired conversion was reached, the reaction was stopped by oxygenating and cooling down the solution simultaneously. The PAA-TTC macro-RAFT agent in solution was precipitated dropwise into a diethyl ether (Di-ether) bath at room temperature with a high speed stirring in order to remove unreacted monomers. Upon precipitation, PAA-TTC macro-RAFT sedimented in a yellow precipitate and after the last drop was applied; the sludge was left for the sedimentation for 30 minutes. The sludge of PAA-TTC was then removed from the Di-ether bath by vacuum filtration with a sintered disc filter funnel grade 4 (10-16 μm) and re-dissolved into 1,4-dioxane for a second precipitation. The final PAA-TTC sludge (after 2 precipitations) was dried at room temperature overnight and then under vacuum at room temperature for 24 hours. The final product was analysed by ^1H NMR (Appendix A-1) and methylated before analyzing by SEC/THF. Reaction conditions, % conversion, number-average molar mass (M_n) and dispersity (M_w/M_n) of the PAA-TTC macro-RAFT agent synthesized in our study are listed in Table 4.3.

Results of the synthesis

Table 4.3 reveals that several PAA-TTC macro-RAFT agents could be synthesized in a controlled way. The differently sized macro-RAFT agents, M_n ranging from 2.5 to 6 kg.mol^{-1} , showed a dispersity (M_w/M_n) < 1.2 , and the $M_n(\text{exp})$ was very close to $M_n(\text{th})$ which indicated the good control of the polymerization.

	AA-TL01	AA-TL02	AA-TL03	AA-TL04	DG03
Temperature, °C	80	80	80	80	80
Reaction time, min	95	70	106	75	95
AA conc., mol.L ⁻¹	1.6	1.5	1.5	1.5	1.5
TTCA conc., mol.L ⁻¹	14.7×10^{-3}	16.2×10^{-3}	37.1×10^{-3}	36.7×10^{-3}	36×10^{-3}
ACPA conc., mol.L ⁻¹	1.5×10^{-3}	1.7×10^{-3}	4×10^{-3}	4.7×10^{-3}	3.1×10^{-3}
[AA] ₀ / [TTCA] ₀	108	95	40	40	41
% conversion	67	53	69	72	60
M _n (th) ^a , kg.mol ⁻¹	5.6	4	2.4	2.4	2.1
M _n (exp) ^b , kg.mol ⁻¹	5.9	3.9	2.6	2.5	2.6
M _w /M _n ^c	1.2	1.2	1.1	1.1	1.1

Table 4- 3: Polymerization conditions and characteristics of PAA-TTC macro-RAFT agents, ^a M_n(th) calculated by Eq. 4-1, ^b M_n(exp) was determined by SEC in THF with a PS calibration (indicated by index PS: _{PS}) and recalculated to designate the non-methylated mass of; $M_n = [M(AA)/(M(MA))] \times M_{n,PS}$, ^c polydispersity obtained from SEC using PS calibration

2.4.2 PAA-b-PBA latexes

To synthesize the PAA-b-PBA core-shell latexes, the emulsion polymerization of n-butyl acrylate (BA) was performed using the PAA-TTC macro-RAFT agent, summarized in Table 4-3 as a control agent and stabilizer.²² The mechanism of the PAA-b-PBA polymerization is described in Figure 4-16.

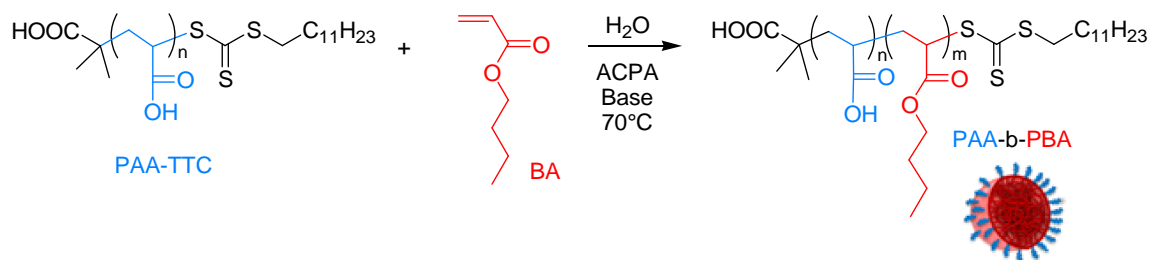


Figure 4- 16: Synthesis of PAA-b-PBA latexes

Experimental section

At first, the PAA-TTC macro-RAFT agent was dissolved into distilled water before adding a specific volume of a stock solution of 4,4'-azobis(4-cyanovaleric acid), ACPA, ($t_{1/2} = 150$ min at 80°C), prepared by dissolving ACPA in water and with a small drop of NH_4OH . Then the PAA-TTC solution was stirred for a while and the pH was adjusted with a 30% ammonium hydroxide (NH_4OH) solution. The pH of the PAA-TTC solution was set to a specific pH, generally between pH 6.0 to 6.8 depending on the size of the PAA-TTC macro-RAFT agent (M_n). After fine tuning the pH, BA was added into the solution and stirred at room temperature for a night.

The solution was then deoxygenated with argon bubbling in an ice bath for 30 minutes. Then, the polymerization was carried out at 70°C at a stirring speed of 275 rpm. During the polymerization, the reaction medium turned from a transparent solution to a whitish liquid, which was the sign of the particle formation by the polymerization of the BA. To monitor the conversion, samples were collected with a syringe and analyzed by gravimetric analysis. After the polymerization reached at least 85% conversion, the polymerization was quenched in an ice bath and oxygenated by opening the septum. The white finished latex solution is presented in Figure 4-17.

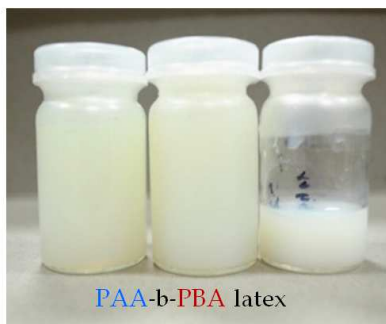


Figure 4- 17: White solution of the final latexes.

To characterize the size and morphology of latex particles, dynamic light scattering (DLS) and transmission electron microscopy (TEM) were performed. The M_n and molar mass dispersity of polymers ($M_w/M_n = \bar{D}$) were characterized by SEC/THF after methylation.

After polymerization, the PAA-b-PBA latexes were kept at 4°C until used. To distinguish easily latexes, they were named as ($\text{AA} + M_n$, $\text{BA} + M_n$), for example ($\text{AA}2.6\text{k}$, $\text{BA}100\text{k}$) meaning a latex synthesized with a PAA-TTC macro-RAFT agent of $M_n \sim 2.6 \text{ kg.mol}^{-1}$ and the final M_n of the latex is $\sim 100 \text{ kg.mol}^{-1}$ (we assume that the M_n of the final latex $\sim M_n$ of BA due to the small M_n of PAA-TTC, considered as negligible).

Results of the synthesis

Latexes with different thicknesses of the PAA shell

The shell thickness of PAA-b-PBA latex is controlled by the molar mass of the PAA block, hence PAA-TTC of different M_n ; 6, 4 and 2.6 kg.mol⁻¹, were used to polymerize BA via RAFT-mediated emulsion polymerization. The polymerization conditions were kept constant, 70 °C, 275 rpm, under argon gas and using 30% NH₄OH for pH adjusting.

We found that the molar mass of the PAA in the macro-RAFT agent had an influence on the control of the polymerization. To achieve latexes with a low molar mass dispersity ($M_w/M_n = \bar{D}$) and a small particle size distribution (expressed as the polydispersity index, PDI) the pH of the reaction needed to be finely adjusted. Thus, we decided to study the effect of the pH in the range of 5.5 to 7.0 on the control over the emulsion polymerization of BA for the different PAA-TTC macro-RAFT agents by maintaining the other conditions constant. The results, analyzed by SEC/THF, are shown in Figure 4-18.

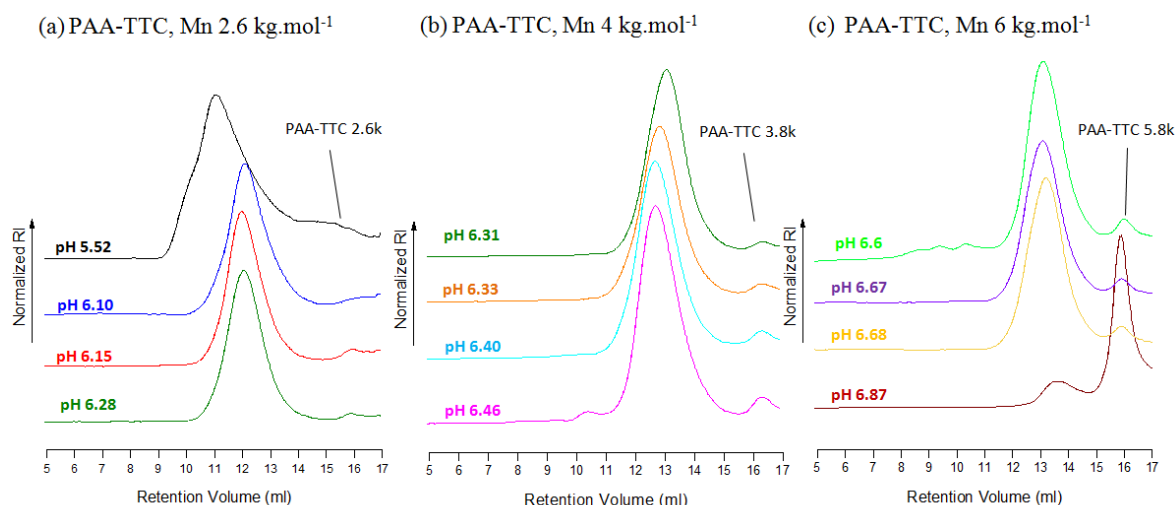


Figure 4- 18: The impact of pH on the PAA-b-PBA latex synthesis using (a) PAA-TTC, M_n 2.6 kg.mol⁻¹, (b) PAA-TTC, M_n 4 kg.mol⁻¹ and (c) PAA-TTC, M_n 6 kg.mol⁻¹

In general, the SEC shows that the pH must be precisely tuned to obtain a good control over the BA polymerization. For the smallest PAA-TTC of M_n 2.6 kg.mol⁻¹ (Figure 4-18 (a)), a good polymerization control can be reached, reproducibly, for pH values between 6.1 - 6.3 with the reasonably low molar mass dispersity (M_w/M_n) 1.7 - 2.0. The medium size PAA-TTC of M_n 4 kg.mol⁻¹ (Figure 4-18 (b)) shows also an optimum pH range of 6.3 - 6.4 that has a low impact on the polymerization with a low molar mass dispersity (M_w/M_n) around 1.7 - 2.0.

In contrast, the longest PAA-TTC of M_n 6 kg.mol⁻¹ (Figure 4-18 (c)) was difficult to use successfully in emulsion polymerization of BA. Little changes in pH had a high impact on the control of the polymerization. For this macro-RAFT, a pH around 6.7 yielding a low molar mass dispersity of 1.6 was chosen for further synthesis. However, as observed in the SEC in THF, some of the macro-RAFT did not react and remained in the latex (especially at high pH). Similarly, Wong et al.^{19, 42} reported for the polystyrene-b-poly(N,N-dimethylacrylamide), (PS-b-PDMA) via RAFT polymerization that the length of the polystyrene macro-RAFT agent had an effect on the block copolymer synthesis. The macro-RAFT agent with a high M_n (> 9 kg.mol⁻¹) led to a bimodal distribution of molar masses, a broadened molar mass dispersity and some remaining free macro-RAFT agents after polymerization. The authors proposed that the length of the macro-RAFT agent limited the accessibility of the thiocarbonylthio end group and delayed the polymerization reaction.⁴² Chenal et al.²² also studied the influence of pH on the RAFT polymerization of the PAA-TTC macro-RAFT agent and BA to create a PAA-b-PBA latex. They reported that at higher pH (pH 6.7), the efficiency of the macro-RAFT agent was reduced, compared to pH 5.4, due to a stronger ionization level of the PAA-TTC macro-RAFT agent. The conformation and partitioning in the different phases of strongly ionized macro-RAFT agents is pH dependent and consequently, the propagating chains might hardly meet and react with the macro raft agent. However, in their study, the impact of the pH of polymerization on the resulting M_n was not clearly elucidated. Considering the high pH used for the high M_n PAA-TTC macro-RAFT agent, it might be less reactive or partially degraded and some PAA chains may consequently remain in the serum after polymerization.

In order to study the effect of the PAA shell thickness on the properties of the film made from PAA-b-PBA latex (using PAA-TTC of different M_n), the M_n of the PBA block should be kept as constant as possible (~ 100 kg.mol⁻¹). In a controlled polymerization, the M_n of the PBA block can be adjusted by tuning the $[BA]_0/[PAA-TTC]_0$ feed ratio. Here, because of the different efficiencies of the macro-RAFT agents for different molar masses, the $[BA]_0/[PAA-TTC]_0$ ratio must be adjusted for each PAA-TTC molar mass in order to reach a final M_n of PBA close to 100 kg.mol⁻¹. As expected the longer PAA-TTC macro-RAFT agent of M_n 6 kg.mol⁻¹ needed a lower $[BA]_0/[PAA-TTC]_0$ ratio than the shorter macro-RAFT agents to achieve the same $M_n \sim 100$ kg.mol⁻¹ due to the lower efficiency of the macro-RAFT, (Figure 4-19).

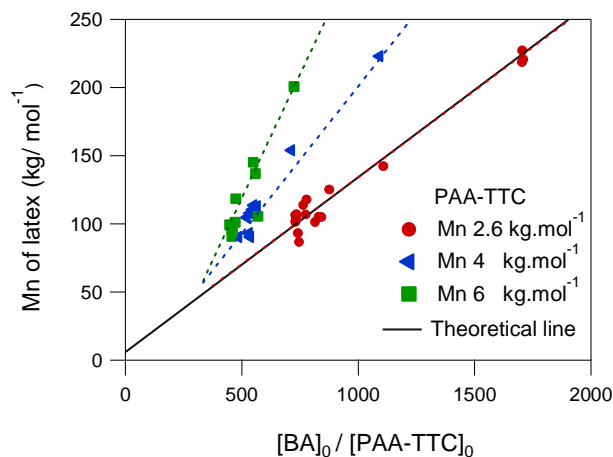
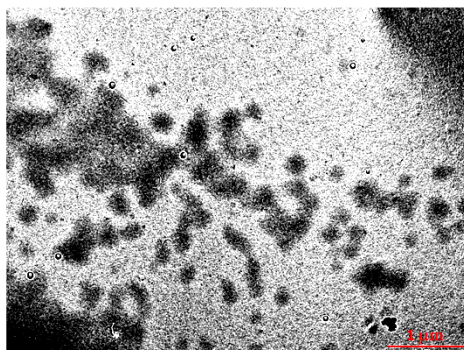


Figure 4- 19: The effect of initial molar ratio of PAA-TTC on the resulting M_n of the PAA-PBA latexes, dashed lines are a guide line for eyes

The latexes were also analyzed by TEM showing soft spherical particles (Figure 4-20 a) and (b)). It seemed that some residue of PAA-TTC macro-RAFT agent could be observed in the latex solution with the PAA-TTC M_n 4 kg.mol^{-1} (Figure 4-20). In the latex with PAA-TTC M_n 6 kg.mol^{-1} , TEM imaging was difficult probably due to a high concentration of residual macro-RAFT. In our study we did not remove the residual macro-RAFT agent. We first assumed that it should be negligible due to its low quantity compared to PBA, some experiments were also performed where free PAA was added to the serum in order to observe its impact on the film formation and properties (section 3.3). Thus, all the latexes synthesized from macro-RAFT agents with different M_n were used without any further purification.

(a) PAA-TTC M_n 2.6 kg.mol^{-1}



(b) PAA-TTC M_n 4 kg.mol^{-1}

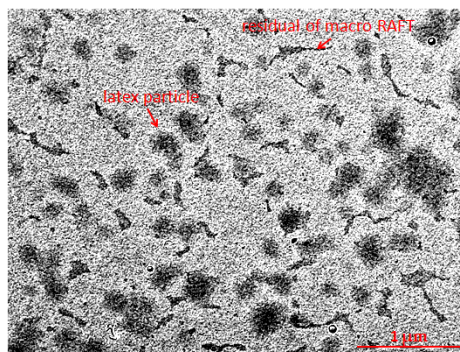


Figure 4- 20: TEM images of latex synthesized with different PAA-TTC (a) The latex TL38 (equal to TL 85) with PAA-TTC M_n 2.6 kg.mol^{-1} , and (b) the latex TL23 with PAA-TTC M_n 4 kg.mol^{-1}

The final latexes with different PAA shell thicknesses were called (PAA2.6k, PBA100k), (PAA4k, PBA100k) and (PAA6k, PBA100k) for the latex synthesized with PAA-TTC M_n 2.6, 4 and 6 kg.mol^{-1} respectively and a M_n of PBA close to 100 kg.mol^{-1} . The characteristics of the different PAA-b-PBA latexes and their polymerization conditions are summarised in Table 4-4. Overall the synthesis of these latexes occurred with acceptable control and the M_n of final latexes was comprised between 100 to 110 kg.mol^{-1} and dispersities were below 2.0. It was found that with increasing M_n of PAA-TTC (from 2.6 to 6k), the particle diameter slightly increased from ~80 nm to ~115 nm.

	TL05	TL06	TL07	TL08	TL85	TL103	TL19	TL23	TL29	TL16	TL22	TL34
Name	(PAA2.6k, PBA100K)						(PAA4k, PBA100K)			(PAA6k, PBA100K)		
Temperature, °C	70	70	70	70	70	70	70	70	70	70	70	70
Reaction time, min	360	220	320	240	272	270	202	160	200	195	190	200
pH ^a	6.15	6.26	6.26	6.28	6.17	6.01	6.40	6.31	6.33	6.66	6.66	6.67
M _n of PAA-TTC, kg.mol ⁻¹	2.6	2.6	2.6	2.6	2.5	2.5	4	4	4	6	6	6
BA conc., mol.L ⁻¹	2.4	2.3	2.3	2.3	2.3	2.3	2.3	2.4	2.4	2.3	2.3	2.3
PAA-TTC conc., mol.L ⁻¹	2.8 × 10 ⁻³	2.7 × 10 ⁻³	2.8 × 10 ⁻³	2.8 × 10 ⁻³	3.1 × 10 ⁻³	3.1 × 10 ⁻³	4.2 × 10 ⁻³	4.6 × 10 ⁻³	4.4 × 10 ⁻³	5.1 × 10 ⁻³	5.2 × 10 ⁻³	5.1 × 10 ⁻³
ACPA conc., mol.L ⁻¹	0.7 × 10 ⁻³	0.7 × 10 ⁻³	0.7 × 10 ⁻³	0.7 × 10 ⁻³	0.7 × 10 ⁻³	1.1 × 10 ⁻³	0.6 × 10 ⁻³	0.9 × 10 ⁻³	0.9 × 10 ⁻³	1.4 × 10 ⁻³	1.1 × 10 ⁻³	1.1 × 10 ⁻³
% conversion	88	96	93	95	92	95	88	89	91	93	87	82
% solids content	21	22	22	22	22	21	21	22	22	23	22	21
% coagulation	0	0	0	0	0	0	0	0	0	0	0	0
M _n (th) ^b , kg.mol ⁻¹	96.8	107.3	97.3	103.9	88.9	91.5	65.6	63.5	66.0	61.3	55.5	53.9
M _n (exp) ^c , kg.mol ⁻¹	104.4	102.4	93.1	99.4	106.4	107	113.5	101.2	107.8	105.5	99.2	95.5
M _w /M _n	1.7	1.7	1.9	1.8	2.0	2.4	2.0	1.7	1.7	1.6	1.50	1.60
wt% PAA ^d	2.6	2.3	2.5	2.4	2.5	2.4	5.7	5.9	5.7	10.3	11.0	11.4
D _z , nm	82	73	76	80	85	66	101	97	97	113	120	117
PDI ^e	0.06	0.06	0.05	0.05	0.08	0.08	0.06	0.08	0.06	0.03	0.05	0.06

Table 4- 4: Polymerization conditions and characteristics of PAA-b-PBA latex with different M_n of PAA, ^a pH of the solution adjusted with a NH₄OH 30% NH₃ basis before polymerization, ^bM_n(th) calculated from Eq. 4-1, ^cM_n(exp) was determined by SEC in THF with a PS calibration and recalculated to designate the non-methylated mass; $M_n = [M(AA)/(M(MA))] \times M_{n,PS}$., ^d poly(acrylic acid) content %wt PAA = $m_0(PAA)/(m_0(BA) \times conv.) \times 100$], ^e polydispersity index obtained from DLS.

Latexes with different core size of PBA

After the study of the effect of changing the thicknesses of the PAA shells in the former section, we were also interested in investigating the effect of changing the PBA core size while keeping the PAA shell constant. To synthesize the latexes with different PBA core sizes, a PAA-TTC of M_n 2.6 kg.mol⁻¹ was used, and latexes were synthesized by changing the initial $[BA]_0 / [PAA-TTC]_0$ ratio (Figure 4-19). The $[BA]_0 / [PAA-TTC]_0$ ratio was increased from 750 to 1750 while the polymerization conditions were kept constant at 70 °C with stirring at 275 rpm. The characterization of the latexes and the polymerization conditions are presented in Table 4-5.

	<i>TL83</i>	<i>TL104</i>
Name	(PAA2.5k, PBA150k)	(PAA2.5k, PBA200k)
Temperature, °C	70	70
Reaction time, min	240	300
pH ^a	5.87	6.04
M_n of PAA-TTC, kg.mol ⁻¹	2.6	2.6
BA conc., mol.L ⁻¹	2.3	2.3
PAA-TTC conc., mol.L ⁻¹	2.4×10^{-3}	1.4×10^{-3}
ACPA conc., mol.L ⁻¹	0.7×10^{-3}	0.9×10^{-3}
$[BA]_0 / [PAA-TTC]_0$	975	1715
% conversion	92	91
% solids content	22	21
% coagulation	0	0
M_n (th) ^b , kg.mol ⁻¹	117.0	202.6
M_n (exp) ^c , kg.mol ⁻¹	148.3	200.1
M_w / M_n	3.0	3.0
wt% PAA ^d	1.9	1.1
D_z , nm	89	95
PDI ^e	0.13	0.07

Table 4- 5: Polymerization conditions and characteristics of PAA-b-PBA latexes with different PBA core sizes, ^a pH of solution adjusted by a NH₄OH 30% NH₃ basis before polymerization, ^b M_n (th) calculated by Eq. 4-1, ^c M_n (exp) was determined by SEC in THF with a PS calibration and recalculated to designate the non-methylated mass of; $M_n = [M(AA)/(M(MA))] \times M_{n,PS}$, ^d poly(acrylic acid) content %wt PAA = $m_0(PAA)/(m_0(BA) \times conv.) \times 100$, ^e polydispersity index obtained from DLS.

Latexes with a larger M_n of PBA had quite a high polydispersity ($M_w/M_n \sim 3$), indicating some loss of control over the polymerization. However, the $M_n(\text{exp})$ of the latexes measured by SEC/THF were close to the theoretical M_n , $M_n(\text{th})$, especially at the high $[\text{BA}]_0 / [\text{PAA-TTC}]_0 = 1715$. The SEC/THF results (Figure 4-21) showed a bimodal distribution at the beginning which is also an indication of some loss of control. The increase of the M_n of the PBA had some effect on the particle size, with the higher M_n of the PBA resulting in a larger particle size.

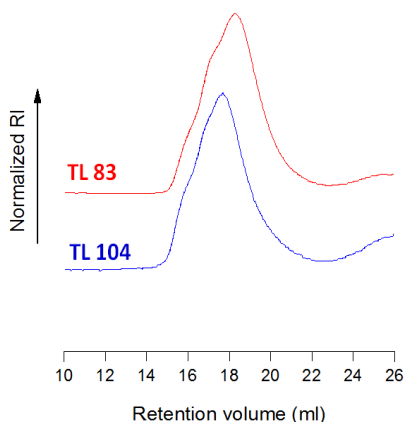


Figure 4-21: SEC in THF of PAA-b-PBA latex with different core size of PBA.

2.4.3 PAA-b-PBA latex with a crosslinked PBA-core

In this study, the PBA core of PAA-b-PBA latex was crosslinked by two kinds of conventional crosslinkers 1,4-butanediol diacrylate (BDA) and divinylbenzene (DVB).

Experimental section

To synthesize these latexes, BDA or DVB was introduced in the PAA-TTC and ACPA solution. After stirring, the pH of the solution was adjusted with NH_4OH to a pH close to 6. Then, BA and the crosslinker (BDA or DVB) were added to the solution under stirring at room temperature for one night. The polymerization was carried out at 70°C with stirring at 275 rpm under argon. After the conversion reached 85%, the reaction was stopped by temperature quenching and oxygenating. The morphology of the latexes with a crosslinked PBA-core was characterized by DLS measurements and by TEM. However, M_n of the crosslinked latexes could not be analyzed by SEC/THF since the dissolved latex did not pass through the $0.2\ \mu\text{m}$ filter used before the SEC analysis which indicated that the crosslinking was indeed efficient even using a low concentration of crosslinker such as 0.3 mol%. A TEM image of a crosslinked PAA-b-PBA latex is displayed in Figure 4-22 and the polymerization conditions of the latexes can be found in Table 4-6.

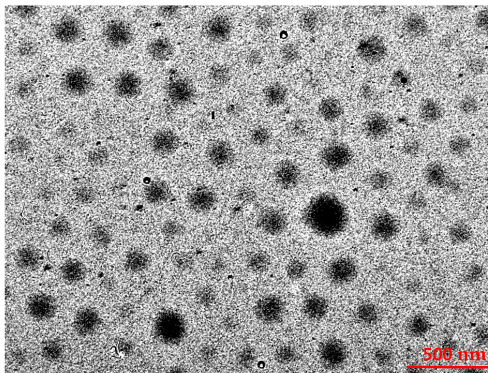


Figure 4- 22: TEM image of PAA-b-PBA latex with 0.3 mol% of BDA crosslinker, (PAA2.6, PBA100) 0.3% BDA.

Results of the synthesis

Crosslinking the PBA-core of latex particles should increase the stiffness of the particles and make interdiffusion of polymers between particles harder. In contrast to the uncrosslinked particles, individual particles of spherical shape could be clearly observed by TEM, (Figure 4-22). The particle diameter did not change much after crosslinking and no coagulum was observed, using 0.1-0.5 mol% of crosslinker.

	<i>TL41</i>	<i>TL43</i>	<i>TL59</i>	<i>TL95</i>	<i>TL90</i>	<i>TL91</i>
Name	(PAA2.6k, PBA100k)0.1%BDA	(PAA2.6k, PBA100k)0.3%BDA	(PAA2.6k, PBA100k)0.5%BDA	(PAA2.6k, PBA100k)0.1%DVB	(AA2.6k, PBA100k)0.3%DVB	(PAA2.6k, PBA100k)0.5%DVB
Crosslinker	BDA	BDA	BDA	DVB	DVB	DVB
Temperature, °C	70	70	70	70	70	70
Reaction time, min	240	240	180	270	330	280
pH ^a	6.24	6.24	6.25	6.14	6.20	6.24
M _n of PAA-TTC, kg.mol ⁻¹	2.6	2.6	2.5	2.5	2.5	2.5
BA conc., mol.L ⁻¹	2.3	2.3	2.4	2.4	2.3	2.3
PAA-TTC conc., mol.L ⁻¹	2.8×10^{-3}	2.7×10^{-3}	3.1×10^{-3}	3.0×10^{-3}	2.9×10^{-3}	3.0×10^{-3}
ACPA conc., mol.L ⁻¹	0.5×10^{-3}	0.5×10^{-3}	0.9×10^{-3}	0.8×10^{-3}	0.7×10^{-3}	0.7×10^{-3}
%mol of crosslink ^b	0.1	0.3	0.5	0.1	0.3	0.5
% conversion	95	94	88	92	94	98
% solids content	22	22	21	22	22	23
% coagulation	0	0	0	0	0	0
wt% PAA ^c	2.2	2.2	2.5	2.3	2.4	2.2
D _z , nm	83	86	104	74	77	72
PDI ^d	0.01	0.09	0.07	0.01	0.01	0.08

Table 4- 6: Polymerization conditions and characteristics of PAA-b-PBA latex with crosslinked PBA core, ^a pH of solution adjusted by NH₄OH 30% before polymerization, ^b molar percentage of crosslinking agents, BDA or DVB = $n_0(\text{crosslinker})/n_0(\text{BA}) \times 100$, ^c poly(acrylic acid) content $\%wt\ PAA = m_0(PAA)/(m_0(BA) \times conv.) \times 100$, ^d polydispersity index obtained from DLS

2.4.4 PAA-b-PBA latex with Na⁺ counter ion

Experimental section

The effect of adding Na⁺ counter ions in the PAA-b-PBA latex was analyzed by adjusting the pH of the PAA-TTC solution with 50% w/w sodium hydroxide (NaOH) solution instead of NH₄OH. The NH₄OH addition yields a counter ion of NH₄⁺ in the latex solution but during the drying process, NH₃ evaporates and results in a clean latex film without removing salt (see section 3.1). On the contrary, NaOH cannot evaporate during the drying process and leaves Na⁺ counter ions in the dried latex. The polymerization conditions, using NaOH for adjusting the pH were similar to the latex synthesized by using NH₄OH; at 70°C and stirring at 275 rpm under argon. The characteristics of the PAA-b-PBA latexes with Na⁺ counter ion and their polymerization conditions are summarized in Table 4-7.

	TL78	TL106
Name	(PAA2.6k, PBA100k)Na ⁺	(PAA2.6k, PBA100k)Na ⁺
Temperature, °C	70	70
Reaction time, min	300	270
pH ^a	6.04	6.06
M _n of PAA-TTC, kg.mol ⁻¹	2.6	2.6
BA conc., mol.L ⁻¹	2.3	2.3
PAA-TTC conc., mol.L ⁻¹	3.3 × 10 ⁻³	3.1 × 10 ⁻³
ACPA conc., mol.L ⁻¹	0.8 × 10 ⁻³	0.9 × 10 ⁻³
% conversion	96	91
% solids content	23	21
% coagulation	0	0
M _n (th) ^b , kg.mol ⁻¹	91.1	88.0
M _n (exp) ^c , kg.mol ⁻¹	111.7	106.4
M _w / M _n	1.8	2.5
wt% PAA ^d	2.3	2.5
D _z , nm	84	80
PDI ^e	0.08	0.02

Table 4- 7: Polymerization conditions and characteristics of PAA-b-PBA latex with Na⁺ counter ion, ^a pH of solution adjusting by NaOH 50% w/w before polymerization, ^b M_n (th) calculated by Eq. 4-1, ^c M_n (exp) was determined by SEC in THF with a PS calibration and recalculated to designate the non-methylated mass of; $M_n = [M(AA)/(M(MA)) \times M_{n,PS}]$, ^d poly(acrylic acid) content %wt PAA = $m_0(PAA)/(m_0(BA) \times conv.) \times 100$, ^e polydispersity index obtained from DLS.

Results of the synthesis

Stable latexes presenting no coagulum were obtained with an average diameter ~ 80 nm, similar to the latexes where the pH was adjusted by adding NH_4OH . Comparing with the standard conditions, the polymerization in presence of NaOH remained controlled to a certain degree. The $M_n(\text{exp})$ from SEC/THE was quite close to the theoretical M_n ($M_n(\text{th})$).

3. Latex film formation

3.1 Drying process and conditions

In our study, PAA-b-PBA latex particles are dispersed in aqueous solution. To create a homogeneous and transparent film, the surface characteristic of the supports are important. In our study silicone cooking molds were used to cast the films. However, due to the different characteristics of our latexes different drying behaviors were observed. In some types of latexes such as the latex with a high M_n of PAA some dewetting is observed during drying. In this case, the silicone mold needed to be modified to use another silicone base plate with a higher wettability. The dimension and characteristics of the silicone cooking mold and modified silicone mold are presented in Figure 4-23 (a) and (b).

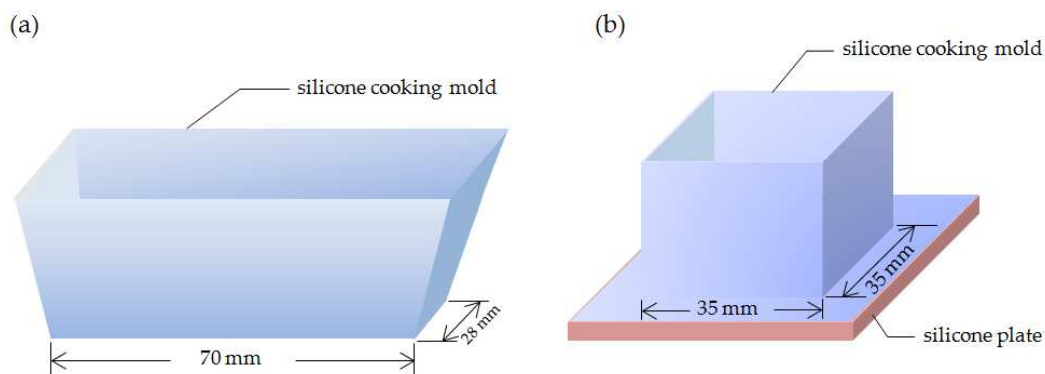


Figure 4- 23: Dimension of the silicone cooking molds for drying latexes (a) rectangular silicone mold, and (b) modified square silicone mold.

Experimental section

A certain amount of latex solution was poured into the prepared silicone mold and all air bubbles were eliminated. Then the mold was placed in a closed oven at ambient temperature ($< 25^{\circ}\text{C}$). The air circulation was put to the lowest level in order to decrease the water evaporation rate; in addition, the horizontal surface of the oven was leveled to assure a constant thickness of the dried film. During drying, the latex particles slowly align and pack to create the film. The drying process took around one week to completely dry the film. After that, the dried latex film was further dried at 100°C under vacuum for a night in order to eliminate ammonia and convert carboxylate groups into carboxylic acids. The dried films were stored in between siliconized paper at room temperature and further used

to create latex double network within 3 days in order to avoid any possible aging effect. In our study, we observed that the drying temperature had an impact on the mechanical properties of the resulting films, the details can be found in appendix A-2.

Characteristics of the dried films

For all latexes, transparent films were obtained (Figure 4-24(a). The transparency of the films comes from the deformation of the particles filling the inter-particle voids, resulting in a close packing where light is no longer scattered by heterogeneities in the refractive index.¹ The light yellow color present in most of the film comes from the trithiocarbonate group due to the use of a PAA-TTC macro-RAFT agent. The PBA-core crosslinked latexes gave also transparent films, presented in Figure 4-24(b). These films after drying are less adhesive and stiffer.

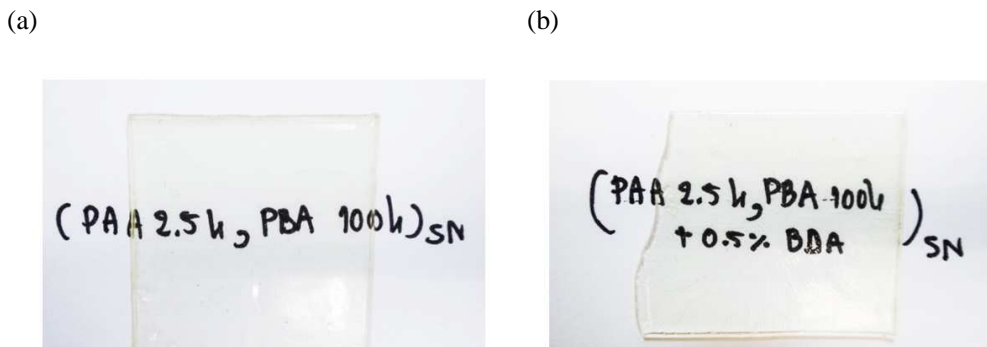


Figure 4-24: PAA-b-PBA films (a) transparent film of latex (PAA 2.5k, PBA 100k), and (b) transparent film of crosslinked latex (PAA 2.5k, PBA 100k) 0.5% BDA.

During this thesis, we did not focus on the microstructure of the films. However, it has been reported that PAA-b-PBA core-shell latex particles should create a network similar to a natural honeycomb structure.¹ Chenal et. al^{2, 6} used wet-Scanning Transmission Electronic Microscopy (wet-STEM) technique to observe the film formation of the PAA-b-PBA latex. They found that by a slow drying process, PAA-b-PBA latex particles formed a nanostructured film, made of soft PBA domain and a hard hexagonal PAA network (Figure 4-25).

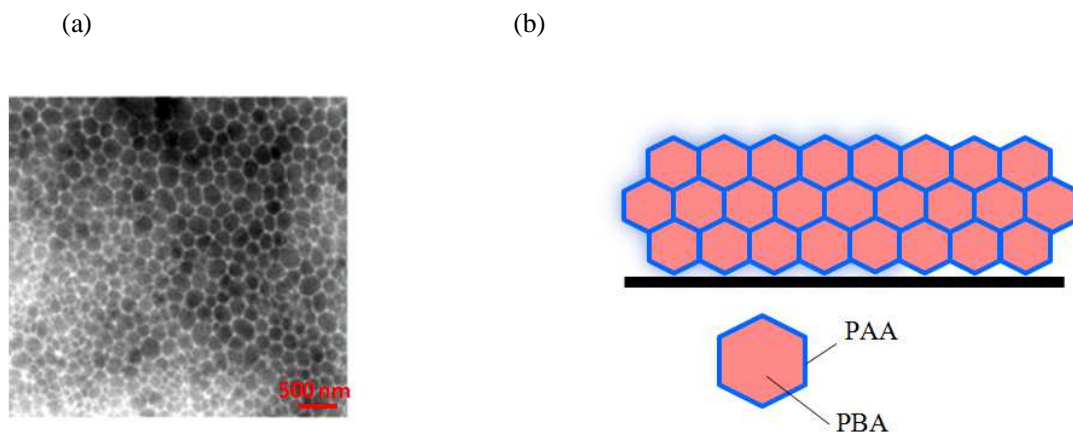


Figure 4-25: Nanostructure of dried latex film. (a) Wet-STEM image of a thin film made by drying a drop of latex (PAA2.8k, PBA110k)Na⁺, studied by Chenal et al.², and (b) schematic of dried latex film.

For the statistically crosslinked P(BA-co-BDA) latex (synthesis in section 2.3), we used the same drying process as for the PAA-b-PBA latexes. This latex showed clearly a skin formation in which the latex particles on the top of the solution coalesced. Consequently, the latex needed a long time, around 2 weeks in a closed oven, to dry completely. The conventional latex film had a rough surface and was less transparent comparing to the core-shell latex, as shown in Figure 4-26.

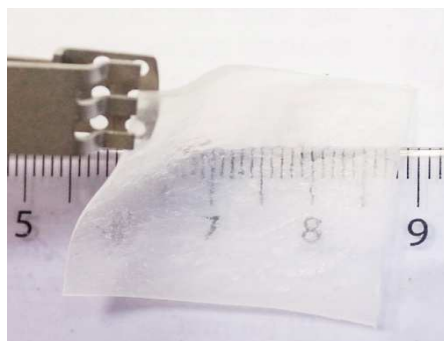


Figure 4-26: Film obtained with crosslinked P(BA-co-BDA) latex synthesized by conventional emulsion polymerization.

In addition, it should be noted that all latexes in our study, core-shell latexes and the statistically crosslinked P(BA-co-BDA) latex, showed a different structure at the edge of the sample after drying in which the edge of the film was more opaque and scattering light (Figure 4-27). The edge of the films was always trimmed before using in latex double network in order to have a homogenous thickness.

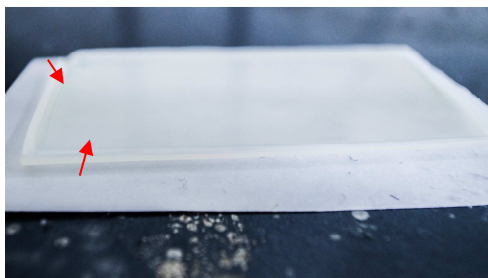


Figure 4-27: Horizontal drying front of latex films (in red arrows).

3.2 PAA-b-PBA film with added PADAME

Experimental section

In this study the (PAA2.5k, PBA100k) latex was selected to observe the effect of ionic interactions with a cationic polymer, poly(N,N-dimethylamino ethyl acrylate) trithiocarbonate or PADAME-TTC, M_n 4.58 kg.mol⁻¹. Before using, PADAME-TTC was purified by removing an observed insoluble part after dissolving it in distilled water, passing through a 0.2μm filter membrane and drying at room temperature. The amount of purified PADAME-TTC was dissolved in distilled water and the pH was adjusted with 30% NH₄OH to pH ~ 8. Then the PADAME-TTC solution was introduced into the latex TL103 (Table 4.8), the pH of which was also adjusted with 30% NH₄OH to pH ~ 8 and stirred over night at room temperature. Two different molar ratios of ADAME units to AA units of the latex, namely 0.2 and 0.65 equivalents, were investigated.

The pH adjustment of the PADAME-TTC solution was performed in order to inhibit the protonation of the amino groups (pKa value of PADAME ~ 6.5)⁴³. To create dry films, latexes with PADAME-TTC were filled in the prepared mold and dried following the drying process in section 3.1. During drying, NH₄OH evaporates and the resulting protonated amino groups of PADAME-TTC interact via ionic interaction with the negatively charged carboxylate groups of the shell of PAA. A network which is crosslinked by ionic interactions between PAA shells and PADAME-TTC is then formed as shown in Figure 4-28.

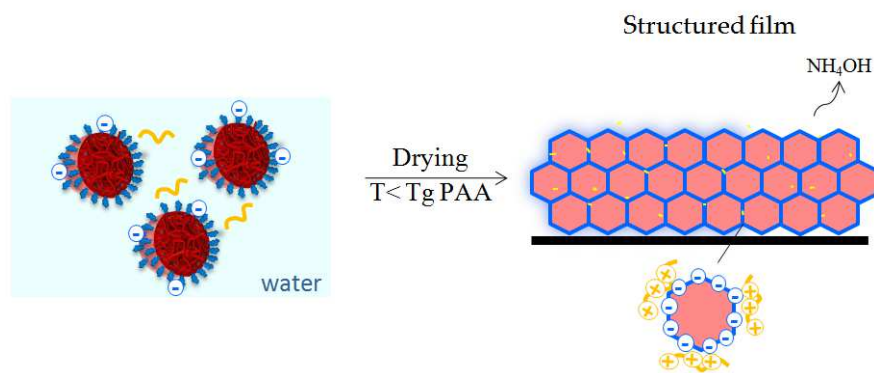



Figure 4- 28: Schematic of core-shell latex with ionic crosslink where  is PADAME-TTC.

The latexes used in this study and wt% of PAA and PADAME in each systems are presented in Table 4-8.

Name	(PAA2.5k, PBA100k) 0.2eq. PADAME	(PAA2.5k, PBA100k) 0.65eq. PADAME
Latex, batch	TL103 ^a	TL103 ^a
[ADAME] / [AA] ^b	0.2	0.65
wt% PAA ^c	2.4	2.4
wt% PADAME ^d	1.1	3.4

Table 4- 8: PAA-b-PBA films with ionic crosslinks, ^a Synthesis conditions and latex characteristics of TL 103 are presented in Table 4-4 section 2.4.3, ^b molar ratio of ADAME to AA = $n_0(ADAME)/n_0(AA \text{ from PAA} - TTC)$, ^c poly(acrylic acid) content (%wt PAA) = $m_0(PAA)/(m_0(BA) \times conv.) \times 100$, ^d PADAME content %wt PADAME = $m_0(PADAME - TTC)/[m_0(PAA - b - PBA) \times (\%solid/100)] \times 100$.

Characteristics of the dried films

After drying, a transparent film was obtained as shown in Figure 4-29. It was found that introducing PADAME-TTC to the film did not have a visible impact on the film formation. The latex film remains as transparent as the film without PADAME-TTC (Figure 4-24). This film shows also an opaque region near the edge which needs to be trimmed before using in double network.

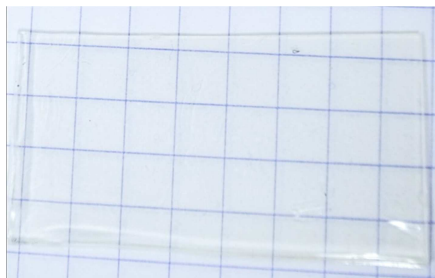


Figure 4-29 : PAA-b-PBA latex film containing PADAME-TTC.

3.3 P(AA-co-BDA) and PAA-b-PBA film with added PAA homopolymer

Experimental section

In addition to studying the addition of a polyamine (PADAME-TTC), a low molar mass homopolymer of poly(acrylic acid), 50 wt% in water; M_n 5 kg.mol⁻¹, pH 3, was added to the P(BA-co-BDA) statistical crosslinked latex and to the PAA-b-PBA core-shell latexes. PAA is a water-soluble polymer. After introducing the solution in the P(BA-co-BDA) latex, the PAA should dissolve in the water phase and should not diffuse into the core of the latex. After drying, if the mixture is homogeneous, these free PAA chains should surround the PBA particles and increase the thickness of the PAA shell in the core-shell latex films (Figure 4-30). These latexes with additional PAA will then be compared to the PAA-b-PBA core-shell latexes synthesized with the PAA-TTC macro-RAFT agent of 6 kg.mol⁻¹, containing 11wt% PAA (in the polymer, see in section 2.3). For the mixtures with PAA, we therefore targeted a total of 11% of PAA in the dried samples.

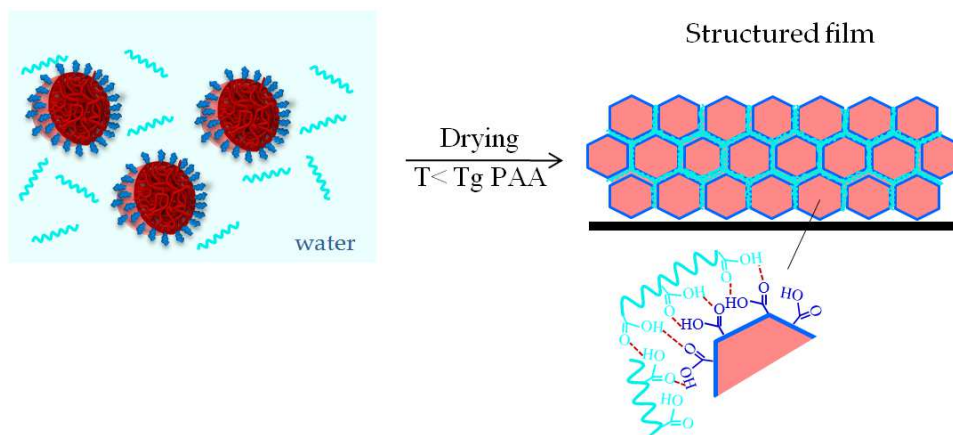


Figure 4- 30: Schematic of core-shell latex with added PAA, where are PAA chains

A PAA solution (pH 3) was slowly added to the statistically crosslinked latex (TLL01, see section 2.3) and to the core-shell latexes (TL85 (PAA2.6k, PBA100k) and TL104 (PAA2.6k, PBA200k), see section 2.4.3) and the latexes were stirred overnight. After the addition of the PAA solution, there was some coagulum found in the latex (~1.5%). The coagulum was removed from the latex by decantation, before the drying process which followed the protocol presented in section 3.1. The characteristics of the latexes used in this study are presented in Table 4-9.

<i>Name</i>	<i>(PBA_{no-shell})11%AA</i>	<i>(PAA2.5k, PBA100k)9%PAA</i>	<i>(PAA2.5k, PBA200k)10%PAA</i>
Latex, batch	TLL01 ^a	TL85 ^b	TL104 ^c
% solids content	26	22	21
% coagulation	0	1.2	1.6
wt% PAA _{initial} ^d	0	2.5	1.1
wt% PAA _{additional} ^e	11	9.3	10.8
wt% PAA _{final} ^f	11	11.8	11.9

Table 4- 9: P(BA-co BDA) latex and PAA-b-PBA latexes with addition of PAA, ^a The synthesis conditions and latex characteristics of TLL01 are presented in Table 4-2 section 2.3, ^b TL85 is presented in Table 4-4 section 2.4.3, ^c TL104 is presented in Table 4-5 section 2.4.3, ^d Poly(acrylic acid) content at initial state before adding PAA_{5k} % wt PAA_{initial} = $m_0(PAA)/[m_0(BA) \times Conv.] \times 100$, ^e Additional poly(acrylic acid) from PAA_{5k} % wt PAA_{additional} = %wt PAA_{final} – % wt PAA_{initial}, ^f Poly(acrylic acid) content after adding PAA_{5k} %wt PAA_{final} = $[m_0(PAA_{latex}) + m(PAA_{5k})]/[m_0(BA) \times Conv.] \times 100$.

Characteristics of the dried films

After drying, the formed latex films containing additional PAA chains were less transparent, probably because too much PAA was added. The PAA-b-PBA core-shell latex film changed from a transparent appearance to a frosted appearance (Figure 4-31 (a)) which may come from the insertion of clusters of free PAA chains in between particles which are large enough to scatter light. In contrast for the P(BA-co-BDA) latex, the addition of free PAA chains might fill the voids between particles, resulting in a smoother film surface (compared to the reference sample). The observed frosted to opaque appearance (Figure 4-31(b)) might again be explained by the formation of PAA clusters possessing a different refractive index than the particle copolymer and resulting in an opaque appearance through light scattering.

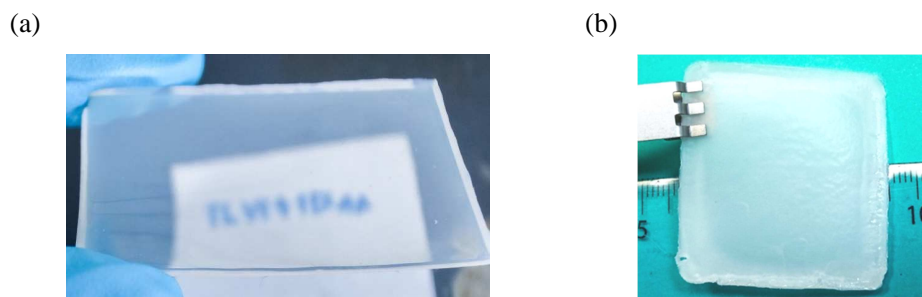


Figure 4- 31: Latex films containing free PAA chains, (a) PAA-b-PBA latex of (PAA2.6k, PBA100k) with PAA_{final} 11 wt%, and (b) P(BA-co-BDA) latex or latex_{no-shell} with PAA_{final} 11 wt% .

3.4 Thermally annealed latex films

Experimental section

Thermal annealing (TA) was applied to core-shell latex films dried formerly under standard conditions at 160 °C for 72 hours. The annealing temperature was set to be higher than the T_g of PAA (~110°C) in order to reach a thermodynamically stable microstructure of the film. Chenal et. al^{2, 6} had indeed reported that the increase of the temperature above the T_g of the PAA-b-PBA latex shell triggered a phase inversion and led to the loss of the initial honeycomb-like network structure of the film into spherical micelles with a very small PAA core and a large PBA shell (Figure 4-32).

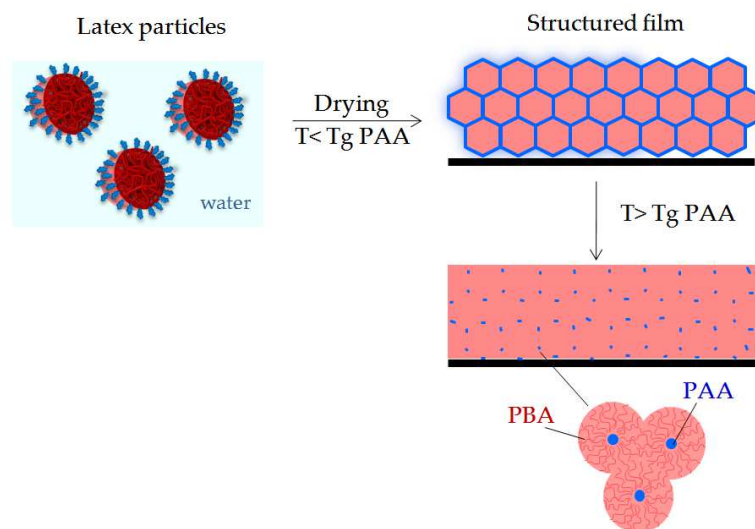


Figure 4- 32: Schematic of core-shell latex, the formation of the honeycomb-like structured network film, and phase inversion into micelles after thermal annealing

Characteristics of the dried films

Latex films after TA showed a change in aspect. The initially transparent film were yellowish but became orange; especially for latex films containing free PAA chains the color turned to brown (Figure 4-33). The effect of the TA process on the color of the films is currently not fully understood; the change of color may come from some side reaction of residual NH_3 during the annealing process. The aspects of different films are presented in Figure 4-33.

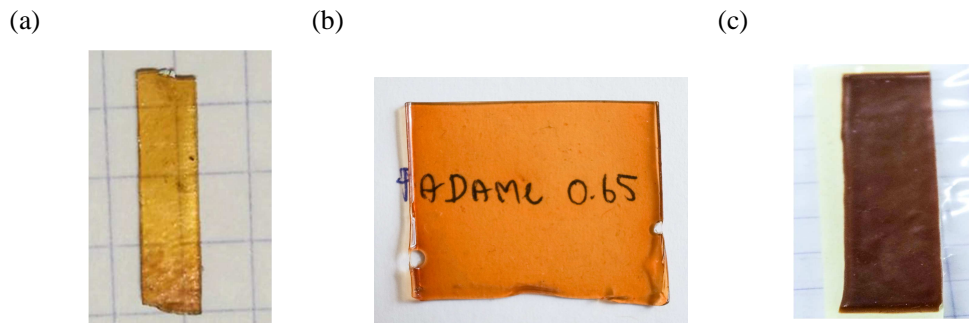


Figure 4- 33: Latex films after TA synthesized from, (a) latex TL85 (PAA2.5k, PBA100k) (b) latex TL103 (PAA2.5k, PBA100k) with 3.4wt% PADAME (0.65 eq, and (b) latex TL85 (PAA2.5k, PBA100k) with additional PAA solution.

4. Latex double network films

In our study, latex films have been synthesized to serve as reinforcement to extensible elastomers as a polymeric filler. Poly(n-butyl acrylate) elastomer was selected as a standard network because it is the same polymer as the core of PAA-b-PBA particles, avoiding any problems arising from phase separation due to polymer incompatibility. Thus, after swelling the latex film in BA monomer, the core of the latex particles should be swollen by BA monomers, and in the course of their photopolymerization, PBA chains should interpenetrate the core of individual PAA-b-PBA particles, without breaking the initial structure of the first film obtained from the latex (Figure 4-34). This technique was called a sequential interpenetrating polymer network technique.^{44, 45, 46, 47} The resulting PBA elastomers with latex reinforcement were named latex double networks (latex DN).

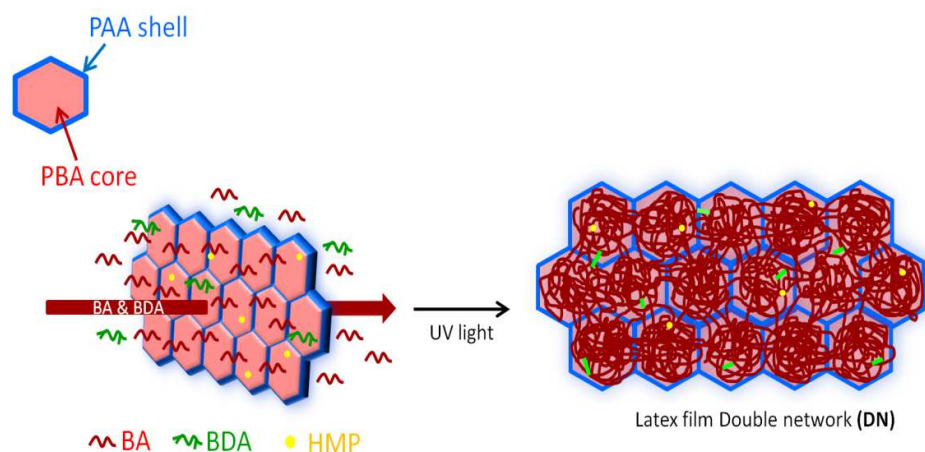


Figure 4-34: Swelling process of core-shell latex film to create latex DN.

Experimental section

The latex DN was synthesized in the glove box under nitrogen atmosphere, with less than 5 ppm of oxygen (MBraun Unilab) to avoid side reactions. All reactants and monomers used to create the latex DN inside the glove box were deoxygenated by bubbling with nitrogen for 45 minutes to avoid oxygen contamination in the glove box and stored in a freezer at -20°C. After swelling of the dried latex film in BA bath (containing BA, BDA and HMP), the polymerization of the samples was carried out in the glass mold, similar to the one used in Chapter 2 (Figure 2-7) and exposed to UV light (Vilbert Lourmat lamp (model VL-215.L), centered on 365 nm) in order to create radicals, from the UV-initiator (hydroxyethyl-2-methylpropiophenone or HMP). A low power UV irradiation (10 $\mu\text{W}/\text{cm}^2$) was selected in order to decrease the number of chains growing simultaneously and to decrease the number of termination reactions.⁴⁷ To perform this, the UV intensity was decreased by

covering with PET sheets and the power was measured with a radiometer (VLX-3W from Vilber Lourmat). The details to create the latex DN and other related studies are presented in the following sections.

4.1 Swelling study of the latex films

According to the sequential interpenetrating network technique, the double network is created by swelling a principal network (latex film) with a solution of the interpenetrating network monomer, a crosslinker and an initiator, and subsequently polymerization occurs in situ. In order to control the swelling ratio we need to understand the swelling behavior of the latex film..

As an example, a latex film (TL104; PAA2.5, PBA200) was cut into a piece and immersed into a monomer bath of BA without introducing any crosslinker (BDA) and initiator (HMP). The bath was left at room temperature without light exposure. During distinct time intervals, the sample was taken out, wiped with tissue paper to remove the excess monomer and weight was recorded. The %swelling of latex film can be calculated as in Eq. 2-3 and the result of the swelling behavior of the film TL104 is shown in Figure 4-35.

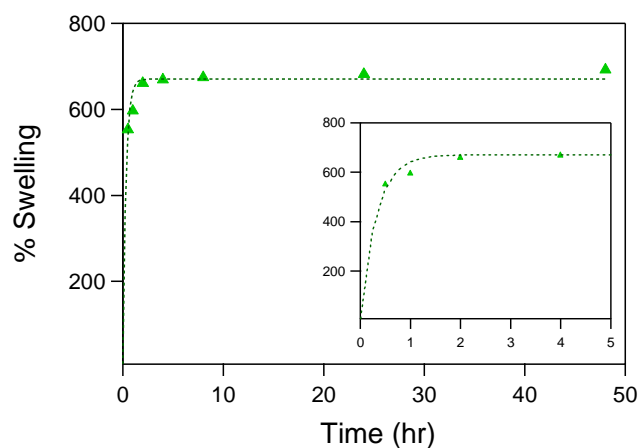


Figure 4- 35: Swelling behaviour of the film TL104 (PAA_{2.5k}-b-PBA_{200k}), $\%swelling = \left(\frac{w_t - w_i}{w_i} \right) \times 100$

We found that the swelling of latex film TL04 is very rapid, and after less than 1 hour, 600% swelling is reached. Afterwards the swelling rate decreased and an equilibrium swelling is reached at 2 hours. Therefore, in order to create latex double networks, we decided to swell the latex films for 2 hours corresponding to the swelling equilibrium point.

4.2 PBA elastomer, serving as an interpenetrating network to DN

PBA elastomer was used as an interpenetrating network in our study. In addition to BA, a little amount (≤ 0.05 mol%) of 1,4-butanediol diacrylate (BDA) crosslinker was introduced in order to maintain the physical properties of elastomers, such as shape, degradation and solubility properties after immersing in solvents. In order to study the mechanical properties of the interpenetrating network alone, some simple PBA networks were created by UV polymerization in the bulk, with different concentrations of BDA crosslinker.

Experimental section

A set amount of BA, BDA crosslinker and HMP UV- initiator were mixed until homogenous in the glove box. Then, the mixture was transferred to the glass mold, in which the glass plates were covered with a thin layer of PET in order to avoid the adhesion between the glass and polymer (Figure 2-7, in chapter 2). The thickness of the sample was controlled by the gap between the glass plates with 1 mm metal slides. The mold was subsequently exposed to UV irradiation ($10 \mu\text{W}/\text{cm}^2$) for 2 hours to complete the reaction. The concentration of each composition can be found in Table 4-10.

After 2 hours of polymerization, the PBA networks formed and they were removed from the glass mold and from the glove box. Unreacted monomer from the sample was then removed by drying at 80°C under vacuum for a night. The samples were kept at room temperature until uniaxial extension tests were performed. The mechanical properties of the PBA networks in uniaxial extension were analysed with the Rubinstein Panyukov model⁴⁸ and they will be presented and discussed in the next chapter.

Name	[BDA] ^a (mol%)	[HMP] ^b (mol%)	$m_0(\text{BA})$ (g)	$v_0(\text{BDA})$ (μl)	$v_0(\text{HMP})$ (μl)
PBA 0.01%BDA	0.01	0.01	7	1.03	0.83
PBA 0.03%BDA	0.03	0.01	7	3.09	0.83
PBA 0.05%BDA	0.05	0.01	7	5.15	0.83

Table 4- 10: Formulation of the PBA interpenetrating network swelling bath, ^a is the molar percentage of BDA = $n_0(\text{BDA})/n_0(\text{BA}) \times 100$, where n_0 is a number of initial moles, ^b is the molar percentage of HMP = $n_0(\text{HMP})/n_0(\text{BA}) \times 100$, where n_0 is a number of initial moles.

4.3 Latex double network synthesis

Experimental section

To create latex double networks, first a monomer bath was prepared in a plastic box by mixing BA monomer with a 0.01 mol% of BDA as crosslinker and HMP as UV-initiator. The chemical composition of the monomer bath is presented in Table 4-11. Then a piece of dried latex film (with the edge trimmed) of a known initial weight was swollen in the monomer bath, which was tightly closed to avoid the evaporation of monomer. In this stage, the molecules of the bath swell the core of latex particles as PBA is soluble in BA.

Name	[BDA] ^a (mol%)	[HMP] ^b (mol%)	m ₀ (BA) (g)	v ₀ (BDA) (μl)	v ₀ (HMP) (μl)
PBA network	0.01	1	15	2.2	178.4

Table 4- 11: Formulation of the PBA interpenetrating network swelling bath, ^a Molar percentage of BDA = $n_0(BDA)/n_0(BA) \times 100$, where n_0 is a number of initial moles, ^b Molar percentage of HMP = $n_0(HMP)/n_0(BA) \times 100$, where n_0 is the initial mole number.

The swelling to equilibrium of the PAA-b-PBA core-shell latex films took about 2 hours, however, for the P(BA-co-BDA) conventional latex, only 30 minutes were applied in order to prevent the re-dispersion of the latex particles. This reference latex is therefore swollen to a set amount. After swelling to equilibrium, the swollen film was carefully removed from the bath and the excess monomer was eliminated by a wiper. The swollen film was then placed in between the glass plates covered by a PET sheet. The glass mold was gently tightened and exposed to UV light for 2 hours. After polymerization, the latex DN was removed from the mold and from the glove box. The sample was weighed and dried under vacuum at 80°C for one night. The final DN latexes were stored at room temperature until performing mechanical tests.

The swelling ratio (%), the weight fraction of latex (ϕ_{latex}) and the prestretching of the chains of the latex film (λ_0), assuming that the densities are equal, were determined by the weight of latex in the initial state $W_0[L]$, the weight of the swollen latex after polymerization with UV irradiation $W_S[DN]$ and the weight of the DN latex after vacuum drying $W_D[DN]$ as shown in Eq.4-8, Eq. 4-9 and Eq. 4-10.

$$\%Swelling = \frac{W_S[DN] - W_0[L]}{W_S[L]} \times 100 \quad (Eq. 4 - 8)$$

$$\phi_{latex} = \frac{W_0[L]}{W_D[DN]} \quad (Eq. 4 - 9)$$

$$\lambda_0 = \frac{1}{(\phi_{latex})^{1/3}} \quad (Eq. 4 - 10)$$

The results of latex DN synthesized in our study are summarized in Table 4-12.

P(BA-co-BDA) conventional latex

Sample name	Latex (batch)	% swelling	Φ_{latex} (%)	λ_0
(latex _{no-shell}) _{DN}	TLL01	446	18	1.77

PAA-b-PBA latex with different PAA-shell thickness

Sample name	Latex (batch)	% swelling	Φ_{latex} (%)	λ_0
(PAA2.6k, PBA100k) _{DN}	TL08	409	20	1.70
(PAA2.6k, PBA100k) _{DN}	TL85	397	21	1.68
(PAA4k, PBA100k) _{DN}	TL23	293	26	1.57
(PAA6k, PBA100k) _{DN}	TL22	Incapable to do DN		
[(PAA2.6k, PBA100k) TA] _{DN}	TL99	781	11	2.09

PAA-b-PBA latex with different PBA-core size

Sample name	Latex (batch)	% swelling	Φ_{latex} (%)	λ_0
(PAA2.6k, PBA150k) _{DN}	TL83	601	15	1.88
(PAA2.6k, PBA200k) _{DN}	TL104	669	13	1.97

PAA-b-PBA latex with PBA-core crosslink

Sample name	Latex (batch)	% swelling	Φ_{latex} (%)	λ_0
[(PAA2.6k, PBA100k)0.1%BDA] _{DN}	TL41	342	23	1.63
[(PAA2.6k, PBA100k)0.3%BDA] _{DN}	TL43	236	30	1.49
[(PAA2.6k, PBA100k)0.5%BDA] _{DN}	TL59	167	37	1.39
[(PAA2.6k, PBA100k)0.1%DVB] _{DN}	TL95	319	24	1.61
[(PAA2.6k, PBA100k)0.3%DVB] _{DN}	TL90	297	26	1.57
[(PAA2.6k, PBA100k)0.5%DVB] _{DN}	TL91	220	32	1.46

PAA-b-PBA latex with counter ions

Sample name	Latex (batch)	% swelling	Φ_{latex} (%)	λ_0
[(PAA2.6k, PBA100k)Na ⁺] _{DN}	TL106	362	22	1.66
[(PAA2.6k, PBA100k)Na ⁺ (TA)] _{DN}	TL106	342	23	1.63

PAA-b-PBA latex with ionic crosslink

Sample name	Latex (batch)	% swelling	Φ_{latex} (%)	λ_0
[(PAA2.6k, PBA100k) 0.2eq PADAME] _{DN}	TL103	294	26	1.57
[(PAA2.6k, PBA100k) 0.65eq PADAME] _{DN}	TL103	309	25	1.59
[(PAA2.6k, PBA100k) 0.65eq PADAME(TA)] _{DN}	TL103	Incapable to do DN		

PAA-b-PBA latex with PAA adding

Sample name	Latex (batch)	% swelling	Φ_{latex} (%)	λ_0
[(PAA2.6k, PBA100k)9%PAA] _{DN}	TL85	329	24	1.61
[(PAA2.6k, PBA200k)10%AA] _{DN}	TL104	566	15	1.88
(latex _{noshell} 11%AA) _{DN}	TLL01	366	22	1.66

Table 4-12: Characteristic and composition ratio of latex DN films.

Most of the latex films could be used to create DN films. However some latex films, namely [(PAA2.6k, PBA100k) 0.65eq PADAME(TA)]_{DN}, and (PAA6k, PBA100k)_{DN} could not be used to create the double network because the swollen films were too fragile and it was not possible to remove them intact from the bath after swelling in the BA monomer. Moreover, the thermally annealed film [(PAA2.6k, PBA100k) TA]_{DN} could be swollen without dissociation, but after polymerization, cracks were observed and the film was curly, and thus not usable for further mechanical testing.

The results of the equilibrium swelling ratio (% swelling) and the weight fraction of latex (Φ_{latex}) presented in Table 4-12 show that different latexes had different swelling behaviours as summarized on Figure 4-36. From the results in Table 4-12 and Figure 4-36, it can be concluded that

- A larger PBA-core size in the latex (higher M_n of PAA-b-PBA) results in a higher % swelling and ultimately in a smaller weight fraction of the first latex network (Φ_{latex} of a large core latex < Φ_{latex} of a small core latex).
- The increase of PAA-shell thickness, i. e. using a higher M_n PAA-TTC macro-RAFT agent in latex polymerization, decreases the swelling ability and leads to higher weight fractions of the first network in the resulting DN (Φ_{latex} of a thick shell latex > Φ_{latex} of a thin shell

latex). A high PAA wt% in the latex film restricts probably the deformability of the particles which causes a lower swelling ratio.

- iii, iv) As expected, the presence of a PBA crosslinker inside the particles leads to a lower swelling ratio, and eventually higher fractions of the first network.
- v, vi), vii) Adjusting the pH with NaOH instead of NH_4OH , and addition of PADAME or PAA results in a slightly lower swelling ratio, which might indicate a reinforcement of the interactions between particle shells.

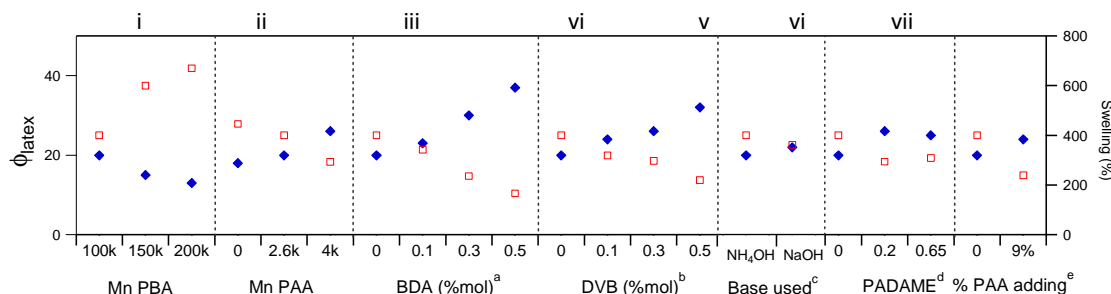


Figure 4-36: Effect of different latex compositions on the volume fraction of latex in the respective DN films, ^a BDA crosslinker in latex (PAA2.6k, PBA100k), ^b DVB crosslinker in latex (PAA2.6k, PBA100k), ^c different bases used to adjust the pH of latex before polymerization in latex (PAA2.6k, PBA100k), ^d Equivalent number of PADAME in the ionically crosslinked latex (PAA2.6k, PBA100k), ^e % PAA solution (M_n 5 kg.mol⁻¹) added into the latex (PAA2.6k, PBA100k)

4.4 HMP consumption effect

During the first polymerizations of DN using a typical bath composition used before for other systems⁴⁷ (BDA 0.01mol%, HMP 0.01mol%), we found that the polymerization was not complete and very low conversions were reached, about 30% as indicated by the weight loss of up to 70% after drying under vacuum. The incomplete polymerization may come from the reaction of HMP with the reactive end group of PAA-b-PBA.

In order to determine the HMP concentration necessary to complete the polymerization within 2 hours, we studied the impact of the amount of HMP in the latex DN polymerization. The HMP concentration was increased from 0.01 mol% to 1 mol% and the latex double network was created following the procedure described in section 4.3. The monomer conversion can be calculated by the weight of swollen latex after being exposed to UV radiation for 2 hours ($W_S[\text{DN}]$) and the weight after vacuum drying for one night ($W_D[\text{DN}]$) as shown in Eq. 4-10. The detail of monomer bath composition and the latex film characteristics are summarized in Table 4-12.

$$\% \text{ monomer conversion} = \left[1 - \left(\frac{W_s[DN] - W_D[DN]}{W_s[DN]} \right) \right] \times 100 \quad (\text{Eq. 4 - 11})$$

Latex film	[HMP] ^b (mol%)	[BDA] ^a (mol%)	m ₀ (BA) (g)	v ₀ (BDA) (μl)	v ₀ (HMP) (μl)	% monomer Conv.
TL05	0.01	0.01	20.1	3.0	2.4	28
TL05	0.03	0.01	7.4	1.1	2.6	53
TL06	0.05	0.01	7.4	1.1	4.4	56
TL06	0.1	0.01	7.4	1.1	44	97
TL07	1	0.01	7.4	1.1	88	98

Table 4- 13: Formulation of the PBA interpenetrating network swelling bath, ^a Molar percentage of BDA = $n_0(BDA)/n_0(BA) \times 100$, where n_0 is the initial mole number, ^b Molar percentage of HMP = $n_0(HMP)/n_0(BA) \times 100$, where n_0 is the initial mole number.

By increasing the concentration of the initiator HMP in the monomer bath up to 1 mol%, we found that monomer conversion became quasi quantitative. It should be noted that with 1 mol% HMP the concentration was 100 times larger than the amount needed for the normal BA network (Figure 4-37 (a)).

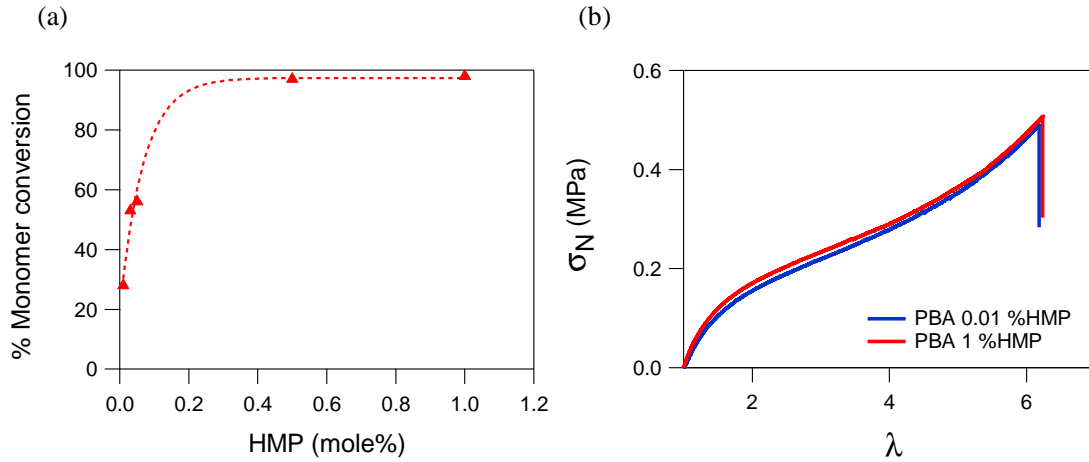


Figure 4- 37: The result of HMP consumption study, (a) % monomer conversion versus the concentration of HMP, (b) stress-strain curve of PBA 2nd network with different HMP concentration.

It was thus necessary to check that the high concentration of HMP did not affect the mechanical properties of the PBA 2nd network. The PBA 2nd network was synthesized alone with two different concentration of HMP, 0.01mol% (normal condition) and 1mol% (latex DN condition) respectively

(Table 4-14). The mechanical properties of both PBA latexes were checked with a tensile test at the cross head velocity of 50 $\mu\text{m/s}$ and the stress-strain curves of these two PBA networks are presented in Figure 4-37 (b). It can be observed that the increase of HMP did not impact the mechanical properties of the PBA network.

Name	[BDA] ^a (mol%)	[HMP] ^b (mol%)	$m_0(\text{BA})$ (g)	$v_0(\text{BDA})$ (μl)	$v_0(\text{HMP})$ (μl)
PBA 0.01%HMP	0.01	0.01	7	1	0.8
PBA 1%HMP	0.01	1	7	3.1	85

Table 4- 14: Formulation of the PBA 2nd network swelling bath, ^a Molar percentagof BDA = $n_0(\text{BDA})/n_0(\text{BA}) \times 100$, where n_0 is the initial mole number, ^b Molar percentagof HMP = $n_0(\text{HMP})/n_0(\text{BA}) \times 100$, where n_0 is the initial mole number.

Conclusions

In our study, we used for the first time a nanostructured latex as the polymeric reinforcement filler for an elastomeric system. A P(BA-co-BDA) crosslinked latex and a PAA-b-PBA core-shell latex were used to reinforce PBA elastomers. Various latexes were synthesized in different conditions. Conventional emulsion polymerization was used to synthesize the P(BA-co-BDA) crosslinked latex and RAFT-emulsion polymerization in batch conditions was used to create PAA-b-PBA a core-shell latex with different PAA shell thicknesses (via different M_n of PAA) and different PBA core sizes (different M_n of the PBA). In addition the particle's core was crosslinked with BDA or DVB, whereas shell interactions were reinforced via the use of NaOH (instead of NH_4OH yielding ionized PAA shells via carboxylate formation), or the addition of PAA or PADAME (promoting shell crosslinking through supramolecular interaction). From these different latexes formulations nanostructured films were prepared by slow drying at room temperature, resulting in a percolating network.

The P(BA-co-BDA) crosslinked latex film showed a rough surface and cloudy appearance, while the PAA-b-PBA core-shell latex films were transparent. However, when PAA homopolymer was added before film formation, the films turned cloudy indicating the presence of large PAA clusters, while thermal annealing led to yellow-orange discoloration.

To create latex double networks (latex DN), the latex films, which are insoluble but swellable in BA monomer, were swollen in a monomer bath until equilibrium, and subsequently polymerized under UV irradiation, following the sequential interpenetrating network technique. By controlling these synthesis conditions, latex double networks could be successfully created.

References

1. Keddie, J. and A.F. Routh, *Fundamentals of Latex Film Formation: Processes and Properties*. 2010: Springer Netherlands.
2. Chenal, M., *Particules cœur-écorce par polymérisation raft en émulsion pour des matériaux nanostructurés sans solvants*, 2013. (Thèse de doctorat Physique et Chimie des matériaux): University Pierre and Marir Curie, Paris, France. p. 265
3. Ferguson, C.J., et al., *Effective ab Initio Emulsion Polymerization under RAFT Control*. *Macromolecules*, 2002. **35**(25): p. 9243-9245.
4. Ferguson, C.J., *Core-shell polymers from styrene and vinyl acetate for use as wood adhesives*, 2000. (published doctoral dissertation): University of Canterbury, New Zaland.
5. Pérez, E. and J. Lang, *Internal Structure of Core-Shell Latex Particles Studied by Fluorescence Nonradiative Energy Transfer*. *Langmuir*, 1996. **12**(13): p. 3180-3187.
6. Chenal, M., et al., *Soft nanostructured films with an ultra-low volume fraction of percolating hard phase*. *Macromol Rapid Commun*, 2013. **34**(19): p. 1524-9.
7. Urbani, C.N. and M.J. Monteiro, *RAFT-Mediated Polymerization in Heterogeneous Systems*, 2008. (Handbook of RAFT Polymerization), Wiley-VCH Verlag GmbH & Co. KGaA. p. 285-314.
8. Steward, P.A., J. Hearn, and M.C. Wilkinson, *An overview of polymer latex film formation and properties*. *Advances in Colloid and Interface Science*, 2000. **86**(3): p. 195-267.
9. Thickett, S.C. and R.G. Gilbert, *Emulsion polymerization: State of the art in kinetics and mechanisms*. *Polymer*, 2007. **48**(24): p. 6965-6991.
10. Bonham, J.A., M.A. Faers, and J.S. van Duijneveldt, *Non-aqueous microgel particles: synthesis, properties and applications*. *Soft Matter*, 2014. **10**(47): p. 9384-9398.
11. Harkins, W.D., *A General Theory of the Mechanism of Emulsion PolymerizationI*. *Journal of the American Chemical Society*, 1947. **69**(6): p. 1428-1444.
12. Vega-Rios, A. and A. Licea-Claverie, *Controlled Synthesis of Block Copolymers containing N-isopropylacrylamide by Reversible Addition-Fragmentation Chain-Transfer (RAFT) Polymerization*. *Journal of the Mexican Chemical Society*, 2011. **55**(1): p. 21-32.
13. Ganeva, D.E., et al., *Particle Formation in ab Initio RAFT Mediated Emulsion Polymerization Systems*. *Macromolecules*, 2007. **40**(17): p. 6181-6189.
14. Keddie, D.J., *A guide to the synthesis of block copolymers using reversible-addition fragmentation chain transfer (RAFT) polymerization*. *Chemical Society Reviews*, 2014. **43**(2): p. 496-505.
15. Barner-Kowollik, C., *Introduction*, 2008. (Handbook of RAFT Polymerization), Wiley-VCH Verlag GmbH & Co. KGaA. p. 1-4.

16. Rizzardo, E., G. Moad, and S.H. Thang, *RAFT Polymerization in Bulk Monomer or in (Organic) Solution*, 2008. (Handbook of RAFT Polymerization), Wiley-VCH Verlag GmbH & Co. KGaA. p. 189-234.
17. Moad, G., E. Rizzardo, and S.H. Thang, *Living radical polymerization by the RAFT process*. Australian Journal of Chemistry, 2005. **58**(6): p. 379-410.
18. Chiefari, J., et al., *Thiocarbonylthio Compounds (SC(Z)S-R) in Free Radical Polymerization with Reversible Addition-Fragmentation Chain Transfer (RAFT Polymerization). Effect of the Activating Group Z*. Macromolecules, 2003. **36**(7): p. 2273-2283.
19. Stenzel, M.H., *Complex Architecture Design via the RAFT Process: Scope, Strengths and Limitations*, 2008. (Handbook of RAFT Polymerization), Wiley-VCH Verlag GmbH & Co. KGaA. p. 315-372.
20. Rieger, J., et al., *Amphiphilic Poly(ethylene oxide) Macromolecular RAFT Agent as a Stabilizer and Control Agent in ab Initio Batch Emulsion Polymerization*. Macromolecules, 2008. **41**(12): p. 4065-4068.
21. Wang, X., et al., *Ab Initio Batch Emulsion RAFT Polymerization of Styrene Mediated by Poly(acrylic acid-*b*-styrene) Trithiocarbonate*. Macromolecules, 2009. **42**(17): p. 6414-6421.
22. Chenal, M., L. Bouteiller, and J. Rieger, *Ab initio RAFT emulsion polymerization of butyl acrylate mediated by poly(acrylic acid) trithiocarbonate*. Polymer Chemistry, 2013. **4**(3): p. 752-762.
23. Rieger, J., et al., *Surfactant-Free RAFT Emulsion Polymerization Using Poly(N,N-dimethylacrylamide) Trithiocarbonate Macromolecular Chain Transfer Agents*. Macromolecules, 2010. **43**(15): p. 6302-6310.
24. Zhang, X., et al., *Well-Defined Amphiphilic Block Copolymers and Nano-objects Formed in Situ via RAFT-Mediated Aqueous Emulsion Polymerization*. Macromolecules, 2011. **44**(11): p. 4149-4158.
25. Divry, V., et al., *Drying Mechanisms in Plasticized Latex Films: Role of Horizontal Drying Fronts*. The Journal of Physical Chemistry B, 2016. **120**(27): p. 6791-6802.
26. Singh, K.B., *Understanding film formation mechanism in latex dispersions*, 2008. (published doctoral dissertation): Indian institute of technology Bombay, Mumabi, India.
27. Vanderhoff, J.W., E.B. Bradford, and W.K. Carrington, *The transport of water through latex films*. Journal of Polymer Science: Polymer Symposia, 1973. **41**(1): p. 155-174.
28. Croll, S.G., *Heat and Mass Transfer in Latex Paints during Drying*. Journal of Coatings Technology, 1987. **59**(751): p. 81-92.
29. Routh, A.F. and W.B. Russel, *Horizontal drying fronts during solvent evaporation from latex films*. AIChE Journal, 1998. **44**(9): p. 2088-2098.
30. Routh, A.F. and W.B. Russel, *A Process Model for Latex Film Formation: Limiting Regimes for Individual Driving Forces*. Langmuir, 1999. **15**(22): p. 7762-7773.

31. Vanderhoff, J.W., et al., *Theoretical Consideration of Interfacial Forces Involved in Coalescence of Latex Particles*. Rubber Chemistry and Technology, 1967. **40**(4): p. 1246-1269.
32. Dillon, R.E., L.A. Matheson, and E.B. Bradford, *Sintering of synthetic latex particles*. Journal of Colloid Science, 1951. **6**(2): p. 108-117.
33. Brown, G.L., *Formation of films from polymer dispersions*. Journal of Polymer Science, 1956. **22**(102): p. 423-434.
34. Sheetz, D.P., *Formation of films by drying of latex*. Journal of Applied Polymer Science, 1965. **9**(11): p. 3759-3773.
35. Ribeiro, T., C. Baleizão, and J. Farinha, *Functional Films from Silica/Polymer Nanoparticles*. Materials, 2014. **7**(5): p. 3881.
36. Balci, M., *1 - Introduction*, 2005. (Basic ¹H- and ¹³C-NMR Spectroscopy), Elsevier Science: Amsterdam. p. 3-8.
37. Oberlerchner, J.T., T. Rosenau, and A. Potthast, *Overview of methods for the direct molar mass determination of cellulose*. Molecules, 2015. **20**(6): p. 10313-10341.
38. Podzimek, S., *Size Exclusion Chromatography*, 2011. (Light Scattering, Size Exclusion Chromatography and Asymmetric Flow Field Flow Fractionation), John Wiley & Sons, Inc. p. 99-206.
39. Orata, F., *Derivatization Reactions and Reagents for Gas Chromatography Analysis*, 2012. (Advance gas chromatography- Progress in agricultural, biomedical and industrial applications), INTECH Open Access Publisher.
40. Kühnel, E., et al., *Mechanism of Methyl Esterification of Carboxylic Acids by Trimethylsilyldiazomethane*. Angewandte Chemie International Edition, 2007. **46**(37): p. 7075-7078.
41. Couvreur, L., et al., *First Nitroxide-Mediated Controlled Free-Radical Polymerization of Acrylic Acid*. Macromolecules, 2003. **36**(22): p. 8260-8267.
42. Wong, K.H., et al., *Honeycomb structured porous films from amphiphilic block copolymers prepared via RAFT polymerization*. Polymer, 2007. **48**(17): p. 4950-4965.
43. Liu, C., M.A. Hillmyer, and T.P. Lodge, *Multicompartment Micelles from pH-Responsive Miktoarm Star Block Terpolymers†*. Langmuir, 2009. **25**(24): p. 13718-13725.
44. Gong, J.P., et al., *Double-Network Hydrogels with Extremely High Mechanical Strength*. Advanced Materials, 2003. **15**(14): p. 1155-1158.
45. Nakajima, T., et al., *True chemical structure of double network hydrogels*. Macromolecules, 2009. **42**(6): p. 2184-2189.
46. Ducrot, E., et al., *Toughening Elastomers with Sacrificial Bonds and Watching them Break*. Science, 2014. **344**(6180): p. 186-189.

47. Ducrot, E., *Innovative tough elastomers: Designed sacrificial bonds in multiple networks*, 2013. (Unpublished doctoral dissertation): University Pierre and Marie Curie, Paris, France.
48. Rubinstein, M. and S. Panyukov, *Elasticity of Polymer Networks*. *Macromolecules*, 2002. **35**(17): p. 6670-6686.

-CHAPTER 5-

**Structure and Mechanical properties of latex films and DN made
from latex films**

Chapter 5: Structure and Mechanical properties of latex films and DN made from latex films.....	171
Introduction.....	174
Part I: Mechanical properties of latex films.....	179
1. Mechanical properties of the PBA, serving as an interpenetrating network for DN films.....	180
2 The differences between P(BA-co-BDA) latex films and PAA-b-PBA core-shell latex films..	182
2.1 P(BA-co-BDA) crosslinked latex films (0.5 mol% BDA).....	182
2.2 PBA-b-PAA core-shell latex films.....	183
2.3 Differences between crosslinked latex, P(BA-co-BDA), and core-shell latex, PAA-b-PBA.....	185
3 Mechanical results of PAA-b-PBA core-shell latex films with modified compositions.....	191
3.1 PAA-b-PBA latex film with a crosslinked PAA-Shell.....	191
3.1.1 Crosslinked PAA-shells by added PADAME.....	191
3.1.1-1 SN films of PAA-b-PBA with added PADAME.....	191
3.1.1-2 DN films based on PAA-b-PBA with added PADAME.....	192
3.1.2 Ionic interactions through PAA deprotonation with NaOH instead of NH_4OH	196
3.1.2-1 SN films of PAA-b-PBA with Na^+ counter ions.....	197
3.1.2-2 DN films based on PAA-b-PBA with Na^+ counter ions.....	197
3.2 PAA-b-PBA latex film with a crosslinked PBA-core.....	201
3.2.1 Crosslinked PBA-core by BDA.....	201
3.2.1-1 SN films of PAA-b-PBA crosslinked by BDA.....	201
3.2.1-2 DN films based on PAA-b-PBA crosslinked by BDA.....	202
3.2.2 Crosslinked PBA-core by DVB.....	206
3.3 The effect of the M_n on the PAA (shell thickness).....	207
3.3.1 SN films of PAA-b-PBA with different M_n of the PAA.....	208
3.3.2 DN films based on PAA-b-PBA with different M_n of the PAA.....	208
3.4 The effect of the PBA-core size on the PAA-b-PBA latex film	212
3.4.1 SN films of PAA-b-PBA with different M_n of the PBA	212
3.4.2 DN films based on PAA-b-PBA with different M_n of the PBA.....	213
3.5 PAA-b-PBA films with added PAA_{5k}	217
3.5.1 Standard latex (PAA 2.5k, PBA 100k) with added PAA_{5k}	217
3.5.1-1 SN films of PAA-b-PBA with added PAA_{5k}	217
3.5.1-2 DN films based on PAA-b-PBA with added PAA_{5k}	218
3.5.2 High M_n PBA latex, (PAA2.5k, PBA200k) with added PAA_{5k}	221
3.5.2-1 SN films of (PAA2.5k, PBA200k) with added PAA_{5k}	222
3.5.2-2 DN films based on (PAA2.5k, PBA200k) with added PAA_{5k}	222
Part II: Summary and discussion of the mechanical properties of the different SN and DN films..	227
1. Method of data analysis.....	228

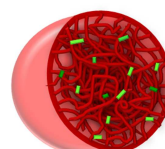
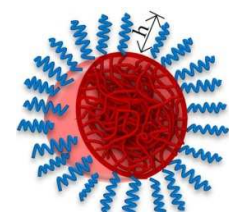
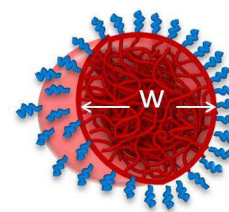
2. Swelling equilibrium of modified latex films.....	231
3. Toughness of DN films.....	232
4. Dissipation energy in DN films.....	235
5 Fracture toughness of DN films.....	237
Conclusion.....	238
References.....	240

Introduction

In chapter 4, we explained the procedure to synthesize unstructured P(BA-co-BDA) crosslinked latexes and PAA-b-PBA *core-shell* latexes, by conventional radical emulsion polymerization and by RAFT mediated emulsion polymerization, respectively. For the unstructured reference P(BA-co-BDA) latex, PBA_{no-shell}, it was necessary to copolymerize BA with 0.5% mol BDA as a crosslinker, to prevent the dissolution of the resulting film in BA monomer during the creation of the double network. For PAA-b-PBA core-shell latexes, various synthesis conditions and compositions were used to create different core-shell latexes, such as

- varying the M_n of the PAA block to create core-shell latex with different thicknesses of the PAA-shell,
- Varying the M_n of PBA block to increase the size of the PBA-core,
- using NaOH and not NH_4OH as the pH controller to leave ions in the shell of the core-shell latex after drying and/or promote ionic interactions.
- introducing two different effective crosslinkers; BDA and DVB to crosslink the PBA-core.

For a better understanding of the different structures, all latexes synthesized in this study are summarized in Table 5-1.

Type of latex	Abb. name	Latex structure
P(BA-co-BDA) crosslinked latexes (synthesis chapter 4 section 2.3)	(latex _{no-shell})	
PAA-b-PBA core-shell latex with different M_n of PAA-shell (synthesis chapter 4 section 2.4.2)	(PAA+ M_n PAA, PBA+ M_n PBA) - (PAA2.5k, PBA100k) - (PAA4k, PBA100k) - (PAA6k, PBA100k)	
PAA-b-PBA core-shell latex with different M_n of PBA-core (synthesis chapter 4 section 2.4.2)	(PAA+ M_n PAA, PBA+ M_n PBA) - (PAA2.5k, PBA100k) - (PAA2.5k, PBA200k)	

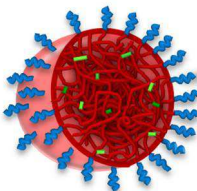
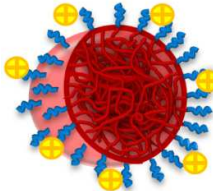



PAA-b-PBA core-shell latex with crosslinked PBA-core (synthesis chapter 4 section 2.4.3)	(PAA+M _n PAA, PBA+M _n PBA)+ % crosslinker) - (PAA2.5k, PBA100k)0.3%BDA ^a - (PAA2.5k, PBA100k)0.3%DVB ^b	
PAA-b-PBA core-shell latex with Na ⁺ counter ion (synthesis chapter 4 section 2.4.4)	(PAA+M _n PAA, PBA+M _n PBA)Na ⁺ - (PAA2.5k, PBA100k)Na ⁺	

Table 5- 1: Latex structures and names synthesized in this study, where  is PBA,  is PAA, and  is a crosslink, ^a mol% BDA used are 0.1, 0.3 and 0.5%, ^a mol% DVB using are 0.1, 0.3 and 0.5%.

Latex single network films (SN films)

The latexes (generally at solids contents around 22 wt%) were slowly dried at a controlled temperature below 25°C for a week to form simple latex single network films (SN film) with a thickness about 0.3-0.5 mm.

As shown in Table 5.1 (last line) we were also interested in reinforcing the interactions between PAA-shells during the drying process. Alternatively PADAME, a tertiary amine functional polymer ($M_n = 4.5 \text{ kg.mol}^{-1}$) was introduced at pH 8 into the core-shell latex (PAA2.5k, PBA100k). Upon evaporation of NH₃ and water during film formation and drying, the tertiary amines become partially protonated ($pK_a \sim 6.5$), and the ionic bonds formed between the ammonium groups of PADAME and the carboxylate groups of PAA should result in physical ionic crosslinks between the PAA-shells. The resulting core-shell latex films were called (PAA2.5k, PBA100k) 0.2eq PADAME and (PAA2.5k, PBA100k) 0.65eq PADAME. The details of the preparation of the films with PADAME addition can be found in chapter 4, section 3.2.

Moreover, a certain amount of PAA homopolymer solution ($M_n(\text{PAA}) = 5 \text{ kg.mol}^{-1}$) was added to the PAA-b-PBA latex, (PAA2.5k, PBA100k) to thicken the PAA shell of the latex. The % of PAA in the dry film was determined by weighing the PAA-TTC RAFT initiator ($m_0(\text{PAA})$) and the polymerized BA monomer($m_0(\text{BA})$) as presented in Eq. 5-1. Note that because not all the PAA-TTC will initiate the BA polymerization the %wt PAA in the film is larger than the %wt PAA in the PAA-b-PBA block copolymer.

$$(\%wt\ PAA)_{SN} = \frac{m_0(PAA)}{m_0(BA) \times conv.} \times 100 \quad (Eq. 5 - 1)$$

The overall % of PAA was increased by PAA_{5k} homopolymer to 11.5 wt% (original latex is about 2.5 wt% of PAA, see in Chapter 4; Table 4-4) and the blend was named (PAA2.5k, PBA100k) 9% PAA_{5k} (“9” wt% PAA added, meaning the quantity of PAA was increased by a factor of 4). The mechanical properties of the resulting films and the DN prepared afterwards will be compared with films made of a PAA-b-PBA latex with a high M_n of PAA, (PAA 4k, PBA100k), containing 6 wt% of PAA (see Table 4-4). Unfortunately, we could not compare these PAA loaded films with the latex (PAA 6k, PBA100k), containing 11%PAA as was our initial intention since we found later that we could not prepare DN films from the core-shell latex with a high M_n of PAA.

Figure 5-1, summarizes the different types of latex SN films and their proposed nanostructures, as synthesized in our study. The mechanical properties of the latex SN films were characterized in uniaxial extension. Once the films are prepared (as described in Chapter 4), the testing method and conditions are similar to those used for the silicone networks and can be found in chapter 3.

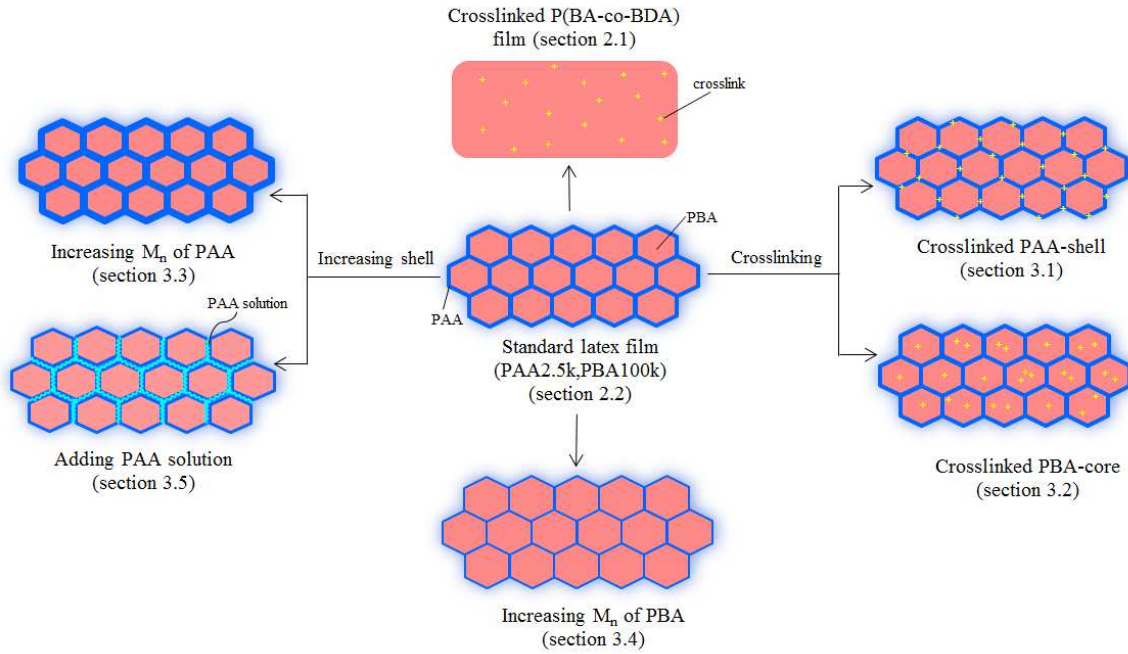


Figure 5- 1: Schematic of the latex films and their nanostructure

Double network films from latex precursors (DN films)

The dry films made from the synthesized latexes were used as a polymeric filler to reinforce a PBA elastomer and will be called in the following latex SN films. We introduced these films into PBA by the sequential interpenetrating network technique, where the latex SN films are first swollen in a BA monomer and BDA crosslinker mixture, and later polymerized to form an interpenetrating double network film (DN). We assumed that the PAA content in the SN films, $(\%wt\ PAA)_{SN}$, was the same as that in the latex which could be calculated from Eq.5-1 and for latex DN films, we calculated the % PAA content, $(\%wt\ PAA)_{DN}$, as shown in Eq. 5-2.

$$(\%wt\ PAA)_{DN} = \frac{(\%wt\ PAA)_{SN} \times \Phi_{latex}}{100} \quad (Eq. 5 - 2)$$

Where $m_0(PAA)$ is the mass of PAA macro-RAFT agent, $m_0(BA)$ is the mass of BA monomer used for latex synthesis and Φ_{latex} is the weight fraction of latex in the DN film.

The standard mechanical properties of the latex DN films were characterized in uniaxial extension until failure and also with single-edge notch fracture tests (method described in Chapter 3, as used for silicone elastomers). However, since these DN films are much more extensible and viscoelastic elastomers than the silicones, it was also interesting to characterize their energy dissipation properties by using loading-unloading cyclic extension tests as described in chapter 3. However, due to the high extensibility of the latex DN films, each step of extension needed to be adjusted to $\lambda = 3$. A typical deformation history for a cyclic deformation test can be found in Figure 5-2.

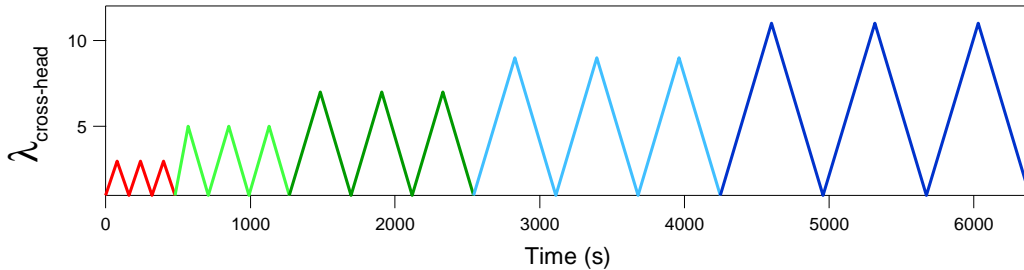


Figure 5- 2: Applied stretch ratio (λ) during a cyclic extension test for the latex DN films.

In this chapter, we will present the mechanical properties of the films made from the latex SN and of their corresponding DN films in two parts. In part I, we will expose in detail the mechanical properties of the latex SN and latex DN films for different modified systems. In Part II, we will summarize and compare the mechanical properties of modified DN. Finally, the DN, which shows the best properties based on the volume of glassy polymeric filler, will be highlighted.

Part I:

Mechanical properties of latex films

1. Mechanical properties of the PBA, serving as an interpenetrating network for DN films

A PBA elastomer is used as the interpenetrating network in latex DN films, (i.e. the swelling network). As a mechanical reference, PBA films were therefore also fabricated as standalone single network films with different BDA crosslinker concentrations, 0.01 mol%, 0.03 mol%, and 0.05 mol%. The polymerization of BA and BDA was initiated with an HMP UV-initiator inside an oxygen-free glove box. The detail of the PBA synthesis can be found in Chapter 4, section 4.2. The mechanical properties of the PBA networks were characterized in uniaxial extension as described in chapter 3, section 1.2.1.

Unsurprisingly, increasing the amount of BDA crosslinker resulted in an increase in stress and modulus at high strain, and in a reduction in extensibility (Figure 5-3(a)). The Mooney stress plot versus λ^{-1} in Figure 5-3 (b) (read from right to left) shows an obvious strain softening of the network beginning at $\lambda^{-1} = 0.9$. The decrease in Mooney stress along λ^{-1} is due to the presence of chain entanglements in the networks. The strain stiffening, due to the finite extensibility of the chains, can be easily detected for $\lambda^{-1} < 0.2$.

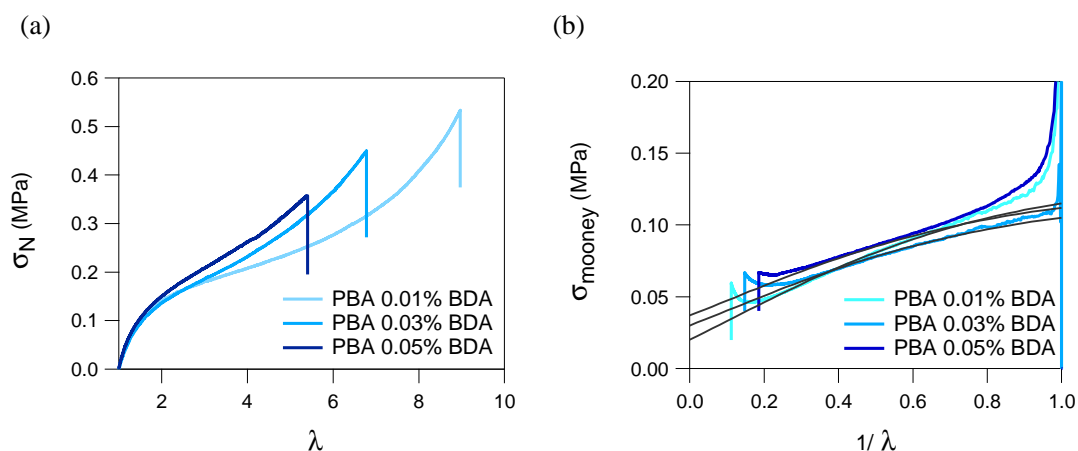


Figure 5- 3: Stress-strain curve and Mooney plot of PBA interpenetrating networks containing different concentrations of BDA, (a) stress-strain curve and (b) Mooney stress plot with the best fit (black line) of the Rubinstein-Panyukov equation

In addition, by fitting the Rubinstein-Panyukov model to the Mooney plot (black line in Figure 5-3 (b)), the contribution of the Young's modulus from entanglements (E_e), and from crosslinks (E_c) can be estimated as presented in Table 5-2.

Sample	E (MPa)	E_c (MPa)	E_e (MPa)
PBA 0.01% BDA	0.30	0.06	0.29
PBA 0.03% BDA	0.29	0.09	0.23
PBA 0.05% BDA	0.32	0.11	0.23

Table 5- 2: Young's modulus of PBA networks with different crosslinker concentrations. Measured from the initial modulus (E), or from fitting in Figure 5-3 (b) the entanglements (E_e) and crosslinks (E_c) contribution

It was found that by increasing the crosslinker concentration, E_c of the networks slightly increases while E_e of the network remains approximately constant. The unreliable value of the E_e contribution for the 0.01% BDA material may be due to viscoelastic relaxation. In the concept of the interpenetrated networks, the interpenetrating network is the loose network which provides extensibility, while the core or the host network is the stiff network which creates the sacrificial bonds in the overall network. For this reason, PBA 0.01% BDA which shows the best performance in terms of extensibility was selected to create latex double networks and will be the reference elastomer before reinforcing it with the latex film. .

2. The differences between P(BA-co-BDA) latex films and PAA-b-PBA core-shell latex films

In our study, two different methods, conventional radical emulsion polymerization, and RAFT-mediated emulsion polymerization, were used to synthesize simple and core-shell structured latexes, respectively. This resulted in a simple crosslinked latex of P(BA-co-BDA), called $\text{PBA}_{\text{no-shell}}$, and a series of core-shell latexes constituted of amphiphilic PAA-b-PBA diblock copolymers, . In this section, the mechanical properties of these two latex films and their corresponding DN films will be characterized and compared.

2.1 P(BA-co-BDA) crosslinked latex films (0.5 mol% BDA)

The simple P(BA-co-BDA) latex film, also named $(\text{PBA}_{\text{no-shell}})_{\text{SN}}$, and its DN network $(\text{PBA}_{\text{no-shell}})_{\text{DN}}$, were first characterized by uniaxial extension and the results are shown in Figure 5-4. The $(\text{PBA}_{\text{no-shell}})_{\text{SN}}$, crosslinked with 0.5 mol% BDA, shows a poor toughness, low stress at break and extensibility. A disappearance of the strain stiffening in the stress-strain curve of $(\text{PBA}_{\text{no-shell}})_{\text{SN}}$ which generally comes from the entanglements between polymer chain belonging to different latex particles, reveals that latex particles are probably poorly coalesced. The PBA chains have fewer entanglements with chains of neighboring particles due to the presence of crosslinks, resulting in a low toughness of the films and the presence of free surfactant was responsible of the cloudy aspect of the films, which we have already reported in chapter 3.

However, after introducing the PBA interpenetrating network to create DN films, the mechanical properties of $(\text{PBA}_{\text{no-shell}})_{\text{DN}}$ dramatically change. The initial modulus of $(\text{PBA}_{\text{no-shell}})_{\text{DN}}$ increases slightly relative to that of $(\text{PBA}_{\text{no-shell}})_{\text{SN}}$ and the strain hardening can be clearly observed at $\lambda \sim 2$ until fracture occurs and the nominal stress at break increases significantly from 0.1 to 1.1 MPa. Such strain stiffening in the DN is obviously due to the presence of crosslinks in the PBA latex. By the sequential interpenetrating network technique, the polymerized PBA linked the crosslinked latex particles together resulting in significant mechanical reinforcement of the PBA network. It is interesting to note however that the extensibility of the PBA original film (red curve) has been reduced by the introduction of the chemically crosslinked latex particles.

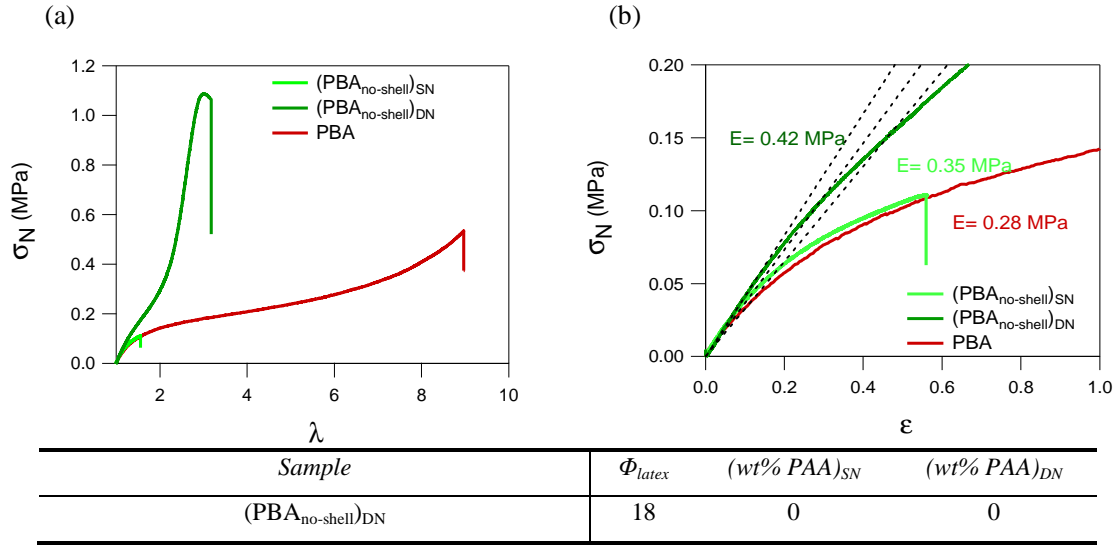


Figure 5- 4: Stress- strain curve of $PBA_{no-shell}$ latex films and the DN network film where the red line represent a reference PBA elastomer with 0.01wt% BDA (see in section 1) In figure (b), the dashed lines represent the fits to the initial modulus.

2.2 PBA-b-PAA core-shell latex films

The PBA-b-PAA core-shell latexes showed a distinctly different mechanical behavior from the $PBA_{no-shell}$ latex films. The stress-strain curve of a core-shell latex ($PAA_{2.5k}, PBA_{100k}$)_{SN}, shown in Figure 5-5 (a) and (b) as a light yellow line, shows a high initial modulus while maintaining a good extensibility. Generally, in rubber compounds the increase in modulus at low deformation, which induces the nonlinear behavior, comes from filler-filler interactions.^{1, 2} In our study, the SN films of PAA-b-PBA latexes also show this behavior, the initial modulus of the film is much higher than that of the pure PBA (red line) until $\epsilon = 0.2$ which is certainly related to interactions between PAA-shells. After this point, the PAA shells are broken into pieces and the material softens very markedly. The mechanical behavior of the films after the breaking of PAA shells is dominated by the PBA core and the extensibility of the latex films is related to the M_n of the PBA block.

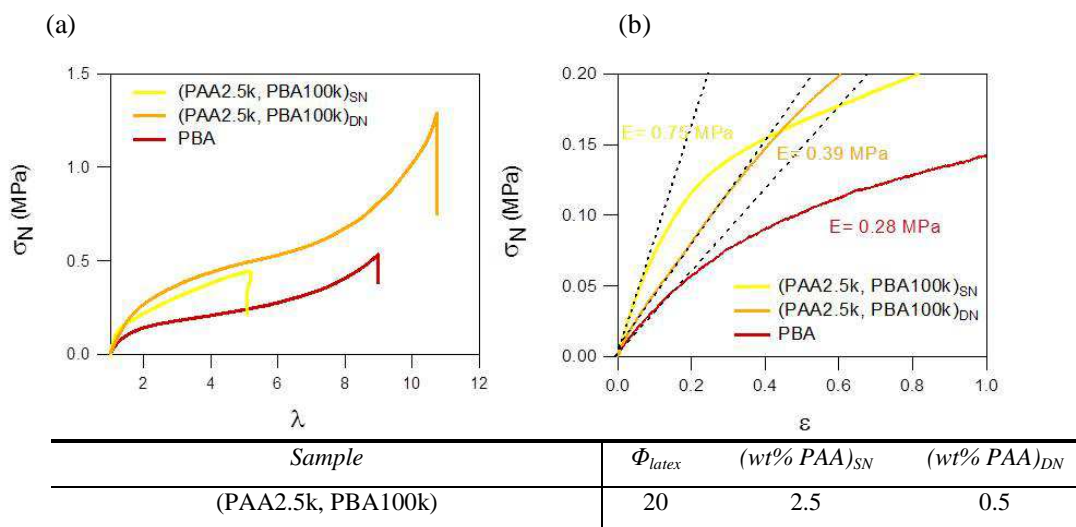


Figure 5- 5: Stress- strain curve of PBA-b-PBA core-shell latex films, type (PAA2.5k, PBA100k) and their DN network films where the red line represent a reference PBA elastomer with 0.01wt% BDA (see in section 1)

The result for the latex DN film is shown as an orange line in Figure 5-5 (a) and (b). Compared to the SN, the initial modulus of (PAA2.5k, PBA100k)_{SN} decreases as it is now interpenetrated with PBA (Figure 5-5 (b)). This decrease is expected since the shell structure is now diluted from 2.5 wt% to 0.5wt% of PAA (Figure 5-6). Yet the presence of the latex stiffens the pure reference PBA elastomer (red line in Figure 5-5) by almost a factor of 2 at 100% strain and increases markedly the strain at break with a pronounced strain stiffening starting at $\lambda \sim 6$ and increasing until break at $\lambda \sim 11$.

Remarkably, this increase in modulus and stress at break with only 0.5%wt of dispersed PAA shells, occurs without any reduction in extensibility and may be due to a combination PBA entanglements and the interaction between PAA shells during deformation.

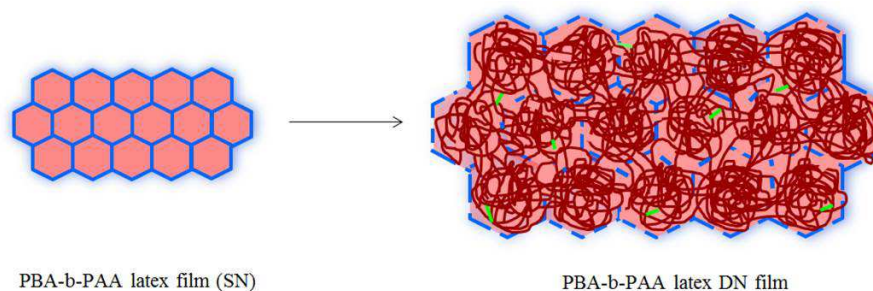


Figure 5- 6: Proposed nanostructure of PBA-b-PBA latex simple film (SN) and PBA-b-PBA latex DN film.

2.3 Differences between crosslinked latex, P(BA-co-BDA), and core-shell latex, PAA-b-PBA

To understand better the mechanical differences between the chemically crosslinked latex P(BA-co-BDA) film and the core-shell latex PAA-b-PBA films, latex SN films and latex DN films are plotted in the same stress-strain curve in Figure 5-7.

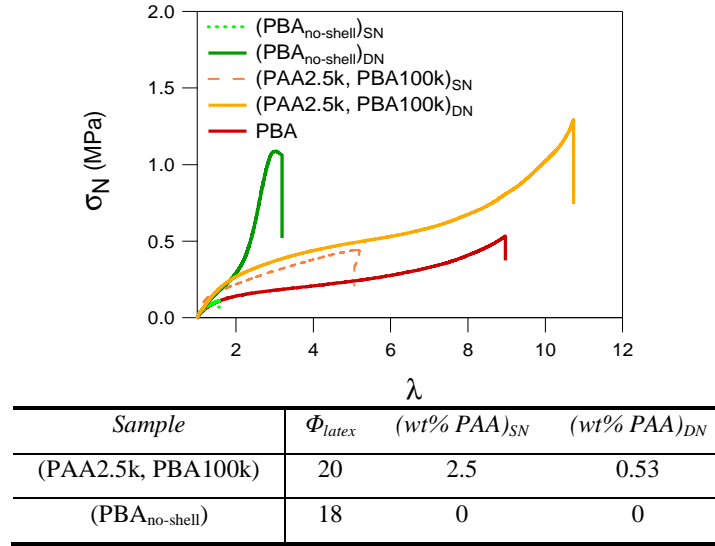


Figure 5- 7: Stress-strain curve of PBA_{no-shell} film and PAA-b-PBA film, SN and DN network, and their PAA composition where the red line represent a reference PBA elastomer with 0.01wt% BDA (see in section 1)

In SN films (dashed lines), the two films show dramatic differences. The core-shell latex film (PAA2.5k, PBA100k)_{sn} shows significantly higher mechanical performance compared to films made from plain crosslinked latex particles as previously reported in the study of Chenal et al. on a series of similar latexes.³ Thanks to the unique properties of PAA, which remains in the glassy state at room temperature ($T_g = 106\text{ }^{\circ}\text{C}$)^{4, 5} and creates physical crosslinks (through hydrogen bonding or ionic interactions) with other PAA chains, the films can create a relatively continuous network and stiffen the material.

After creating DN films, the mechanical properties of the films (full line) show significant improvements in modulus, stress at break and elongation at break relative to the PBA film alone or to the SN films. The (PBA_{no-shell})_{DN} shows a very steep strain stiffening at relatively low deformation probably due to the limited extension of the chains between crosslinks of the PBA particles embedded in the material. On the other hand, the DN film made from the PAA-b-PBA latex film shows a decrease in the initial modulus relative to the SN film (Figure 5-8) and the strain stiffening is shifted to

very high deformations. The decrease of the initial modulus of the PAA-b-PBA latex in the DN film indicates a dilution of the structure but in this case PAA shells do not have any intrinsic finite extensibility and the structure may even be partially disrupted by the swelling process, as proposed in Figure 5-6.

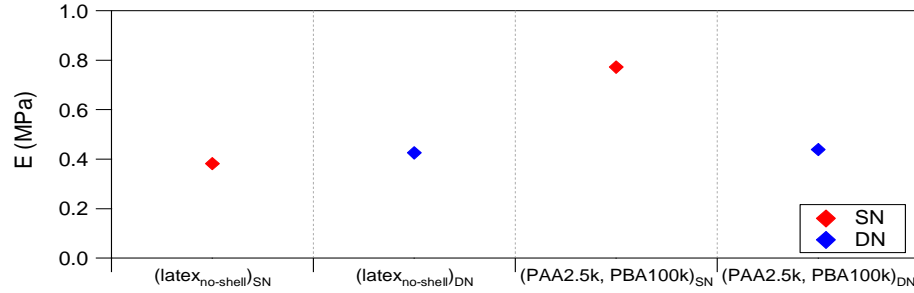


Figure 5- 8: Initial modulus of PBA_{no-shell} film and PAA-b-PBA film, SN and DN network.

Fracture toughness of latex films

Latex SN films and latex DN films were cut into a strip and a single notch (1-1.5 mm) was cut in the center edge of the specimens. The details of testing conditions and the sample dimensions can be found in Chapter 3. The fracture toughness of these notched latex films was characterized in mode I (extension) at 500 $\mu\text{m}.\text{sec}^{-1}$ at room temperature. The fracture energy of the samples was determined by using the Greensmith approximation (Chapter 1 and 3). However, as we found some variations in the properties of our DN films, the strain energy density $W(\lambda_c)$, used for the fracture energy calculation (Eq. 5-3) will be calculated from the integral of the area under the stress-strain curves of the actual notched samples. As a result the values of Γ may have been slightly underestimated.

$$\Gamma = \frac{6cW(\lambda_c)}{\sqrt{\lambda_c}} \quad \text{Eq.5 - 3}$$

where Γ is fracture energy in $\text{J}.\text{m}^{-2}$, c is the initial length of the crack and λ_c is the stretch ratio at the maximum stress before the crack propagation.

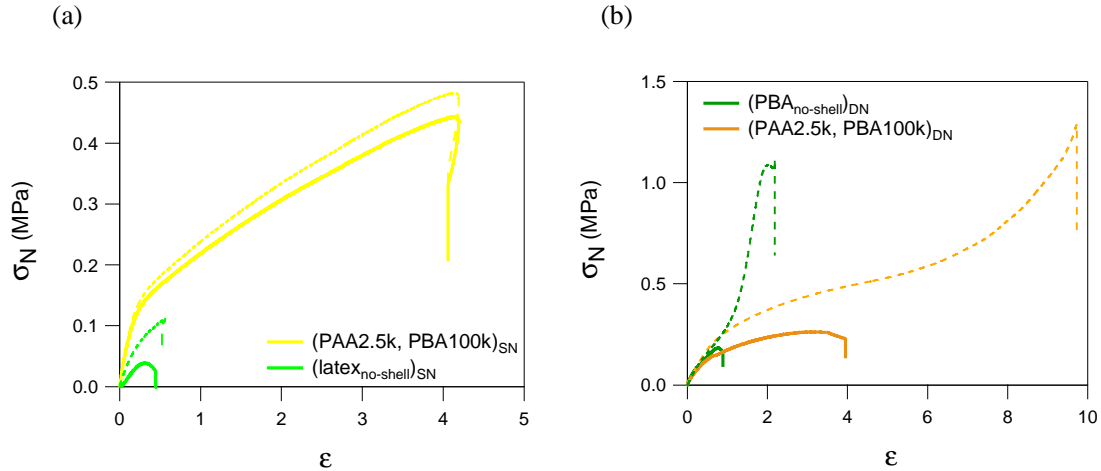


Figure 5- 9: Stress-strain curves of notched (full lines) and unnotched (dashed lines) samples of (PBA_{no-shell}) and (PAA2.5k, PBA100k), (a) SN and (b) DN

In the latex SN films (Figure 5-9 (a)), it is obvious that the core-shell latex of (PAA-b-PBA)_{SN} has a much better fracture resistance than the crosslinked P(BA-co-BDA) or (PBA_{no-shell})_{SN}. Due to the nanostructure of the film and the glassy nature of the PAA, the (PAA2.5k, PBA100k)_{SN} with a single edge cut does not show a significantly different behavior from that of an un-notched sample (shown as a dashed line). The sample can absorb and distribute well the stress around the crack tip and prevent the crack propagation very effectively. It should be noted here that such a core-shell film without any chemical crosslinks is able to flow at high strains and undergo significant plastic deformation, a desirable feature to reduce stresses at the crack tip but also source of irreversible and permanent deformation after removal of the stress.

After creating DN films (Figure 5-9 (b)), in the (PAA2.5k, PBA100k)_{DN}, the nanostructure of the PAA shell remains but the PBA network creates now a continuous lightly crosslinked network throughout the film which suppresses most of the irreversible plasticity of the SN. This increase in elasticity while reducing the fracture properties compared with the viscoplastic SN.

For the crosslinked latex, P(BA-co-BDA), the notched-sample of (latex_{no-shell})_{DN} shows an obvious increase in fracture energy by a factor of 5 (Figure 5-9 and Table 5-3). This increase in fracture toughness in the DN films may come from the internal fracture of covalent bonds in the particles at the crack tip analogously to what has been observed in acrylate double network elastomers.⁶

Sample	Γ (kJ/m ²)
(PBA _{no-shell}) _{SN}	0.07
(PBA _{no-shell}) _{DN}	0.63 ± 0.04
(PAA2.5k, PBA100k) _{SN}	3.95 ± 1.50
(PAA2.5k, PBA100k) _{DN}	2.53 ± 0.36

Table 5- 3: Fracture energy of SN and DN of (PBA_{no-shell}) and (PAA2.5k, PBA100k)Energy dissipation

Understanding the energy dissipation mechanisms of a material is a key to optimize the reinforcement of the mechanical properties and in particular the toughness. It is therefore interesting to verify the nature of the dissipative properties of the latex DN films, which possess a high toughness. The dissipation properties of the DN films were characterized with loading-unloading cyclic extension tests at increasingly large values of strain. The experimental method and testing conditions are described in Chapter 3 and the applied strain history is the one shown in Figure 5-2.

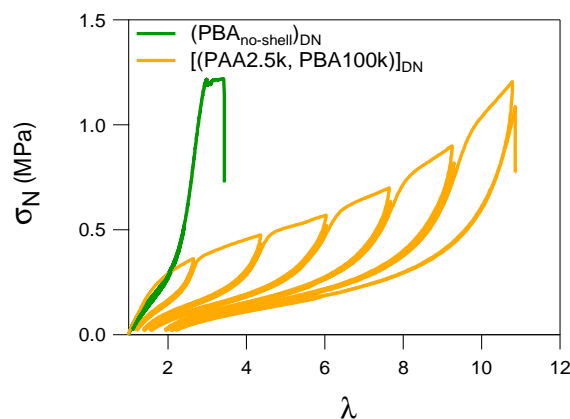
Figure 5- 10: Step-cycle extension tests of latex DN films of (PBA_{no-shell}) and (PAA2.5k, PBA100k).

Figure 5-10 shows the data for the (PBA_{no-shell})_{DN} in green, and (PAA2.5k, PBA100k)_{DN} in orange. Clearly, these two kinds of latex DN films have very different dissipative behaviours. The DN made from the crosslinked latex, (PBA_{no-shell})_{DN}, shows very little bulk hysteresis suggesting that there is very little bond breaking of the crosslinked networks in the particles. In contrast, in the core-shell latex films, (PAA2.5k, PBA100k)_{DN}, dissipation is found both in the first cycle (which we will call the major loop) and in the stabilized cycle (the minor loop). The dissipation energy of each loop (major and minor) in each step extension are then analyzed with the method described below.

Analysis method for energy dissipation

The dissipated energy for each step extension can be calculated by integrating the area of the stress-strain curve of each loop.^{7, 8} The analysis of the dissipation of energy was characterized for the major loop (the 1st cycle), Hys_{maj} , and for the minor loop (the 2nd repeating loop), Hys_{mi} , for each step extension. In general, the major loop of each step is related to irreversible damage to the internal structure of the material. The hysteresis of the minor loop or repeating loop is due to viscoelastic dissipation at fixed structure, the hysteresis shows the effect of pendant chains and free chains. The normalized hysteresis (Hys_{maj}/W) which is the ratio of a major hysteresis to a total work done to the system is also characterized as described in Figure 5-11. The input work of each extension loop can be determined by the area under the stress-strain curve.

Moreover, the residual deformation or permanent set of each major loop which shows the viscoelastic effect also can be analyzed and shown as Def_{res} . The initial modulus of each major loop, E_{maj} is also the key to characterize the damage to the network. The E_{maj} can be determined by fitting the loading curve at low deformation (Figure 5-11).

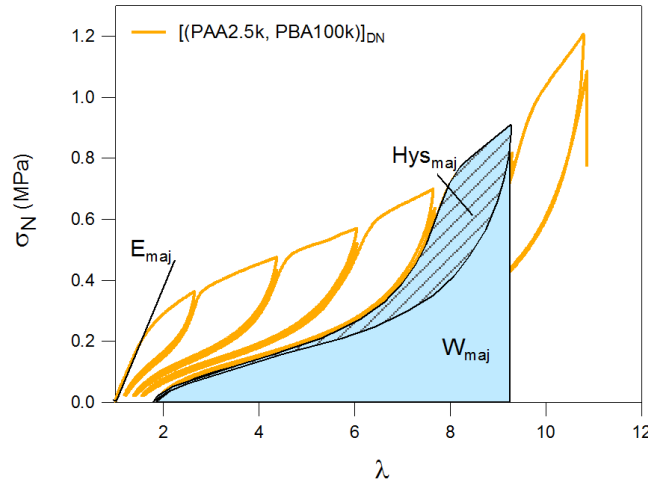


Figure 5- 11: The calculation of the hysteresis of the major loop (Hys_{maj}), relative hysteresis (Hys_{maj}/W), and initial modulus of major loop (E_{maj})

The evolution of the dissipated energy of the $(PAA2.5k, PBA100k)_{DN}$ as a function of λ is shown in Figure 5-12. The dissipated energy, shown as Hys_{maj} and Hys_{mi} , increases markedly with applied strain along with the residual deformation (Def_{res}) which reaches $\lambda_{min} = 2.25$ in the last cycle ($\lambda_{max} = 11$) before breaking. The Hys_{maj} which is characterized in a hysteresis loop by an unloading curve shows significant softening. This behavior is known as the Mullins effect⁹ and it is mostly found in filled elastomers. The origin of the Mullins effect in filled elastomers was described by two main

approaches¹⁰, i) the hard rubber phases are transformed into soft rubber during unloading⁹, and ii) the damage corresponds to breaking of polymer chains.¹¹

In our study, we filled a soft PBA elastomer with polymeric fillers (PAA-b-PBA) in which PAA forms a network of harder shells. The hysteresis of the latex from $\lambda_{\max} = 0$ to $\lambda_{\max} = 2.5$ (interval I) slightly increases and then a dramatic increase can be found in interval II. The hysteresis at low deformation (phase I) may be due to the progressive breaking of PAA shells and to the breaking of connections between them while the hysteresis at high deformation (phase II) may be more related to the disentangling and breaking of PBA chains. The Def_{res} of the latex DN film also increases monotonously with applied maximum λ . The Def_{res} was observed to correlate with the softening¹² and we found clearly this effect in our latex DN. The variation in initial modulus observed in the major hysteresis loop is shown in Figure 5-12 (b). A dramatic decrease of E_{maj} can be clearly observe after 1st cycle ($\lambda_{\max} = 2.5$). This confirms that the damage of the network occurred, especially in the beginning of the loading to $\lambda_{\max} = 6$ due to the breaking of the network of PAA shells. The effect of breaking the PAA-shell also can be seen by plotting the normalized hysteresis $\text{Hys}_{\text{maj}}/W$, which is highest for the 1st and 2nd cyclic extension, where more energy is needed to break the PAA-shells.

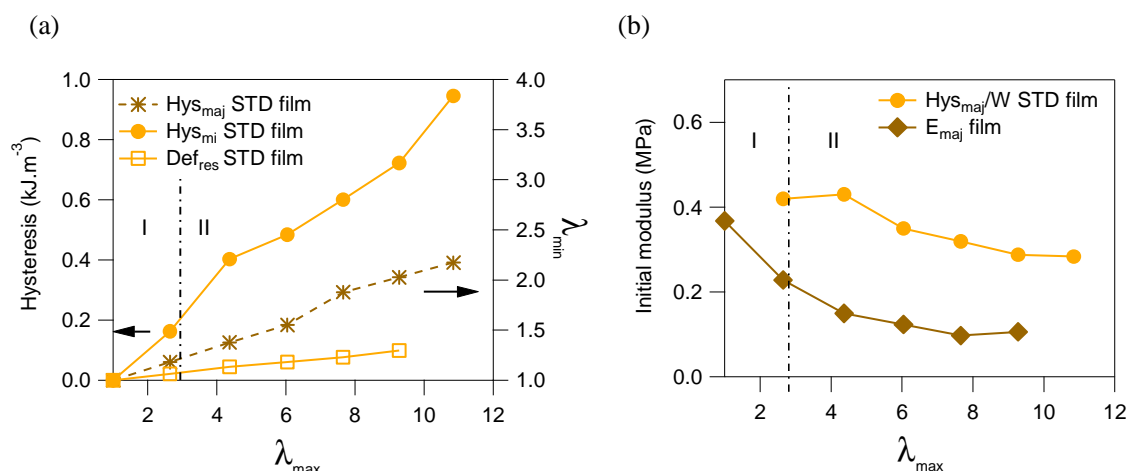


Figure 5- 12: Energy dissipation analysis of each step extension of the standard latex film (PAA2.5k, PBA100k)_{DN}

3. Mechanical results of PAA-b-PBA core-shell latex films with modified compositions

3.1 PAA-b-PBA latex film with a crosslinked PAA-Shell

In this section, the objective was to reinforce the interactions between PAA shells of the PAA-b-PBA core-shell latexes. Two methods were used:

- i) Creating physical crosslinks by introducing a cationic polymer (PADAME) in the water phase, creating therefore ionic bonds with the carboxylate group of PAA-shells.
- ii) Introducing ionic interactions between carboxylate groups of PAA (COO^-) and cations generated by NaOH (Na^+), which were used for the pH adjustment during the synthesis of the core-shell latexes.

The impacts of these ionic interactions in the PAA shell on the mechanical properties of the films are reported in this section.

3.1.1 Crosslinked PAA-shells by added PADAME

To create physical crosslinks between PAA-shells, a PADAME cationic polymer was added into the PAA-b-PBA latex solution before drying to create the films. The step by step preparation of the PADAME addition was described in Chapter 4, section 3.2. In this study, two different amounts of PADAME were added to the latex solution (0.2 eq. and 0.65 eq., corresponding to 1.1 and 3.4 wt% in the dried film respectively). The effect of the quantity of PADAME on the mechanical properties of the latex films is presented in Appendix A. Here we will only present the results for 0.65 eq. PADAME addition and compare the mechanical properties of the resulting films with those of the unfilled PBA or those of the standard latex film ($\text{PAA2.5k, PBA100k}_{\text{DN}}$).

3.1.1-1 SN films of PAA-b-PBA with added PADAME

The mechanical performance of the dried films of PAA-b-PBA latex films with additional PADAME were tested in uniaxial extension. The stress-strain curves are shown in Figure 5-13 in comparison with the standard PAA-b-PBA latex films.

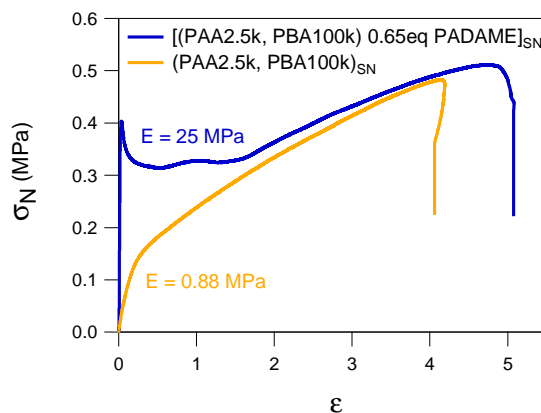


Figure 5- 13: Stress-strain curve of PAA-b-PBA latex SN film with PADAME addition, and standard latex film

The initial modulus of the latex simple films with 0.65 eq. PADAME addition is remarkably increased ($E = 25$ MPa). The physical crosslinks imparted by the PADAME/PAA interactions to the PAA shells result in a better organization of the latex particles. The particles can form a tightly packed structure. The extensibility at break of the core-shell latex films appears to be mainly controlled by the M_n of the PBA. However, a slight difference in extension at break can be found when comparing with the standard latex films which could be due to a small difference in M_n of PBA, M_n of the standard latex being lower than of M_n of latex used for the latex with the PADAME addition (see the details in chapter 4, Table 4-4 for TL103 was used for creating a latex film with PADAME addition, and TL85 for the standard latex film).

In addition, considering the overall mechanical behaviour of the latex films, latex films with PADAME addition are qualitatively different from the standard latex film. At low deformation, the modulus of the latex simple films with 0.65 eq PADAME addition is very high and beyond the values expected from entropic elasticity, until a critical stress (σ_c) is reached, $\sigma_c = 0.4$ MPa. After this point, the specimens undergoes a yield process and a large deformation with a small increase in the applied load. Presumably in this regime, the PAA shell network is broken irreversibly and the behaviour is then dominated by the rheology of the PBA core. A similar result was also reported by Chenal et al ^{13, 14}. In addition the latex film with 0.2 eq PADAME was reported to form a necking during the tensile test.

3.1.1-2 DN films based on the PAA-b-PBA with added PADAME

DN latex films were synthesized from the formerly discussed nanostructured SN, containing 0.65 eq. PADAME. The mechanical properties of the DN films were then characterized in uniaxial extension, strain controlled step-cycle extension and single edge notch fracture tests. We will start the analysis with the results of uniaxial extension as shown in Figure 5-14.

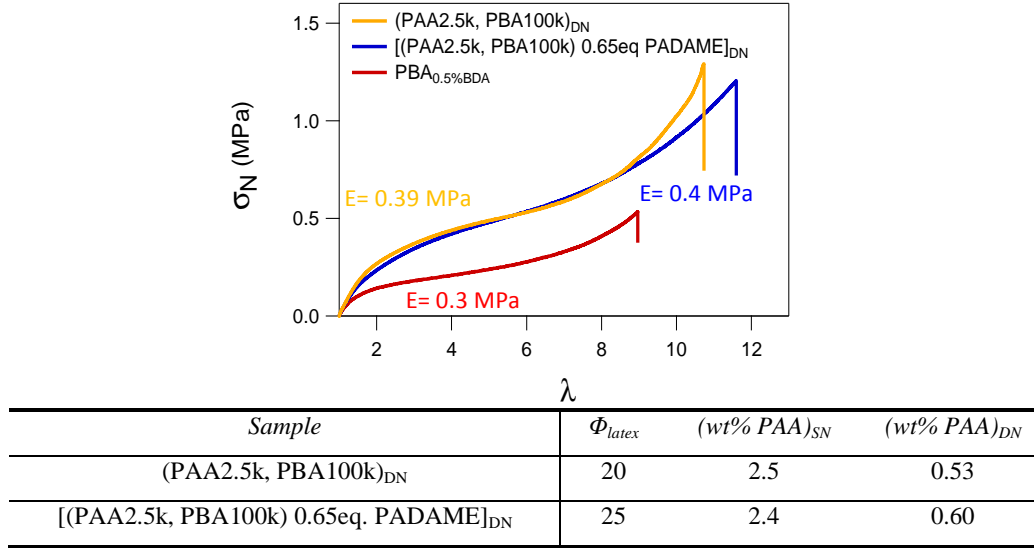


Figure 5- 14: Stress-strain curves and wt% of PAA for PAA-b-PBA DN films with 0.65 eq. PADAME, standard DN films, and reference film (SN PBA film).

Intuitively we would have expected that the difference in stiffness and yield stress of the latex SN films (Figure 5-13) should also result in differences in the DN. Unfortunately little difference can be observed in the stress-strain curve and the PADAME added films result in even lower stresses at a higher volume fraction of PAA. This is particularly surprising given the large difference in moduli in the SN and suggests that either the swelling process has significantly disrupted the PAA structure formed by the ionic interactions or the PADAME was dissolved in the BA bath during the swelling process. Since particles need to swell to form the double networks, the shell should not be mechanically too strong to be able to deform to accommodate the change in volume without breaking apart. The collapse of the shell decreases significantly the toughness of the latex film. Moreover, we did not test the solubility of PADAME in the BA monomer; PADAME may dissolve and leave from the film during the swelling process, resulting in less effect of PADAME on the DN.

Fracture toughness

Fracture tests on notched samples studied with single edge notched DN latex films are shown in Figure 5-15. The fracture energy calculated by the Greensmith equation using the strain energy density calculated in notched sample, presented in Table 5-4.

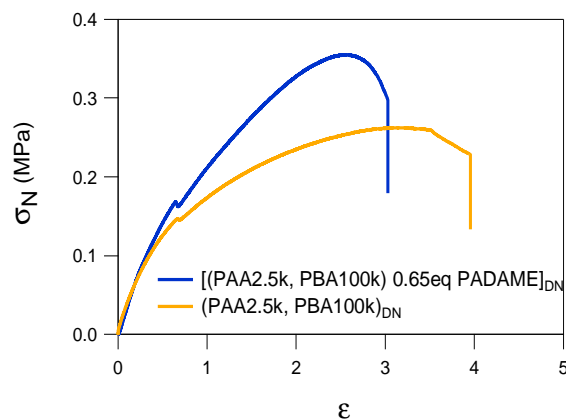


Figure 5- 15: Stress-strain curves of notched samples of (PAA2.5k, PBA100k) latex DN with 0.65 eq. PADAME addition, and standard latex DN films

We observe slight differences in the stress-strain curve of the notched samples in fracture tests compared with the tensile test in un-notched samples. The core-shell latex with 0.65 eq. PADAME added shows a better stress at break and lower elongation at break, while the initial modulus is similar to that of the standard latex film ($E = 0.33$ MPa and 0.34 MPa for standard DN and 0.65 eq. PADAME DN respectively). These small differences may be due to ionic interactions between PADAME and PAA.^{3, 6} The fracture energy has a variability for the DN films made from the latexes with PADAME, however, it seems to slightly increase relative to the standard film, as shown in Table 5-4

Sample	Γ (kJ/m ²)
(PAA2.5k, PBA100k) _{DN}	2.53 ± 0.36
[(PAA2.5k, PBA100k)0.65 eq PADAME] _{DN}	3.16 ± 0.15

Table 5- 4: Fracture energy of (PAA2.5k, PBA100k) latex DN with 0.65 eq PADAME addition, and standard latex DN films

Energy dissipation

The dissipative properties of the PAA-b-PBA latex DN films with PADAME addition, were characterized by step-cycle tests, and compared with the standard latex DN films, (PAA2.5k, PBA100k)_{DN} (Figure 5-16).

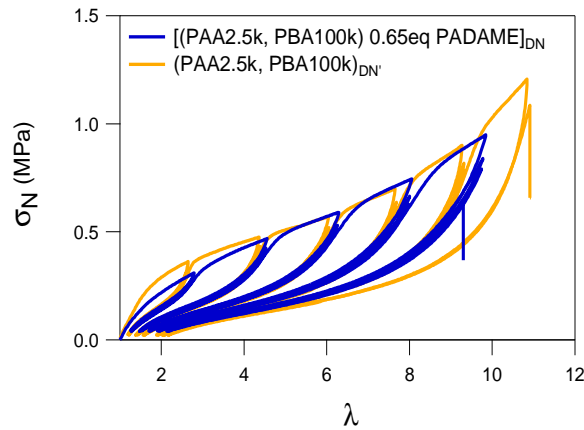


Figure 5- 16: Cyclic extension of (PAA2.5k, PBA100k) latex DN with 0.65 eq. PADAME addition, and standard latex DN films

Again, the DN films prepared from latexes with PADAME addition do not show significant differences from the standard DN film. All latex DN films show obviously the Mullins effect, which is the presence of strain softening under unloading condition. The dissipative properties of each DN films were characterized as explained in Chapter 3, section 1.2.2 and analysed as explained in the analysis method of energy dissipation, section 2.3. A plot of the evolution of the major and minor hysteresis, permanent set, relative hysteresis and initial modulus of the major extension loop as a function of the applied λ_{\max} are shown in Figure 5-17.

Overall, the dissipation energy of the latex DN film with 0.65 eq. PADAME does not show significant differences from that of a standard latex DN film. A slightly higher Hys_{mi} can be found in DN PADAME film which may be due to the free PADAME after the breaking of physical bonds with the PAA-shells. In Figure 5-17 (b), we found that the initial modulus of the 1st major loop in DN PADAME film was a bit lower than for the standard latex DN film. The relative hysteresis (Hys_{maj}/W) is slightly lower at low deformations ($\lambda < 5$). These results indicate that the PADAME chains do not perform well as physical crosslinks in the latex DN film. PADAME may act as free polymer which diminishes the homogeneity of the film, resulting in a lower energy to break the PAA bond (lower in Hys_{maj}/W) and lowering the initial modulus of the films.

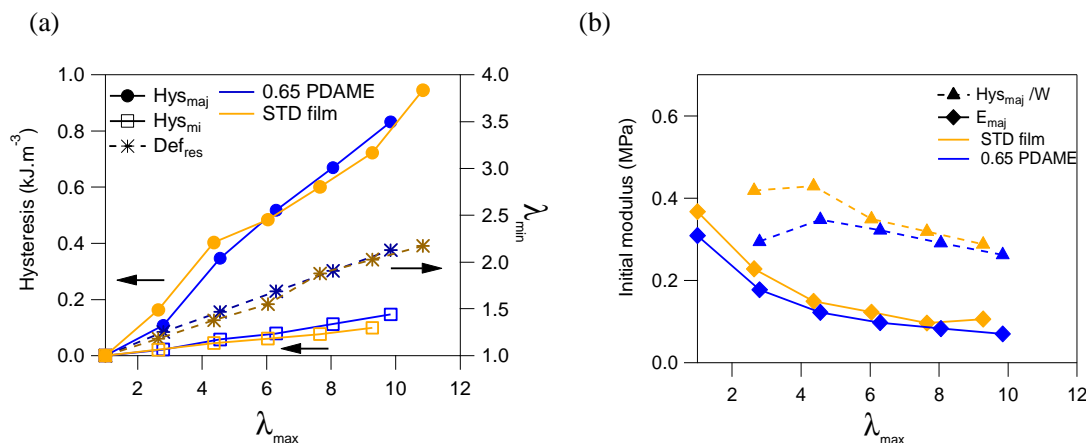


Figure 5- 17: Energy dissipation analysis of each step extension of (PAA2.5k, PBA100k) latex DN film with 0.65 eq PADAME addition relative to the standard latex DN film

In conclusion, the addition of PADAME to PAA-b-PBA latex significantly reinforces the latex SN film, especially the initial modulus of the film. However, it has little positive effects on reinforcing PBA in the DN films. The swelling process to create DN film probably disturbs the physical crosslinks between the PAA-shells or PADAME may dissolve in BA bath during swelling.

3.1.2 Ionic interactions through PAA deprotonation with NaOH instead of NH₄OH

Leaving residual ions in latexes to form ionic bonds is another way to create physical crosslinks between PAA-shells. Cationic ions can form physical bonds with carboxylate ions (COO⁻) in the PAA-shells, and may create different types of physical crosslinks relative to those created between PADAME and COO⁻.

In our standard latex synthesis, NH₄OH was used to adjust the pH of the monomer mixed solution according to former studies by Chenal et al^{3, 13}, the acrylic acid units in latex film are in their acid form since NH₃ is evaporated during film formation and also by evaporation at 100 °C. Now, in order to play with the degree of ionization of the PAA (i.e. to transform at least partially the PAA in a carboxylate anion), NaOH was used instead of NH₄OH. The latex synthesis using NaOH for pH adjustment released residual Na⁺ during the film formation process, while water formed through acid-base reaction (OH⁻ with H⁺ from PAA) evaporated with the serum water and leaves COO⁻ anions and Na⁺ cations in the latex film, which can form physical “crosslinks” through ionic interactions.

3.1.2-1 SN films of PAA-b-PBA with Na⁺ counter ions

The mechanical properties observed in uniaxial extension at room temperature of PAA-b-PBA latex films with Na⁺ counter ions are shown in Figure 5-18. Similarly to what was observed with PADAME crosslinked PAA-shells (see in section 3.1) the initial modulus of the films significantly increases at the beginning until it reaches a critical stress (σ_c), $\sigma_c = 0.2$ MPa. Then the deformation of the specimens continues to deform up to $\varepsilon = 2.8$ before breaking without observing any necking. The stress at break of latex films with Na⁺ counter ions is around 0.4 MPa.

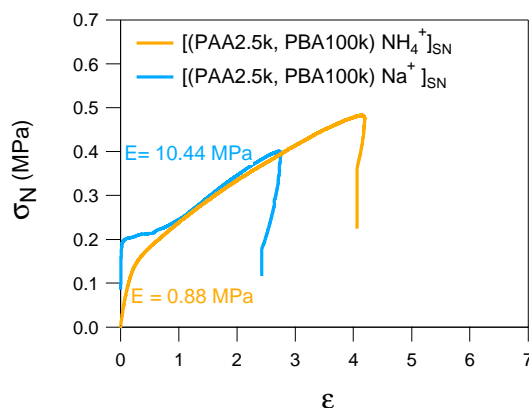
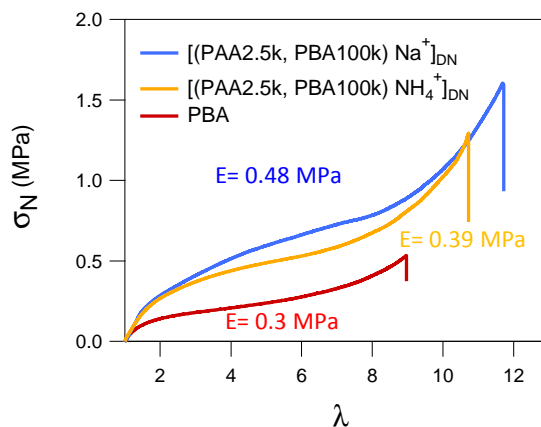


Figure 5- 18: Stress-strain curve of PAA-b-PBA latex films with Na⁺ counter ions and latex films.

The two studies introducing reinforcing interactions to the PAA-shell of the latex, using a cationic polymer (PADAME) or ionic interactions (COO⁻ / Na⁺), show that the shell-shell interactions probably promote a better organized, or at least a stronger interface between particles in the films as demonstrated by the drastic increase of the initial modulus of the films. They do not however affect much the extensibility of the films.

3.1.2-2 DN films based on PAA-b-PBA with Na⁺ counter ions

The tensile stress-strain curves of a DN film made from PAA-b-PBA with Na⁺ counter ions is shown in Figure 5-19.



Sample	Φ_{latex}	(wt% PAA) _{SN}	(wt% PAA) _{DN}
[(PAA2.5k, PBA100k) NH ₄ ⁺] _{DN}	20	2.5	0.53
[(PAA2.5k, PBA100k) Na ⁺] _{DN}	22	2.5	0.55

Figure 5- 19: Stress-strain curve and wt % of PAA for PAA-b-PBA latex DN films with Na⁺ counter ions, standard latex films and the reference film (SN PBA film).

The stress-strain curve of the latex DN film with Na⁺ is slightly higher than that of the standard latex DN film made with NH₄OH. In addition, the initial modulus of the two films is similar and it is intermediate between that of the latex SN films and that of the simple PBA elastomer, indicating that the network formed by the PAA shells was broken during swelling and that the nanostructure of PAA shells has changed in the DN film.

Fracture toughness

A slightly higher fracture toughness is found in the DN film with Na⁺ counter ions, [(PAA2.5k, PBA100k) Na⁺]_{DN}, (Figure 5-20 and Table 5.5). This reinforcement is invisible in the modulus but appears in the extensibility of the notched films and hence in the fracture energy. It is possible that the stronger interactions between PAA broken shells and presence of ions in the films introduces more energy dissipation at large strain (the strains at the crack tip must be very large).

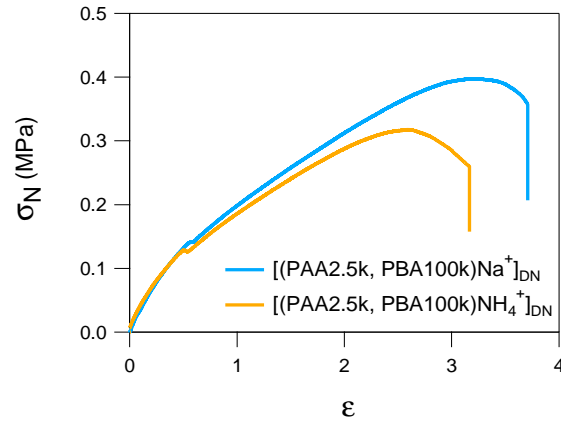


Figure 5- 20: Stress-strain curves of single-edge notch samples of DN made from PAA-b-PBA latex films with Na^+ counter ions and from standard latex films

Sample	Γ (kJ/m^2)
$[(\text{PAA}2.5\text{k}, \text{PBA}100\text{k})\text{NH}_4^+]_{\text{DN}}$	2.53 ± 0.36
$[(\text{PAA}2.5\text{k}, \text{PBA}100\text{k})\text{Na}^+]_{\text{DN}}$	3.38 ± 0.08

Table 5- 5: Fracture energy of PAA-b-PBA latex DN films with Na^+ counter ions and standard latex films, ^a the fracture energy determined by Greensmith approach and ^b the fracture energy determined by the area under stress-strain curve of notched sample

Energy dissipation

The energy dissipation properties of DN films $[(\text{PAA}2.5\text{k}, \text{PBA}100\text{k})\text{Na}^+]_{\text{DN}}$ and of DN made from standard latexes $[(\text{PAA}2.5\text{k}, \text{PBA}100\text{k})\text{NH}_4^+]_{\text{DN}}$, are characterized by loading-unloading cyclic extension tests and the stress-strain curves are shown in Figure 5-21.

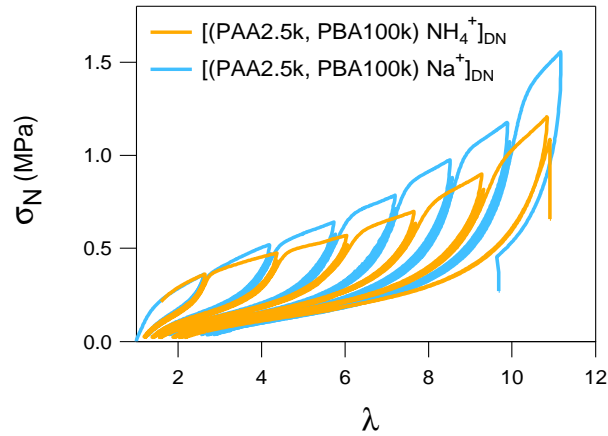


Figure 5- 21: Cyclic extension of PAA-b-PBA latex DN films with Na^+ counter ions and standard latex films

DN films of [(PAA2.5k, PBA100k) Na^+]_{DN}, show 20% higher values of stress at break and energy dissipation for equivalent levels of strain again showing some reinforcement. The stress of the latex DN films with Na^+ counter ions obviously increases along the extension and notably increases at high deformation. To improve the understanding, the dissipation of energy during the cyclic tests was analysed using the method previously presented in section 2.3. The correlated plots of hysteresis, residual deformation and initial modulus can be found in Figure 5-22 (a) and (b).

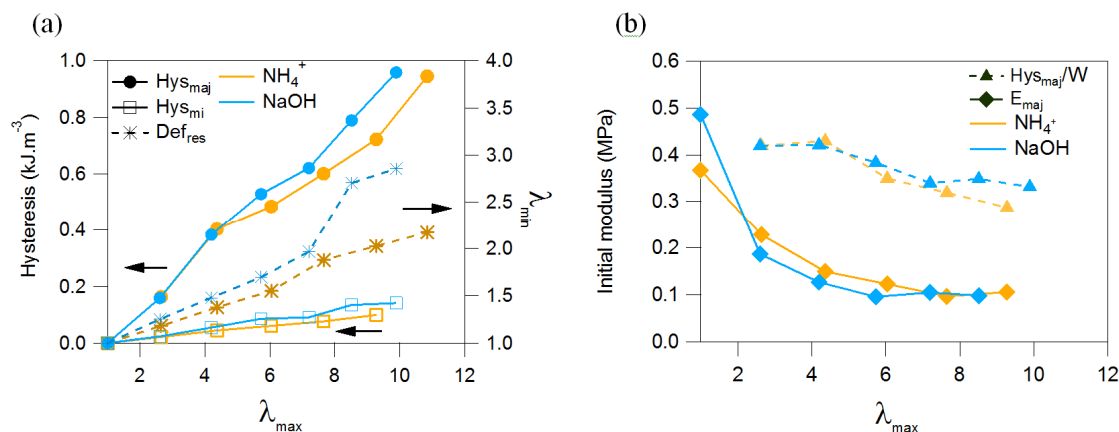


Figure 5- 22: Energy dissipation analysis of each step extension of PAA-b-PBA latex DN films with Na^+ counter ions and standard latex films

By the analysis, we found that both the damage hysteresis (Hys_{maj}) and viscoelastic hysteresis (Hys_{mi}) of the latex DN film with Na^+ counter ions are higher than the standard DN film using NH_4OH . The residual deformation (Def_{res}) of the latex DN film with Na^+ counter ions is markedly higher, especially at high deformation as the result of Def_{res} of DN film with Na^+ is ~ 2.9 while Def_{res} of DN film with NH_4OH is ~ 2.2 . All these results point to a more extended permanent damage during loading in latex DN film with Na^+ counter ions, which may be due also to the structure of the network of shells that is probably already rather discontinuous after the swelling. The softer shells of the standard latex may be less dissipative as they deform in the soft matrix and give therefore a lower level of hysteresis and a lower residual deformation, i.e. more reversible elasticity.

This same conclusion can also be inferred by the evolution of the initial modulus of the major hysteresis loop or E_{maj} , shown in Figure 5-22(b). The sharper decrease of E_{maj} in the latex DN film with Na^+ can be clearly observed in the second major loop ($\lambda > 3$), due to the breaking of PAA-shells. The much lower E_{maj} in the latex DN film with Na^+ counter ions indicates the more damage occurs in the film and is consistent also with the higher fracture energy.

3.2 PAA-b-PBA latex film with a crosslinked PBA-core

Multifunctional monomers or crosslinkers have been used to control particle morphology and the mechanical properties of the latex, synthesized by emulsion polymerization.¹⁵ It has been reported that by using a core-shell latex with a chemically crosslinked core, hardness, resistance to solvents, chemicals and detergents can be increased.^{15, 16} In our study, we explored the potential of this crosslinking technique to toughen the PAA-b-PBA latex and for that purpose two kinds of crosslinkers, BDA and DVB were used. The crosslinkers of our study are hydrophobic, therefore during the synthesis of the latex they remained with BA and crosslinked the PBA-core. The method of synthesis and latex characteristics are reported in chapter 4, section 2.4.3. The effect of crosslink type on the mechanical properties of the films will be discussed in this section.

3.2.1 Crosslinked PBA-core by BDA

1,4-Butanediol diacrylate or BDA is a linear bifunctional monomer, used as a crosslinker in various formulations.¹⁷ BDA possesses two polymerizable acryloyl groups, which are linked via a flexible chain of four carbon atoms. The structure of BDA is shown in Figure 5-23. The crosslinking with BDA is performed during the RAFT emulsion polymerization process while creating PAA-b-PBA latex. The resulting latex SN films showed a higher rigidity and lower stickiness compared to the uncrosslinked samples. The physical appearance of the films is shown in Chapter 4, section 3.1.

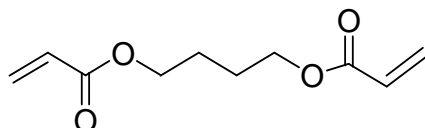


Figure 5- 23: BDA structure

In our study, the films were prepared with 3 different BDA concentrations (0.1, 0.3, 0.5 mol%). However, in order to see more easily the effect of crosslinking PBA with BDA, we show here the latex SN films and DN films of latex with 0.3% BDA compared with the standard latex film. The results for the other crosslinker concentrations can be found in Appendix A.

3.2.1-1 SN films of PAA-b-PBA crosslinked by BDA

The mechanical properties of the latex SN films of PAA-b-PBA with a PBA-core crosslinked by BDA are very different from those of the standard latex films (Figure 5-24). The BDA crosslinked films have a lower initial modulus compared with standard films and a much lower extensibility, probably due to the presence of the crosslinker which limits chain stretching.

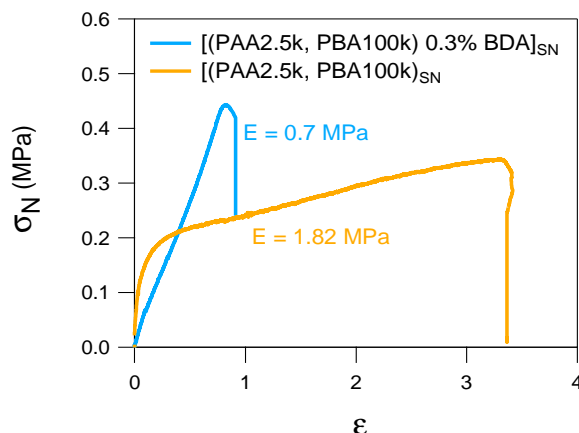
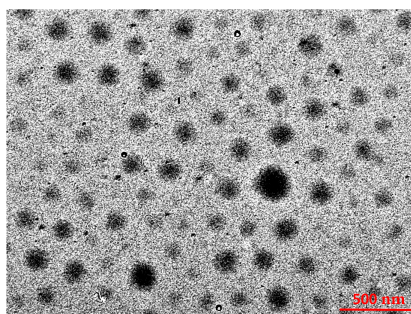


Figure 5- 24: Stress-strain curves of PAA-b-PBA latex films with a PBA-core crosslinked by 0.3% BDA, and standard PAA-b-PBA latex films

The lower initial modulus of crosslinked films ($E = 0.7$ MPa) suggests that the nanostructure of these crosslinked films is different and less well organized. TEM images (Figure 5-25) show that the latex particles are at least more rigid (they do not flatten and appear round). This may result in a less well organised structure or at least less percolating, therefore reducing the stiffness of the film.

(a) (PAA2.5, PBA100) 0.3% BDA



(b) (PAA2.5, PBA100), standard latex

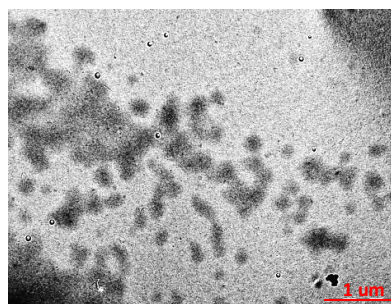


Figure 5- 25: TEM image of latex (PAA2.5 PBA100) 0.3% BDA, and standard latex (PAA2.5, PBA100)

3.2.1-2 DN films based on PAA-b-PBA crosslinked by BDA

DN films were synthesized from core-shell latex films with PBA-cores crosslinked by BDA, using the sequential interpenetrating network technique. As expected, the presence of BDA in the latex films limits the swelling of the film and as a result, Φ_{latex} is higher in the corresponding DN (Figure 5-26).

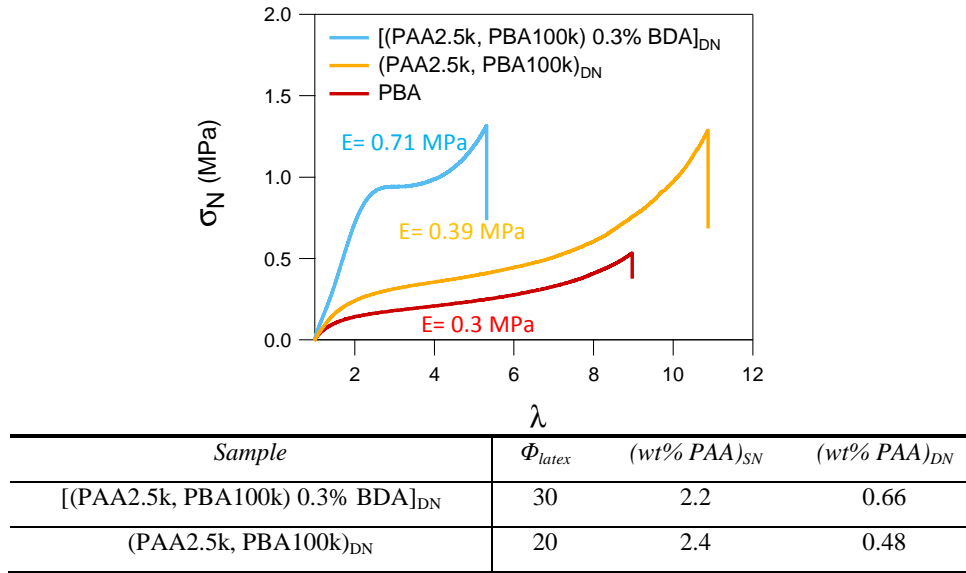


Figure 5- 26: Stress-strain curve and wt% of PAA of PAA-b-PBA latex DN film with crosslinked PBA-core by 0.3% BDA, standard PAA-b-PBA latex film, and reference film (PBA film)

The stress-strain curves of the latex DN films, carried out in uniaxial extension at room temperature show that the strain stiffening comes at a much lower extension in DN films containing BDA crosslinker (Figure 5-26). As we saw before, the initial modulus of the standard latex DN film decreases relative to its SN counterpart because of the changing nanostructure of the films occurring during swelling. However, in DN films made from latexes containing BDA crosslinker, the initial modulus does not change much relative to that of the latex precursors (Figure 5-27).

By crosslinking the PBA-core, the latexes probably form more rigid particles and therefore create a less connected network of PAA shells during the film formation process. SN films show therefore a lower initial modulus and swell less compared with standards latex SN film. The swelling of these latex SN films is limited by the chemical crosslinks introduced by the BDA, resulting in a lower swelling equilibrium. However, the nanostructure of the SN film seems unaffected by the swelling process. Finally, the DN film of latex containing BDA crosslinker shows an extensibility which is intermediate between that of the the respective SN (compare figures 5-24 and 5-26) and that of the simple PBA elastomer, while the initial modulus of DN remaining similar to that of the SN film (Figure 5-27).

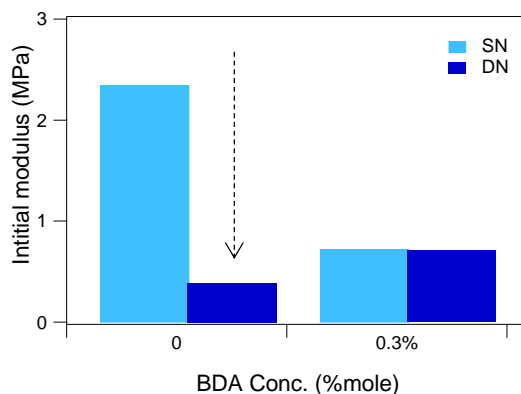


Figure 5- 27: Initial modulus of latex SN films and latex DN films of PAA-b-PBA with crosslinked PBA-core by 0.3% BDA

Fracture toughness

Results of fracture tests on DN films made from latexes of PAA-b-PBA with BDA crosslinker are shown in Figure 5-28. The fracture energies of the DN films calculated with the Greensmith approximation and the energy of notched sample are shown in Table 5-6.

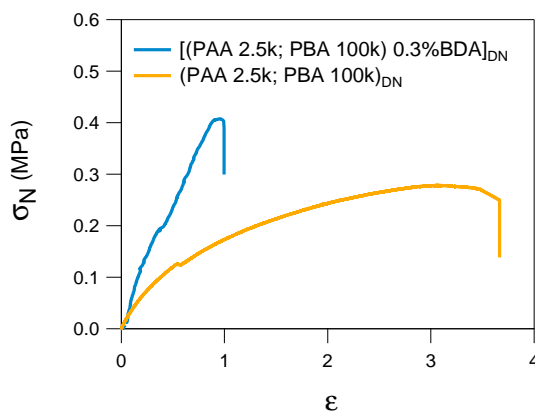


Figure 5- 28: Stress-strain curve of single-edge notch samples of DN films made from PAA-b-PBA with BDA crosslinker and from a standard PAA-b-PBA latex film

A marked decrease in fracture energy of DN with BDA crosslinker relative to that of the standard DN is observed due to the greatly reduced extensibility of the notched samples. Although, the presence of the crosslinker increases the modulus of unnotched samples and give interesting intermediate properties, the resistance to crack propagation is worse than the standard DN. This is a somewhat surprising result since the strong softening in the stress-strain curves of the unnotched sample (Figure 5-26) suggests a damage mechanism that usually also toughens the material. This suggests that once the stiff phase responsible for the high modulus is broken (after $\lambda = 2$ in Figure 5-

26) the material must retain considerable elasticity and is not able to dissipate much energy. We now check this hypothesis by performing step-cycle tests.

Sample	Γ (kJ/m ²)
(PAA2.5k, PBA100k) _{DN}	2.53 ± 0.36
[(PAA2.5k, PBA100k)0.3% BDA] _{DN}	1.50

Table 5- 6: Fracture energy of DN films made from PAA-b-PBA latex with BDA crosslinker and from the standard PAA-b-PBA latex, ^a the fracture energy determined by Greensmith approach and ^b the fracture energy determined by the area under stress-strain curve of notched sample.

Energy dissipation

The stress-strain curves during the loading-unloading step cycle extension tests for the DN containing the BDA crosslinker compared with the standard latex can be found in Figure 5-29. The DN films with BDA crosslinker shows a very significant dissipation of energy (due to irreversible damage) in the 2nd and the 3rd extension step ($\lambda_{\max} = 4.2$ and 6 respectively). In contrast, the latex DN standard film shows a consistent level of energy dissipation until the final loop ($\lambda_{\max} = 10.5$) which has a higher dissipation before breaking.

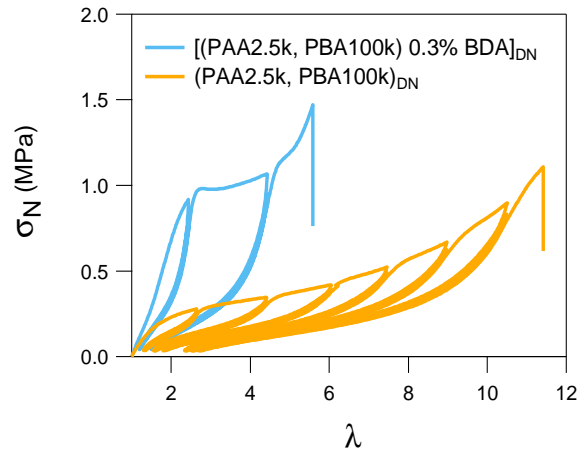


Figure 5- 29: Strain controlled loading-unloading step cycle test of PAA-b-PBA latex DN films with a crosslinked PBA-core with 0.3% added BDA, and standard PAA-b-PBA latex films

The results of the hysteresis analysis, described in section 2.3 can be found in Figure 5-30. The hysteresis of the damage loop in each step extension (Hys_{ma}) is markedly higher for the DN film with 0.3% BDA, [(PAA2.5k, PBA100k) 0.3% BDA]_{DN}, relative to the standard latex. At low deformation, the difference is small. However, the hysteresis of the major loop (Hys_{ma}) shows significant differences at high deformation. The irreversible damage of [(PAA2.5k, PBA100k) 0.3% BDA]_{DN} at

high deformation probably comes from the breakage of the BDA crosslinks and maybe some PBA polymer chains resulting in a much higher value of Hys_{ma} than that of the standard latex at $\lambda > 3$.

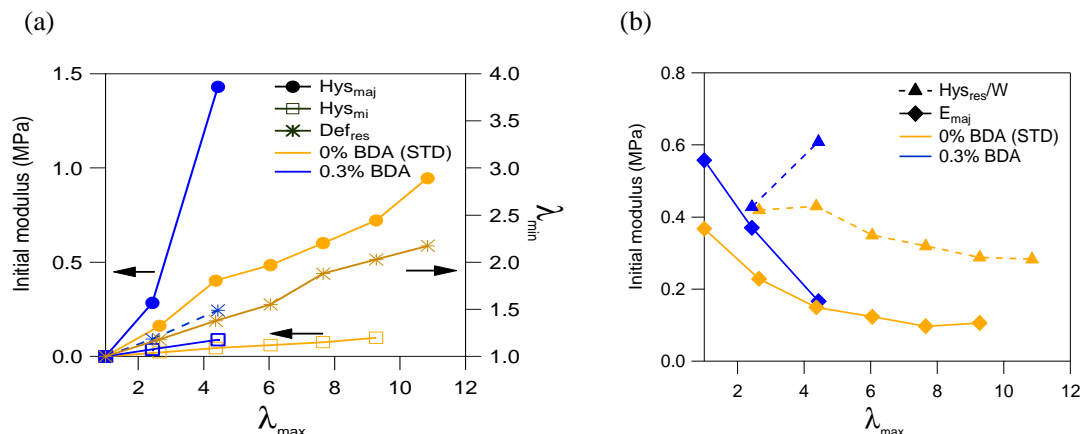


Figure 5- 30: Energy dissipation analysis of each step extension of PAA-b-PBA latex DN films with a crosslinked PBA-core with 0.3% added BDA, and standard PAA-b-PBA latex films

Interestingly, the minor loop hysteresis (Hys_{mi}) of each sample which comes from the viscoelastic dissipation of free chains and branches is barely higher for [(PAA2.5k, PBA100k) 0.3% BDA]_{DN} than for the standard DN film. This may be due to the specific structure resulting from the damage through bond breaking. The connecting network of the PAA shells breaks first and then creates more imperfection. It is interesting to note however that the residual deformation is not very high, so that these crosslinked materials damage but maintain a very good elastic recovery being in this sense more similar to chemically crosslinked filled elastomers. Despite the large dissipative damage at large strain, this reversible elasticity, combined with the low extensibility due to the presence of the chemical crosslinks may be the key factor reducing the fracture toughness of the material.

In Figure 5-30 (b), the initial modulus observed in the major extension loop is higher for the latex DN with BDA. The BDA crosslinker reinforces the initial modulus as seen in the tensile tests (Figure 5-26). The relative hysteresis (Hys_{ma}/W) does not show differences at low deformation since presumably the energy is needed there to break PAA shells, but the differences increase at high deformation where hysteresis may be due to the breaking of BDA crosslinks in the core of the particles.

3.2.2 Crosslinked PBA-core by DVB

Divinylbenzene or DVB is a versatile chemical crosslinking agent containing two reactive vinyl groups (Figure 5-31). DVB is generally used as a crosslinking agent in the polymerization of styrene and copolymers of styrene. Moreover, it can be copolymerized with various other monomers,

such as chlorostyrene, butadiene, isoprene, cyclopentadiene, methyl methacrylate, vinyl acetate and other vinyl derivatives.¹⁸

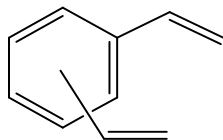


Figure 5- 31: DVB structure

DVB is more hydrophobic than BDA, and has water solubility closer to that of BA than BDA does, where the solubility in water of DVB is 0.054%, of BDA is 1.7% and of BA is 0.2%. It has been reported in other studies of crosslinked ethyl acrylate that a very different hydrophobicity of crosslinker vs monomer, causes a less uniform distribution of crosslinks within the polymer matrix.^{19,20, 21} Thus, regarding the differences in water-solubility and in reactivity ratios of BDA and DVB with BA the respective crosslinked latexes might have some differences in the crosslinking distribution, which might result in different mechanical properties of the dry films.

In our study, the effect of DVB addition was qualitatively very similar to that of adding BDA. Therefore, the mechanical characterization of latex SN and DN with different DVB loading are discussed in Appendix A.

3.3 The effect of the M_n on the PAA (shell thickness)

PAA is a homopolymer of acrylic acid which has a T_g of 106 °C in its acid form.^{4, 5} In the PAA-b-PBA copolymer latex, PAA is a soft shell swollen in water. However, after drying to create latex films the PAA transforms from a soft shell to a glassy shell and forms an imperfect network of shells through hydrogen bonds between each PAA polymeric chain. In the PAA-b-PBA latex, a variation of the M_n of PAA is also a key factor in changing the mechanical properties of the latex films.

In our study, the PAA of the latex was increased by using different sizes (M_n) of the PAA macro-RAFT agents, M_n 2.5, 3.8 and 5.8 kg.mol⁻¹. In order to study the effect of the PAA block length on the mechanical properties of the latex films, the M_n of PBA was controlled to be stable as much as possible, $M_n \sim 100$ kg.mol⁻¹. The method to synthesize PAA-b-PBA latexes with different M_n of PAA-shell and the effect of the size of the macro-RAFT agent on the polymerization process can be found in Chapter 4, section 2.41 and 2.42. In this section, the mechanical properties of the films made with different M_n of PAA or different PAA-shell thicknesses will be reported.

3.3.1 SN films of PAA-b-PBA with different M_n of the PAA

The mechanical properties of PAA-b-PBA latex films with different M_n of PAA, characterized in uniaxial extension at room temperature are presented in Figure 5-32.

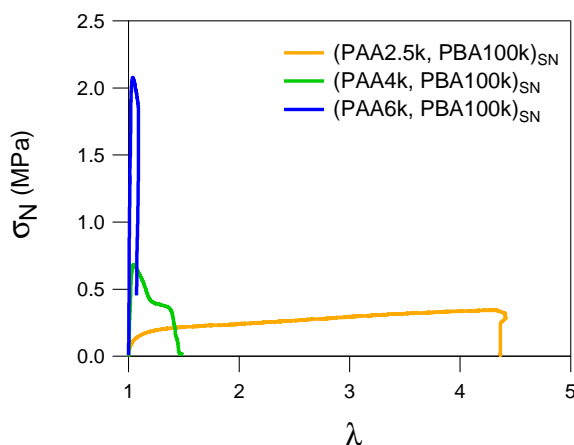


Figure 5- 32: Stress-strain curve of PAA-b-PBA latex films with different M_n of PAA

The M_n of PAA has clearly a dramatic effect on the mechanical properties of the SN film. Latex films with a thick shell (PAA 6k, PBA100k)_{SN} present a very steep slope of the stress-strain curve and after reaching the critical stress (σ_c), $\sigma_c = 2.1$ MPa, the films suddenly breaks at low strains ($\lambda < 1.2$). The extremely high initial modulus indicates a strong network of PAA shells and latex particles packed into a stiff but brittle nanostructure. Since the critical stress used to break the PAA network is very high, the PBA is not able to resist fracture once the shell network is broken. Lower M_n of PAA result in a decrease of the initial modulus and increased extensibility. However only (PAA2.5k, PBA100k)_{SN} results in a really extensible film.

3.3.2 DN films based on PAA-b-PBA with different M_n of the PAA

The mechanical properties of DN films made from latexes with different M_n of PAA (PAA4k, PBA100k)_{DN}, and (PAA2.5k, PBA100k)_{DN} were studied in uniaxial extension tests, and results are shown in Figure 5-33.

The higher M_n of PAA, (PAA4k, PBA100k)_{DN} shows a higher initial modulus and stress at break, while keeping a high extensibility. Increasing the M_n of the PAA limits the swelling ability of the latex films, resulting in a higher Φ_{latex} in (PAA4k, PBA100k)_{DN} and a much higher PAA content (wt% PAA) in DN films. The higher M_n of PAA gives rigidity to the latex SN film. However, during the fabrication of the DN, we found difficulties in using a high M_n PAA films such as (PAA6k, PBA100k)_{SN}. The films were broken during swelling in the monomer bath, and DN films could not be obtained.

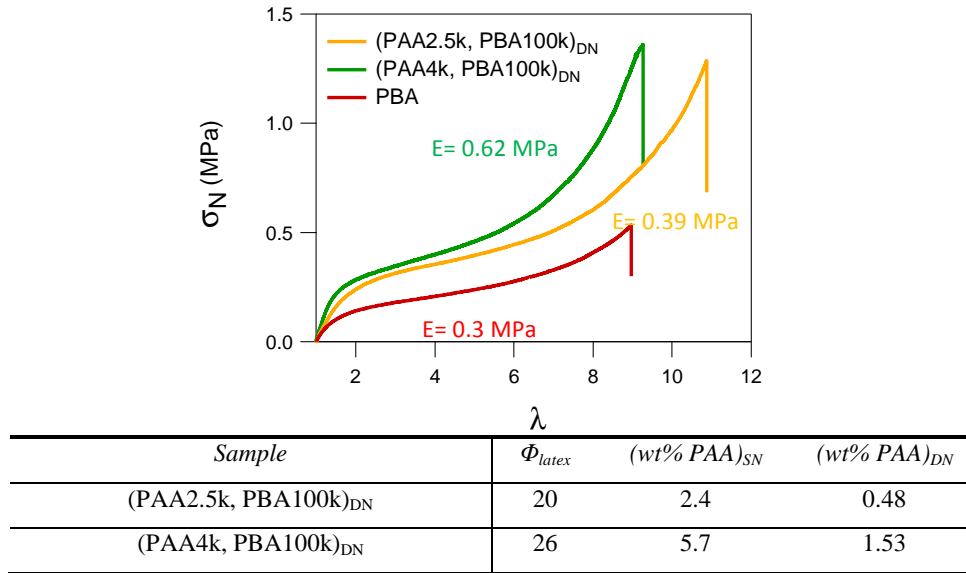


Figure 5- 33: Stress-strain curves and wt% of PAA in DN films made from PAA-b-PBA latexes with different M_n of PAA

From Figure 5-33, the (PAA4k, PBA100k)_{DN} shows a more pronounced strain stiffening around $\lambda = 6$ relative to what is observed with the standard latex that has a thinner shell. Once the shell network is broken (leading to the softening) one can imagine that the broken shells act as fillers and higher filler contents lead to an earlier strain hardening. Apparently this could be analogous to what is observed for filled elastomers.²² However one should point out that the volume fraction of PAA is here only of a few percent (< 2 wt%), while these effects are observed in filled elastomers at 15-20 vol%. It is likely therefore that the covalent link between the PAA and PBA is responsible for this strong effect of the small volume fraction of PAA in the material.

Fracture toughness

The fracture properties of the latex DN films of PAA-b-PBA with high M_n of PAA (PAA 4k, PBA 100k) and the standard latex (PAA2.5k, PBA 100k) were studied by fracture in a single edge notch test. The stress-strain curve of notched samples are shown in Figure 5-34.

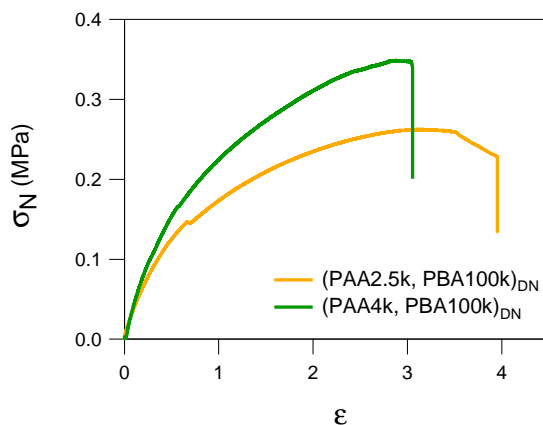


Figure 5- 34: Fracture tests of DN films made from PAA-b-PBA latexes with different M_n of PAA

For these notched samples the modulus and stress at break of the latex DN films of (PAA4k, PBA100k)_{DN} are higher but their extensibility at the point of crack propagation is lower. Hence, a slightly higher fracture toughness was found for the (PAA4k, PBA100k)_{DN} as shown in Table 5-7. Increasing the M_n of the PAA and therefore the average thickness of the shell results in an improvement in fracture resistance.

Sample	Γ (kJ/m ²)
(PAA2.5k, PBA100k) _{DN}	2.53 ± 0.36
(PAA4k, PBA100k) _{DN}	2.94 ± 0.52

Table 5- 7: Fracture energy of PAA-b-PBA latex DN films with different M_n of PAA.

Dissipation of energy

The loading- unloading cyclic extension tests are shown in Figure 5- 35. The DN film with the higher M_n of PAA, (PAA4k, PBA100k)_{DN} shows a larger major loop hysteresis. However, to be more quantitative the energy dissipation analysis was applied here.

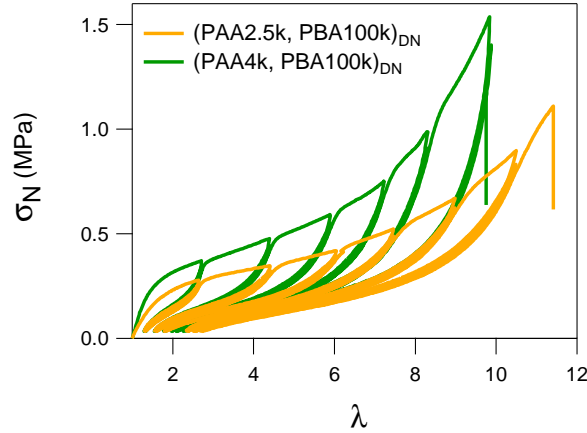


Figure 5- 35: Strain controlled loading-unloading step cycle test of PAA-b-PBA latexes with different M_n of PAA

The analysis of the hysteresis of each major loop (Hys_{ma}) and minor loop (Hys_{maj}) and the residual deformation (Def_{res}) of the film are shown in Figure 5- 36 (a). If we consider the Hys_{maj} and Def_{res} of (PAA4k, PBA100k)_{DN}, we can see that the amount of hysteresis and the residual deformation of the film are similar to that of the standard latex DN film, (PAA2.5k, PBA100k)_{DN} at low deformation where $\lambda_{max} < 8$. At higher deformation, the Hys_{maj} and Def_{res} of (PAA4k, PBA100k)_{DN} significantly increases, similar to what occurs with the strain hardening behaviour in the tensile test. It is unclear why the higher M_n of the PAA induces such a change in the strain hardening for such a small change in volume fraction of PAA but again the connectivity must here be important. Hys_{mi} of (PAA4k, PBA100k)_{DN} is also higher than that of the standard latex DN film which shows that (PAA4k, PBA100k)_{DN} creates more free chains or pendent chains. The deformation may break the PAA into small segments and increase the viscoelastic hysteresis in the minor loop.

In Figure 5- 36 (b), the change in modulus E_{maj} of (PAA4k, PBA100k)_{DN} shows a stronger initial decrease and continues then to be similar to the standard latex until failure occurs. The rapid decrease of E_{maj} in (PAA4k, PBA100k)_{DN} with increasing stretch, clearly shows the breakup of the network of PAA shells. The increase of the relative hysteresis (Hys_{maj}/W) in the first loop is then also due to the breakage of the structure of the shells.

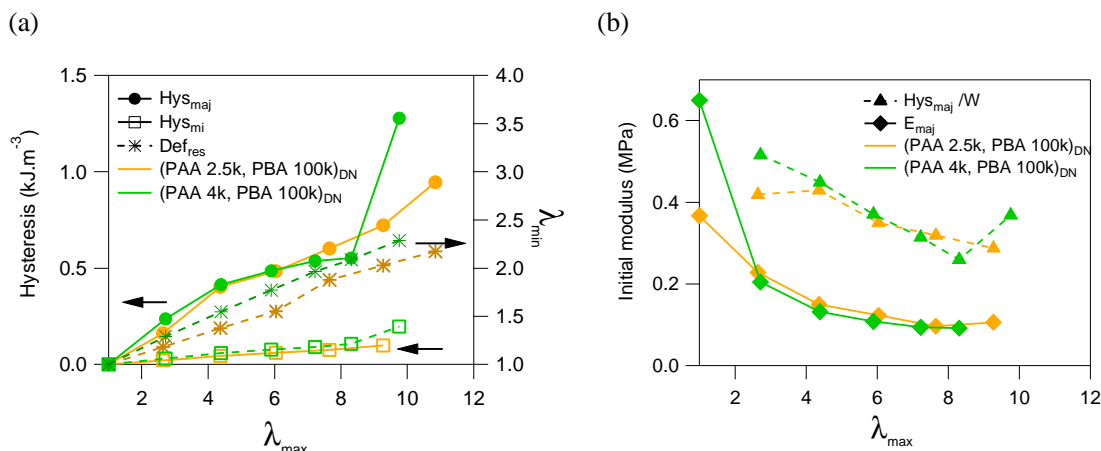


Figure 5- 36: Energy dissipation analysis of each step extension of PAA-b-PBA latexes with different M_n of PAA

In summary, the increase in shell thickness can bring some improvements in stiffness but at the expense of the reversibility of the deformation. The fracture toughness is a little bit higher in the DN film made from the latex with a higher M_n of the PAA, maybe because of the larger amount of PAA in the DN film. Moreover, it is essential to note that much larger shell thicknesses (very high M_n of PAA) result in difficulties in making the samples. As a result, we can conclude that a M_n of the PAA around 4 kg.mol^{-1} is optimum to create a percolating structure of shells that can also swell and retain their structure.

3.4 The effect of the PBA-core size on the PAA-b-PBA latex film

We were also curious to see the effect of the M_n of the PBA core on the mechanical properties of the PAA-b-PBA latex films. A PAA-macro RAFT agent, $M_n 2.5 \text{ kg.mol}^{-1}$ was synthesized to create PAA-b-PBA latexes with different M_n of PBA which were (PAA2.5k, PBA100k) or standard latex, (PAA2.5k, PBA150k) and (PAA2.5k, PBA200k). The procedure to create these latexes can be found in Chapter 4 section 2.4.

By dynamic light scattering and TEM, we found that the high M_n of the PBA increases the size of the latex particles as presented in Chapter 4, Table 4-5. Of course this expansion of the core size of the particles reduces mechanically the volume fraction of PAA.

3.4.1 SN films of PAA-b-PBA with different M_n of the PBA

The mechanical properties of the latex simple films with different M_n of the PBA were studied by the tensile test and are shown in Figure 5-37. It should be noted that in this study the M_n of the PAA is

kept constant, thus the differences in mechanical performance are due only to the effect of the M_n of the PBA.

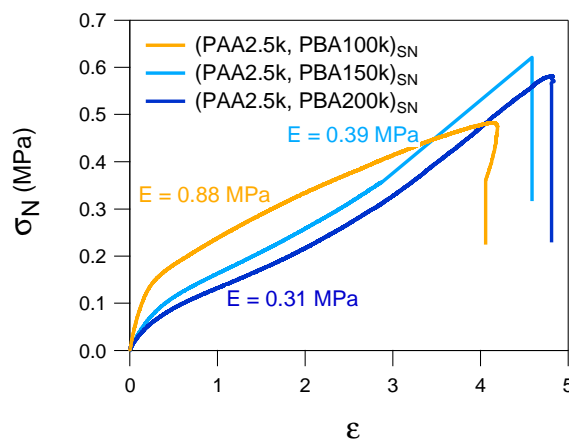


Figure 5- 37: Stress-strain curve of PAA-b-PBA latex simple films with different M_n of PBA core.

In uniaxial extension, we found that increasing the M_n of the PBA decreases the initial modulus of the film. The lower initial modulus may come from changes in the particles organization or from the lower % PAA in the composition. Moreover, in the latex synthesis of the high M_n of PBA, the polydispersity (M_w/M_n) was found to be broader which may lead to less well defined block copolymers, resulting in a less well defined core-shell structure of the particles. In addition, unsurprisingly the extensibility of the film is slightly higher in the film with higher M_n of PBA.

3.4.2 DN films based on PAA-b-PBA with different M_n of the PBA

The stress-strain curves of the latex DN films made from PAA-b-PBA with different M_n of the PBA are displayed in Figure 5-38. The latex simple film of (PAA2.5k, PBA150k)_{SN} was not selected to fabricate DN since it was not very different from (PAA2.5k, PBA200k)_{SN}.

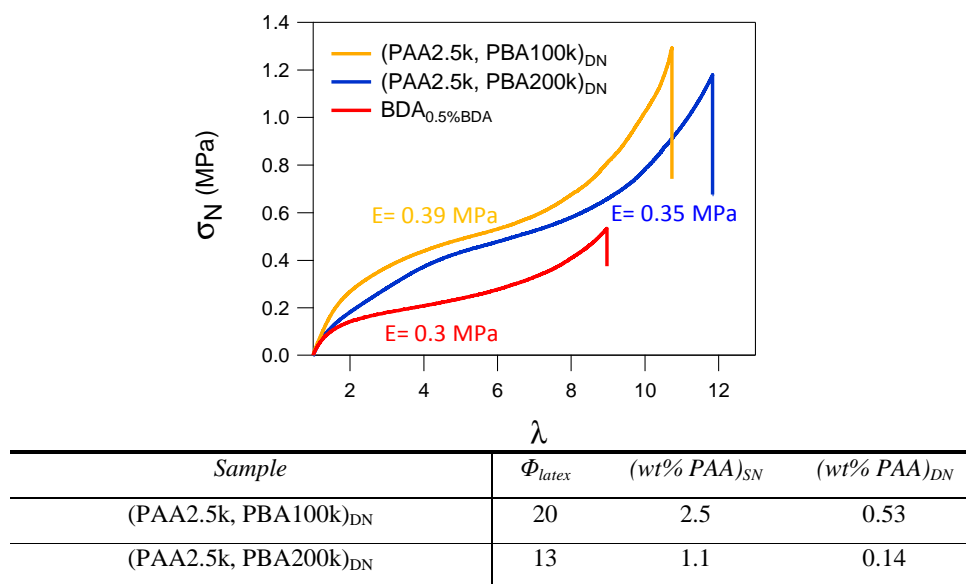


Figure 5- 38: Stress-strain curve and wt% PAA of PAA-b-PBA latex DN films with different M_n of PBA core

In Figure 5-38, we observe that the SN films containing a high M_n of PBA, (PAA2.5k, PBA200k)_{SN}, had a higher equilibrium swelling ratio and therefore a decreased value of Φ_{latex} in the DN. The high M_n of the PBA creates a larger PBA core, and a lower percentage of PAA in the film, which can swell more. After polymerization, the wt% of PAA decreases then dramatically in (PAA2.5k, PBA200k)_{DN}.

Latex DN of (PAA2.5k, PBA200k)_{DN} shows a slightly increased extensibility. However, the initial modulus, and stress at break of the film are a bit lower comparing with the standard film (PAA2.5k, PBA100k)_{DN}. It is interesting that with only 0.14 wt% of PAA, we still have a significant reinforcement relative to pure non-reinforced PBA material (red line)

Fracture toughness

The fracture toughness of the latex DN film of PAA-b-PBA with different M_n of the PBA, tested with a tensile test of notched samples, is shown in Figure 5-39. The fracture energy of the DN films was calculated with the Greensmith model. The results of fracture toughness calculation are shown in Table 5-8.

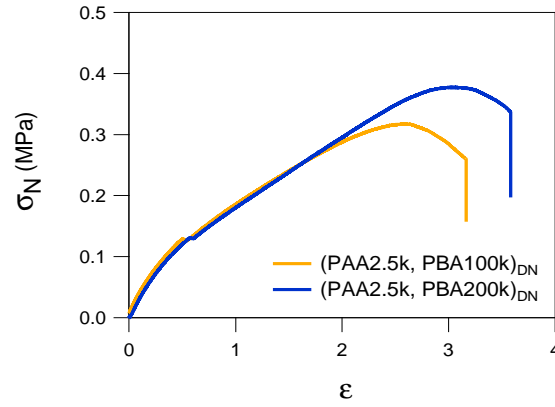


Figure 5- 39: Stress-strain curves of notched samples of PAA-b-PBA latex DN films made from SN with different M_n of PBA

The stress-strain curves of the notched samples do not show significant differences, except that the latex DN of (PAA2.5k, PBA200k)_{DN} has a slightly higher extensibility as a result of the higher M_n of PBA and PBA content. However, from the calculation with the Greensmith model, the fracture energy of (PAA2.5k, PBA200k)_{DN} is very similar to that of the standard latex DN. It can be concluded that increasing the M_n of the PBA does not increase the fracture toughness of the DN film.

Sample	Γ (kJ/m ²)
(PAA2.5k, PBA100k) _{DN}	2.53 ± 0.36
(PAA2.5k, PBA200k) _{DN}	2.47 ± 0.26

Table 5- 8: Fracture energy of PAA-b-PBA latex DN films with different M_n of PBA

Dissipation of energy

The dissipation of energy of the latex DN films was characterized with loading-unloading cyclic extension tests and is shown in Figure 5-40. We obviously see that the hysteresis loop of the latex DN with a higher M_n of PBA, (PAA2.5k, PBA200k)_{DN} is smaller than that of the standard latex DN film, (PAA2.5k, PBA100k)_{DN}. The initial modulus at the first extension loop of (PAA2.5k, PBA200k)_{DN} is clearly lower than the standard one, which is similar to the tensile test result. The extensibility of both films does not show much difference with the materials failing at $\lambda_{\max} \sim 11$. The standard DN latex, which has a higher PAA content shows a higher stress at break, $\sigma_{\text{at break}} \sim 1.2$ MPa while $\sigma_{\text{at break}}$ of (PAA2.5k, PBA200k)_{DN} is around 1 MPa.

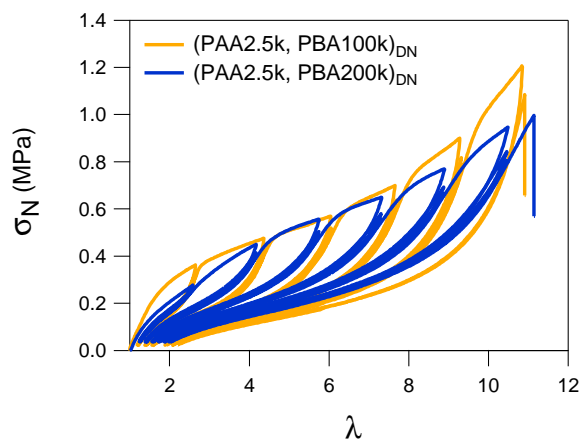


Figure 5- 40: Strain controlled loading-unloading step cycle tests of PAA-b-PBA latex DN films with different M_n of PBA

For a better understanding of the dissipation energy of the DN films, the hysteresis analysis was applied and the results are shown in Figure 5-41.

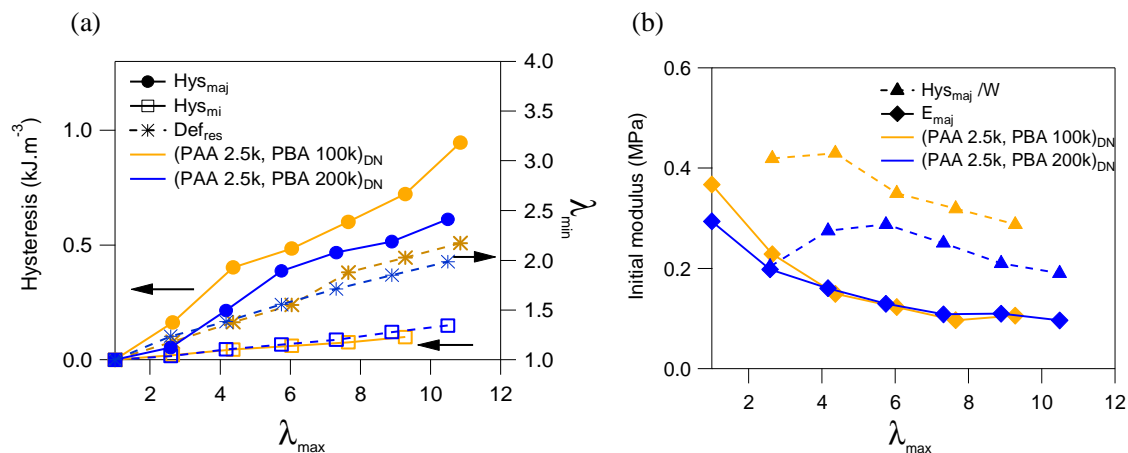


Figure 5- 41: Energy dissipation analysis of each step extension of PAA-b-PBA latex DN films with different M_n of PBA

In Figure 5-41 (a), we observe that the Hys_{maj} of the standard latex DN, (PAA2.5k, PBA100k)_{DN} is much higher than that of the latex DN films of (PAA2.5k, PBA200k)_{DN}. The higher %wt of PAA in the standard latex dissipates more energy at low deformation since it is used to break the network of the PAA shells. This difference can be seen in Figure 5-41 (b) when the initial modulus (E_{maj}) and relative hysteresis ($\text{Hys}_{\text{maj}}/W$) at $\lambda_{\text{max}} < 6$ are obviously higher for (PAA2.5k, PBA100k)_{DN}. Interestingly the increase of the M_n of PBA in the (PAA2.5k, PBA200k)_{DN} increases the value of Hys_{mi} relative to the standard latex, i.e. the material becomes more viscoelastic.

In conclusion, the increase of the M_n of PBA in the PAA-b-PBA latex increases the swelling ability of the film. However, the lower %wt of PAA in the final DN film does not inhibit the reinforcement of the DN film. The latex with a higher M_n of the PBA block, (PAA2.5k, PBA200k)_{DN} still shows good mechanical properties, a high stress at break with a good extensibility but also shows a lower level of dissipated energy through damage.

3.5 PAA-b-PBA films with added PAA_{5k}

3.5.1 Standard latex (PAA 2.5k, PBA 100k) with added PAA_{5k}

In order to increase the thickness of the PAA shells in the dry films and possibly reinforce shell interactions, we tried to add an aqueous solution of polyacrylic acid homopolymer, $M_n = 5 \text{ kg.mol}^{-1}$ (PAA_{5k}), to our PAA-b-PBA standard latex, (PAA2.5k, PBA100k). We speculated that PAA_{5k} would remain around the shell of the latex particles, i.e. in the interstices between particles in the film, resulting in a mechanical reinforcement similar to that obtained with a latex with high M_n of PAA. In our study PAA_{5k} was introduced to the latex and the final wt% of PAA was adjusted from the original, 2.5 wt% to 11 wt% which is similar to what is present in the (PAA 6k, PBA100k)_{SN}. The calculation of wt% of PAA for PAA_{5k} addition and the method of the simple film preparation have been described in Chapter 4, section 3.3. Moreover, PAA_{5k} was also introduced to the P(BA-co-BDA) crosslinked latex, but in the mechanical analysis, there were some variations between the different samples films and therefore no conclusions on mechanical properties could be drawn. Thus the results of the mechanical tests carried out with the P(BA-co-BDA) with a PAA_{5k} addition are presented in Appendix A.

3.5.1-1 SN films of PAA-b-PBA films with added PAA_{5k}

The mechanical properties in uniaxial tension of the latex SN films of (PAA 2.5k, PBA 100k) reinforced with PAA_{5k} homopolymer are shown in Figure 5-42 compared to those of the standard film.

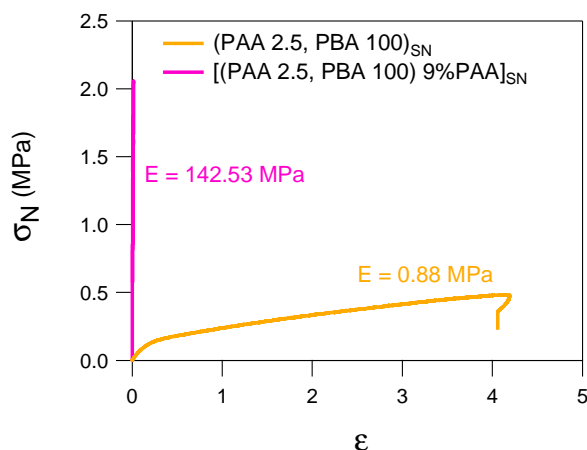


Figure 5- 42: Stress-strain curve of PAA-b-PBA latex SN films with and without added PAA_{5k} homopolymer

The addition of PAA homopolymer causes a large increase in initial modulus and stress at break, before the material breaks at very low deformation. This behaviour is very similar to what was observed for the simple latex film with high M_n of PAA or (PAA6k, PBA 100k)_{SN} in section 3.3.1. The stress at break $\sigma_{at\ break}$ of these two films: (PAA6k, PBA 100k)_{SN} and [(PAA2.5k, PBA 100k)9% PAA_{5k}]_{SN}, is similar, around 2 MPa.

3.5.1-2 DN films based on PAA-b-PBA films with added PAA_{5k}

The mechanical properties of the DN made from the latex films with 9% added PAA_{5k} homopolymer were tested in uniaxial tension, loading-unloading cyclic extension and finally its fracture toughness was measured with notched samples. The stress-strain curves of the DN films made from precursor films with and without PAA_{5k} homopolymer are shown in Figure 5-43.

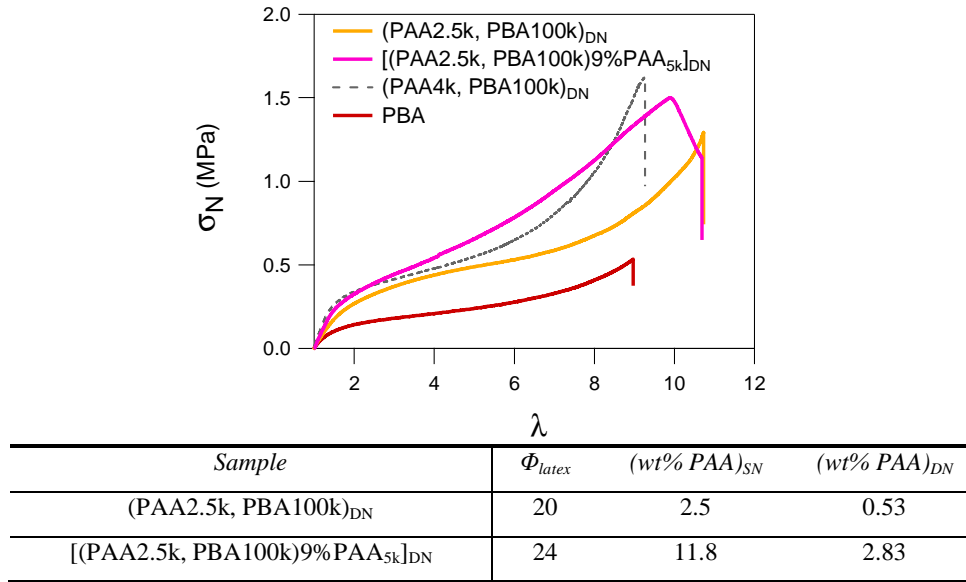


Figure 5- 43: Stress-strain curve and wt% PAA of PAA-b-PBA latex DN films with and without added PAA $_{5k}$

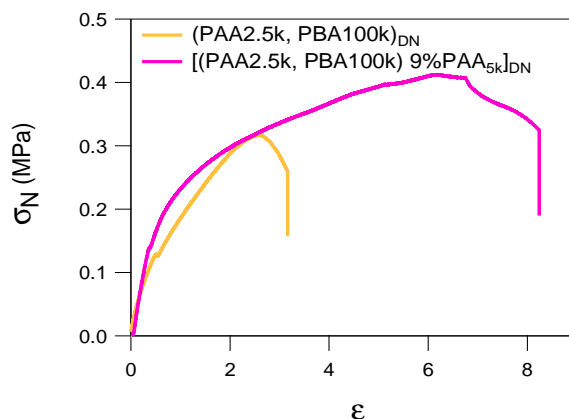
An increase of initial modulus and stress at break is clearly observed in the DN film with PAA $_{5k}$, [(PAA2.5k, PBA 100k)9% PAA $_{5k}$] $_{\text{SN}}$ relative the reference PBA film. Latex films containing PAA $_{5k}$ homopolymer swell less than the standard film. The thicker shell formed by the PAA $_{5k}$ may limit the extensibility of the particles, resulting in a much higher wt% of PAA in the DN films compared to the reference sample without PAA $_{5k}$.

If the results are compared with those obtained with the latex DN made from the high M_n of PAA block copolymer or (PAA4k, PBA 100k) $_{\text{DN}}$ (Fig. 5-43, dashed line), the DN film with added PAA $_{5k}$ shows less softening, but also much less hardening, suggesting some disruption of the percolating PAA network of particle shells.

Fracture toughness

The fracture toughness of the notched DN samples is shown in Figure 5-44. It was found that adding PAA $_{5k}$ homopolymer distinctly improves the resistance to crack propagation of the film and in particular their extensibility even in the presence of a notch. The notched sample of the DN film with PAA $_{5k}$ homopolymer shows a higher stress at break, similar to that of the DN made from a high M_n PAA4K shell latex, see Fig.5-34, but has in addition a significantly higher extensibility before the crack propagates.

Confirmed by the fracture energy calculation (Table 5-9), the fracture energy of the DN film with PAA $_{5k}$ addition, [(PAA2.5k, PBA100k) 9%PAA $_{5k}$] $_{\text{DN}}$ is much higher than for the standard latex, (PAA2.5k, PBA100k) $_{\text{DN}}$ about double calculated with the Greensmith approximation.

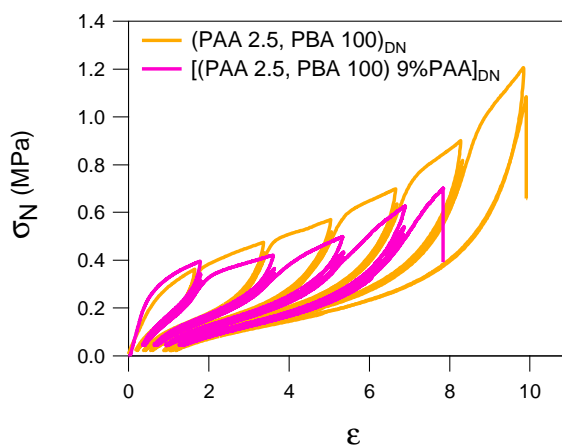
Figure 5- 44: Fracture mechanics of PAA-b-PBA latex DN films with and without PAA_{5k} addition

Sample	Γ (kJ/m ²)
(PAA2.5k, PBA100k) _{DN}	2.53 ± 0.36
[(PAA2.5k, PBA100k) 9%PAA _{5k}] _{DN}	4.56 ± 0.36

Table 5- 9: Fracture energy of PAA-b-PBA latex DN films with and without PAA_{5k} addition

Energy dissipation in cyclic loading

The dissipation of energy in cyclic loading of these DN films with added PAA_{5k}, [(PAA2.5k, PBA100k) 9%PAA_{5k}]_{DN}, is quite different from the standard latex DN film, (PAA2.5k, PBA100k)_{DN}. We observed that the hysteresis in standard latex DN films is generally greater at all extensions, than the hysteresis in the standard film as shown in Figure 5-45. However, the modulus of the latex DN film with added PAA_{5k} begins higher than that of the standard film and slightly decreases with increasing extension, until the material failed at $\lambda_{\max} > 8$.

Figure 5- 45: Strain controlled loading-unloading step cycle of PAA-b-PBA latex DN films with and without PAA_{5k} addition

Applying the analysis, described in section 2.3, sheds some additional light as shown in Figure 5-46.

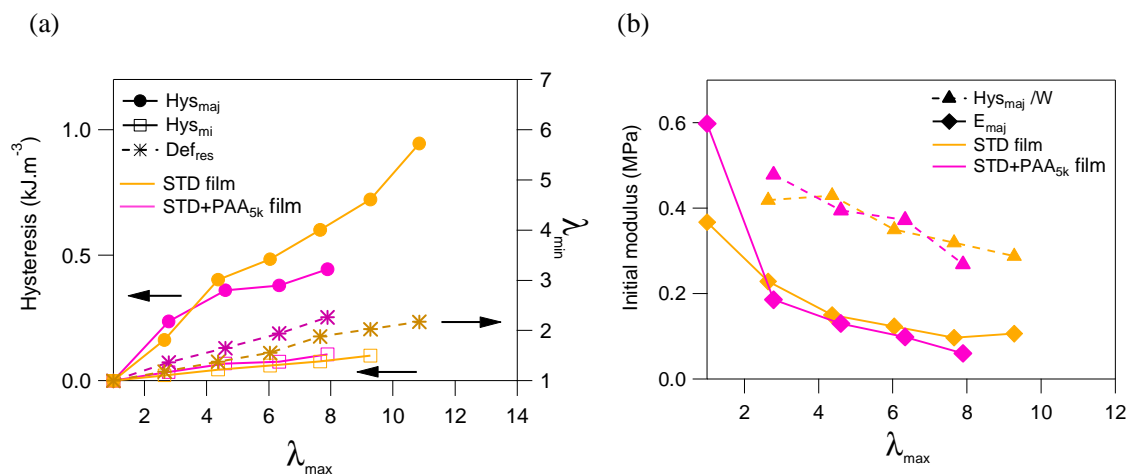


Figure 5- 46: Energy dissipation analysis of each step extension of PAA-b-PBA latex DN films with and without PAA_{5k} addition

The latex DN film with added PAA_{5k} has a higher initial modulus and relative hysteresis in the first extension loop, Figure 5- 46 (b). However, subsequent extension loops (beginning at $\lambda_{max} = 3$) show a much more pronounced decrease of the initial modulus in the DN film with added PAA_{5k} than for the standard latex. The added PAA_{5k} homopolymer makes a stiffer but more fragile network of shells. The analysis of the major hysteresis loop (Hys_{maj}), Figure 5-46 (a), shows that the Hys_{maj} of [(PAA2.5k, PBA100k) 9%PAA_{5k}]_{DN} becomes clearly lower than the standard DN film at high deformation ($\lambda_{max} > 4.5$). This behavior shows that the PAA shells with added PAA_{5k} damage at low strain and then have a more stable structure and less additional damage. This is confirmed by the analysis of the residual deformation (Def_{res}), which increases more for the DN with added PAA_{5k}. This effect is classically observed in filled elastomers when the amount of filler increases.^{23, 24}

3.5.2 High M_n PBA latex, (PAA2.5k, PBA200k) with added PAA_{5k}

We reported previously that introducing 9% of PAA_{5k} to the standard latex limited considerably the extensibility properties of the simple SN film, but increases the fracture toughness of the DN film. In order to increase the extensibility while maintaining the fracture toughness, we designed new films with added PAA_{5k} based on the latex with high M_n PBA, (PAA2.5k, PBA200k), ~1%wt PAA. To be comparable, we adjust the wt% PAA content of latex simple film to 11% relative to PBA, thus 10 % of additional PAA was introduced in the latex (PAA2.5k, PBA200k) by using PAA_{5k}.

3.5.2-1 SN film of (PAA2.5k, PBA200k) with added PAA_{5k}

The mechanical properties of the SN films of (PAA2.5k, PBA200k) with added PAA_{5k} are similar to those of the standard latex without adding PAA_{5k}, (PAA2.5k, PBA100k)_{SN}. The modulus is double at low deformation and the material breaks faster at $\varepsilon \sim 1.3$ (Figure 5-47). As observed in section 3.5.1, the addition of PAA_{5k} increases the initial modulus while drastically reducing the extensibility of the films, becoming brittle. By using a base latex with a high M_n of PBA, (PAA2.5k, PBA200k), one can reach a compromise where the modulus increases without making the materials fully brittle.

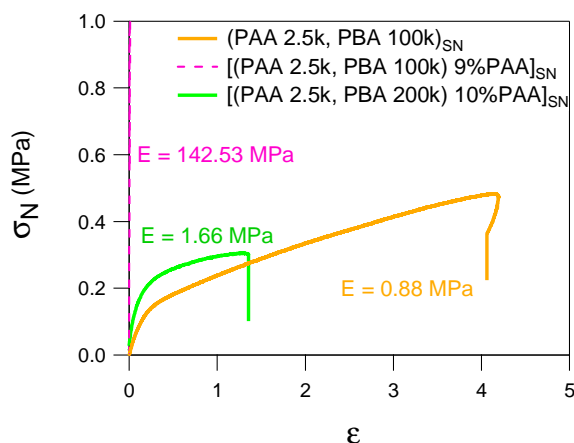
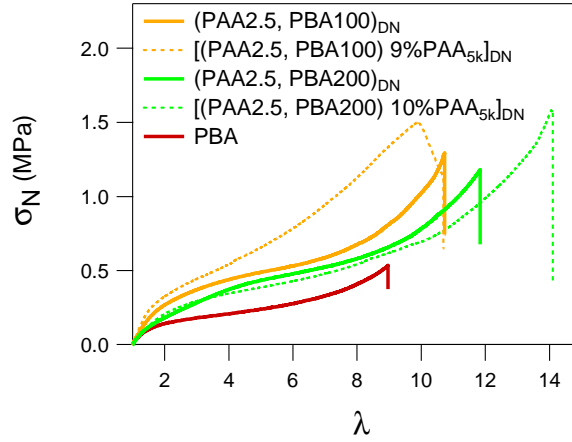


Figure 5- 47: Stress-strain curve of PAA-b-PBA latex simple films, type [(PAA2.5k, PBA100k)9%PAA_{5k}]_{SN}, [(PAA2.5k, PBA200k)10%PAA_{5k}]_{SN}, and standard latex film (PAA2.5k, PBA100k)

3.5.2-2 DN film based on (PAA2.5k, PBA200k) with added PAA_{5k}

The stress-strain curves of latex DN films made from the standard latex (PAA2.5k, PBA100k) with and without added PAA_{5k} and from the latex (PAA2.5k, PBA200k) with and without added PAA_{5k}, are shown in Figure 5-48. It should be noted that the respective PAA content of each DN films is 0.11, 0.53, 1.79 and 2.83 wt% for (PAA2.5k, PBA200k)_{DN}, standard latex (PAA2.5k, PBA100k)_{DN}, [(PAA2.5k, PBA200k)_{DN}10%PAA_{5k}]_{DN} and [(PAA2.5k, PBA100k)_{DN}9%PAA_{5k}]_{DN} respectively or %PAA; (PAA2.5k, PBA200k)_{DN} < (PAA2.5k, PBA100k)_{DN} < [(PAA2.5k, PBA200k)_{DN}10%PAA_{5k}]_{DN} < [(PAA2.5k, PBA100k)_{DN}9%PAA_{5k}]_{DN}.



Sample	Φ_{latex}	(wt% PAA) $_{\text{SN}}$	(wt% PAA) $_{\text{DN}}$	E (MPa)
(PAA2.5k, PBA100k) $_{\text{DN}}$	20	2.5	0.53	0.39
[(PAA2.5k, PBA100k)9%PAA $_{5k}$] $_{\text{DN}}$	24	11.8	2.83	0.62
(PAA2.5k, PBA200k) $_{\text{DN}}$	13	1.1	0.14	0.35
[(PAA2.5k, PBA200k)10%PAA $_{5k}$] $_{\text{DN}}$	15	11.9	1.79	0.31

Figure 5- 48: Stress-strain curve, wt% PAA and initial modulus of PAA-b-PBA latex DN films, type [(PAA2.5k, PBA100k)9%PAA $_{5k}$] $_{\text{DN}}$, [(PAA2.5k, PBA200k)10%PAA $_{5k}$] $_{\text{DN}}$, (PAA2.5k, PBA200k) $_{\text{DN}}$, and standard latex DN film

The addition of PAA $_{5k}$ in the latex (PAA2.5k, PBA200k) causes a slight decrease in its swelling ability. The (PAA2.5k, PBA200k) $_{\text{DN}}$ has a Φ_{latex} around 13% while [(PAA2.5k, PBA200k) $_{\text{DN}}$ 10%PAA $_{5k}$] $_{\text{DN}}$ swells a bit less to yield $\Phi_{\text{latex}} = 15\%$. In general, a lower PAA content in the latex DN film, results in a lower initial modulus and increased extensibility. However, it is unclear for [(PAA2.5k, PBA200k)10%PAA $_{5k}$] $_{\text{DN}}$, showing a similar initial modulus to (PAA2.5k, PBA200k) $_{\text{DN}}$ while the % PAA is much higher.

Fracture toughness

The stress-strain curves of the notched DN films with and without added PAA $_{5k}$ are shown in Figure 5-49.

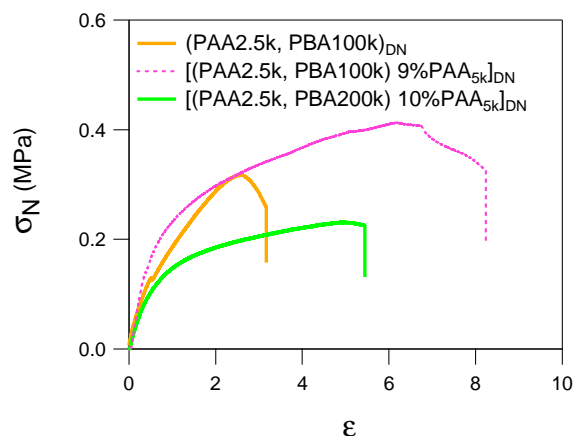


Figure 5- 49: Stress-strain curves of notched samples of PAA-b-PBA latex DN films, type [(PAA2.5k, PBA100k)9%PAA_{5k}]_{DN}, [(PAA2.5k, PBA200k)10%PAA_{5k}]_{DN}, and standard latex DN film.

The DN film made from the (PAA2.5k, PBA200k) with 10%PAA_{5k} has a lower fracture toughness than its lower molar mass counterpart. Compared to [(PAA2.5k, PBA100k)9%PAA_{5k}]_{DN} (pink dashed line), the fracture energy of [(PAA2.5k, PBA200k)10%PAA_{5k}]_{DN} is much lower, about 60% less than [(PAA2.5k, PBA100k)9%PAA_{5k}]_{DN} (Table 5-10). The reason may be the higher swelling degree of the SN films decreasing hence the wt% PAA content, resulting in insufficient hard phase to prevent crack propagation.

Sample	Γ (kJ/m ²)
(PAA2.5k, PBA100k) _{DN}	2.53 ± 0.36
[(PAA2.5k, PBA100k)9%PAA _{5k}] _{DN}	4.56 ± 0.36
[(PAA2.5k, PBA200k)10%PAA _{5k}] _{DN}	1.94 ± 0.34

Table 5- 10: Fracture energy of PAA-b-PBA latex DN films, type [(PAA2.5k, PBA100k)9%PAA_{5k}]_{DN}, [(PAA2.5k, PBA200k)10%PAA_{5k}]_{DN}, and standard latex DN film

Energy dissipation in cyclic extension

The energy dissipation behaviours of the standard latex DN with and without PAA_{5k} addition have been presented in the last section (Figure 5-45). Here, we compare the effect of the M_n of the PBA at equivalent PAA_{5k} content. Two samples [(PAA2.5k, PBA100k) 9%PAA_{5k}]_{DN} and [(PAA2.5k, PBA200k) 10%PAA_{5k}]_{DN} are compared in loading-unloading cyclic extension and results are shown in Figure 5-50

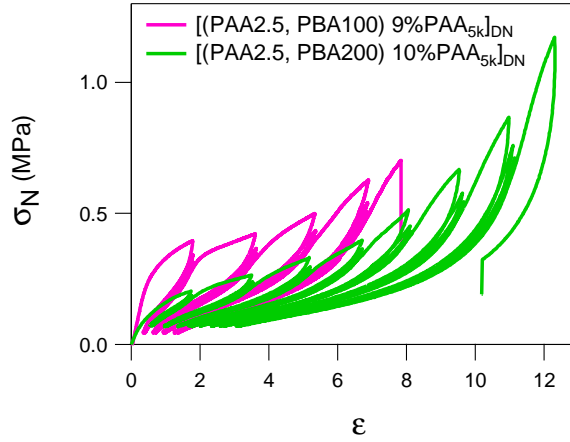


Figure 5- 50 : Strain controlled loading-unloading step cycle tests of PAA-b-PBA latex DN films
 $[(PAA2.5k, PBA100k) 9\%PAA_{5k}]_{DN}$, $[(PAA2.5k, PBA200k) 10\%PAA_{5k}]_{DN}$

In the latex $[(PAA2.5k, PBA200k) 9\%PAA_{5k}]_{DN}$ (Figure 5-50 green line) the lower hysteresis (area of each hysteresis loop) along the deformation axis does not appear clearly as in $[(PAA2.5k, PBA100k) 9\%PAA_{5k}]_{DN}$ (Figure 5-50 pink line). In contrast, the 1st loop hysteresis of $[(PAA2.5k, PBA200k) 10\%PAA_{5k}]_{DN}$ is obviously lower than other further loops. The quantitative hysteresis analysis was applied and the results are plotted as a function of λ_{max} and presented in Figure 5-51.

Interestingly, the major loop hysteresis (Hys_{maj}) of $[(PAA2.5k, PBA200k) 10\%PAA_{5k}]_{DN}$ is significantly lower than that of the $[(PAA2.5k, PBA100k) 9\%PAA_{5k}]_{DN}$, for each incremental extension loop (Figure 5-51 (a)). Presumably the lower PAA content and the high M_n of PBA is responsible for that difference which was already found in section 3.4.2, Figure 5-41. This lower hysteresis (i.e. lower damage) however, results also (and unexpectedly) in an increase in the residual deformation (Def_{res}) which is also a sign of higher damage of the film. In the stabilized cycle (Hys_{mi}) however, the dissipated energy is higher for $[(PAA2.5k, PBA100k) 9\%PAA_{5k}]_{DN}$.

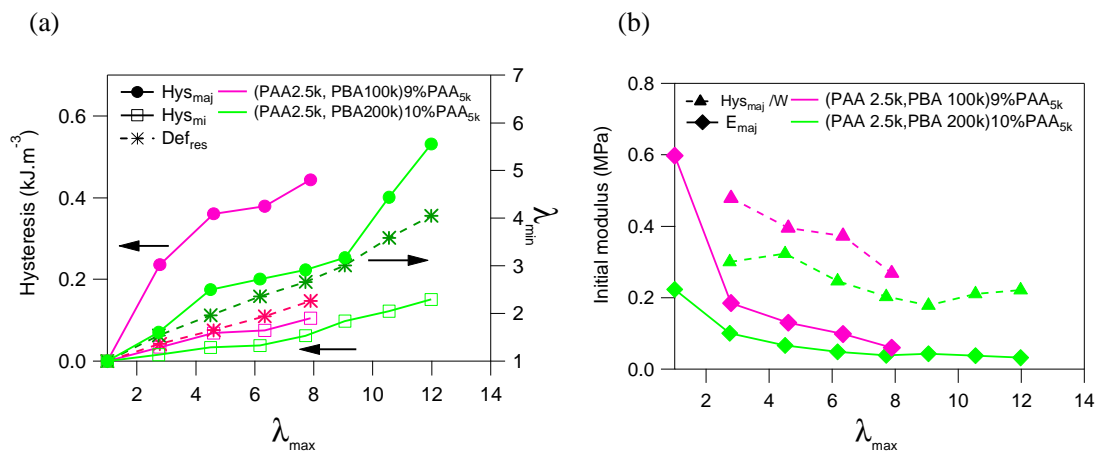


Figure 5- 51: Energy dissipation analysis of each step extension of PAA-b-PBA latex DN films, type [(PAA2.5k, PBA100k)9%PAA_{5k}]_{DN}, [(PAA2.5k, PBA200k)10%PAA_{5k}]_{DN}, and standard latex DN film

In Figure 5-51 (b) the distinct decrease in relative hysteresis (Hys_{maj}/W) and initial modulus of major loop (E_{maj}) can be observed in [(PAA2.5k, PBA200k)10%PAA_{5k}]_{DN}, but they are less drastic than for the [(PAA2.5k, PBA100k)9%PAA_{5k}]_{DN}.

Part II:

**Summary and discussion of the mechanical properties of the
different SN and DN films**

1. Method of data analysis

In this part, we summarize and compare the main structural and mechanical properties of the different DN films. First, the structure of the films due to the process of swelling with PAA and polymerization will be discussed. Since we did not characterize the structure of the D_n by microscopy or scattering we can only compare the volume fraction of latex (Φ_{latex}) and the PAA content in the DN films. These properties were calculated and presented for each material in Chapter 4. Then, the main mechanical properties of the films, which are tested by tensile tests, loading-unloading step cycle extension and a single notched fracture test, presented in details in Part I are compared and discussed. The main mechanical characteristics of the film are:

- i) The initial modulus of the latex film
We report the initial modulus of latex DN film and the differential in initial modulus between the latex SN and the DN film (ΔE). This indicator helps us to understand the changes occurring in the films nanostructure after making the DN film where an increase of ΔE means that the particles are less organized after passing through the swelling process.
- ii) The stress and elongation at break
Stress and elongation at break can be determined from uniaxial extension. Stress at break shows the strength of the film while the elongation at break gives us the extensibility of the film.
- iii) Breaking energy
Breaking energy can be defined as the area under the stress-strain curve, obtained from uniaxial extension. Breaking energy provides the toughness of the DN films.
- iv) Fracture energy
Thanks to the fracture test on notched sample, the fracture energy can be calculated by the Greensmith approach. However, it should be noted that in our study, the strain energy density is calculated from the integral of the area under the stress-strain curve of the notched sample before crack propagation.
- v) Dissipation of energy in cyclic extension
The dissipation of energy can be quantified through loading-unloading step cycle extension tests; we analyze the hysteresis and residual deformation by measuring the energy dissipated in each hysteresis loop. The hysteresis of the major (1st) loop, minor (2nd to the same extension) loop and the residual deformation at each λ_{max} are plotted and the slope of the curve was calculated by linear regression (dashed line), as shown in Figure 5-52. The higher the slope is the more changes occur in the data series. This slope

valuation will be used to compare hysteresis amount between each latex modification system.

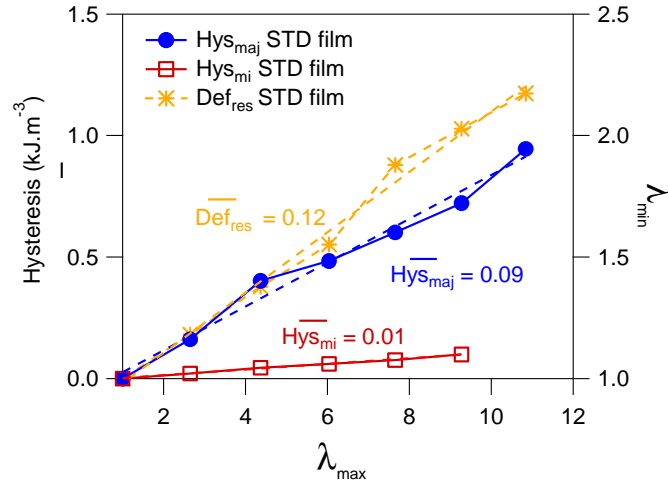


Figure 5- 52: Energy dissipation analysis of each step extension and their fit curve with linear regression (in dashed line).

As explained above, the main physical and mechanical properties of each latex DN modification can be found in Table 5-11.

We will now present a series of figures aimed at comparing these different properties. The question of which should be the governing parameter came up and I decide to plot the data as a function of the volume fraction of PAA in the DN. It is in fact remarkable that such large differences are seen relative to the PBA simple elastomer, with such small weight fractions of glassy PAA.

Sample	Latex (batch)	Symbol	Φ_{latex} (%) ^(a)	%PAA (DN)	Initial modulus (E)		σ at break (MPa)	ε at break	$W_{\text{Break}}^{(d)}$ (kJ/m ³)	Γ (kJ/m ²)	Hysteresis analysis		
					$E_{\text{DN}}^{(b)}$	$\Delta E^{(c)}$					$\overline{Hys}_{ma}^{(g)}$	$\overline{Hys}_{mi}^{(h)}$	$\overline{Def}_{res}^{(i)}$
PBA network (section 1)													
PBA 0.01%BDA	-	PBA	0	0.00	0.3 ^(j)	-	0.53	8.0	2.04	-	-	-	-
P(BA-co-BDA) crosslinked latex films (section 2.1)													
(latex _{noshell}) _{DN}	TLL01	PBA _{no-shell}	18	0.00	0.43	0.04	1.09	2.2	1.02	0.63 ± 0.04	-	-	-
PAA-b-PBA standard latex films (section 2.2)													
(PAA2.5k, PBA100k) _{DN}	TL08	standard	20	0.48	0.36	-2.29	1.29	9.9	7.61	2.52 ± 0.15	0.056	0.019	0.190
(PAA2.5k, PBA100k) _{DN}	TL85	standard	21	0.53	0.39	-0.49	1.29	9.7	5.52	2.33 ± 0.35	0.087	0.011	0.126
PAA-b-PBA latex film with crosslinked PAA-Shell (section 3.1)													
[(PAA2.5k, PBA100k) 0.2eq PADAME] _{DN}	TL103	+0.2PADAME	26	0.62	0.49	-10.67	1.33	10.7	6.64	3.45 ± 0.62	0.062	0.016	0.092
[(PAA2.5k, PBA100k) 0.65eq PADAME] _{DN}	TL103	+PADAME	25	0.60	0.41	-33.76	1.18	10.6	6.12	3.16 ± 0.15	0.101	0.017	0.124
[(PAA2.5k, PBA100k)Na+] _{DN}	TL106	Na+	22	0.55	0.48	-10.86	1.46	10.7	7.09	3.38 ± 0.08	0.105	0.016	0.234
PAA-b-PBA latex film with crosslinked PBA-core (section 3.2)													
(PAA2.5k, PBA100k)0.1%BDA] _{DN}	TL41	BDA0.1%	23	0.51	0.50	0.07	1.31	6.4	5.21	1.93 ± 0.05	0.269	0.022	0.128
[(PAA2.5k, PBA100k)0.3%BDA] _{DN}	TL43	BDA0.3%	30	0.66	0.71	-0.01	1.29	4.3	3.60	1.50	0.573	0.026	0.153
[(PAA2.5k, PBA100k)0.5%BDA] _{DN}	TL59	BDA0.5%	37	0.93	1.47	0.11	1.01	1.1	0.78	1.07	-	-	-
[(PAA2.5k, PBA100k)0.1%DVB] _{DN}	TL95	DVB0.1%	24	0.55	0.43	-0.05	1.75	11.0	7.61	3.10 ± 0.01	0.061	0.017	0.202
[(PAA2.5k, PBA100k)0.3%DVB] _{DN}	TL90	DVB0.3%	26	0.62	0.56	0.05	1.40	8.4	5.49	3.2 ± 0.76	0.074	0.021	0.185
[(PAA2.5k, PBA100k)0.5%DVB] _{DN}	TL91	DVB0.5%	32	0.70	0.75	0.07	0.96	5.8	3.50	1.86 ± 0.26	0.070	0.027	0.111
PAA-b-PBA latex with different PAA-shell thickness (section 3.3)													
(PAA4k, PBA100k) _{DN}	TL23	+M _n PAA	26	1.53	0.62	-26.27	1.36	8.3	4.58	2.94 ± 0.52	0.117	0.020	0.141
PAA-b-PBA latex with different PBA-core size (section 3.4)													
(PAA2.5k, PBA200k) _{DN}	TL104	+M _n PBA	13	0.14	0.35	0.03	1.18	10.8	5.68	2.47 ± 0.26	0.068	0.017	0.096
PAA-b-PBA latex with different PBA-core size (section 3.5)													
[(PAA2.5k, PBA100k)9%PAA _{5k}] _{DN}	TL85	(+PAA _{5k}) _S	24	2.83	0.62	-141.91	1.50	9.69	7.84	4.56 ± 0.36	0.1758	0.0378	0.0129
[(PAA2.5k, PBA200k)10%PAA _{5k}] _{DN}	TL104	(+PAA _{5k}) _L	15	1.79	0.31	-1.35	1.58	13.10	7.91	1.94 ± 0.34	0.044	0.149	0.267
[(latex _{noshell})11% PAA _{5k}] _{DN}	TLL01	(+PAA _{5k}) _{no-shell}	22	2.42	0.38	-1.35	0.63	6.63	2.13	1.02 ± 0.05	0.0398	0.013	0.0817

Table 5- 11: the summary of main physical and mechanical properties of latex DN film with different reinforcement method, ^a the volume fraction of latex particle in DN film calculated by $\Phi_{\text{latex}} = \frac{W_0[L]}{W_D[DN]}$, ^b initial modulus of latex DN film, ^c the differential initial modulus between latex SN and DN film calculated by $E_{\text{DN}} - E_{\text{SN}}$, ^d energy at break of latex DN films determined by the area under the stress-strain curve of uniaxial extension, ^e fracture energy determined by Green smith approach, ^f breaking energy of notched sample of latex DN films, ^g slope evaluation of major hysteresis, ^h slope evaluation of minor hysteresis, ⁱ slope evaluation of residual deformation or permanent set, and ^j initial modulus of PBA network

2. Swelling equilibrium of modified latex films

As discussed in the previous part, modified latexes show an effect on the swelling equilibrium of the films, resulting in different volume fractions of latex (ϕ_{latex}) in the DN films. As a preliminary remark, it is interesting to note that despite the fact that no crosslinking agent is used in most of the latexes they still are not soluble. This was noted by Chenal et al^{3, 13, 25} and implies that the PAA shells may form a percolating structure strong enough to resist the osmotic pressure.

Figure 5-53, shows that the volume fraction of latex (ϕ_{latex}) in the DN changes with the M_n of PBA. For higher M_n of the PBA (+ M_n PBA) ϕ_{latex} decreases. Moreover, the introduction of chemical crosslinks, (BDA0.3%, DVB0.3%) clearly impacts the swelling equilibrium of the SN latex film, as the films are less flexible, thus they cannot deform as much during the swelling process. Moreover, the addition of PAA_{5k} to the latex films; (+PAA)_s, (+PAA)_L, (+PAA)_{no-shell} also clearly impacts ϕ_{latex} . PAA_{5k} may also increase the interactions between particle shells and limit the swelling behavior of the material.

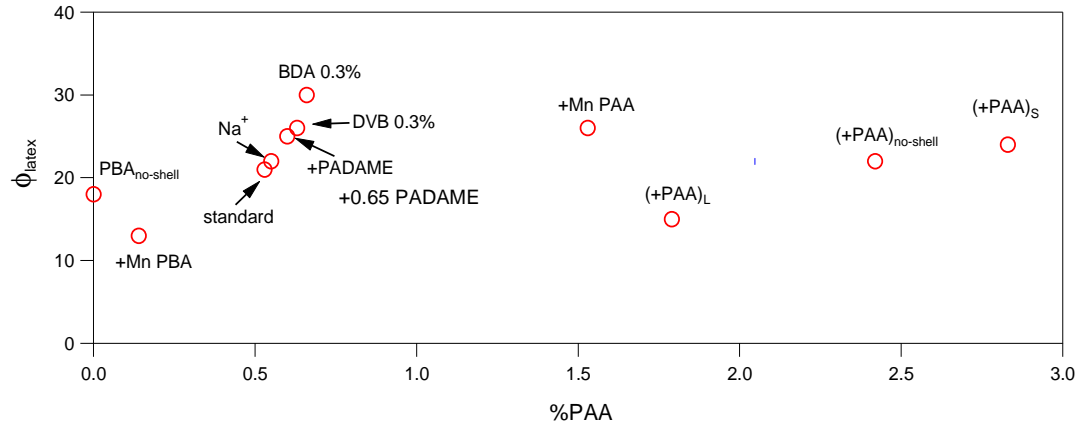


Figure 5- 53: Volume fraction of latex in the different type of DN films, acronyms are defined in Table 5-11

3. Toughness of the DN films

The toughness of the latex films before and after creating the interpenetrated network was discussed in part I. The toughness of the DN films is in absolute terms rather high (several kJ/m²) while retaining a reasonably elastic behavior, which was the initial objective of the study, however the modifications of the latexes do not have a major impact on the fracture toughness of the DN films and it is unclear which kind of latex modification gives the best toughness to the DN film.

First, we considered the initial modulus of the film, which is sensitive to the nanostructure of the film. Figure 5-54 shows that the initial modulus of the latex DN films increases in the DN films containing ether chemical crosslinks, (BDA0.3% and DVB0.3%) or physical crosslinks, (+PADAME and Na⁺), higher M_n of PAA (+M_nPAA), and PAA_{5k} addition [(+PAA)_s, (+PAA)_{no-shell}] comparing with the standard latex. In contrast, the initial moduli of the DN films decrease for the high M_n of PBA film [(+M_nPBA), (+PAA)_L].

The unfilled green dots in Figure 5-54 represent the difference of initial modulus between latex DN and latex SN (ΔE). This value reflects the change of nanostructure in the DN film when ΔE is lower than zero meaning that the structure of the film is being destroyed. It is observed that the nanostructure of the film dramatically changes in the standard latex with PAA_{5k} addition or (+PAA)_s, when ΔE is about -142 MPa, following by the latex with the PADAME addition or (+PADAME) and the high M_n PAA film (+M_nPAA), which ΔE are about -34 MPa and -27 MPa respectively. For other latex films the ΔE does not change much which is around 0 to -2 MPa.

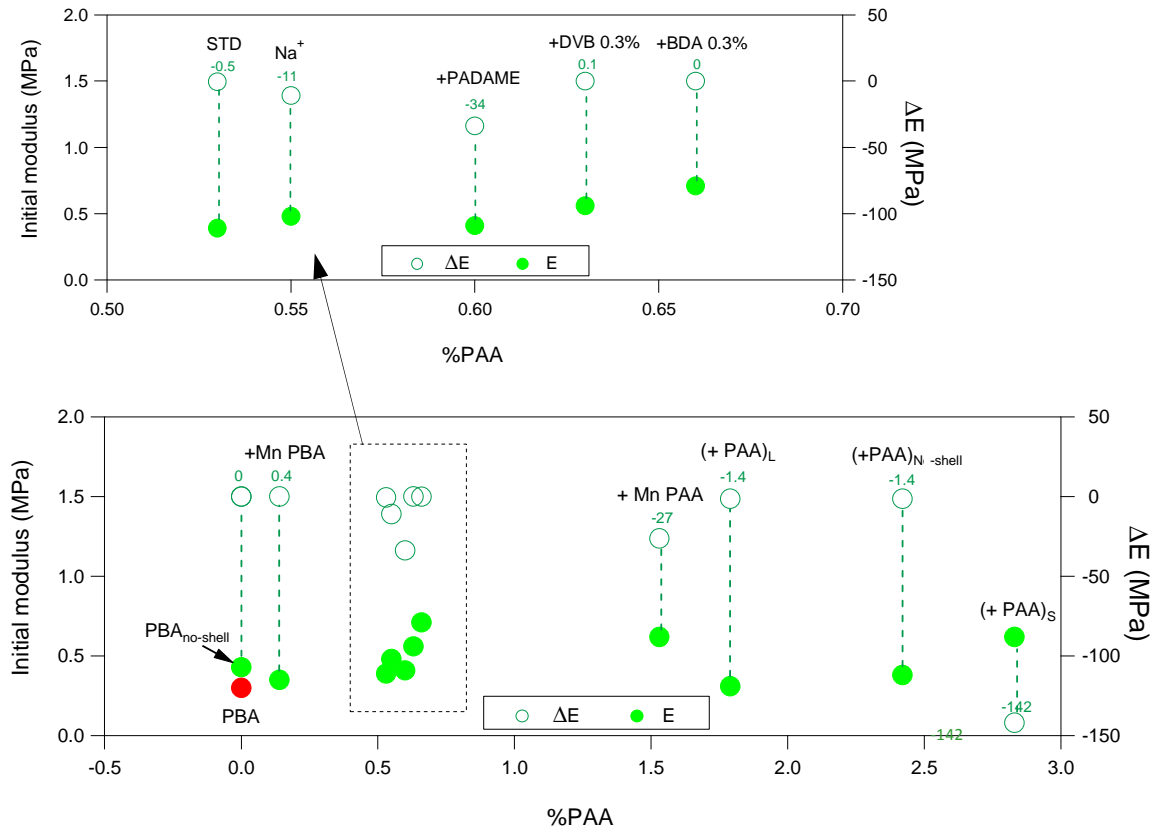


Figure 5- 54: Initial modulus (E) and the differential of initial modulus between latex DN and latex SN (ΔE) of latex DN films, where green dash lines are a guide line for eyes, and acronyms are defined in Table 5-11

Second, the modifications in toughness of the latex DN film can be compared by the stress (σ) and strain (ϵ) at break, and the breaking energy (W_{Break}) which is the integral under the stress-strain curve until failure as shown in Figure 5-55. The highest stress at break is found for the latex DN with PAA_{sk} addition [(+PAA)_S, (+PAA)_L], which is about 1.5-1.58 MPa followed by the DN with Na⁺ (Na⁺) and DN with 0.3 %DVB (DVB 0.3%), which are respectively 1.46 and 1.4 MPa. The latex DN showing the highest strain (ϵ) at break are latex DN with increasing M_n of PBA (+ M_n PBA), and the latex DN with PAA shell-interaction (+PADAME and Na⁺). The ϵ at break is about 10.6-13.1.

As a result the highest true stress at break values ($\sigma_T = \sigma_N \cdot \lambda$) for these highly extensible materials are of the order of 20 MPa a very respectable value for acrylic elastomers without any mineral fillers and a factor of four higher than the value for the simple PBA elastomer (red dot) which is highly viscoelastic.

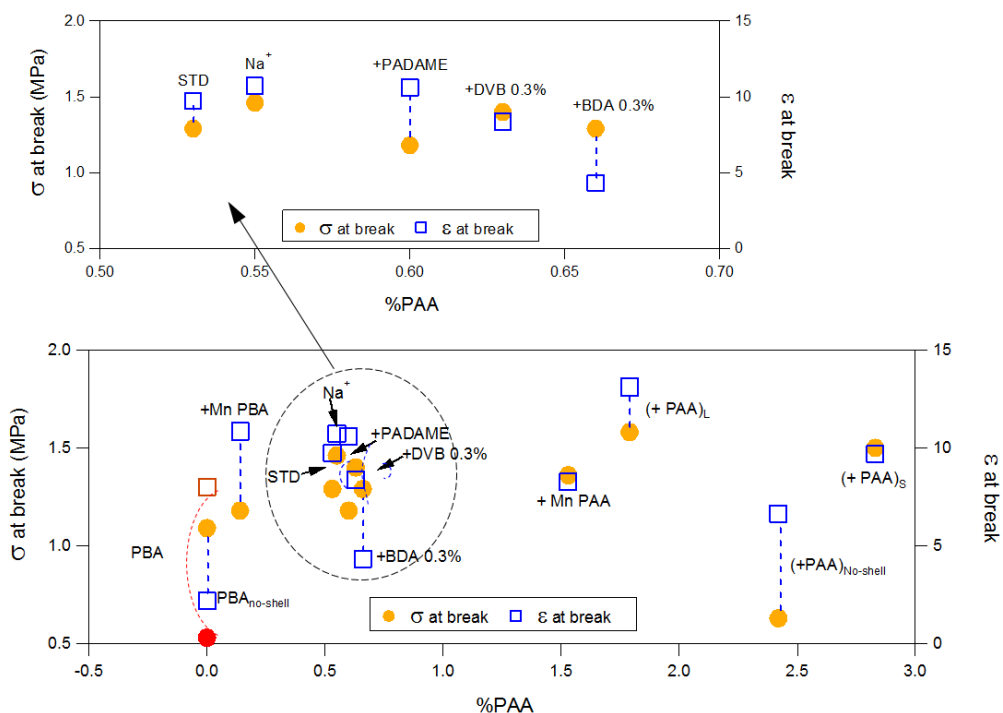


Figure 5- 55: Stress (σ) and strain (ϵ) at break of latex DN films, where green dash lines are a guide line for eyes, and acronyms are defined in in Table 5-11

Finally, the breaking energy of the films determined by the integration of the area under stress-strain curve can represent well the toughness of unnotched latex DN films (Figure 5-56). The results can be summarized as follows: The DN where PAA_{5k} was added to the latex with high M_n PBA or $(+PAA)_L$ shows the highest breaking energy. This latex has both a high breaking stress and strain due to the distinct strain hardening in the material. Increasing the thickness of the PAA-shell by adding PAA_{5k} in the standard latex or $(+PAA)_S$ results in a similar increase in breaking energy. However, this comes at the expense of a larger amount of PAA which will cause water whitening and sensitivity. It is however quite remarkable that with the reinforcement with Na^+ and almost equivalents stress and strain at break can be obtained with only 0.5% of introduced hard phase.

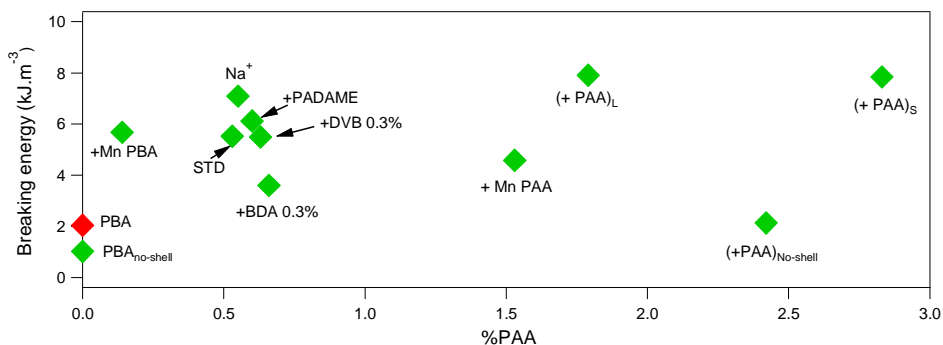


Figure 5- 56: Breaking energy (w_{Break}) calculated by the area under stress-strain curve of latex DN films, acronyms are defined in Table 5-11

4. Energy dissipation in DN films

The energy dissipation analysis is done as described in Figure 5-52, i.e. the level of cumulative hysteresis is plotted as a function of the applied lambda of the major hysteresis loop (Hys_{maj}), the minor hysteresis loop (Hys_{mi}) and the residual deformation (Def_{res}) are summarized in Figure 5-57.

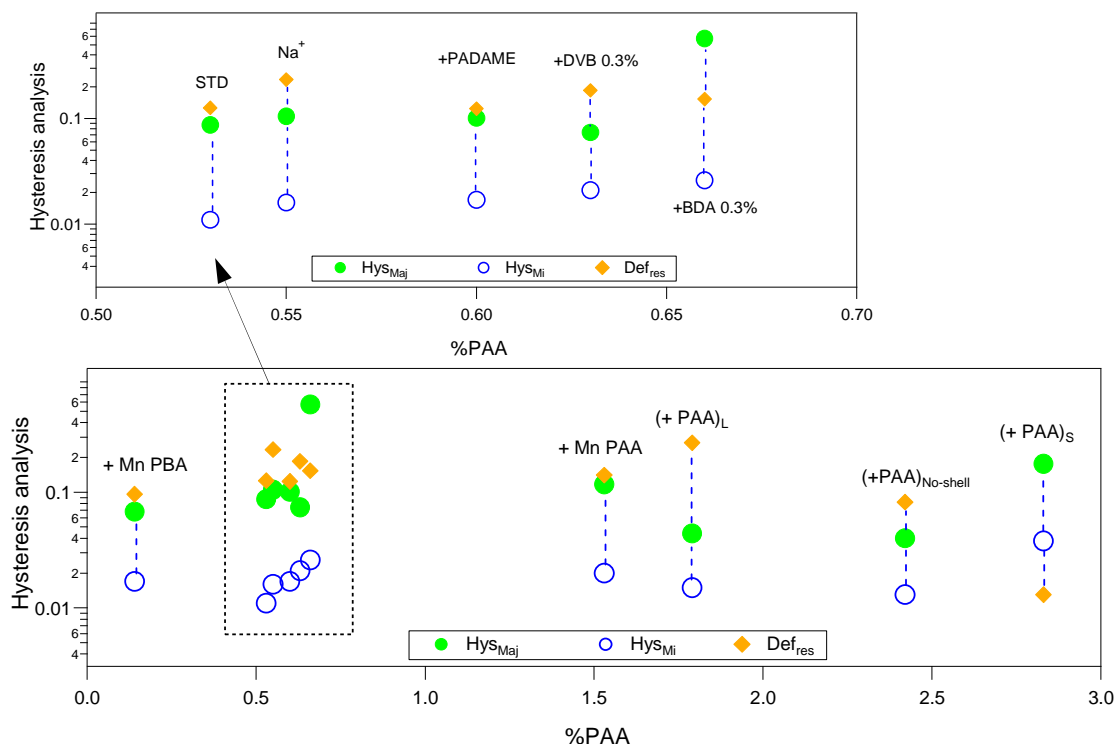


Figure 5- 57: Hysteresis analysis of latex DN films, where green dash lines are a guide line for eyes, and acronyms are defined in Table 5-11

The highest Hys_{maj} can be found in the latex with a core crosslinked with BDA (+BDA 0.3%), in contrast the DN with PAA_{5k} addition in the high M_n of PBA (+PAA)_L and in PBA_{no-shell} (+PAA)_{no-shell} shows the lowest major hysteresis. The Hys_{maj} is due to irreversible deformation or plastic behaviour of the material, the high Hys_{maj} in the latex containing BDA is probably due to the concomitant failure of covalent bonds in the core of the particles and to the breakup of the PAA shells of the latex. However, it is unclear how the addition of PAA_{5k} reduces Hys_{maj} in the latex with the high M_n of PBA (+PAA)_L or for the PBA_{no-shell} (+PAA)_{no-shell}, but not when added to the standard latex (+PAA)_S. It seems that the PAA_{5k} homopolymer and the PAA from the shell are not working cooperatively, resulting in free homopolymer in the film.

The minor hysteresis (Hys_{mi}) is due to reversible dissipation, which mainly comes from pendent chains and free chains in the material. The addition of free molecules to the latex seems to increase

the free chains and pendent chains in the final film. As a result, the latexes modified with chemical-crosslinkers (+BDA 0.3% and +DVB 0.3%), with a cationic polymer (+0.65PADAME), and with the NaOH pH adjust (Na^+) show a clear increase of Hys_{mi} , relative to the standard latex. In addition, Hys_{mi} also significantly increases for the DN with added $\text{PAA}_{5\text{k}}$ in the standard latex $(+\text{PAA})_{\text{S}}$, the increase in Hys_{mi} is due to the breakup of connection between $\text{PAA}_{5\text{k}}$ and PAA shell. However, the Hys_{mi} does not significant increase for other films with added $\text{PAA}_{5\text{k}}$, i.e. $(+\text{PAA})_{\text{L}}$ and $\text{PBA}_{\text{no-shell}}$.

On the other hand, permanent set or residual deformation (Def_{res}) is a result of the viscoelasticity of the material and is related to the softening of the rubber. In our study, the highest residual deformation is clearly found for the latex with the high M_n of PBA and the addition of $\text{PAA}_{5\text{k}}$, $(+\text{PAA})_{\text{L}}$ and is the lowest for the standard latex with an addition of $\text{PAA}_{5\text{k}}$, $(+\text{PAA})_{\text{S}}$.

5. Fracture toughness of DN films

The fracture toughness (Γ) of the latex DN film was investigated by measuring the critical energy release rate of notched samples, using a slight variation of the Greensmith approximation to analyze the data. The results are summarized in Figure 5-58.

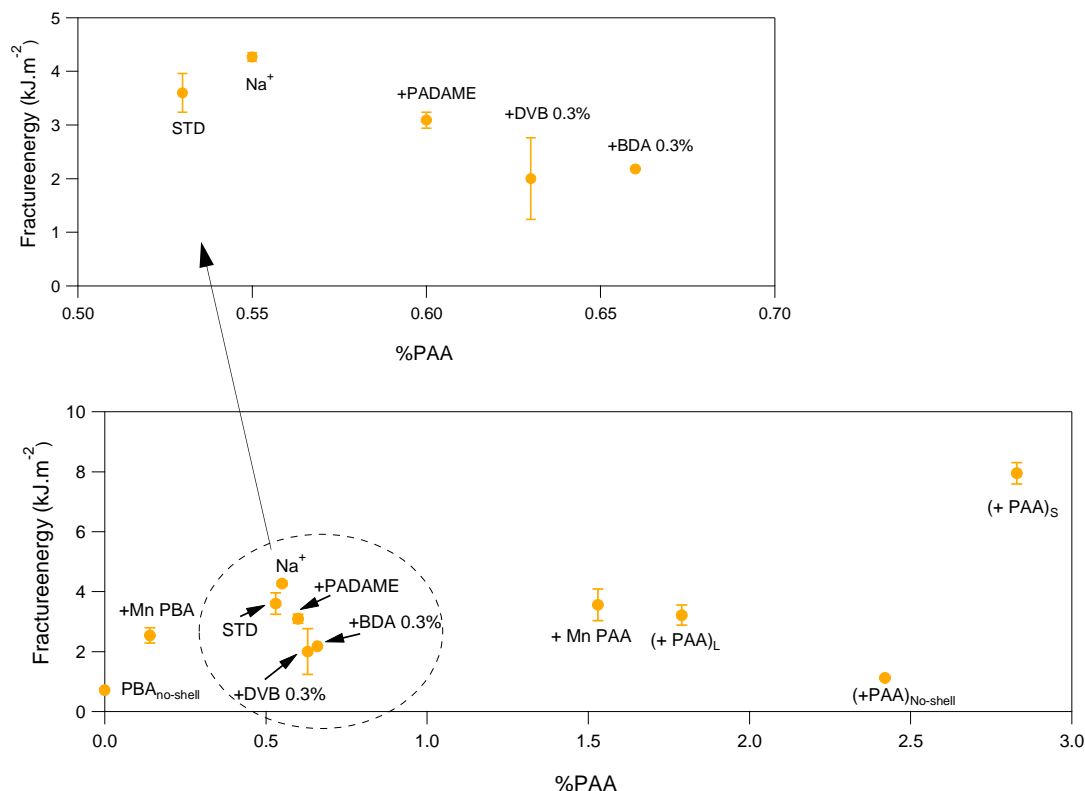


Figure 5- 58: Fracture toughness of latex DN films calculated by Greensmith approach, acronyms are defined in Table 5-11

It can be concluded that the standard latex DN film with added PAA_{5k}, (+PAA)_s shows the best fracture resistance. This is of course due to the higher %PAA composition in latex DN film which can delay crack propagation while maintaining stiffness. However, this conclusion cannot be made for the DN film made from the PBA_{no-shell} latex with added PAA_{5k} or (+PAA)_{no-shell} and for the DN made from high M_n PBA with added PAA_{5k} or (+PAA)_L, where although the %PAA composition is high, the fracture resistant is not improved suggesting that the PAA may not form a homogeneous thicker shell but may be dispersed randomly in the bulk and create larger defects. Thus, the key reinforcement of the fracture toughness appears to come from the embedded and well-dispersed PAA shells of the core-shell latexes containing block copolymers. In contrast, the increase of M_n of PBA (+ M_n PBA) which gives a less well organized shell structure shows the worse fracture toughness while additional crosslinks in the latex particles do not have much impact on the fracture resistance.

Conclusion

We have explored in this chapter the reinforcement of extensible PBA elastomers with a series of core-shell latexes. The basic synthesis method to make the core-shell particles was described in chapter 3 and in this chapter; we characterize and discuss the physical and mechanical properties of the different latex SN and DN films.

In all cases, although we can produce dry SN films with a high modulus by either using physical crosslinks between PAA-shells with the added cationic PADAME or with the COO^- ions created by the introduction of NaOH or by increasing the M_n of the PAA or by adding free PAA_{5k} homopolymer, the organized nanostructure of these films is most likely destroyed during the swelling process, resulting in a sometimes significant decrease in the initial modulus between the latex SN film and the DN. Thus, the method of introducing sacrificial bonds, as explained in Chapter 1 is not responsible for the reinforcement here, since the SN latexes do not contain permanent crosslinks and have no strong bonds between the shells.

In terms of stress and strain behavior the presence of the dispersed shell even after swelling does not change much the elastic modulus of the DN relative to the simple PBA network or relative to the DN made from the standard latex ($\text{PAA}_{2.5k}$, PBA_{100k}). However, the extensibility is increased while maintaining a higher stiffness relative to the M_n of PBA and the extensibility at break is much higher than for the DN reinforced with the simple latex.

The latex DN films show an obvious strain stiffening relative to the pure matrix of PBA thanks to the network formed by the physical bonds between the homogeneously dispersed PAA shells in the core-shell latex which result in a higher stress and strain at break and hence a higher toughness relative to the simple PBA network.

It should be noted that DN films with a high fracture energy and toughness can be obtained by adding PAA_{5k} homopolymer and increasing the %wt PAA. However, this reinforcement method changes the appearance of the films which turn white after adding PAA_{5k} homopolymer. Moreover, the sensitivity of the DN film to water and humidity may change due to the introduction of PAA_{5k} homopolymer which is sensitive to water. Thus, the most interesting method to reinforce the toughness of the PBA is the latex with reinforced physical interactions between the PAA short chains by COO^- (adjusted by added NaOH). In this case the DN film showed a high toughness by using only 0.5 %wt PAA.

The energy dissipation of the DN films depends on the method of reinforcement. Introducing free chains in the DN i.e. a PADAME cationic polymer, Na^+ , crosslinkers, or PAA_{5k} homopolymer increases the hysteresis. The lowest hysteresis can be found in DN films with higher M_n of PAA and fully elastic film is observed in DN of crosslinked PBA.

Last, fracture toughness of the films is significantly increased by adding PAA_{5k} homopolymer. to the standard latex and is clearly decreased when the core of the core-shell latex is crosslinked.

Other modifications are difficult to separate within the reproducibility of the measurement but it should be noted that these values are rather high at 3000-4000 J/m² for a relatively elastic material.

References

1. Payne, A.R., *The dynamic properties of carbon black-loaded natural rubber vulcanizates. Part I.* Journal of Applied Polymer Science, 1962. **6**(19): p. 57-63.
2. Wang, M.-J., *The Role of Filler Networking in Dynamic Properties of Filled Rubber.* Rubber Chemistry and Technology, 1999. **72**(2): p. 430-448.
3. Chenal, M., *Particules cœur-écorce par polymérisation raft en émulsion pour des matériaux nanostructurés sans solvants*, 2013. (Thèse de doctorat Physique et Chimie des matériaux): University Pierre and Marir Curie, Paris, France. p. 265
4. Haynes, W.M., *CRC Handbook of Chemistry and Physics, 93rd Edition.* 2016: CRC Press.
5. Park, J.-K., et al., *Effect of drying conditions on the glass transition of poly(acrylic acid).* Polymer Engineering & Science, 1991. **31**(12): p. 867-872.
6. Ducrot, E., et al., *Toughening Elastomers with Sacrificial Bonds and Watching them Break.* Science, 2014. **344**(6180): p. 186-189.
7. Ducrot, E., *Innovative tough elastomers: Designed sacrificial bonds in multiple networks*, 2013. (Unpublished doctoral dissertation): University Pierre and Marie Curie, Paris, France.
8. Webber, R.E., et al., *Large Strain Hysteresis and Mullins Effect of Tough Double-Network Hydrogels.* Macromolecules, 2007. **40**(8): p. 2919-2927.
9. Mullins, L., *Effect of Stretching on the Properties of Rubber.* Rubber Chemistry and Technology, 1948. **21**(2): p. 281-300.
10. Cantournet, S., R. Desmorat, and J. Besson, *Mullins effect and cyclic stress softening of filled elastomers by internal sliding and friction thermodynamics model.* International Journal of Solids and Structures, 2009. **46**(11-12): p. 2255-2264.
11. Bueche, F., *Molecular basis for the mullins effect.* Journal of Applied Polymer Science, 1960. **4**(10): p. 107-114.
12. Mullins, L., *Permanent Set in Vulcanized Rubber.* Rubber Chemistry and Technology, 1949. **22**(4): p. 1036-1044.
13. Chenal, M., L. Bouteiller, and J. Rieger, *Ab initio RAFT emulsion polymerization of butyl acrylate mediated by poly(acrylic acid) trithiocarbonate.* Polymer Chemistry, 2013. **4**(3): p. 752-762.
14. Chenal, M., et al., *Mechanical properties of nanostructured films with an ultralow volume fraction of hard phase.* Polymer, 2017. **109**: p. 187-196.
15. Bouvier-Fontes, L., et al., *Seeded Semicontinuous Emulsion Copolymerization of Butyl Acrylate with Cross-Linkers.* Macromolecules, 2005. **38**(4): p. 1164-1171.
16. Srivastava, S., *Co-polymerization of Acryla.* Designed Monomers and Polymers, 2009. **12**(1): p. 1-18.

17. *Technical Information Petrochemicals (Specialty Monomers)*. 2012: BASF Group.
18. Benson, H.L., *Divinylbenzene polymerization inhibitors*. 1970, Google Patents.
19. Cui, Z., et al., *Using intra-microgel crosslinking to control the mechanical properties of doubly crosslinked microgels*. *Soft Matter*, 2016. **12**(33): p. 6985-6994.
20. Errede, L.A., *Polymer swelling. 5. Correlation of relative swelling of poly(styrene-co-divinylbenzene) with the Hildebrand solubility parameter of the swelling liquid*. *Macromolecules*, 1986. **19**(6): p. 1522-1525.
21. Dechant, J., *Polymer handbook. 3rd edition. J. BRANDRUP and E. H. IMMERGUT (editors)*. ISBN 0-471-81244-7. New York/Chichester/Brisbane/Toronto/Singapore: John Wiley & Sons 1989. Cloth bond, ca. 1850 pages, £ 115.00, \$175.00. *Acta Polymerica*, 1990. **41**(6): p. 361-362.
22. Donnet, J.-B. and E. Custodero, *Chapter 8 - Reinforcement of Elastomers by Particulate Fillers*, 2013. (The Science and Technology of Rubber (Fourth Edition)), Academic Press: Boston. p. 383-416.
23. Dorfmann, A., B.A. Trimmer, and W.A. Woods, *A constitutive model for muscle properties in a soft-bodied arthropod*. *Journal of the Royal Society Interface*, 2007. **4**(13): p. 257-269.
24. Rothon, R., *Particulate-filled Polymer Composites*. second edition ed., United Kingdom: Rapra Technology Limited.
25. Chenal, M., et al., *Soft nanostructured films with an ultra-low volume fraction of percolating hard phase*. *Macromol Rapid Commun*, 2013. **34**(19): p. 1524-9.

-CHAPTER 6-

General conclusion and outlook

The idea of reinforcing mechanically elastomers with interpenetrating polymer networks (IPNs) to avoid macro phase separation has been developed and used in both elastomers and hydrogels since 1914.¹ By combining two or more polymers in the network form, it is possible to obtain a material with physical and mechanical properties that are a compromise between those of the individual polymers while maintaining a homogeneously mixed structure. In general interpenetrating polymer networks can be prepared in many ways. In our study we focus on the sequential interpenetrating polymer networks technique (sequential IPNs) which has recently been successfully applied to the acrylate polymeric system.^{2,3} By a proper design of an IPN based on the combination of a stretched stiff network (synthesized first) and an extensible network (synthesized in further steps), the acrylate multiple networks were both stiff and tough and the increase in toughness has been attributed to the presence of sacrificial bonds. Inspired by this recent work, we tried to broaden the concept of introducing sacrificial bonds, and create sequential IPNs with different polymeric system, silicone elastomers and core-shell acrylate latexes.

One way to synthesize silicone elastomer is the hydrosilylation reaction which is based on the addition of Si-H to a vinyl group. Fillers such as nanosilica are well known to be effective fillers and have been commonly used to reinforce silicone elastomers. However, to avoid the use of filler, IPNs have also been developed for silicone elastomers.^{4,5,6} Unfortunately, due to the phase separation the mechanical reinforcement was not well successful and ideal IPNs were not pursued.⁵ In our study, we synthesized silicone multiple networks by using sequential IPNs. Based on the experience gained on acrylates⁷, the most efficient stoichiometry was selected for both the silicone initial single network and for the silicone extensible network, serving as host network and interpenetrating networks respectively. However, since the same chemical reaction was applied in both silicone single networks and in the multiple networks, the presence of residual unreacted Si-H groups in the SN resulted in some coupling between the networks and the mechanical reinforcement in the multiple networks was not as strong as expected. The results of mechanical testing suggested that actually the silicone simple network and silicone interpenetrating network were bonded together by too many covalent bonds, creating an unorganized and heterogeneous coupled silicone multiple network. In those conditions the mechanical properties of the stiff and extensible network were not separated enough to create sacrificial bonds. However, we still found significant improvements of stress and strain at break comparing with its simple network. As shown in Table 6-1, the weight fraction of $\% \phi_{wt}^{SN}$ in DN decreases with the number of swelling steps. The multiple networks made from the SN synthesized in the presence of solvent showed as expected and increase in modulus and some strain hardening as the number of polymerization steps increased. Values of the fracture energy and toughness was 80-100% higher than for the corresponding simple network without trace of energy dissipation. However for the multiple networks made from SN synthesized in the bulk, the modulus decreased and there was no fracture energy or toughness improvement suggesting that the structure of this “bulk” first network

was very heterogeneous and the swelling steps did not cause any chain prestretching but rather some scission of chemical bonds.

(a) Silicone multiple network based on PDMS- V_{6k} and 66 %w/v toluene

[2 nd network]	-	[0.01 H _{D4}]			[0.02 H _{D4}]			[0.03 H _{D4}]		
Silicone network	SN	DN	TN	QN	DN	TN	QN	DN	TN	QN
ϕ_{wt}^{SN} (%)	100	44	21	13	42	17	11	56	22	9
λ_0	1	1.31	1.69	1.98	1.33	1.81	2.09	1.21	1.67	2.24
E (MPa)	0.35	0.35	0.34	0.35	0.43	0.47	0.49	0.52	0.58	0.67
Toughness (kJ/m ³)	112	480	477	378	359	362	396	379	536	578
Hysteresis (J/m ³)	-	-	-	-	-	-	-	-	-	0
Γ (J/m ²)	50	-	-	-	-	-	-	-	-	110

(b) Silicone multiple network based on PDMS- V_{17k} and 0 %w/v toluene

[2 nd network]	-	[0.01 H _{D4}]			[0.02 H _{D4}]			[0.03 H _{D4}]		
Silicone network	SN	DN	TN	QN	DN	TN	QN	DN	TN	QN
ϕ_{wt}^{SN} (%)	100	48	25	11	46	22	10	45	24	12
λ_0	0.83	1.28	1.59	2.06	1.29	1.67	2.15	1.30	1.62	2.05
E (MPa)	357	0.62	0.48	0.42	0.67	0.56	0.44	0.72	0.59	0.5
Toughness (kJ/m ³)	100	372	448	298	447	374	342	511	531	258
Hysteresis (J/m ³)	-	-	-	-	-	-	-	-	0	-
Γ (J/m ²)	52	-	-	-	-	-	-	-	54	-

(c) Silicone multiple network based on PDMS- V_{17k} and 0 %w/v toluene

[2 nd network]	-	[0.01 H _{D4}]			[0.02 H _{D4}]			[0.03 H _{D4}]		
Silicone network	SN	DN	TN	QN	DN	TN	QN	DN	TN	QN
ϕ_{wt}^{SN} (%)	100	34	17	7	29	13	9	32	13	6
λ_0	1	1.43	1.79	2.39	1.52	2.00	2.24	1.46	1.97	1.46
E (MPa)	0.22	0.20	0.21	0.23	0.24	0.24	0.36	0.22	0.37	0.33
Toughness (kJ/m ³)	462	290	245	359	710	380	314	526	287	360
Hysteresis (J/m ³)	-	-	-	-	0	-	-	-	-	-
Γ (J/m ²)	47	-	-	-	66	-	-	-	-	-

Table 6- 1: Physical and mechanical properties of silicone SN and their multiple network, where (a) silicone network based on PDMS- V_{6k} and 66 %w/v toluene, (b) silicone network based on PDMS- V_{17k} and 0 %w/v toluene, and (c) silicone network based on PDMS- V_{17k} and 66 %w/v toluene. The best silicone networks are highlighted in green

Our study on double networks (DN) based on core-shell acrylate latexes is the first of its kind to the best of our knowledge. Generally, latex IPNs are synthesized by creating a polymer II latex inside the polymer I latex and it is called as micro-IPNs^{1, 8, 9} or by mixing two or more latex and then create the crosslink at high temperature¹, this latex is called as interpenetrating elastomeric Networks (IEN).¹

In our study, the core-shell latex of PAA-b-PBA and crosslinked latex P(BA-co-BDA) were synthesized in controlled condition. The simple latex films were created by slow drying at temperature below 20 °C and then DN were created by using sequential-IPNs with BA monomer. The effect on the mechanical properties of different modifications of the latexes such as a latex with a crosslinked PBA-core, a latex with physical crosslinks between the PAA shells, a latex with a high M_n of the PBA-core, a latex with a high M_n of the PAA-shell and a latex with added PAA_{5k} solution etc. were investigated. We found that the modifications in the synthesis of the latex creates a different nanostructure of the film, resulting in differences in mechanical properties of the latex SN film. SN films with PAA modification such as high M_n of PAA in diblock copolymer, PAA-shells with physical crosslinks by adding a cationic polymer or cationic counter ion and adding PAA homopolymer show obviously high stiffness in the initial modulus. In contrast, SN films with PBA modification such as high M_n of PBA and PBA-cores crosslink have a low initial modulus (the detail can be found in Chapter 5 part 2).

However, after creating a DN film based on that latex by using sequential-IPNs, the initial modulus of the latex films always decreased due to the collapse of nanostructure during the second step of the synthesis process, i.e. the swelling by BA and subsequent polymerization. Despite our efforts, the shells of our latex SN films did not couple together, during the swelling/polymerization process to create DN films, so the PAA shell could break into the small pieces and was not really able to form a continuous network able to create sacrificial bonds. From this hypothesis, the PAA in the latex DN should stay homogeneously dispersed and work as a classical reinforcing filler.

The mechanical properties of the modified latexes DN suggest that to increase the initial modulus of the DN, the best strategy is to crosslink the PBA-core. Introducing crosslinks to the PBA-core reduces the collapse of the latex particles after the swelling/polymerization steps (sequential IPNs process) which is probably due to the less swellable core fixed in shape by the presence of the crosslinks. The physical crosslinking between PAA-shells by adding a cationic polymer or a cationic counter ion did contribute some reinforcement to the latex DN films, especially the Na⁺ counter ion results in DN films with excellent toughness and fracture resistance while containing only 0.5% PAA. In addition, the adjustment of the M_n of the PAA or of the PBA of core-shell latex has a very strong impact on the mechanical properties of the DN film: a higher M_n of the PAA increases the modulus of the film while increasing the M_n of the PBA has an impact on the extensibility of the film. The dissipation of energy of the DN films in cyclic extension depend on the method of modification of the latex. We found that by either adding free polymer (crosslinks, cationic polymer, homopolymer) or counter ions, the hysteresis increases. Finally, the fracture toughness of the latex DN films showed a significant improvement when a small amount of free PAA_{5k} was added to the latex, to the expense however of the transparency of the film and presumably its resistance to water whitening.

References

1. Zhi-zhong, Y. and E.M. Pearce, *Interpenetrating polymer networks and related materials*, L. H. Sperling, Plenum, New York, 1981, 265 pp. Price: \$35.00. Journal of Polymer Science: Polymer Letters Edition, 1982. **20**(4): p. 244-245.
2. Ducrot, E., et al., *Toughening Elastomers with Sacrificial Bonds and Watching them Break*. Science, 2014. **344**(6180): p. 186-189.
3. Ducrot, E., *Innovative tough elastomers: Designed sacrificial bonds in multiple networks*, 2013. (Unpublished doctoral dissertation): University Pierre and Marie Curie, Paris, France.
4. Hamurcu, E.E. and B.M. Baysal, *Interpenetrating polymer networks of poly(dimethylsiloxane) with polystyrene, polybutadiene and poly(glycerylpropoxytriacylate)*. Macromolecular Chemistry and Physics, 1995. **196**(4): p. 1261-1276.
5. Mazurek, M., *Silicone Copolymer Networks and Interpenetrating Polymer Networks*, 2000. (Silicon-Containing Polymers ,The Science and Technology of Their Synthesis and Applications), W.A. Richard G. Jones, Julian Chojnowski, Editor, Springer Netherlands. p. 113-137.
6. Clarson, S.J., *Silicones and Silicone-Modified Materials: A Concise Overview*, 2003. (Synthesis and Properties of Silicones and Silicone-Modified Materials), American Chemical Society. p. 1-10.
7. Millereau, P., *Large Strain and Fracture of Multiple Networks Elastomer*, 2017. (Unpublished doctoral dissertation): University Pierre and Marie Curie, Paris, France.
8. Sheu, H.R., M.S. El-Aasser, and J.W. Vanderhoff, *Phase separation in polystyrene latex interpenetrating polymer networks*. Journal of Polymer Science Part A: Polymer Chemistry, 1990. **28**(3): p. 629-651.
9. El-Aasser, M.S., et al., *Morphology, design and characterization of IPN-containing structured latex particles for damping applications*. Colloids and Surfaces A: Physicochemical and Engineering Aspects, 1999. **153**(1): p. 241-253.

-ANNEXES-

Annexes.....	249
Annex: A.....	251
Annex: B.....	253

Annex: A

1. NMR results of PAA-TTC macro-RAFT agent

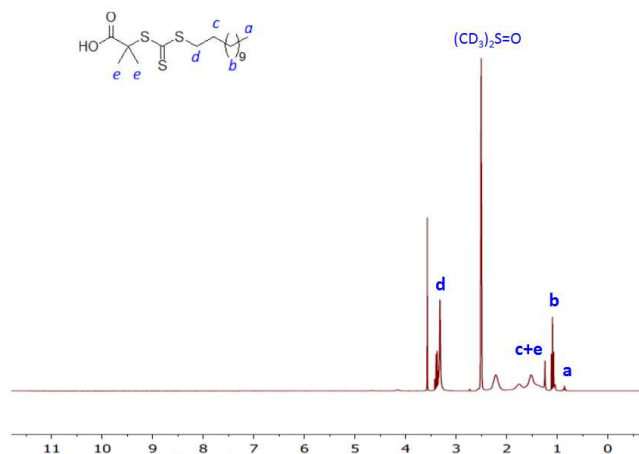


Figure A- 1: ^1H NMR spectra of TTCA by 200 MHz NMR with Deuterated DMSO

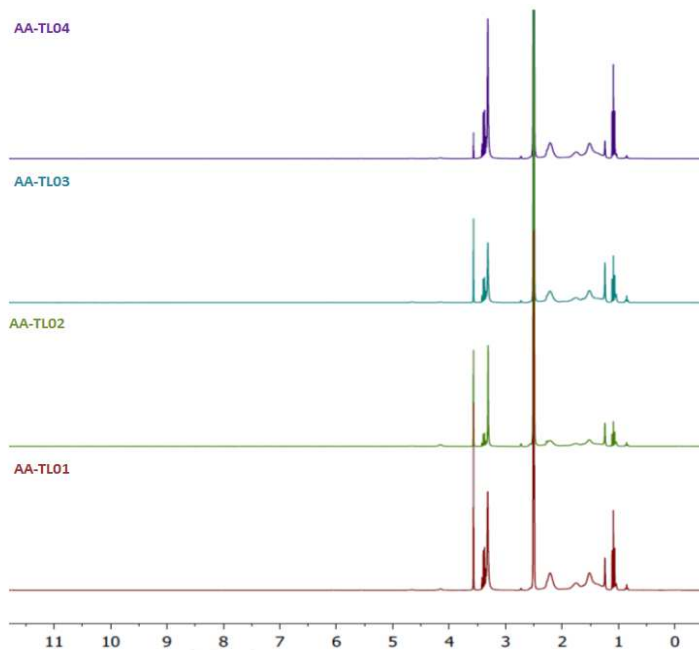


Figure A- 2: ^1H NMR spectra of TTCA with different M_n of PAA by 200 MHz NMR with Deuterated DMSO

2. The effect of the drying process on the structure and properties of the PAA-b-PBA latex SN

The precise drying temperature (T) used in the drying process to create PAA-b-PBA latex SN films had an impact on the initial modulus and on the toughness of the films. In our study, we found this effect very obvious in the film made from the latex (PAA2.5k, PBA100k) which we called our standard latex film (Figure A-1). Films with a higher modulus and stress at break can be obtained from drying the latex at a temperature lower than 22 °C. While, a drying process at a temperature higher than 25 °C ($T > 25$ °C) gives a more extensible and much less stiff film (see Figure A-3).

This study suggests that the drying process at high temperature disturbs the packing process of the latex particles to create the film. Resulting in a lower initial modulus and a higher extensibility. Comparing latex films at $T > 25$ °C to latex films with thermal annealing process (TA) at 160 °C for 72 hr, presented in Chapter 3 section 4, the annealed films showed a similar initial modulus as the latex film at $T > 25$ °C but the extensibility of the film was much lower ($\lambda=0.4$). The change of mechanical properties in the annealed film was expected and it may come from the inversion of the core-shell structure into a micellar structure as reported by Chenal et al.^{1,2}

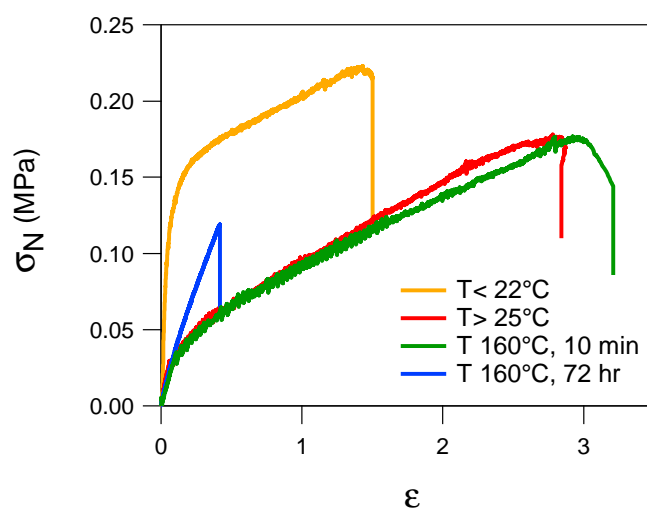


Figure A- 3: Mechanical properties of latex SN films obtained from the same latex but with different drying processes.

Annex: B

1. Difference amount of PDAME to latex SN and DN

1.1 Latex simple films of PAA-b-PBA with added PADAME

The mechanical properties of the dried films of PAA-b-PBA latex with added PADAME were characterized in uniaxial extension. The stress-strain curves, compared with the standard PAA-b-PBA latex film are shown in Figure B-1.

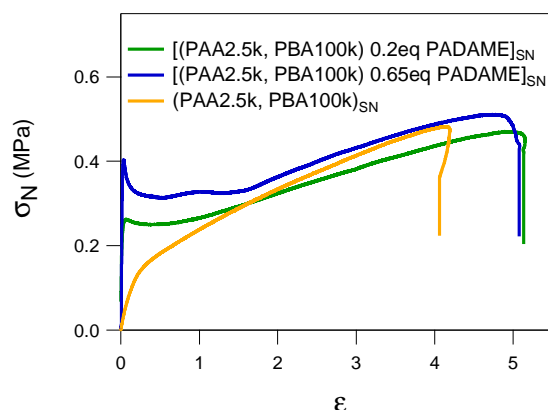
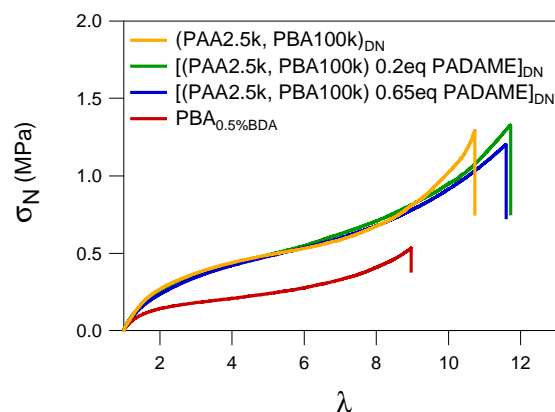


Figure B- 1: Stress-strain curve of (PAA2.5k, PBA100k) latex DN films with 0.2 eq. and 0.65 eq., and standard latex (PAA2.5k, PBA100k)_{DN}

The addition of PADAME clearly increase the initial modulus while it has little influence on the extensibility. This suggests that the physical crosslinks between PAA shells promote a better organization of the network of shells.

1.2 Latex DN films of PAA-b-PBA with added PADAME

The mechanical properties of the DN films made from SN films with different PADAME concentrations have been characterized in uniaxial extension and are presented in Figure B-2.



Sample	Φ_{latex}	(wt% PAA) _{SN}	(wt% PAA) _{DN}
(PAA2.5k, PBA100k) _{DN}	20	2.5	0.53
[(PAA2.5k, PBA100k) 0.2eq. PADAME] _{DN}	26	2.4	0.62
[(PAA2.5k, PBA100k) 0.65eq. PADAME] _{DN}	25	2.4	0.60

Figure B- 2: Stress-strain curve and %wt PAA of (PAA2.5k, PBA100k) latex DN films with 0.2 eq. and 0.65 eq., and standard latex (PAA2.5k, PBA100k)_{DN}

We expected that the better particle organization and initial modulus seen in latex SN films would also give a higher toughness in the respective DN. Unfortunately this was not the case. The mechanical properties of the DN films with PADAME addition do not show any improvement of mechanical strength, and the stress-strain curve of the films are not different from those of the standard latex film for both PADAME concentrations. In particular there is no difference in initial modulus suggesting that the stronger initial structure was disrupted by the swelling process. The steep initial modulus which is distinctive in latex SN film with PADAME addition disappears in DN.

Fracture toughness

Fracture mechanic studied by single edge notched sample of DN latex films are shown in Figure B-3. The fracture energy calculated with the Greensmith equation is shown in Table B-1.

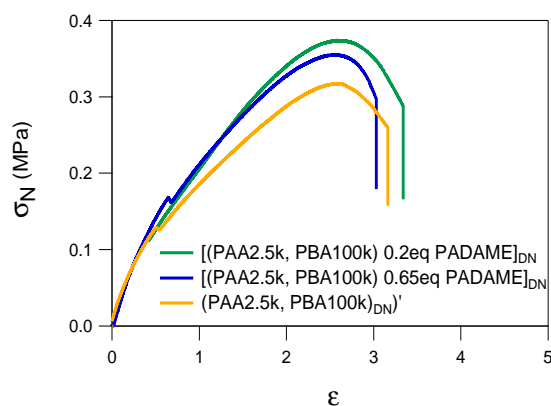


Figure B- 3: Fracture mechanics of (PAA2.5k, PBA100k) latex DN films with 0.2 eq. and 0.65 eq., and standard latex (PAA2.5k, PBA100k)_{DN}

The latex DN films with PADAME addition (0.2 eq. PADAME and 0.65 eq. PADAME) shows a slightly better fracture energy than the standard latex. Through PADAME addition, which is a short chain polymer (M_n 4.58 kg.mol⁻¹) may not impact the fracture toughness this improvement may come from the higher of %PAA content in latex DN with added PADAME addition (Figure B-2).

Sample	Γ (kJ/m ²)
(PAA2.5k, PBA100k) _{DN}	2.53 ± 0.36
[(PAA2.5k, PBA100k)0.2 eq PADAME] _{DN}	3.45 ± 0.62
[(PAA2.5k, PBA100k)0.65 eq PADAME] _{DN}	3.16 ± 0.15

Table B- 1: Fracture energy of (PAA2.5k, PBA100k) latex DN with 0.2 eq. and 0.65 eq., and standard latex (PAA2.5k, PBA100k)_{DN}

Energy dissipation

The dissipative properties of the PAA-b-PBA latex DN films with different concentrations of added PADAME, characterized with strain-control loading and unloading step extension tests are presented in Figure B-4.

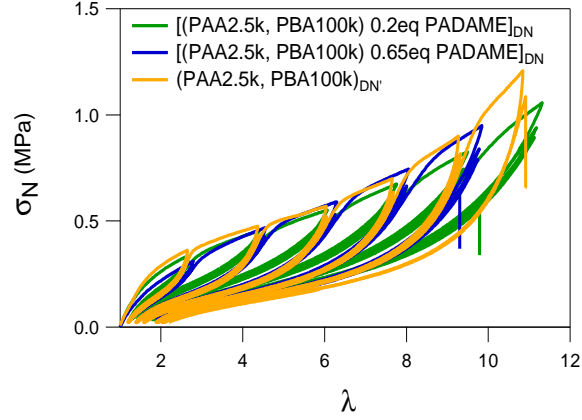


Figure B- 4: Strain controlled loading-unloading step cycle tests of (PAA2.5k, PBA100k) latex DN with 0.2 eq. and 0.65 eq., and of the standard latex (PAA2.5k, PBA100k)_{DN}

Latex DN films with added PADAME, both 0.2 and 0.65 eq. do not show significantly different stress-strain curves from those of the latex DN standard film. However, to understand better the dissipation mechanisms of each DN film, we apply the analysis as explained in Chapter 5 and the results are shown in Figure B-5.

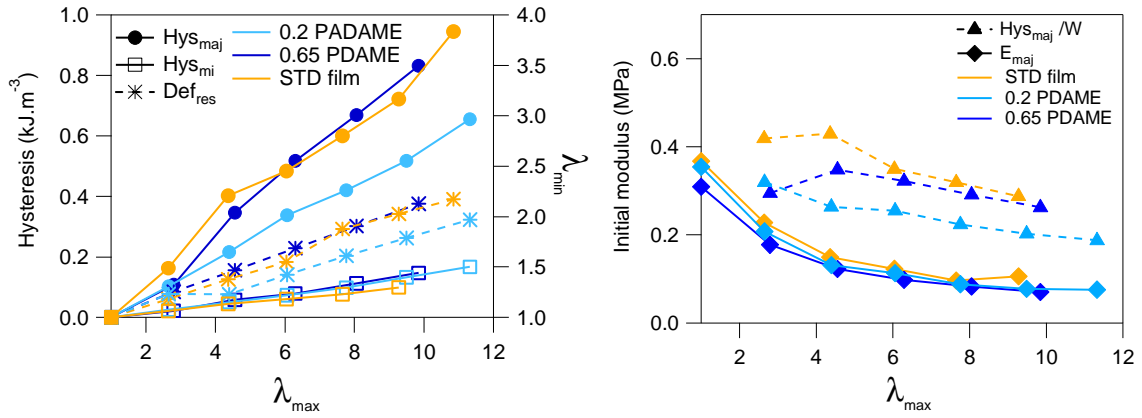


Figure B- 5: Dissipation energy analysis of, of (PAA2.5k, PBA100k) latex DN with 0.2 eq. and 0.65 eq., and standard latex (PAA2.5k, PBA100k)_{DN}

Major hysteresis (Hys_{maj}) and permanent set in latex DN with 0.65 eq. of added PADAME is similar to that of the standard latex DN film while for the latex DN with 0.2 eq. of added PADAME the hysteresis is lower. It is unclear to explain why Hys_{maj} and the permanent set of the latex DN with 0.2 of added PADAME has a lower level of damage.

2. Effect of a BDA amount on the latex SN and DN films

2.1 SN films of PAA-b-PBA with crosslinked PBA-core by BDA

The mechanical toughness of latex SN film with a PBA-core crosslinked by BDA shows a different behaviour from that of the standard latex films (Figure 5-22(a)). The BDA crosslinked films have a lower initial modulus compared with the one made from a standard film (Figure 5-22 (b)). However the initial modulus of the films with a crosslinked core increases with added amount of BDA crosslinker.

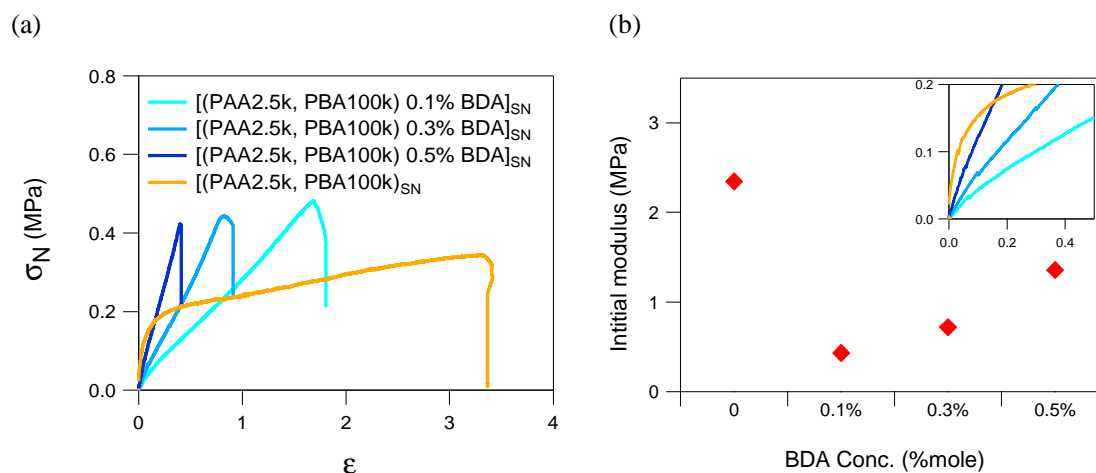
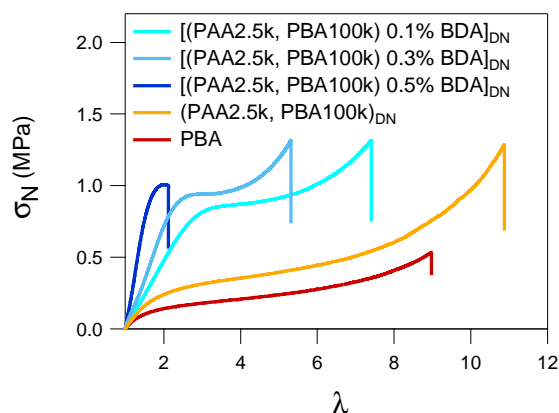


Figure 5- 59: (a) Stress-strain curve, and (b) initial modulus of PAA-b-PBA latex films with crosslinked PBA-core by 0.1%, 0.3% and 0.5% BDA, and normal PAA-b-PBA latex films

2.2 DN films of PAA-b-PBA with crosslinked PBA-core by BDA

Latex DN films synthesized by the sequential interpenetrating network technique of latex SN films with different concentrations of BDA crosslinker were tested in uniaxial extension (Figure B-6). An increase in crosslinker amount, results in a lower level of equilibrium swelling of the films and an increase of the final % PAA in the DN films.



Sample	Φ_{latex}	(wt% PAA) _{SN}	(wt% PAA) _{DN}
[(PAA2.5k, PBA100k) 0.1% BDA] _{DN}	23	2.2	0.51
[(PAA2.5k, PBA100k) 0.3% BDA] _{DN}	30	2.2	0.66
[(PAA2.5k, PBA100k) 0.5% BDA] _{DN}	37	2.5	0.93
(PAA2.5k, PBA100k) _{DN}	20	2.4	0.48

Figure B- 6: Stress-strain curves of PAA-b-PBA latex DN films with crosslinked PBA-core by 0.1%, 0.3% and 0.5% BDA, and normal PAA-b-PBA latex films

The stress-strain curves of the latex DN films made from SN films with a core crosslinked with BDA show a strain stiffening at lower levels of λ . Also interestingly, while the initial modulus of the standard latex DN film dramatically decreases relative to the SN because of the change in the nanostructure of the films (Figure B-7), for the DN films with BDA crosslinker the initial modulus does not change much relative to its Sn counterpart and increases with increasing BDA crosslinker.

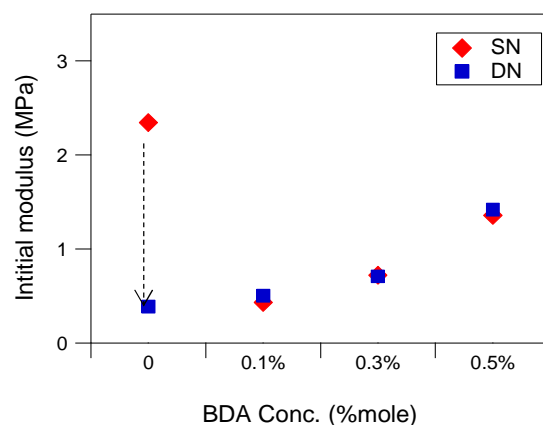


Figure B- 7: Initial modulus of latex SN films and latex DN films of PAA-b-PBA with crosslinked PBA-core by BDA

Fracture toughness

Fracture mechanics tests of latex DN films of PAA-b-PBA with different BDA concentration and standard latex DN film are shown in Figure B-8. The effect of the BDA crosslinker on the latex DN films is clearly shown by the increase of the initial modulus but also the decrease of the stretch at which the crack propagates.

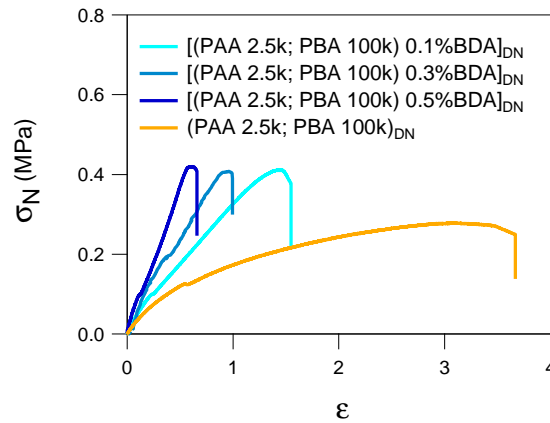


Figure B- 8: Fracture mechanic of latex DN films of PAA-b-PBA with BDA crosslink and normal PAA-b-PBA latex films

The fracture energy of the latex DN films calculated with the Greensmith model are shown in Table B-2. The fracture energy clearly decreases after introducing the BDA cross linker. Although, the crosslinker increases the modulus, it does also embrittle the material.

The effect of crosslinking concentration on the fracture toughness of the polymer matrix was also studied in the composite material of Drayton gasifier slag and poly(acrylic acid).³ It was found that by increasing the degree of crosslinker, the initial modulus of the cement composite increased. The presence of crosslinks can potentially increase the fracture toughness of the material; however, a high degree of crosslinking can also reduce the fracture toughness due to the high modulus of material.³

Sample	Γ (kJ/m ²)
(PAA2.5k, PBA100k) _{DN}	2.53 ± 0.36
[(PAA2.5k, PBA100k)0.1%BDA] _{DN}	1.93 ± 0.05
[(PAA2.5k, PBA100k)0.3%BDA] _{DN}	1.50
[(PAA2.5k, PBA100k)0.5%BDA] _{DN}	1.07

Table B- 2: : Fracture energy of latex DN films of PAA-b-PBA with BDA crosslink and normal PAA-b-PBA latex film

Energy dissipation

The stress-strain curve of loading-unloading step cycle extension of latex DN films with added BDA crosslinker compared with the standard latex can be found in Figure B-9. Latex DN films with added BDA crosslinker in the core of the particles obviously show a high level of dissipation in the cycle 2 ($\lambda_{\max}=4.2$) and 3 ($\lambda_{\max}=6$).

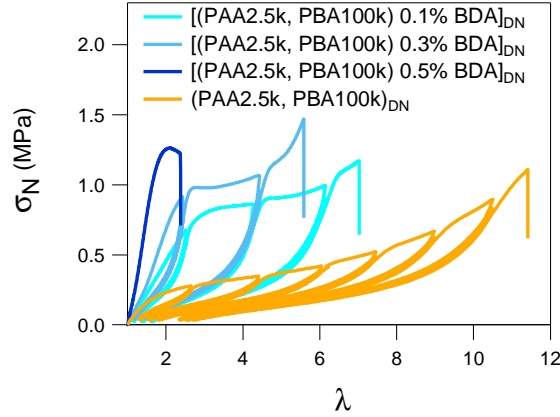


Figure B- 9: Strain controlled loading-unloading step cycle tests of PAA-b-PBA latex DN films made from SN with a PBA-core with 0.1%, 0.3% and 0.5% BDA, compared to the standard PAA-b-PBA latex films

The hysteresis analysis plots are shown in Figure B-10. The latexes DN made from SN with different concentrations of BDA showed similar Hys_{maj} at the beginning. Then the Hys_{maj} of the latex DN with 0.1% BDA had a higher hysteresis while there was no significant different of Hys_{mi} between the two latex DN films with different concentrations of BDA. The Def_{res} of latex DN with 0.3% BDA was higher due to the higher crosslinking reducing the viscoelasticity of the film. Moreover, E_{maj} of the latex DN was proportional to the concentration of BDA crosslinker as noted in uniaxial extension.

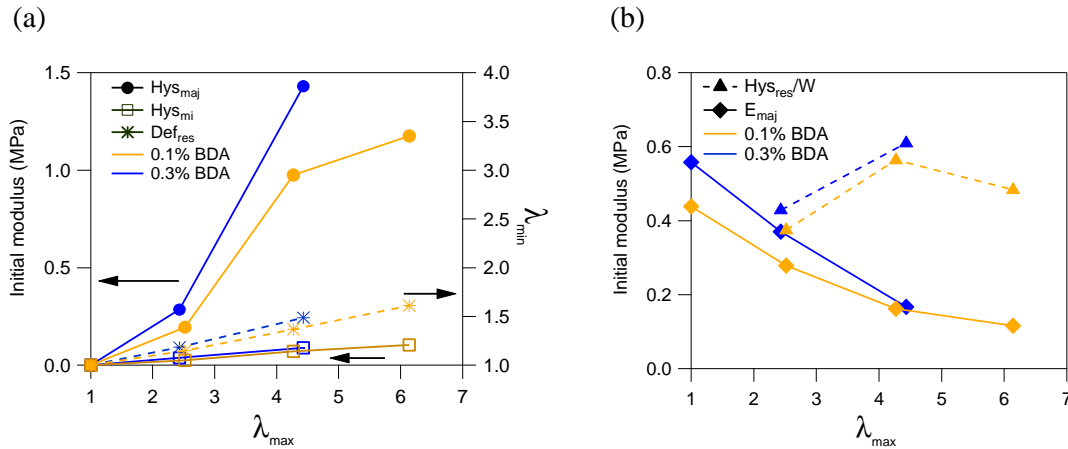


Figure B- 10: Dissipation energy analysis of, of (PAA2.5k, PBA100k) latex DN with different BDA crosslink concentrations, and standard latex (PAA2.5k, PBA100k)_{DN}

3. Effect of a DVB amount on the latex SN and DN films

3.1 SN films of PAA-b-PBA with a PBA-core crosslinked by DVB

In a qualitatively similar way as for the BDA crosslinker both modulus and strain at break decrease relatively to the uncrosslinked latex. The concentration of DVB crosslinker is related to the initial modulus of the film and limiting extension properties of the film, (figure B-11).

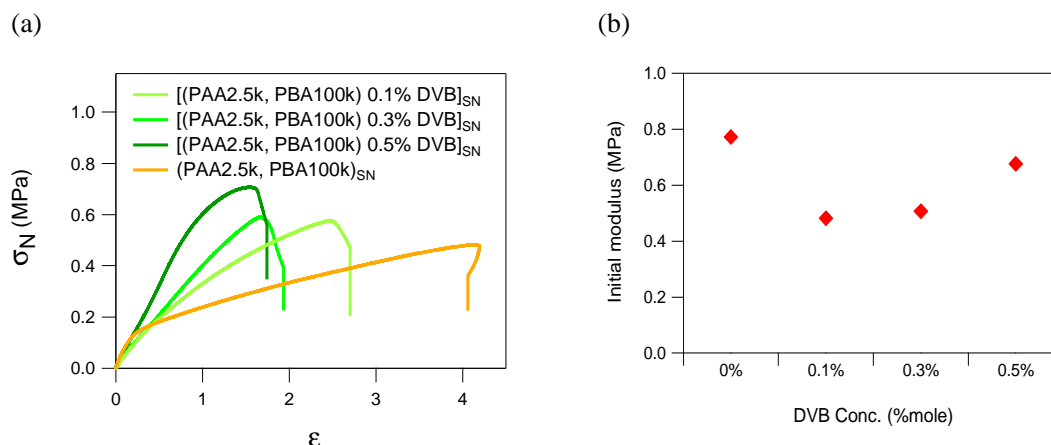


Figure B- 11: (a) Stress-strain curve and (b) initial modulus of PAA-b-PBA latex films with crosslinked PBA-core by 0.1%, 0.3% and 0.5% DVB, and normal PAA-b-PBA latex films

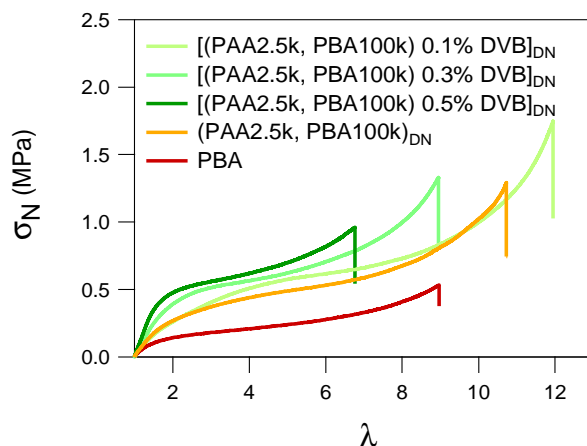
However, comparing with the system crosslinked with BDA, the latex films crosslinked with BDA have a lower initial modulus, but higher stress at break and deformation at break (Table B-3). These differences come from the nature of crosslinker and the different distribution of crosslinks as discussed above.

Mechanical properties	Conc. BDA (% mole)			Conc. DVB (% mole)		
	0.1	0.3	0.5	0.1	0.3	0.5
Initial modulus	0.43	0.72	1.35	0.48	0.51	0.68
Stress at break	0.42	0.44	0.42	0.58	0.59	0.71
Strain at break	1.81	0.91	0.41	2.70	1.94	1.74

Table B- 3: Mechanical properties of PAA-b-PBA latex SN films with crosslinked PBA-core by BDA and DVB crosslinker

3.2 Latex DN films made from PAA-b-PBA with DVB

In the DN films made from PAA-b-PBA latexes with DVB crosslinker, the stress-strain curve of the films studied in uniaxial extension at room temperature are shown in Figure B-12. Compared to the standard DN film, the latex DN films with DVB crosslinker has a significantly higher initial modulus and the strain stiffening comes at lower extension; it begins at $\lambda \sim 6$ for latex DN with DVB.



Sample	Φ_{latex}	(wt% PAA) _{SN}	(wt% PAA) _{DN}
(PAA2.5k, PBA100k) _{DN}	20	2.5	0.53
[(PAA2.5k, PBA100k) 0.1% DVB] _{DN}	24	2.3	0.55
[(PAA2.5k, PBA100k) 0.3% DVB] _{DN}	36	2.4	0.62
[(PAA2.5k, PBA100k) 0.5% DVB] _{DN}	32	2.2	0.70

Figure B- 12: Stress-strain curves and wt% of DN films made from PAA of PAA-b-PBA latexes with a PBA-core crosslinked by 0.3% DVB, compared with the standard DN film.

The comparison of the initial modulus between latex DN films and their SN counterparts is presented in Figure B-13. In the standard uncrosslinked core-shell latex, the initial modulus decreases markedly after passing through the swelling/polymerizing process. However, only a slight decrease in initial modulus relative to the precursor latex is observed for DN films made from precursor latexes containing DVB crosslinker.

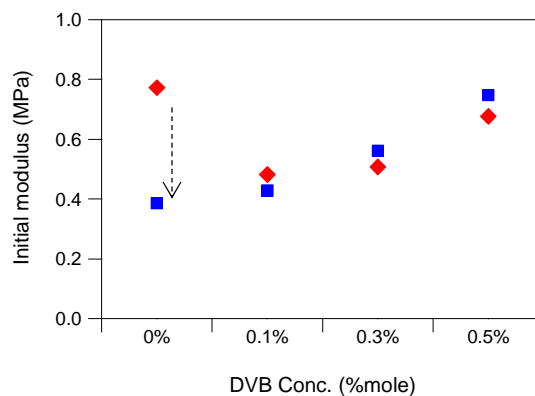


Figure B- 13: Initial modulus of PAA-b-PBA latex SN films and DN films with crosslinked PBA-core by 0.1%, 0.3% and 0.5% DVB

Comparing with latex DN films with the BDA system (section 3.2.2-1), latex DN films with DVB crosslinking show much better extension properties (Figure 5-30). Especially in latex films with 0.1% mole of DVB, the λ is about 12 and higher than the standard latex film ($\lambda=11$). The higher hydrophobicity of the DVB crosslinker creates more uniformly crosslinked cores. The latex DN films with DVB crosslinker can be reinforced by crosslinks while retaining a high swelling equilibrium which has an advantage to reinforce DN films. However, latex films with DVB crosslinker show an obvious decrease in swelling ability when introducing a high degree of DVB crosslinker ($>0.3\%$), resulting in an improvement of the initial modulus and high strain modulus, but limiting the extension at break.

Fracture toughness

Fracture tests of DN films made from PAA-b-PBA with DVB crosslinker, measured with single edge notch samples are shown in Figure B-14.

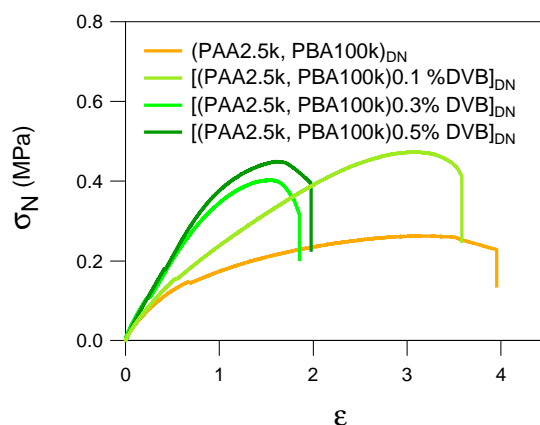


Figure B- 14: Fracture tests of DN films made from PAA-b-PBA latexes with different DVB crosslinker, compared with a standard DN film.

Introducing a crosslinker in the PBA-core, increases the initial modulus and this property remains in the fracture test. However, due to the limitation of extensibility due to the crosslinking effect, the sample breaks early. The fracture toughness, calculated by Greensmith approximation are presented in Table B-4 and show that the film containing a higher concentration of BDA (>0.3%) has a lower fracture energy , while a low concentration of BDA (0.1%), gives the best results in terms of fracture toughness.

Sample	Γ (kJ/m ²)
(PAA2.5k, PBA100k) _{DN}	2.53 ± 0.36
[(PAA2.5k, PBA100k)0.1%DVB] _{DN}	3.10 ± 0.01
[(PAA2.5k, PBA100k)0.3%DVB] _{DN}	3.2 ± 0.76
[(PAA2.5k, PBA100k)0.5%DVB] _{DN}	1.86 ± 0.26

Table B- 4: Fracture energy of PAA-b-PBA latex DN films with different DVB crosslinkers, and standards PAA-b-PBA latex DN film

Dissipation of energy

The dissipative behavior of DN films made from PAA-b-PBA with DBA crosslinker were investigated by step-cycle extension. The stress-strain curve of DN films are shown in Figure 5-36 and compared with the standard latex DN film (without crosslinker).

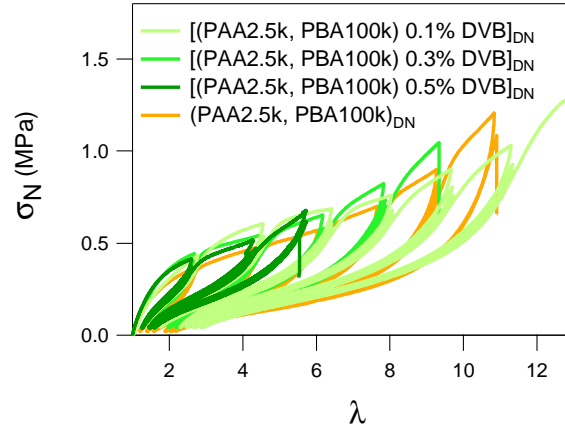


Figure 5- 60: Strain controlled loading-unloading step cycle test PAA-b-PBA latex DN films with different DVB crosslinker, and standards PAA-b-PBA latex DN film

We found that the dissipative properties are not significantly different from those of the standard DN. The modulus of the films with DVB increases a bit (1-5%) but the overall hysteresis in each step cycle is quite similar. In order to be precise, the analysis method to clarify energy dissipation described in Chapter 5, section 2.3 was applied here. The analyzed data are plotted as the function of λ_{\max} of each step extension, and they were presented in Figure B-15 (a) and (b).

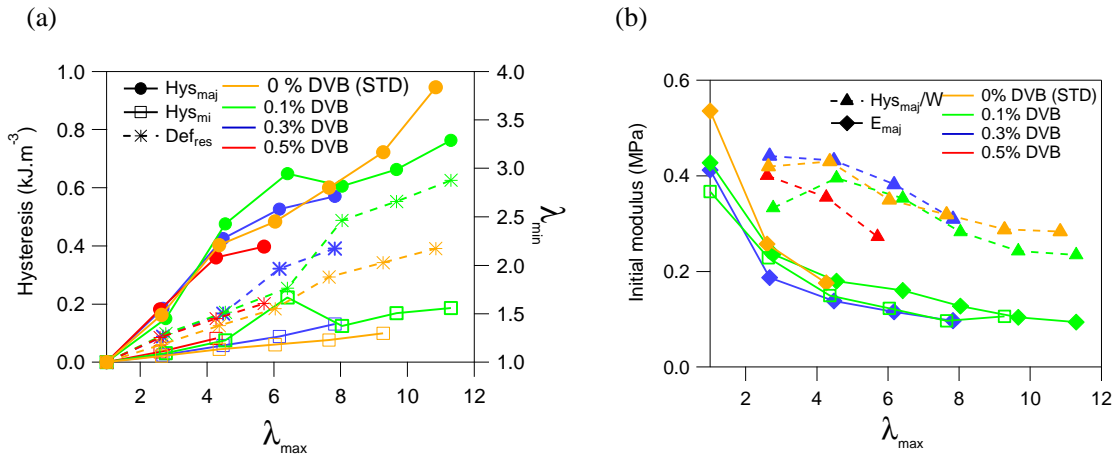


Figure B- 15: Energy dissipation analysis of each step extension of PAA-b-PBA latex DN films with different DVB crosslinker, and standards PAA-b-PBA latex DN film

In Figure B-15 (a), it was found that Hys_{maj} at low deformation of the latex DN films with different concentrations of DVB, starting from 0% or a standard latex DN film to 0.5% DVB) do not show significant differences. The differences of Hys_{maj} can be noticed at high deformation ($\lambda > 3$) where the lower concentration of DVB gives the higher Hys_{maj} . The Hys_{maj} at low deformation is due to the breaking of PAA-shells and crosslink while Hys_{maj} at high deformation may come from the

breaking of PBA. The low concentration of PBA gives the longer PBA chain between crosslink point which can be extended and absorb better the energy. Moreover, the increase of Hys_{mi} and permanent set or residual deformation (Def_{res}) are clearly observed in latex DN with high concentration of DVB crosslink. It may be due to damage process during the first loop creating more chain ends and causing a higher viscoelastic hysteresis, related to the increasing of Def_{res} in latex DN with DVB crosslinker. In Figure B-15 (b), The E_{maj} of latex DN shows similar result to those in uniaxial extension, the higher concentration of DVB showing a higher initial modulus.

4. Latex P(BA-co-BDA) films with added PAA

4.1 SN films of P(BA-co-BDA) with added PAA_{5k}

In this study, we try to mimic the structure of the core-shell latex of the PAA-b-PBA film by introducing additional PAA_{5k} in water to the P(BA-co-BDA) latex before creating the film. Uniaxial extension was used to observe the mechanical properties of latex SN films with and without adding PAA_{5k} and the results are presented in Figure B-16. The SN film of PBA_{no-shell} with added PAA_{5k} shows a similar behavior as the latex SN of PBA_{no-shell}. An increase of initial modulus can be obviously observed in the film made from the latex with added PAA_{5k}, however, the toughness of the film is much lower than that of the standard latex film.

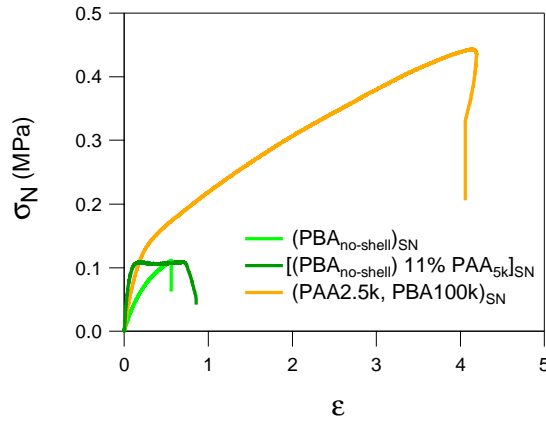


Figure B- 16: Stress-strain curve of SN films of PBA_{no-shell} films with and without PAA_{5k} addition compared to a standard film.

4.2 DN films of PBA_{no-shell} with added PAA_{5k}

The mechanical properties of the latex DN films made from latexes with and without added PAA_{5k} are shown in Figure B-17. The strain hardening could be observed clearly in the latex without added PAA_{5k} or (PBA_{no-shell})_{DN} which is due to the crosslinking of the PBA. However, a surprising result is found in the latex with added PAA_{5k} or with [(PBA_{no-shell})11%PAA_{5k}]_{DN}, the strain hardening in [(PBA_{no-shell})11%PAA_{5k}]_{DN} is barely observed and the effect of crosslinking and of added PAA seem to cancel each other. This surprising result shows that in [(PBA_{no-shell})11%PAA_{5k}]_{DN} the PAA may be poorly dispersed.

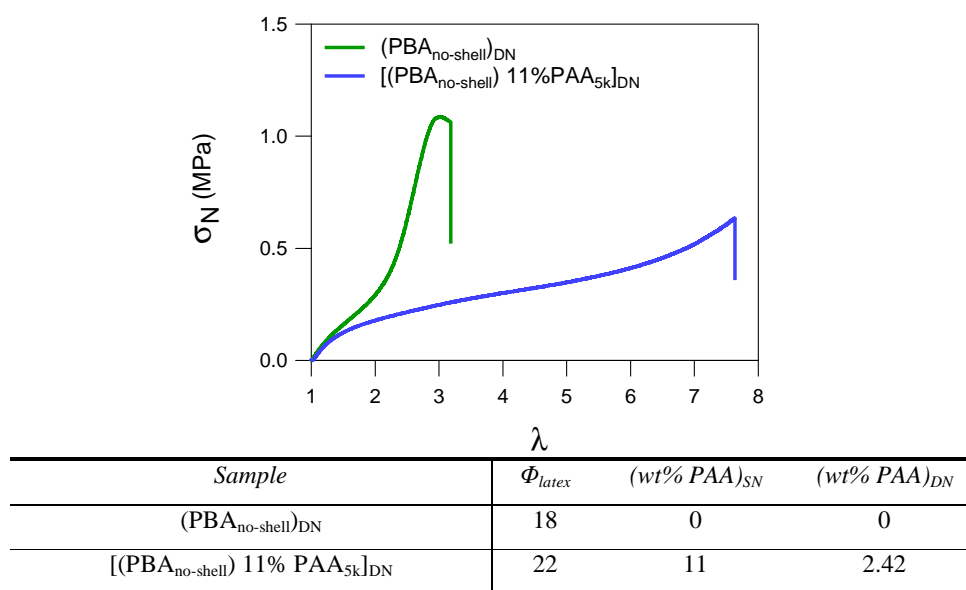


Figure B- 17: Stress-strain curve and wt% PAA of P(BA-co-BDA) latex DN films with and without PAA_{5k} addition

Fracture toughness

The results of fracture toughness tests of the samples as determined by uniaxial extension on notched samples are shown in Figure B-18.

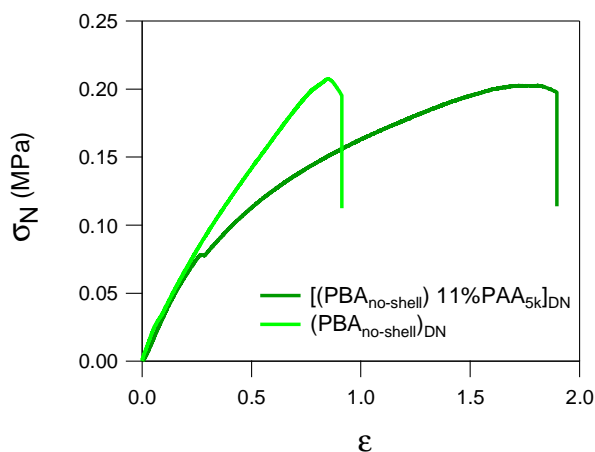


Figure B- 18: Fracture mechanics test of PBA_{no-shell} latex DN films with and without PAA_{5k} addition

An obvious improvement in fracture toughness is observed for [(PBA_{no-shell})11%PAA_{5k}]_{DN}. Although the strain at break of [(PBA_{no-shell})11%PAA_{5k}]_{DN} decreases, the extensibility of the film is much better, resulting in an increase in fracture toughness as shown in Table B-5.

Sample	Γ (kJ/m ²)
(PBA _{no-shell}) _{DN}	0.63 ± 0.04
[(PBA _{no-shell})11%PAA] _{DN}	1.02 ± 0.05

Table B- 5: Fracture energy of P(BA-co-BDA) latex DN films with and without PAA_{5k} addition.

Energy dissipation

The energy dissipation of the PBA_{no-shell} latex DN films with and without PAA_{5k} addition are presented in FigureB-19. The DN of the PBA_{no-shell} shows a fully elastic behavior where the hysteresis loop is negligible. However, after introducing PAA_{5k} to the PBA_{no-shell} latex, the hysteresis loops clearly appear and are mainly due to the breakup of the PAA chains.

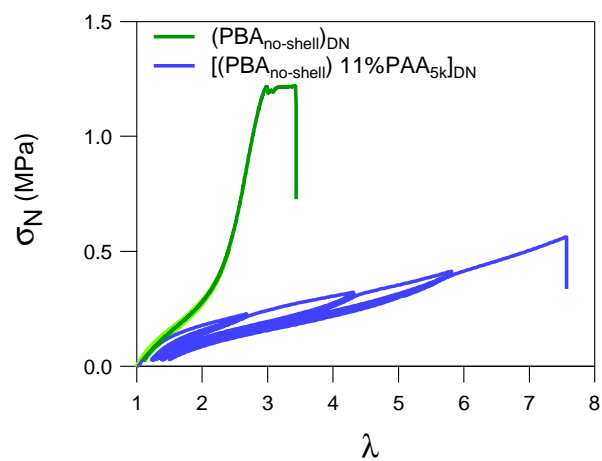


Figure B- 19: Strain controlled loading-unloading step cycle of P(BA-co-BDA) latex DN films with and without PAA_{5k} addition

References

1. Chenal, M., et al., *Soft nanostructured films with an ultra-low volume fraction of percolating hard phase*. Macromol Rapid Commun, 2013. **34**(19): p. 1524-9.
2. Chenal, M., *Particules cœur-écorce par polymérisation raft en émulsion pour des matériaux nanostructurés sans solvants*, 2013. (Thèse de doctorat Physique et Chimie des matériaux): University Pierre and Marir Curie, Paris, France. p. 265
3. Sullivan, A. and R. Hill, *Influence of poly(acrylic acid) molar mass on the fracture properties of glass polyalkenoate cements based on waste gasifier slags*. Journal of Materials Science, 2000. **35**(5): p. 1125-1134.

Résumé:

Récemment, une nouvelle technique pour renforcer les élastomères acryliques non chargés a été développée. L'élastomère a été préparé par séquences de gonflement par du monomère acrylique et polymérisation radicalaire en faisant des réseaux interpénétrés. Le prétrempage des chaînes du premier réseau créent des liaisons sacrificielles qui améliorent de manière significative les propriétés mécaniques de l'élastomère sans modifier sa Tg. Il est donc intéressant d'étendre cette méthode à d'autres familles d'élastomères. Ainsi, dans cette étude, la stratégie des réseaux interpénétrés a été appliquée à deux matériaux intéressants. Premièrement, un élastomère silicone a été synthétisé en utilisant une polymérisation par polycondensation par réaction d'hydrosilylation qui est significativement différente de la polymérisation utilisée pour les réseaux acryliques. Les réseaux multiples ont été ensuite synthétisés en gonflant ce réseau avec des précurseurs de petite masse et un faible pourcentage de réticulant D₄H. Ces réseaux multiples en silicone ont les propriétés d'un élastomère classique, avec une énergie de rupture améliorée d'environ 100%. Deuxièmement, des particules cœur-ecorce formées de copolymères dibloc amphiphiles de poly(acide acrylique)-b-poly(acrylate de n-butyle) ou PAA-b-PBA ont été synthétisés par auto-assemblage simultané par polymérisation RAFT et préparés sous la forme de films. Ensuite, les films ont été utilisés comme des charges polymères en poly (acrylate de butyle) en utilisant une technique de réseau interpénétrés multiples. Nous avons réussi pour la première fois à renforcer l'élastomère par des particules de latex. Grâce à cette stratégie d'interpénétration qui distribue des particules de latex de manière très homogène dans l'élastomère, les films interpénétrés montrent de bonnes caractéristiques mécaniques, une résistance à la fracture et une ténacité extrêmement élevées en utilisant moins de 1% de PAA vitreux et pas de réticulant ajouté dans la particule renforçante.

Mots clés: Élastomères, double réseau, renforcement mécanique, polydiméthyl siloxane, particules cœur-ecorce, polymérisation RAFT

Abstract:

Recently, a new technique to reinforce unfilled acrylic elastomers has been established. The elastomer was prepared by sequential free radical polymerization and swelling of acrylic monomers making interpenetrated networks. By introducing sacrificial bonds, the elastomer had significantly enhanced mechanical properties without changing the Tg of the material. We extended this method to two different elastomeric system to probe its generality. First, a silicone elastomer was synthesized by using polycondensation polymerization via a hydrosilylation reaction which is significantly different from the free radical polymerization used for acrylic networks. The multiple networks were synthesized by sequential swelling and polymerization steps with low molecular weight precursors and a small amount of D₄H crosslinker. The resulting silicone multiple networks were fully elastic elastomer with a mechanical toughness improved by about 100%. Second, core-shell latexes made of amphiphilic diblock copolymers Poly(acrylic acid)-block-poly(butyl acrylate) or PAA-b-PBA were synthesized by RAFT polymerization induced self-assembly and prepared into thin films. Different types of core-shell latexes and crosslinked latexes were synthesized and characterized both in the aqueous state and in the dry film state. The films were then used as a polymeric filler to a poly(butyl acrylate) by using the interpenetrated network technique. We succeeded for the first time to reinforce elastomers by latex particles. Thanks to interpenetrated networks strategy which distributed homogeneously latex particles through the entire material, the interpenetrated films show extremely enhanced mechanical characteristics, fracture energy and toughness by using less than 1 % of glassy PAA content and no crosslinker in the reinforcing particles.

Keywords: unfilled elastomers, multiple network design, mechanical reinforcement, silicone networks, core-shell latex, RAFT polymerization

Résumé: Récemment, une nouvelle technique pour renforcer les élastomères acryliques non chargés a été développée. L'élastomère a été préparé par séquences de gonflement par du monomère acrylique et polymérisation radicalaire en faisant des réseaux interpénétrés. Le prétrempement des chaînes du premier réseau créent des liaisons sacrificielles qui améliorent de manière significative les propriétés mécaniques de l'élastomère sans modifier sa Tg. Il est donc intéressant d'étendre cette méthode à d'autres familles d'élastomères. Ainsi, dans cette étude, la stratégie des réseaux interpénétrés a été appliquée à deux matériaux intéressants. Premièrement, un élastomère silicone a été synthétisé en utilisant une polymérisation par polycondensation par réaction d'hydrosilylation qui est significativement différente de la polymérisation utilisée pour les réseaux acryliques. Les réseaux multiples ont été ensuite synthétisés en gonflant ce réseau avec des précurseurs de petite masse et un faible pourcentage de réticulant D₄H. Ces réseaux multiples en silicone ont les propriétés d'un élastomère classique, avec une énergie de rupture améliorée d'environ 100%. Deuxièmement, des particules cœur-ecorce formées de copolymères dibloc amphiphiles de poly(acide acrylique)-b-poly(acrylate de n-butyle) ou PAA-b-PBA ont été synthétisés par auto-assemblage simultané par polymérisation RAFT et préparés sous la forme de films. Ensuite, les films ont été utilisés comme des charges polymères en poly(acrylate de butyle) en utilisant une technique de réseau interpénétrés multiples. Nous avons réussi pour la première fois à renforcer l'élastomère par des particules de latex. Grâce à cette stratégie d'interpénétration qui distribue des particules de latex de manière très homogène dans l'élastomère, les films interpénétrés montrent de bonnes caractéristiques mécaniques, une résistance à la fracture et une ténacité extrêmement élevées en utilisant moins de 1% de PAA vitreux et pas de réticulant ajouté dans la particule renforçante.

Mots clés: Élastomères, double réseau, renforcement mécanique, polydiméthyl siloxane, particules cœur-ecorce, polymérisation RAFT

Abstract: Recently, a new technique to reinforce unfilled acrylic elastomers has been established. The elastomer was prepared by sequential free radical polymerization and swelling of acrylic monomers making interpenetrated networks. By introducing sacrificial bonds, the elastomer had significantly enhanced mechanical properties without changing the Tg of the material. We extended this method to two different elastomeric system to probe its generality. First, a silicone elastomer was synthesized by using polycondensation polymerization via a hydrosilylation reaction which is significantly different from the free radical polymerization used for acrylic networks. The multiple networks were synthesized by sequential swelling and polymerization steps with low molecular weight precursors and a small amount of D₄H crosslinker. The resulting silicone multiple networks were fully elastic elastomer with a mechanical toughness improved by about 100%. Second, core-shell latexes made of amphiphilic diblock copolymers Poly(acrylic acid)-block-poly(butyl acrylate) or PAA-b-PBA were synthesized by RAFT polymerization induced self-assembly and prepared into thin films. Different types of core-shell latexes and crosslinked latexes were synthesized and characterized both in the aqueous state and in the dry film state. The films were then used as a polymeric filler to a poly(butyl acrylate) by using the interpenetrated network technique. We succeeded for the first time to reinforce elastomers by latex particles. Thanks to interpenetrated networks strategy which distributed homogeneously latex particles through the entire material, the interpenetrated films show extremely enhanced mechanical characteristics, fracture energy and toughness by using less than 1 % of glassy PAA content and no crosslinker in the reinforcing particles.

Keywords: unfilled elastomers, multiple network design, mechanical reinforcement, silicone networks, core-shell latex, RAFT polymerization
